RICE UNIVERSITY

Probabilistic Determination of Thermal Conductivity and Cyclic Behavior of Nanocomposites via Multi-Phase Homogenization

by

Atakan Tamer

A THESIS SUBMITTED
IN PARTIAL FULFILLMENT OF THE
REQUIREMENTS FOR THE DEGREE

Doctor of Philosophy

APPROVED, THESIS COMMITTEE:

Pol D. Spanos, Chair
Lewis B. Ryon Professor of Mechanical Engineering and Material Science

Enrique V. Barrera
Professor of Mechanical Engineering and Materials Science

Satish Nagarajaiah
Professor of Civil and Mechanical Engineering

Houston, Texas
May, 2013

Abstract

Probabilistic Determination of Thermal Conductivity and Cyclic Behavior of Nanocomposites via Multi-Phase Homogenization

by

Atakan Tamer

A novel multiscale approach is introduced for determining the thermal conductivity of polymer nanocomposites (PNCs) reinforced with single-walled carbon nanotubes (SWCNTs), which accounts for their intrinsic uncertainties associated with dispersion, distribution, and morphology. Heterogeneities in PNCs on nanoscale are identified and quantified in a statistical sense, for the calculation of effective local properties. A finite element method computes the overall macroscale properties of PNCs in conjunction with the Monte Carlo simulations. This Monte Carlo Finite Element Approach (MCFEA) allows for acquiring the randomness in spatial distribution of the nanotubes throughout the composite. Furthermore, the proposed MCFEA utilizes the nanotube content, orientation, aspect ratio and diameter inferred from their statistical information.

Local SWCNT volume or weight fractions are assigned to the finite elements (FEs), based on various spatial probability distributions. Multi-phase homogenization techniques are applied to each FE to calculate the local thermal conductivities. Then, the

Monte Carlo simulations provide the statistics on the overall thermal conductivity of the PNCs. Subsequently, dispersion characteristics of the nanotubes are assessed by incorporating nanotube agglomerates. In this regard, a multi-phase homogenization method is developed for enhanced accuracy and effectiveness. The effect of the nanotube orientation in a polymer is studied for the cases where the SWCNTs are randomly oriented as well as longitudinally aligned.

The influence of voids existing in the polymer is investigated on the thermal conductivity, to capture the uncertainties in PNCs more extensively. Further, a unique damage evaluation model is proposed to assess the degradation of PNCs when subjected to thermal cycling. The growth in void content is represented with a Weibull-based equation, to quantify the deterioration of the thermal and mechanical properties of PNCs under thermal fatigue. In addition, the MCFEA considers the interface resistance of the carbon nanotubes as one of the key factors in the thermal conductivity of nanocomposites.

Parametric studies are performed comprehensively. The numerical results obtained are compared with available analytical techniques at hand and with the data from pertinent independent experimental studies. It is found that the proposed MCFEA is capable of estimating the thermal conductivity with good accuracy.

Acknowledgements

I wish to extend my deep gratitude to my advisor, Dr. *Pol D. Spanos*, for his mentorship and thorough guidance, and for challenging me in every aspect. His extensive knowledge and expertise in both academic and industrial world have been of a great value to me, both personally and professionally.

I would like to express my thanks to Dr. *Enrique V. Barrera* for introducing me to the world of nanotechnology. I am sincerely grateful to Dr. *Satish Nagarajaiah* for being a part of my academic education.

Further, I hereby thank all of my fellow colleagues and dear friends from the bottom of my heart for our collaborations, numerous stimulating discussions made, and for their constant support and help during my hard times, and all the fun we have had, and most importantly, for being part of my life. In this regard, special appreciation is due to *Esen Erdemir-Üngör, Milton Esteva, Georgeos Evangelatos, Güneş Avcı, Onur İnce, Jay Ghosh, J.N. Swamy*.

Subsequently, I would like to thank my *family* for their endless support, for providing me encouragement through my entire life, and for not giving up their hopes on me during my studies.

Finally, it is an unexplainable pleasure to express my immeasurable gratitude to the woman of my life, my beloved wife, *Pınar Tamer*, for her patience, courage, support, and for all the love, passion, joy, caring and inspiration that she has brought into my life.

I dedicate this dissertation to my dear mother, Mrs. *Muzaffer Alaftar*, whose son I am most proud to be.

Contents

List of Figures

Chapter 1

Introduction

1.1. Motivation

Composites have proven to be an exceedingly effective and efficient class of materials in engineering for decades. Essentially, they are heterogeneous structures composed of reinforcing constituents embedded in a matrix phase. While the reinforcing phase enhances the overall properties of the structure, the matrix acts as load transferring agent and protects the integrity of the structure against the environmental and operational damages. Therefore, the performance characteristics of a composite are superior to the components taken individually. Among all, polymers have been the material of choice as the matrix due to their low density, versatility of their processing methods, and ability to be shaped and molded at relatively low temperatures compared to traditional materials such as metals. A choice of the reinforcing filler emerges from the design requirements in engineering, such as improved mechanical or thermal properties. With their exceptional

mechanical, thermal and electrical properties, carbon nanotubes (CNTs) are considered to be the ultimate reinforcing materials for composite applications.

In recent years, a vast number of efforts have been made to incorporate CNTs into polymers with the aim of utilizing their desirable properties. In particular, polymer nanocomposites (PNCs) with enhanced thermal conductivity are great candidates to replace conventional materials in thermal applications in engineering vis-à-vis efficient heat removal. However, a considerable number of studies report that the thermal conductivity of PNCs is far below their potential. This limited thermal behavior of the polymer nanocomposites essentially stems from non-uniform distribution and poor dispersion of the nanotubes in polymers, the interaction and compatibility of the nanotubes and polymer, as well as CNTs size and orientation effects. These complex uncertainties in PNC structure evidently require pragmatic modeling to take advantage of the full potential of the nanotubes.

This dissertation introduces a novel approach with the purpose of simulating the thermal conductivity of polymer nanocomposites (PNCs) that comprise polymer matrix reinforced with single-walled carbon nanotubes (SWCNTs). The proposed Monte Carlo Finite Element Approach (MCFEA) relies on a multi-scale method to capture the randomness of the problem at hand. The emphasis is specifically on dispersion and distribution characteristic of the nanotubes in the polymer. There has been no work performed unifying these parameters for solving this inhomogeneity problem in steady state heat conduction. The Monte Carlo simulation based finite elements method is used

to capture the spatial randomness of PNCs, represented by the local nanotube volume/weight fraction as random variable. Local degree homogenization in a FE on the thermal conductivity is performed by expanding the two-phase Eshelby's equivalent inclusion method to the multi-phase. Note that the precision of the proposed MCFEA is highly dependent on the FE mesh sizing and the number of realizations used in the Monte Carlo simulations.

Various parameters pertinent to the dispersion of SWCNTs in polymers are employed, such as their properties, orientation, aspect ratio and diameter, which are deduced from their statistical information. To that extent, nanotubes with perfectly random orientation and longitudinally aligned nanotubes are taken into account. Moreover, the level of dispersion is controlled by the agglomeration of the nanotubes, which is defined as certain variables by the proposed model. On the other hand, spatial distribution of SWCNTs in polymers is implemented by using random fields that represent the spatial variations of the local SWCNT volume or weight fraction. Local nanotube characteristics can easily be detected from image analysis of PNCs. Therefore, the proposed approach depends solely on a small fraction of the actual morphology of the filler and its statistical data. Variations of the effective thermal conductivity (K_{eff}) of PNCs are presented for a number of local SWCNT volume fraction distributions. That is, Weibull, Log-Normal and Uniform.

As highlighted in numerous experimental studies, thermal resistivity between the nanotubes and polymer is one of the main reasons of the poor thermal conductivity. Thus,

an attempt here is made to identify its influence. Experiments also show the existence of voids and impurities inherently present within PNCs due to the manufacturing or operational conditions. The proposed approach investigates their impact. In this regard, this dissertation makes an effort to further understand the long term effects of the voids when the PNC is subjected to thermal cycling. The intent is to simulate the real operational conditions, predicting the degradation in PNC properties and expected life.

The performance of the proposed model is assessed by comparison with the related experimental results, and its advantages over other thermal conductivity methods are demonstrated. Pertinent mathematical, physical and engineering background is also provided to give the reader a broad perspective on the established model, and on the critical parameters that affect the thermal conductivity of polymer nanocomposites.

The objective of this work is to establish a synthesis of the probabilistic analysis of the thermal behavior and the homogenization techniques. It aims to address the problem of thermal conductivity of randomly distributed and dispersed single walled carbon nanotube reinforced polymer composites. Regarding the significant advances and developments in nano technology, particularly in nanotubes and nanocomposites, a broader use of such statistical based models due to their ease of applicability is anticipated in engineering.

1.2. Overview

The development of the proposed probabilistic multi-scale approach to the thermal problem at hand is described in detail in this dissertation that comprises nine chapters and five appendices.

Chapter 1 provides an introduction and underlines the motivation and the objectives of the work undertaken. The organization of the dissertation and the summary of the topics discussed in each chapter are also included.

Chapter 2 presents the necessary background on the carbon nanotube reinforced polymer composites by extensive literature survey. First, the carbon nanotubes (CNTs) are introduced by appropriately defining their atomic structure, formation, production and their properties. Next, the use of nanotubes as reinforcements in polymer composites is discussed by experimental studies as well as numerical and analytical modeling techniques for predicting the thermal conductivity of polymer nanocomposites (PNCs).

In Chapter 3 the problem of extreme randomness and uncertainty with the existing polymer nanocomposites is identified by the demonstration of actual images and statistical studies. Definitions of distribution and dispersion are plainly established. It is clearly presented that the PNCs are intrinsically heterogeneous due to quality pertinent to the random distribution and poor dispersion of the CNTs. Initial stage of the proposed MCFEA is also developed in this chapter by defining the material volume element which

is a representative unit cell. Due to the high randomness in the structure, each discretized material region contains different nanotube volume content. In this regard, a statistical representation of the volume fraction of the nanotubes mixed in polymers is established. Actual images of PNCs are provided, quantifying the length and diameter distributions of CNTs. Formulations are developed to regenerate the statistical information obtained from the images.

Chapter 4 provides the theoretical and analytical details to develop the homogenization techniques in accordance with the physics of the problem. Homogenization is performed locally for a given material region with certain nanotube volume content. Primary technique described only estimates the thermal conductivity of a single inclusion in matrix, which is then enhanced to an extent that enables the technique to model multiple inclusions in the matrix. This homogenization technique is effectively known as the Hatta-Taya method. Formulations are derived for composites reinforced with misoriented inclusions. Parameters used in homogenization of a heterogeneous material region are introduced. Eventually, the thermal conductivity value calculated locally by this technique is fed into the finite element scheme.

A novel finite element approach is introduced to simulate the thermal conductivity of a polymer nanocomposite. The PNC is discretized into a number of finite elements (FEs) vis-à-vis material region (MR). Each element assumes a different nanotube volume content due to the heterogeneous nature of the composite. The nanotube content in each MR can be extracted from image analysis. However, since it is practically impossible to

scan the whole structure, sample MRs are scanned and the CNT content values obtained are fit by a probability distribution function (PDF). Consequently, the spatial randomness of the CNTs in a polymer is replicated. The thermal conductivity values for the given CNT content calculated by the local homogenization technique are fed into the finite element scheme.

The method also accounts for the uncertainty in size (i.e., length and diameter) and shape of nanotubes mixed in the polymer, based on their statistical characterization. Nevertheless, an adequate number of image analyses are required to obtain reliable results. Due to the limitation in performing such analysis, the proposed MCFEA employs various probability distribution functions (PDFs) to generate nanotube volume fraction values. CNT content values are numerically generated and fed into each finite element. Subsequently, a Monte Carlo simulation is carried out in conjunction with the finite element analysis which yields estimates for the effective thermal conductivity of PNCs. It is noted that adopting specific PDFs does not limit the applicability of the proposed approach; it simply illustrates its versatility.

In Chapter 5, the dispersion of nanotubes in the polymer is characterized by applying two distinct multi-phase homogenization methods in the local level. The need for a multi-phase method arises with the introduction of the agglomerates; as such the material region now comprises individual SWCNTs, spherical nanotube agglomerates, and the polymer matrix. However, the original technique is only for two-phase composites; matrix and reinforcing constituent. First, a hybrid approach is followed. The original two-

phase technique is used to calculate the thermal conductivity of matrix and individual SWCNTs forming a hybrid matrix. Then, the agglomerates are added into this hybrid matrix, and the local thermal conductivity is computed similarly. A second approach, which is adopted by the proposed MCFEA, is a direct multi-phase technique that uses each constituent as a separate phase. In this regard, the original two-phase homogenization theory is extended to a multi-phase theory. Rigorous derivation of this multi-phase approach consisting of randomly oriented inclusions is included in this chapter. Comparison of these techniques is pursued by several numerical examples. The influence of the agglomeration parameters on the effective thermal conductivity is also addressed.

Chapter 6 investigates the effectiveness of the developed MCFEA to the thermal problem at hand by comparison to the pertinent experimental findings. Proper assumptions are utilized for the agglomeration parameters in accord with the experimental information. The effectiveness and robustness of the proposed approach are also demonstrated by comparison with various models. The versatility of the MCFEA is further shown with the incorporation of the voids/cracks into the polymer matrix. Consecutively, the impact of interfacial thermal resistance between the carbon nanotubes and the polymer is characterized in reference to relevant experimental studies. Finally, in the interest of engineering design and application, PNCs with longitudinally aligned SWCNTs are modeled. To assess the influence of the nanotube orientation, simulation results are compared to that of the previously built randomly oriented SWCNT composites and the Hatta-Taya method.

In Chapter 7, an attempt is made to further understand the effects of voids present in a nanotube reinforced composite in temperature cycling. The intent is to simulate actual operating conditions. Presence of voids causes the PNC properties to deteriorate. The number of voids within a matrix is known to increase with the number of thermal cycles. To this end, progression of void volume fraction is modeled with a Weibull equation based approach. The model takes into account the strain energy density, stress and elastic modulus of the composite. The effective elastic modulus and coefficient of thermal expansion of the PNC are obtained by the well known Mori-Tanaka method. The Hatta-Taya method is employed to compute the effective thermal conductivity. Degradation of the PNC properties and the consequent PNC life are estimated. Pertinent theoretical and analytical background is established. A comprehensive parametric study is performed and the numerical results are presented.

In Chapter 8, concluding remarks along with potential future extensions of the proposed Monte Carlo Finite Element Approach are provided.

Appendices A to D give the detailed plots of the computed PNC property degradations and appendix E summarizes the Hatta-Taya method.

Chapter 2

Carbon Nanotubes as Reinforcing Fillers

2.1. Carbon Nanotubes

2.1.1. Introduction

Carbon is an extraordinary element in nature, a fundamental component of the living systems. It has a great capability of bonding with other atoms as well as with itself, and forming multiple bonds. These remarkable properties of carbon make it exist in the vicinity of ten million different compounds. Carbon also has the capability of forming long chains through carbon-carbon bonds which are among the strongest and the most stable bonds in nature.

There are several allotropes of carbon such as graphite, diamond, or fullerene. Fullerenes are lately-discovered class of carbon molecules which have closed cage-like carbon

structures composed of hexagonal and/or pentagonal faces connected by sp^2 bonds. They can be in spherical, ellipsoidal or tubular shapes i.e. buckyball or nanotube. Figure 2-1 shows various allotropes of carbon.

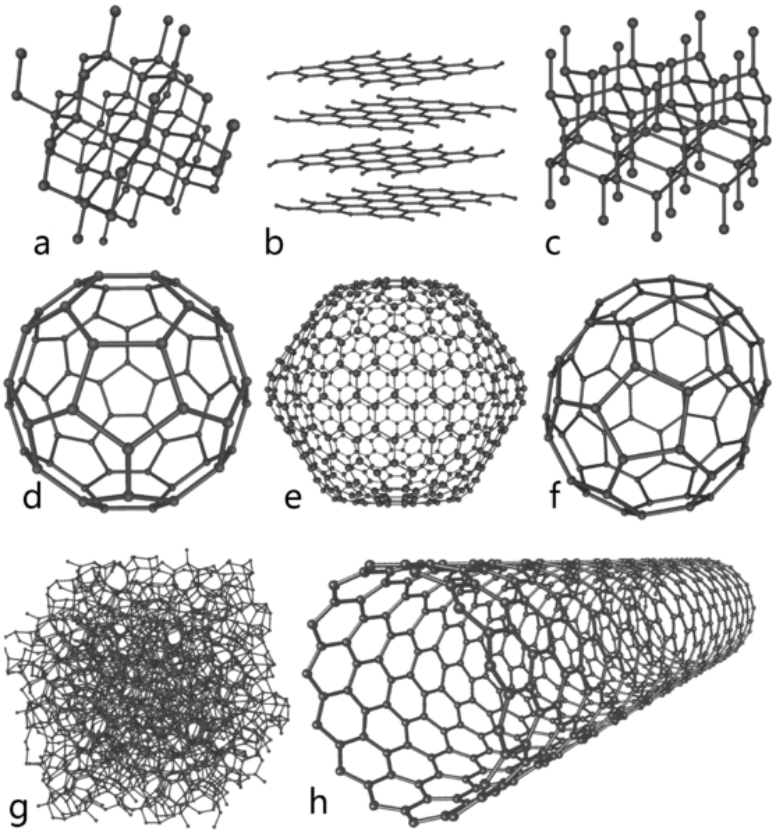

Figure 2-1. Various allotropes of carbon: a) Diamond, b) Graphite, c) Lonsdaleite, d) Buckyball (C_{60}), e) C_{540}, f) C_{70}, g) Amorphous carbon, h) Single-walled carbon nanotube.

Buckyball has a spherical shape and is one of the most famous in the fullerene family. The atoms of carbon come together in a way that they form in 12 pentagons and 20 hexagons (Figure 2-1-d). The buckyball (C_{60}) was discovered by Kroto, Curl, Smalley and their co-workers at Rice University in 1985 [1]. The shape of the buckyball (C_{60}) resembles that of a soccer ball. On the other hand, spherical fullerenes can range from a structure with 20 carbon atoms (C_{20}) [2] to 960 carbon atoms (C_{960})[3].

Another member of the fullerene family is the carbon nanotube (CNT) (Figure 2-1-h). Unlike buckyballs, nanotubes have cylindrical shapes, with ends typically capped with a hemisphere of fullerene molecule. They can be envisioned as seamless cylinders made of rolled-up graphite planes.

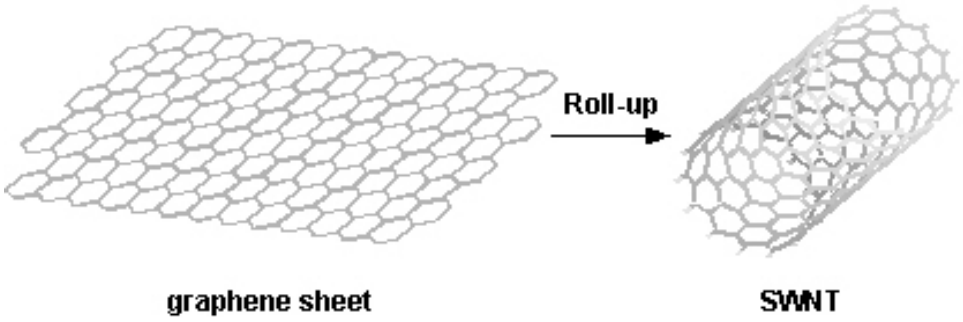

Figure 2-2. The roll-up of graphene sheet to form single-walled carbon nanotube.

The discovery of carbon nanotubes by Iijima [4] in 1991 initiated a huge number of research activities in various areas of science and engineering. Scientists observed that the carbon nanotubes possess unique physical and chemical properties. Their astonishing mechanical, thermal, and electrical properties have made nanotubes exceedingly attractive for a wide range of applications. Several of these applications can be listed as reinforcing of polymers and structures [5], [6]; thermal conductors [7], [8]; field emitters [9], [10]; hydrogen storage [11]; quantum wires; and semi-conductors [12], [13].

While researchers try to utilize the CNTs in optimal and feasible ways, one field among the aforementioned applications appears more promising. Carbon nanotubes are known to possess high aspect ratios (length/diameter); lengths of macro scales (in microns) [14]; densities as low as 1.3g/cm^3; and extraordinary thermal conductivities as high as 6600

W/mK even at room temperature, which is more than two times of that of isotopically pure diamond [7].

Due to these exceptional physical properties, CNTs are ideal candidates as ultimate thermal reinforcing fillers for advanced composite materials. The varieties, structure, properties, production and the area of use of CNTs as reinforcements in composites are discussed in the following sections.

2.1.2. Structure and Synthesis

Atomic Structure

Basically there are two types of carbon nanotubes; single-walled carbon nanotubes (SWCNTs), and multi-walled carbon nanotubes (MWCNTs) (Figure 2-3). SWCNTs can be considered as a single layer of graphene rolled-up to form a seamless cylinder. MWCNTs are coaxial assembly of such cylinders, one inside the other. The distance between each tube in MWCNT (~0.36nm) is similar to that in graphite layers (0.335nm) [15], [4]. However it has been reported that this interlayer distance varies between 0.342 and 0.375 nm due to the curvature and the number of layers of the MWCNT [16]. Transmission electron microscope (TEM) images of a SWCNT and a MWCNT are shown in Figure 2-4.

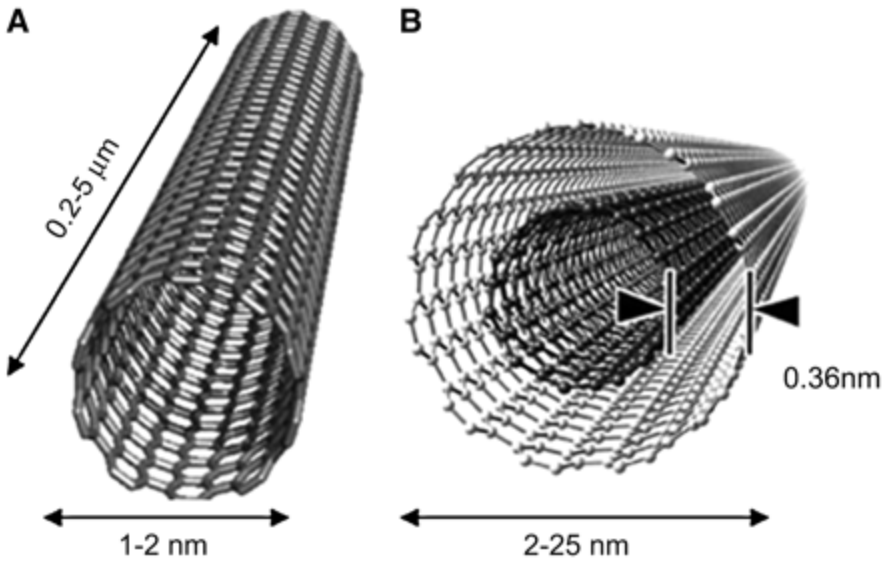

Figure 2-3. Molecular structures of a) single-walled carbon nanotube, b) multi-walled carbon nanotube.

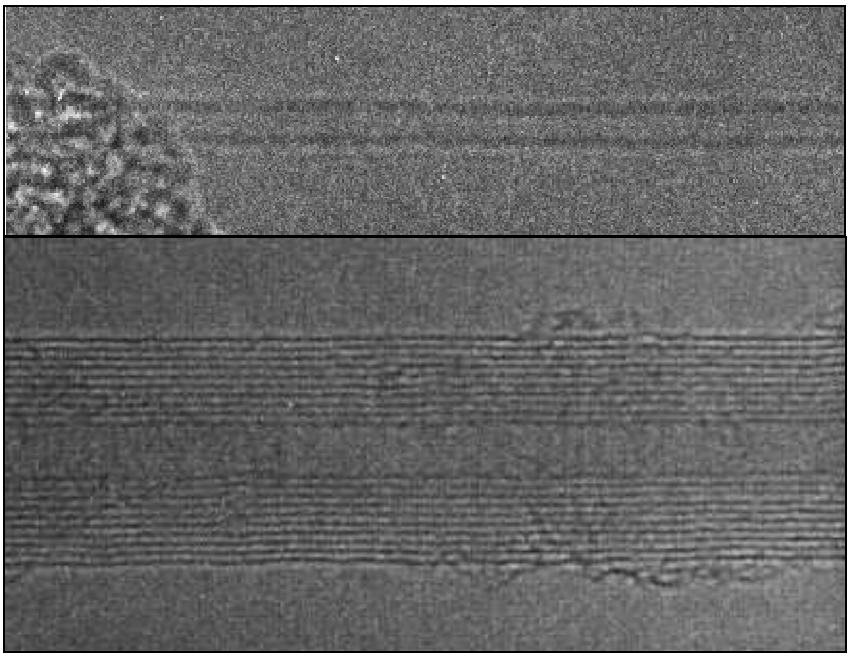

Figure 2-4. Transmission Electron Microscopy (TEM) images of single-walled and multi-walled carbon nanotubes.

The atomic structure of a carbon nanotube is similar to that of graphene sheet which only consists of sp^2 bonds (Figure 2-5). Naturally this sp^2 orbital hybridization is composed of one s-orbital and two p-orbitals which produces 3 sp^2 hybrids [17]. These strong covalent

bonds are also called as σ-bonds which give the CNTs exceptional mechanical properties. The geometry of an sp^2 hybridized atom is trigonal planar, each bond is at 120° to each other within a plane. This structural feature makes carbon atoms form hexagonal shapes. Since carbon 4 vacant electrons, after forming 3 σ-bonds, the left one electron in the p-orbital can form an out-of-plane bond called π-bond (Figure 2-5). The π-bond contributes to the interaction between the layers of MWCNTs, between the CNTs in a CNT bundle, and to the conductivity of SWCNTs.

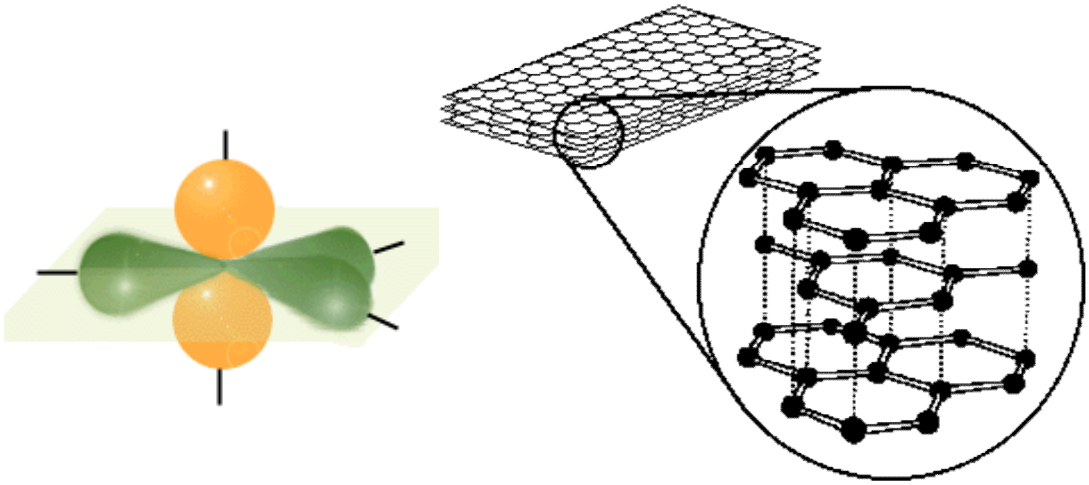

Figure 2-5. Left – sp^2 having a trigonal planar symmetry. **Right** – The atomic structure of graphite.

Single-walled carbon nanotubes (SWCNTs) have diameters in the vicinity of 1.4 nm [18], [19] and aspect ratios that can reach to 10,000 [20]. However, all SWCNTs are not the same. Depending on how the graphene sheet is rolled up, there are three types of nanotubes possible. This can be visualized as the "twist" of the tube and this spiral conformation called "chirality" is characterized by the chiral vector (Figure 2-6). The chiral vector, C_h, is defined by $C_h = n\ a_1 + m\ a_2$ where a_1 and a_2 are unit vectors in the two-dimensional honeycomb lattice of graphene, and *n* and *m* are integers [21]. The angle between zigzag line and C_h vector is called chiral angle which is another important

parameter. The values of *n* and *m* determine the structural forms of the nanotubes. If *m* = 0, which makes the chiral angle 0°, the nanotube is called “Zigzag” type. “Armchair” type nanotube is formed when *n* = *m*, chiral angle is 30°. If the chiral angle is between 0° and 30°, for the other values of *n* and *m*, the nanotubes are called “Chiral”. The vector T in Figure 2-6 shows the nanotube direction, which is perpendicular to chiral vector; C_h. The chirality of SWCNTs is important as their thermal, electrical, and mechanical behaviors [22], [23]. Further, a SWCNT is considered to be metallic when $(n - m)/3$ is integer, otherwise it is semi-conducting. Therefore, all armchair nanotubes are metallic, so are the one-third of other possible nanotube forms.

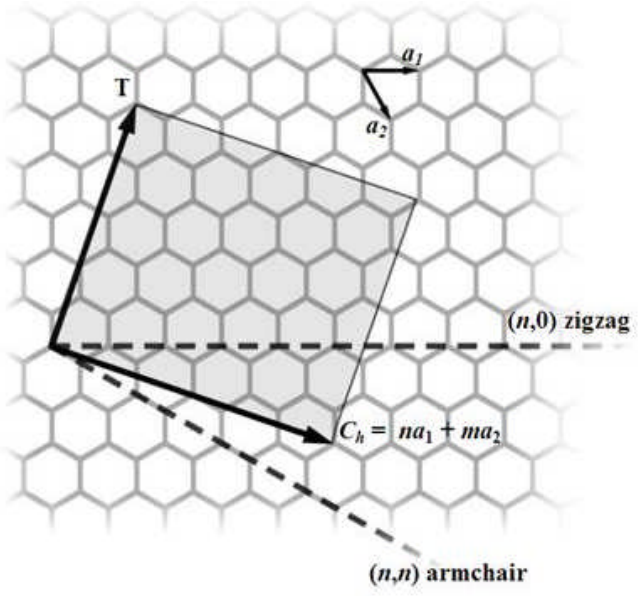

Figure 2-6. Schematic representation of a carbon nanotube described as a graphene sheet. The nanotubes are formed by rolling the sheet in the direction of the chiral vector C_h defined by the unit vectors a_1 and a_2. T vector denotes the nanotube axis.

It is know that the properties of the carbon nanotubes are extremely sensitive to their structure, size, and defect density. The influence of these parameters are extensively discussed and analyzed in the following chapters of this dissertation. Therefore,

controlling the quality of such parameters in the production of SWCNTs is an important research target. Additionally, the mass production is important in terms of widespread use and application of SWCNTs. A brief review of the production processes of SWCNTs is presented below, including electric arc discharge, laser ablation and chemical vapor deposition.

Electric Arc Discharge

The arc discharge method is one of the widely used methods in SWCNT synthesis. An electric current is applied across two carbon-rich electrodes in an inert gas atmosphere. The method is also called plasma arcing. A potential difference of 20-25 V creating a direct current of 50 to 100 A is applied between the electrodes. It results in a very high temperature, capable of vaporizing the surface of one of the carbon electrodes. The detached carbon atoms are then deposited on the other electrode forming a nanotube [24] (Figure 2-7). Quality of the CNT highly depends on the uniformity of the electric arc and the temperature.

Metal catalysts are also added in the SWCNT production where the carbon atoms diffuse on the catalyst particles. Iijima and Ichihashi [25] first reported SWCNT production using iron (Fe) as catalyst. Bethune et al. managed to obtain individual SWCNTs using cobalt (Co) doped electrode [26]. In addition, high purity SWCNTs can be produced in large quantities using metals nickel (Ni) and yttrium (Y) [27], [28].

During the process, an isolated environment must be sustained. Hence, the chamber is filled with gases such as He, H_2, N_2, CH_4 and Ar, or their mixtures. Depending on the procedures and the type of the gases used, the pressure of the chamber also varies [29–31]. This method is not too costly to produce mass amount of SWCNTs. However, the tubes can have structural defects. By-products such as metal particles, fullerenes and amorphous carbon are formed during the process. The nanotubes tend to be short with random sizes and entangles.

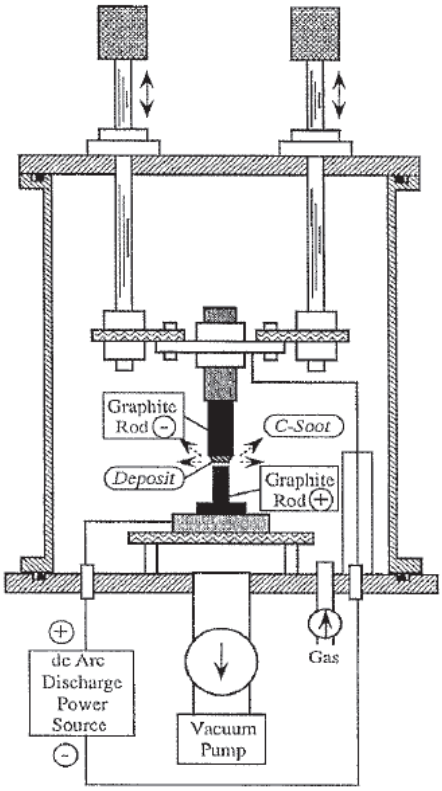

Figure 2-7. Schematic diagram of an arc-discharge apparatus **[24]**.

Laser Ablation

Laser ablation simply refers to the process of removing material from a solid surface by irradiation with a laser beam. The material is heated by the absorbed laser energy, which sublimates at low laser flux, or is converted to plasma at high laser flux. The material can be heated by a pulsed or a continuous wave laser. Computerized setups can be employed for automated operations.

The laser ablation technique was first reported in the production of SWCNTs in 1995 by Guo et al. in Smalley's group at Rice University [32]. A laser is sent on a target consisting of a mixture of graphite and Co-Ni catalyst in an oven at approximately 1200 °C. As the laser vaporizes the carbon electrode, the pure carbon vapor condenses and forms carbon nanotubes. Argon gas is pumped along the direction of the laser point to carry the CNTs onto a cooled collector (Figure 2-8). The nanotube diameter is thought to be controlled by the size of the metal catalyst [33].

While the MWCNTs are synthesized with pure graphite electrodes, metals catalysts must be mixed into the electrodes for the SWCNTs. These metals can consist of elements such as cobalt (Co), nickel (Ni), copper (Cu), niobium (Nb), platinum (Pt) or their combinations. Compared to the electric arc discharge, relatively better quality and purity can be achieved by laser ablation technique [34]. However, the effectiveness of this method is questionable due to expensive equipment and slower synthesis speed.

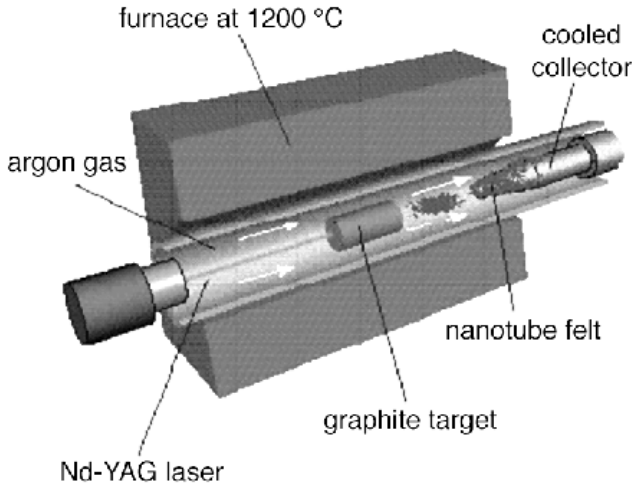

Figure 2-8. Schematics of a laser ablation set-up (Reproduced from **[35]**).

Chemical Vapor Deposition

Rather large scale of SWCNTs can be produced by chemical vapor deposition (CVD) technique [36], [37]. First, a substrate is coated with metal catalysts such as Ni, Co, Fe or their combination. A carbon source in gas phase is passed over the substrate in a carrier gas, e.g., ammonia, nitrogen or hydrogen. The carbon-containing gas can be methane, ethylene, acetylene, benzene or carbon monoxide. An energy source, such as plasma or a resistance heater, heats up the system. This leads the carbon-rich gas to be broken into its atoms. Then the carbon diffuses towards the surface of substrate, forming nanotubes at the tip of the catalyst particles (Figure 2-9).

The diameter of the carbon nanotubes is dependent on the size of the metal catalyst. The relation between the catalyst particle and the substrate determines if the particle stays at the tip or remains at the bottom of the nanotube. Unlike the other methods, metal catalysts are always included in the synthesis of both SWCNTs and MWCNTs.

Moreover, an electric field can be applied during the growth process so as to obtain aligned CNTs perpendicular to the substrate [38], [39].

At Rice University, Richard Smalley's research group developed a novel approach to produce highly-pure SWCNTs at a very large scale (kilogram per day) [40], [41]. The SWCNTs are synthesized by flowing high-pressure carbon monoxide (CO), mixed with a gaseous catalyst precursor ($Fe(CO)_5$), through a heated reactor. During the process, CO reacts with metal particles to form carbon dioxide (CO_2) and carbon atoms, which then bonds together to from carbon nanotubes. The grouped named this method the 'HiPco' process. The method can yield almost pure SWCNTs as small as 0.7 nm in diameter [42]. Purity and diameter of the nanotubes can be controlled by adjusting the pressure and temperature.

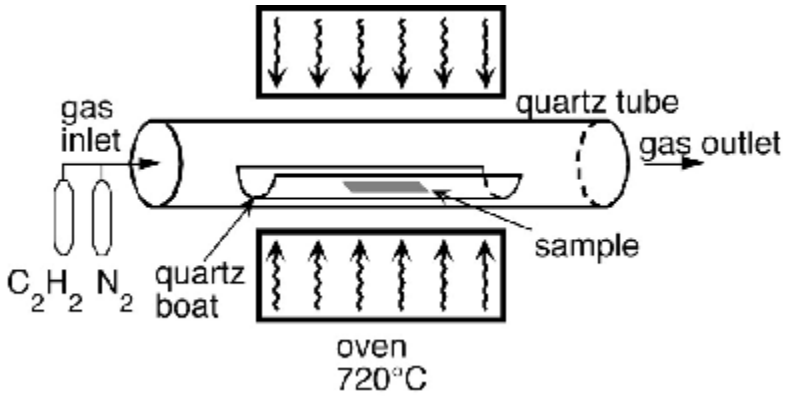

Figure 2-9. Schematics of a CVD deposition oven.

2.1.3. Properties

Electrical Properties

SWCNTs are remarkably powerful candidates as one-dimensional systems, due to their small diameters and their high aspect ratios. Their electric properties vary depending on their structure and dimensions. Chirality determines if the nanotube is metallic or semiconducting. Metallic SWCNTs are considered to be one-dimensional carriers as they do not allow electron scattering unlike their bulk metal counterparts. They are also called ballistic conductors since the electrons in transit do not scatter with too many phonons. With this reduced scattering rate, heat generation within a metallic SWCNT is considerably low. Such phenomenon, in theory, may lead the SWCNTs to possess high current density values of 1E6-1E7 A/mm^2 [43], [44]. This is orders of magnitude larger than the current densities found in existing bulk metals [45]. Conversely, a number of sources of scattering have been identified due to physical bends and defects in the SWCNTs [46].

Semi-conducting single walled carbon nanotubes are of special interest due to their capability to be used as critical components in electronic devices. This ability is attributed to the change in their electrical resistivity with temperature change [47]. Their other advantages are reduced heat output and higher frequency operations which can lead to devices with higher precision. Furthermore, by controlling the chirality, customized SWCNTs can be produced specific to the need. Several examples of such nano scale

electronic applications can be named as high-speed field effect transistors, and chemical or biochemical sensors [48], [49].

Thermal Properties

Potential application of carbon nanotube based devices, such as chips, diodes, field-effect transistors and elementary logic circuits, depends on the efficiency of the heat removal from the active section of the device [50], [49]. As thermal conductivity reflects the ability of a material to transfer heat, it is a key factor for heat dissipation. The in-plane thermal conductivity of graphite is very high (~2000 W/mK), twice that of diamond (~1000 W/mK).

Conversely, the out-of-plane thermal conductivity of graphite is, as one might expect, quite low due to the weakly bound layers, which are attracted to each other only by van der Waals forces [51], [52]. Contribution to a finite in-plane thermal conductivity in graphite at low temperature (<140 K) is thought to be phonon scattering from the edges of the finite crystallites. Even in highly oriented pyrolytic graphite (HOPG), the in-plane coherence length (where wave interference is strong) is typically less than 100 nm. At low temperatures, the phonon free path is controlled mainly by boundary scattering and at temperatures above 140 K, phonon-phonon (umklapp processes) dominates [53],[54]. Transmission electron microscopy (TEM) images suggest that defect-free tubes exist with lengths exceeding several microns, which is significantly longer than the typical crystallite length present in graphite. Hence, it is expected that the axial thermal conductivity of carbon nanotubes may be higher than graphite and diamond.

Another aspect of thermal management of structures or devices is the coefficient of thermal expansion (CTE), which relates the change in temperature to change in their dimensions. Therefore, it is important to control the thermal stress that rises from the difference in temperature during operations of such devices. With their low to negative CTE values similar to graphene, carbon nanotubes can be combined with other material such as polymers to tailor thermal expansion to specific needs. This negative expansion is attributed to the increased polyhedral libration of molecules by higher temperature. That leads to effective bond shortening which, in turn, results in negative thermal expansion.

The potential of carbon nanotubes has driven researches and scientists to delve into discovering their thermal properties, such as thermal conductivity and coefficient of thermal expansion. It is, nevertheless, challenging to quantify the properties of an isolated nanotube, while the measured and theoretical values are widely disputed.

Molecular dynamic simulations were performed by Berber et al. [7] to determine the thermal conductivity of single walled carbon nanotubes. Their results suggest an exceptionally high value of 6600 W/mK for an isolated SWCNT at room temperature. Their calculations also show unusually high value of 37000 W/mK at 100K. This value is quite close to the highest value observed in any solid, which is 12C diamond crystal at 104K with 41000 W/mK [55]. Lastly, Berber et al. [7] also reported that the thermal conductivity has a highly non-linear temperature dependence. These results show that the thermal conductivity of an isolated SWNT increases with the increase in temperature at low temperatures, and shows a peaking behavior at 100 K before falling off at higher

temperatures. The authors believed that the temperature dependence on the SWNT thermal conductivity is attributed to two scattering processes. At low temperatures, the thermal transport in SWNTs occurs by phonon-boundary scattering. As temperature increases, phonon-phonon (umklapp) scattering becomes dominant in heat transfer.

Che and his co-workers [56] used empirical inter-atomic interaction in their numerical calculations. Their molecular dynamic simulations estimated the thermal conductivity of a SWCNT in the vicinity of 3000 W/mK. However, they reported that any natural defects or vacancies present in the nanotubes lead to drastic drops in the values. Even notably low defect percentages, as low as one-thousandth (1/1000), may halve the thermal conductivity values.

Experiments were carried out by Pop et al. [57]. The thermal properties of a suspended metallic single-wall carbon nanotube (SWNT) are extracted from its high-bias (I-V) electrical characteristics over the 300–800 K temperature range, achieved by Joule self-heating. The thermal conductance is found to be approximately 2.4 10^{-9} W/K and the thermal conductivity is nearly 3500 W/mK at room temperature for a SWCNT of length 2.6 μm and diameter 1.7 nm.

Kim et al. [58] designed micro-device to measure thermal conductance of SWNT bundles. They found that 10 nm and 200 nm diameter bundles have thermal conductance about 300 and 3000 W/mK, respectively.

J. Hone [59] studied the thermal conductivity of loosely packed, tangled single wall carbon nanotube mats in the temperature range from 8K to 300 K. Their results show that the thermal conductivity behavior is nearly linear in this range, in contrast to that of graphite and carbon fiber, which shows the dependence on square of the temperature. The thermal conductivity of densely packed bulk sample is approximately 35 W/mK at room temperature. This extremely low value is attributed to high entanglement and bundles. Since the theoretical estimates for an individual SWNT could be as high as 6000 W/m-k at the room temperature, a further attempt was made by Hone et al. [60]. Specifically, SWCNTs were aligned applying high magnetic field. They observed linear conductivity variation with temperature, leading values of greater than 200 W/mK at room temperature.

Kordas et al. [50] demonstrated efficient cooling of a silicon chip using micro-fin structures made of aligned carbon nanotubes. They showed that up to 20% enhancement in heat dissipation is achievable with the superior thermal conductivity of CNTs, compared to other materials such as finned copper structures.

Moreover, thermal conductivity of CNTs is found to be diameter dependent. Fujii et al. [61] investigated the effect of diameter by measuring thermal conductivities of SWCNTs with 3 different diameters of 9.8nm, 16.1nm and 28.2nm. Their measurements showed inverse linear relationship with diameter. While the smallest diameter nanotube has an average conductivity of 2500 W/mK, the largest one has 500 W/mK.

The coefficient of thermal expansion of SWCNTs has also been investigated by the researches. Yosida [62] used X-ray diffraction techniques to measure the thermal expansion of an SWCNT bundle. He monitored the lattice constant of a close-packed trigonal arrangement of the nanotubes in the bundle over a temperature range from 290 to 1600 K. Shrinkage over the entire temperature range is observed and the CTE is estimated to be around $-1.5\times10^{-6}\ K^{-1}$ at 300 K and $-2.5\times10^{-6}\ K^{-1}$ at 1300 K. Maniwa and his co-workers [63] also performed X-ray diffraction study to determine the CTE of SWCNT bundles. The results revealed the axial CTE value of $(-1.5 \pm 2)\times10^{-6}\ K^{-1}$ over a temperature range of 300-950 K, which is comparable to that of graphite. This very low CTE value is considered to be due to the strong in-plane C-C bonds in nanotubes.

Molecular dynamic simulations were carried out by Kwon et al. [64]. They studied the thermal contraction of carbon fullerenes and nanotubes with their temperature dependence and length variations. Their results showed contraction up to 800 K, with the minimum value of $-12\times10^{-6}\ K^{-1}$ computed at 400 K.

Another study employed an analytical model to determine the CTE of SWCNTs. The method developed by Jiang et al. [65] uses the inter-atomic potential and the local harmonic model. Their findings show negative CTE values at low and room temperatures, but positive at higher temperatures. That is $-0.4\times10^{-6}\ K^{-1}$ at 270 K and $3\times10^{-6}\ K^{-1}$ at 1200 K. Diameter dependence was also observed to the effect that CTE decreases as the diameter increases from positive to negative values.

Mechanical Properties

In the design and engineering of new generation composites, specifically PNCs, it is important to understand the properties of carbon nanotubes. Due to the strong carbon-carbon bonds present in graphene, they have superior properties in terms of stiffness and strength. In analogy with graphite, it is expected that the CNTs have also similar mechanical behaviors. Measurements show that graphene has an in-plane elastic modulus of 1.06 TPa and a tensile strength of 20 GPa [66], [67].

A brief literature review is presented here on the mechanical properties of carbon nanotubes obtained by analytical and numerical simulations as well as experimental measurements. Determining the mechanical properties experimentally has been a great challenge for scientists. Part of these difficulties arises from handling of the CNTs due to their nanoscale dimensions and the lack of measurement techniques. Inaccuracy in the obtained data and the uncertainty in the test specimens may also cause discrepancy in the reported experimental values.

First experimental results came from Treacy et al. [68], who observed the amplitude of the thermal vibration of MWCNT continuous beams in transmission electron microscope (TEM). They calculated the Young's moduli of 0.40-4.15 TPa with a mean of 1.8 TPa out of 11 MWCNTs. Applying the same technique, Krishnan et al. [69] measured the elastic moduli (EM) of SWCNTs between 0.9 and 1.7 TPa based on 27 samples. Salvetat et al. [70] obtained an EM of 1 TPa by bending a SWCNT clamped at both ends with an atomic force microscope (AFM) tip. Yu et al. [71] measured an individual SWCNT

bundle performing direct tensile testing. The predicted elastic moduli range from 0.32 to 1.47 TPa with a mean 1.002 TPa for SWCNTs. Lourie et al. [72] observed cooling-induced vibration responses of SWCNTs via micro-Raman spectroscopy. The Young's moduli obtained were from 2.8 to 3.6 TPa.

At this point, the elastic modulus of MWCNTs may be mentioned for comparison purposes. Wong et al. [73] applied a direct measurement method to an individual MWCNT using a cantilevered beam model. They used atomic force microscope (AFM) to measure the Young's modulus of 1.28±0.59 TPa. Similarly, Yu et al. [74] determined the EM between 0.27 and 0.95 TPa for MWCNTs. Salvetat et al. [75] obtained the moduli of a MWCNT as 0.81±0.41 TPa.

The strength of nanotubes is also a critical element in engineering applications as they are used as reinforcing agents. The nanotubes must be able to withstand the local stresses generated within a composite. To that extent, various efforts have been made. Yu et al. [74] measured the tensile strengths of individual MWCNTs ranging from 11 to 63 GPa. Testing of 19 MWCNTs revealed that fractures occur in the outer layer at strains up to 12%. The same research group [71] also reported the strength of SWCNTs between 13 and 52 GPa with a maximum strain of 5.3%. Walters and his co-workers [76] determined the tensile strength of SWCNTs by means of AFM measurements and an average value of 45 GPa is obtained.

These difficulties and uncertainties in the experimental observations have driven scientists to develop alternative numerical and analytical methods. Numerous efforts have been made in the pursuit of characterizing the mechanical properties. These methods, nonetheless, show large inconsistencies as well.

Lu [77] investigated the elastic properties using empirical force-constant model and found the modulus in the vicinity of 1 TPa. Yao and Lordi [78] used molecular dynamic (MD) simulations to calculate the EM of nearly 1 TPa from the thermal vibration frequencies of a SWCNT clamped at one end. Jin and Yuan [79] predicted the effective EM of SWCNTs using MD simulations with force and energy approaches. Their computed values are 1.24 TPa and 1.35 TPa, respectively. Zhang et al. [80] developed a modified potential model and also reported an average EM value of 1 TPa, for the wall thickness (h) of 0.34 nm. Yakobson et al. [81] used MD simulations to compute the EM of a SWCNT as 5.5 TPa, with h=0.066 nm. Seidel and Lagoudas [82] utilized composite cylinder micromechanics technique and obtained effective elastic properties with the EM being around 0.7 TPa. Li and Chou [83] used structural mechanics approach with stiffness matrix method and evaluated the EM ranging from 0.89 to 1.033 TPa with h=0.34 nm. To [84] presented a finite element analysis (FEM) solution computing the elastic modulus and shear modulus as 1.024 TPa and 0.47 TPa respectively. Meo and Rossi [85] predicted nearly 0.9 TPa EM by molecular-mechanics based finite element modeling using nonlinear and torsional springs. Giannopoulos et al. [86] evaluated the effective EM of SWCNTs using a spring based finite element approach, ranging from 1.08 to 1.32 TPa.

Variety of numerical studies was conducted to estimate the strength of carbon nanotubes. Yakobson and Avouris [87] investigated the tensile strength of SWCNTs via MD simulations, yielding a value of 150 GPa with a strain of 30%. Srivastava et al. [88] also used the MD method to observe the fracture mechanics of nanotubes. SWCNTs were subjected to compressive strain up to 12%, resulting in stresses up to 150 GPa. Belytschko et al. [89] showed SWCNT strengths ranging from 93.5 to 112 GPa can be achieved at 16.5% average strain. Their MD simulations take into account the effect of chirality.

2.2. Thermal Conductivity of Polymer Nanocomposites

Due to their exceptional thermal properties, carbon nanotubes (CNTs) are one of the most promising fibers for enhancing the properties of advanced composite materials. Although many groups have studied polymer nanocomposite (PNC) materials for their mechanical properties, their possible thermal properties have only recently attracted attention. Notably high thermal conductivity of CNTs, coupled with their unique structure, make them useful for a number of thermal management applications, such as heat sinking of silicon processors, and increasing the thermal conductivity of plastics in such areas as housing for electric motors. The applications range from sensors, nanobearings and nanoprobes to field emission displays, energy storage, energy conversion devices and heat removal devices [90], [50], [49].

Polymer composites are rather easy to manufacture in comparison to their metal, ceramic, or carbon matrix counterparts [91]. The ease at which the polymer composites are manufactured stems from their low melting temperature. Although this characteristic gives them a great advantage for manufacturing, it limits the applications of polymer composites. Polymer used in these composites can either be thermosetting or thermoplastic polymer. Thermoplastics (e.g., polyethylene) are easier to manufacture than thermosets as a result of their ability to have higher ductility or withstand high temperatures. Thermoset polymers (e.g., epoxy) are widely used as a polymer matrix because of their good mechanical properties, corrosion resistance, adhesion properties, and relatively inexpensive material cost. Epoxies are unique polymers because their low molecular weight prior to curing leads to high molecular mobility. This high molecular mobility quickly and easily wets a filler material. Epoxy composites are widely used in conjunction with carbon fillers [92].

2.2.1. Experimental Studies

Numerous experimental studies have been carried out to determine the thermal conductivity of single-walled carbon nanotube (SWCNT) reinforced polymer composites. Haggenmueller et al. [93] measured the thermal conductivity of PNCs using two kinds of polymers; low-density (0.26 W/mK) and high-density (0.5 W/mK) polyethylene in the presence of SWCNTs. SWCNT-composites prepared with up to 30% in weight (wt %) were tested, and a relative increase of 600% was observed for both polymers. 55% enhancement in thermal conductivity was achieved by Bonnet et al. [94] for 7.3%

SWCNT loading in volume. Yu et al. [95] sought the difference between raw and purified SWCNTs added to epoxy resin in order to observe the effect of quality of dispersion. They concluded that purified nanotubes were much more dispersible in epoxy, while raw ones caused a significant raise in the viscosity of the polymer. In case of 9 wt % SWCNT loading, the improvement almost quintupled.

A unique approach was followed by Du et al. [96] in the fabrication of the PNC by creating a heterogeneous distribution of SWCNT, specifically an interconnected SWCNT-rich phase in epoxy. They compared the thermal conductivity of this new PNC to that of SWCNT-PMMA composite. Even though they observed conductivity approximately 3.5 times of the matrix for 2.3 wt %, their study was not comprehensive. Merely single weight fraction value was presented which does not provide thorough understanding of the method. Xu et al. [97] also used a novel technique by mixing unpurified SWCNTs in a PVDF matrix in powder form. They could attain quite high nanotube volume fraction of 50% but with only a slight increase in thermal conductivity of 230% at 50 °C.

High conductive silicone elastomer (1.1 W/mK) was used as the matrix with the presence of carbon nanotubes by Liu et al [98]. Relatively good nanotube dispersion in the matrix was claimed based on scanning electron microscope (SEM) studies and 65% enhancement was observed with 3.8 wt % CNT loading at 45 °C. Thermal conductivity of MWCNT-Epoxy composites was studied by Song and Youn [99]. Samples loaded up to 1.5 wt % purified and unpurified CNTs showed maximum conductivity of 0.26 W/mK

and 0.18 W/mK, respectively ($K_{epoxy} \approx 0.12$ W/mK). This showed that purified nanotubes have better dispersion in the resin resulting in higher thermal conductivity of the PNC.

All studies concluded that carbon nanotubes improve the thermal conductivity of the polymer, even when they are introduced at very small amounts without a percolation threshold, below which CNTs have no contribution vis-à-vis electrical conductivity. It increases as the CNT loading increases. However considering the SWCNTs' outstanding thermal properties (up to 3000 W/mK), the improvement in the thermal conductivity of the PNCs is moderate. There are several factors and parameters pertinent to these unexpectedly small increases in the thermal properties.

Carbon nanotubes may contain large quantities of defects depending on the synthesis methods. This means that their structure is far from the ideal rolled up hexagonal lattice. Their physical properties thus suffer from the presence of defects with thermal, electronic and mechanical properties deviating significantly from those expected for pristine nanotubes. Another problem is the level of nanotube purification, which relates to the large-scale synthesis of carbon nanotubes, limiting vastly their application. The as-produced (raw) SWCNT soot contains impurities to a significant degree. The main impurities in the soot are graphite (wrapped up) sheets, amorphous carbon, metal catalyst, and the smaller fullerenes. These impurities interfere with most of the desired properties of the SWCNTs, as described by Yu et al. [95].

It should also be pointed out that pristine, isolated SWCNTs can rarely be spotted in scanning electron microscope (SEM) images. Due to their great flexibility, high surface energy and as high as 1000 aspect ratios, SWCNT tend to aggregate into large bundles, agglomerates, and clusters when dispersed in polymers. They contain huge numbers of both metallic and semi-conducting SWCNT in a random mixture, whose properties are generally inferior to those of isolated SWCNT [60]. To disperse the CNTs in the polymer homogeneously, the entanglement of CNTs produced by the synthesis and agglomerates of the CNTs caused by the intermolecular van der Waals force must be broken. The aggregation problems have been partially solved by using magnetic stirring [100], melt mixing [101], [102], and sonication [103], [104] during the CNTs dispersion process. A detrimental effect of these methods is the reported rupture of the CNTs, caused by the local energy input, resulting in a reduction of the effective tube length [105].

Size and orientation of SWCNTs in polymers, and, especially, the interfacial properties between the polymer and the reinforcement filler also have substantial effect in the overall thermal behavior of PNC. For SWCNTs, size stands for length (L) and diameter (D), thus aspect ratio (L/D). A fundamental understanding of SWCNT-size influence on thermal conductivity of PNC is important for the development of more realistic models. This is due to the fact that carbon nanotube properties are not solely dependent on simple mean of the size parameters, but the entire nanotube length and diameter distributions. Thostenson and Chou [106] utilized MWCNT diameter statistical distribution functions, in conjunction with a micromechanics model to determine the associated elastic properties. Similar work was performed by Wang et al. [107] which used statistical

distribution of SWCNT length. In this work, multiple atomic force microscope (AFM) images were analyzed by using an image recognition software, quantifying 651 SWCNTs in total. Both studies reported that statistical variation of length and diameter, therefore aspect ratio, significantly affects the overall elastic properties of PNC. One can expect analogous behavior for thermal properties as well.

It can be clearly discerned from a recent study on SWCNT-epoxy composites, reported by Spanos and Esteva [108], [109] that interface imperfection between the matrix and reinforcement has practically no effect on the Young's modulus of PNC, especially for low CNT volume fractions. On the other hand, many researchers have attributed the unexpectedly low increase in thermal conductivity to interfacial thermal resistance at CNT-CNT and CNT-matrix interfaces [110], [111]. Huxtable et al. [112] measured the interface thermal conductance, G ($Wm^{-2}K^{-1}$) of CNTs suspended in a surfactant in water, which is the inverse of the thermal resistance, R_K (m^2K/W). Their findings indicate that heat transfer in a nanotube composite material is limited by the remarkably small interface thermal conductance, $G \approx 12$ $MWm^{-2}K^{-1}$, that corresponds to $R_K = 8.3x10^{-8}$ m^2K/W, and that the thermal conductivity of the composite is much lower than the value estimated from the intrinsic thermal conductivity of the nanotubes and their volume fraction. Wilson et al. [113] reported that magnitude of thermal resistance between nanoparticles and a variety of matrices ranges from $0.77\ x10^{-8}$ m^2K/W up to $20\ x10^{-8}$ m^2K/W. Furthermore, molecular dynamic simulations show that weak van der Walls forces acting between the nanotube and the matrix provide poor coupling, and consequently the interfacial resistance to heat flow is very significant. Thermal resistance

value of SWCNT-epoxy interface calculated by Bryning et al. [114], ranged from $2.4\pm1.3x10^{-9}$ m^2K/W to $2.6\pm1.3x10^{-8}$ m^2K/W. Their results are based on the thermal conductivity measurements for differently processed PNCs. These remarkably high values of R_K lead to effective thermal conductivity of carbon nanotubes varying from as low as 1 W/mK to as high as 100 W/mK [110].

2.2.2. Modeling Techniques

The thermal conductivity of SWCNT reinforced polymer composites is an important material property for many applications, but still widely unexplored. However, the intrinsic complexity of nanostructures evidently makes them fairly challenging to model realistically. The difficulty is mainly due to the morphology of nanotubes, to their size and orientation after mixing, to the heterogeneous distribution and bad dispersion of nanotubes in the matrix, and to CNT-matrix bonding interactions. Carefully developed realistic modeling techniques are essential for capturing all of these fundamental parameters.

In this context, it is noted that a few techniques for modeling thermal conductivity of PNCs have been reported in the literature. Nan et al. [115] modified an approach, first derived by Hasselman and Johnson [116], including interface thermal resistance by Xue [117]. Their model takes into account the nanotube length, diameter, concentration and interfacial thermal resistance, but since it is an averaging method it fails to capture either CNT distribution or dispersion. Lewis and Nielsen [118] extended the theoretical

formulation of Hamilton and Crosser [119] for heterogeneous two-phase mixtures consisting of a continuous (matrix) and a discontinuous (filler) phase. Their method is capable of incorporating the effect of particle shape, orientation, and distribution characteristics in the calculation of the thermal conductivity of the composite. Even thought the ease of use of this method makes it quite preferable, its accuracy is questionable and it falls short of considering agglomeration and dispersion of the fillers, which are SWCNTs in the case of PNCs.

Hatta and Taya [120] proposed a homogenization technique for thermal conductivity, based on Eshelby's equivalent inclusion method [121]. The method realizes multiple ellipsoidal inhomogeneities, their interaction, size and orientation with a considerably good accuracy for the case of regular composites. However, their model is only capable of incorporating two constituents; matrix and nanotube. Therefore it is a two-phase model and does not capture the agglomeration, in particular dispersion parameters.

The effect of agglomeration in Young's modulus of carbon nanotubes in PNC, which is directly associated with dispersion, was studied by Shi et al. [122]. Their two-parameter model introduces high CNT-concentrated spherical inclusions as agglomerations in the matrix which already has well dispersed individual CNTs. They can control the degree of agglomeration by changing the volume of spheres and their nanotube volume ratio. However, they define a random distribution for both the spherical inclusions and the individual CNTs, which accounts for heterogeneous dispersion but not for distribution characteristic.

To that extent, Spanos and Kontsos [123] proposed a multi scale stochastic finite element model to estimate the mechanical properties of PNCs. Based on Eshelby's two-phase homogenization model, they developed a hybrid model to account for distribution and dispersion of SWCNTs in polymers, consisting of matrix, nanotubes and agglomerates. Due to the limitations of this two-phase model, it fails to capture multi-phase composites, nevertheless. As a result, the potential of their method in modeling the properties of the multi-phase nanocomposites is questionable. The accuracy of their model is discussed later in Chapter 5.

There has been no work performed unifying these methods for solving this inhomogeneity problem in steady state heat conduction. In this dissertation, an attempt is made to determine the thermal conductivity of polymer nanocomposites (PNCs) that comprise polymer matrices reinforced with single-walled carbon nanotubes (SWCNTs). Monte Carlo simulation based finite elements method is used to capture the spatial randomness of PNCs, represented by the local nanotube volume/weight fraction as random variable. Uncertainty of dispersion is incorporated by the level of nanotube agglomeration as well as their orientation, aspect ratio and diameter. Homogenization is performed by extending the two-phase Eshelby's equivalent inclusion method to the multi-phase. This also facilitates the introduction of voids and impurities, which are inherently present in composite, into the model. Additionally, the proposed approach account for the interface thermal resistance between the SWCNT and the polymer.

Chapter 3

Identification of Spatial Randomness in PNCs

Studies reported in the literature provide evidence that the experimentally measured thermal conductivities of PNCs show unsatisfactory consistency compared to the analytically and numerically computed ones [95], [97], [124]. These disappointing results can be attributed to complex nano/micro mechanical characteristics of PNCs, such as CNT distribution, dispersion, aspect ratio, orientation, agglomeration due to van der Walls attraction and high aspect ratio, and CNT-matrix interfacial thermal resistance.

The influences of these factors on the thermal conductivity have not been yet thoroughly understood. In this contest, researches have shown that the thermal properties of polymer nanocomposites depend largely on uniform distribution and homogeneous dispersion of individual CNTs in the matrix. This is essentially attributed to the reduced behavior of the aggregated CNTs compared to the individual CNTs [125], [126]. These aggregations can also initiate voids or damage sites in PNCs, which cause degradation in their properties [127]. In addition, this nanoscale spaghetti-like entanglement of nanotubes

effectively lessens the aspect ratio of the reinforcement [128]. To achieve homogeneous dispersion of SWCNTs in the polymer is, thus, important, yet not readily achieved. Even though there exist certain processes for overcoming bad distribution and dispersion issues, their effectiveness is limited and debatable [99–103].

This dissertation makes an effort to develop a model that can reliably determine the thermal conductivity of polymer composites containing randomly distributed SWCNTs with heterogeneous dispersion. A unique feature of the proposed Monte Carlo Finite Element Approach (MCFEA) lies in the fact that instead of seeking a solution for an ideal PNC structure vis-à-vis other suggested models in the literature; the actual morphology of the SWCNTs is taken out of images.

3.1. Definition of Material Volume Element

In addressing the problem of effective (or overall, macroscopic) properties of material micro-structures, the assumption of the existence of a Representative Volume Element (RVE) is critical. RVE refers to a sample of the material that structurally has the entire characteristics of the mixture on the average. In other words, for a periodic nano/micro structure, the RVE must be a unit cell. Otherwise, it is a statistically representative of the macro response satisfying statistical homogeneity and ergodicity of the material. Furthermore, the RVE must contain a sufficient number of inclusions, which insure the independence of the effective constitutive response (e.g. elastic moduli, thermal conductivity) on the scale and boundary conditions. Consequently, the RVE must be

sufficiently large with respect to the length scale of a single heterogeneity, in which the material appears uniform and the continuum methods of analysis can be applied [129–131].

In reality, materials are not homogeneous continua but rather heterogeneous and random media, where there is no periodicity and/or uniformity in their structure. In this case, the quality of the derived results depends strictly on the size of material region (MR) chosen as the representative sample of the whole structure. To ensure Hill's condition [129] in the case of spatially disordered inclusions having no nano/micro structural periodicity, the scale of the MR must be significantly larger than the single heterogeneity size to satisfy homogenization limit, such that

$$d << L << L_{macro}, \qquad (3\text{-}1)$$

where d is the characteristic length of a nano/micro scale heterogeneity, L is mesoscale size of the MR, and L_{macro} is macroscale body size, shown in Figure 3-1. As the L/d ratio becomes significantly large, the selected mesoscale approaches to the RVE size with deterministic responses. For a finite value of L/d, however, the constitutive response of the MR shows a non-zero statistical scatter depending on the number, size, shape, orientation, dispersion and spatial distribution of the inclusion. Therefore, the amount and the volume of the inclusions in the MR can be considered as stochastic quantities, whose scatter tends to decrease to zero as the MR size is increased, and in the limit of infinite sample size, the quantity becomes deterministic.

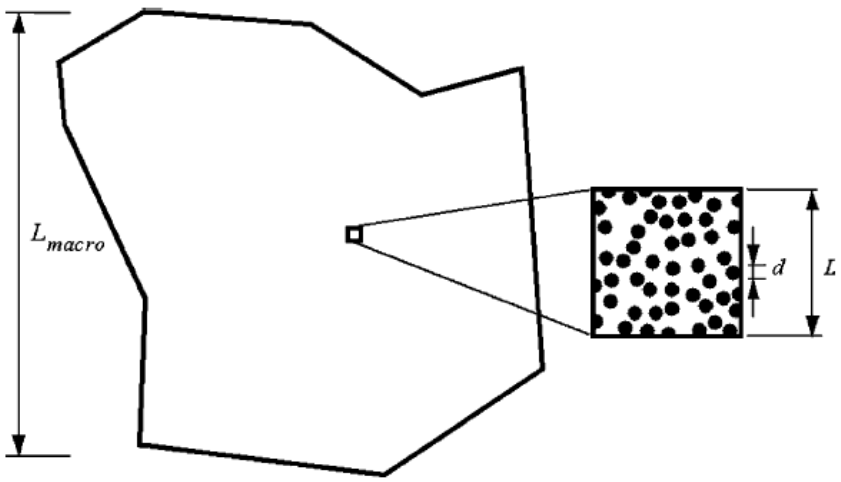

Figure 3-1. Length scales in a material with randomly distributed inclusions; size of a macroscopic body L_{macro}, size of an inclusion d, and a mesoscale window L where material properties are calculated **[131]**.

In the proposed MCFEA, the attributes of this material region can be summarized under two main objectives. First, it is a characteristic sample of the PNC under investigation, the structural morphology of which is observed and modeled. Second, the selected MR is the domain where a mathematical formulation can be developed to determine the thermal conductivity of the polymer nanocomposite.

Advanced microscopy techniques, such as SEM, are utilized to obtain representative MRs, shown in Figure 3-2. The selected MR is a portion of a cross-section of the actual macroscopic PNC. The size of the MR is equal to the size of typical microscopic images of the structures of PNC reported in the literature. Images provide direct information on morphology, dispersion and distribution of the nanotubes within the representative sample, which is then introduced in the MCFEA to investigate the thermal conductivity of polymer nanocomposites. The advantage of the proposed MR over other candidate volume elements is that it homogenizes the material structure in two different scales: the

one defined by the sub-element material structure in each finite element (FE), and the other is specified in the overall MR [132].

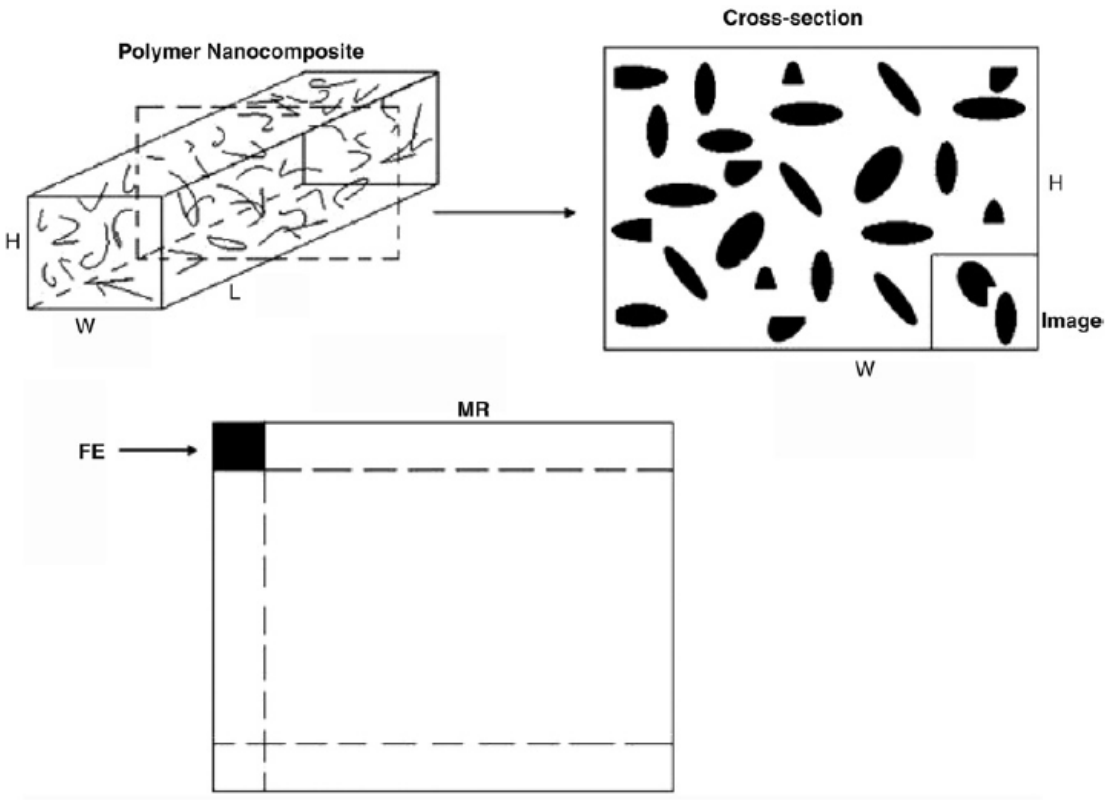

Figure 3-2. The proposed material region (MR) for determining thermal conductivity of PNC. The selected MR corresponds to a portion of a cross-section of the actual PNC and coincides with images obtained by microscopy techniques. MCFEA is then applied on the MR [132].

3.2. PNC as Heterogeneous Media

Physical properties of materials with heterogeneous microstructure (e.g. particle reinforced composites) depend on the production and fabrication procedures. Changes in factors such as orientation and volume fraction of fillers, process temperature, pressure and time, voids, impurities etc. induce variations in the effective constitutive properties of

the macroscale material. These scatter and uncertainties in the material structure and properties are considered to be random. Various actual images of nano/micro material structures are presented in Figure 3-3, verifying the randomness in geometry, orientation and distribution of inclusions in the base material. Effective use of reinforced composites and designing reliable products relies upon an accurate characterization of the inherent random nature of a heterogeneous nano/micro structure in materials. Therefore, the necessity of establishing statistical and probabilistic based models is evident. This section attempts to identify the above mentioned randomness of PNCs on nanoscale, particularly in polymer matrix filled with single-walled carbon nanotubes.

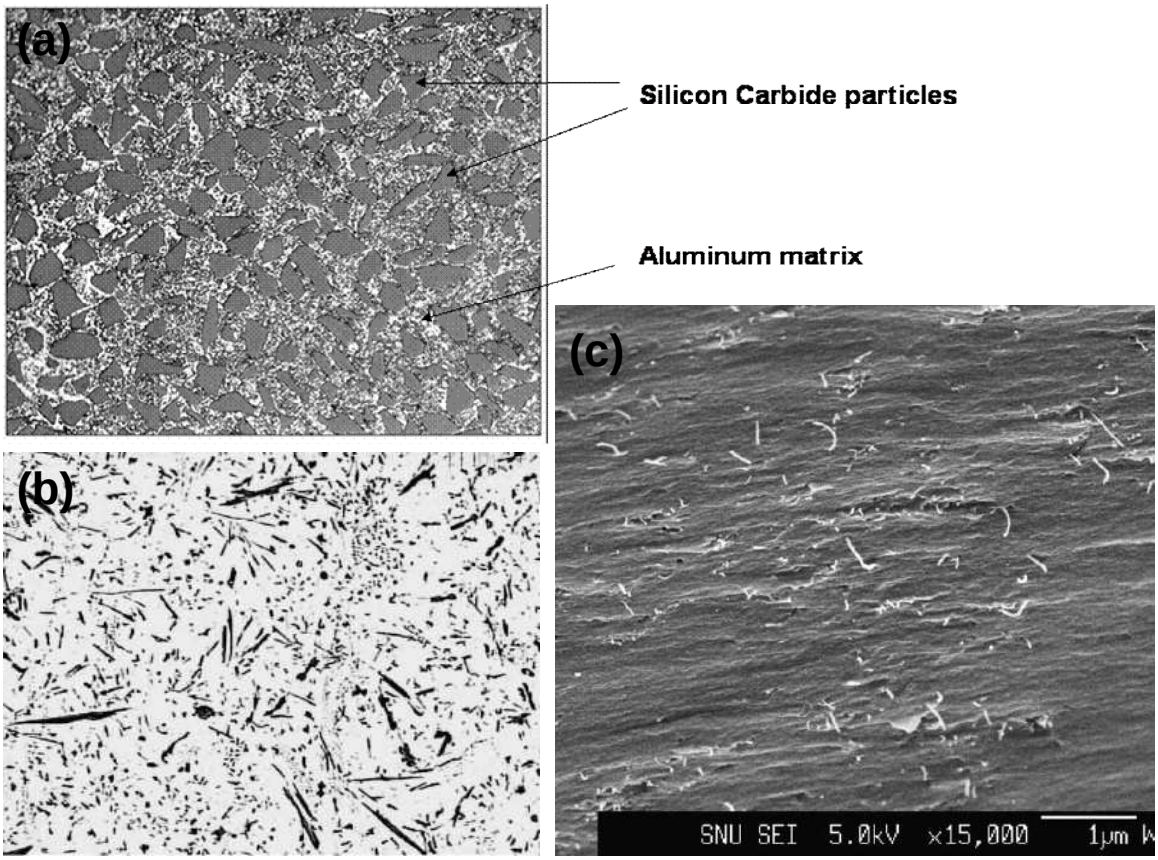

Figure 3-3. (a) Microscopic picture of Al-SiC composite **[133]**. (b) Optical microstructure of Al-2Mg alloy with 2.5 wt % FeCu **[134]**. (c) SEM image of the composite filled with carbon nanotubes **[135]**.

Spatial distribution in a polymer is important to utilize the full potential nanotube fillers. However, it is quite hard to achieve, and highly dependent on fabrication methods. Examples of such distribution are given in Figure 3-4 and Figure 3-5. The images were taken by Li and Shimizu [136]. They mixed unmodified MWCNTs with a concentration of 5 wt % in a thermoplastic elastomer (SBBS). The distribution of the CNTs was examined by optical microscopy, shown in Figure 3-4. Figure 3-5 shows SEM images of the fracture surfaces of the composites prepared with various mixing speeds. In both figures, images (a) and images (b) were produced at 300 rpm and 1000 rpm, respectively. It is seen that quality of distribution increases with higher mixing speeds.

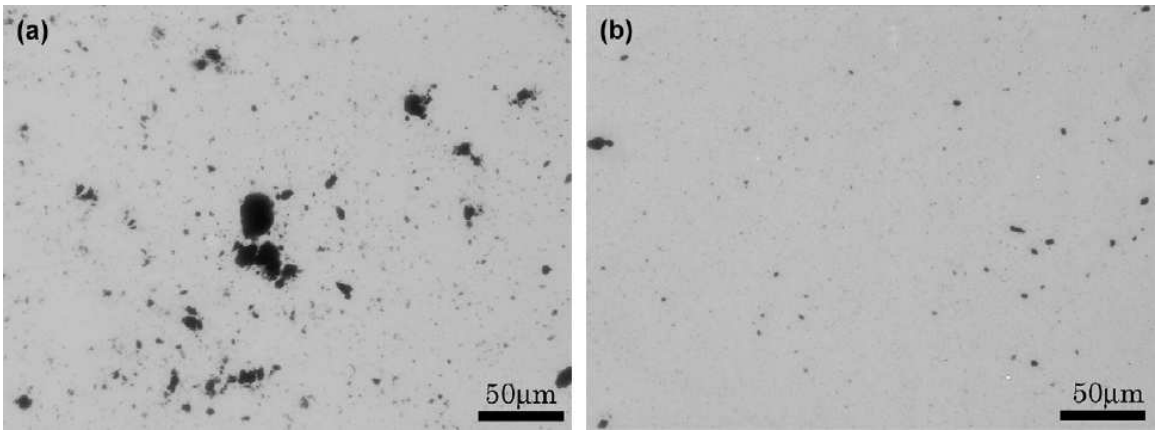

Figure 3-4. Optical micrographs of MWCNT/SBBS composites, produced at. (a) 300 rpm, (b) 1000 rpm **[136]**.

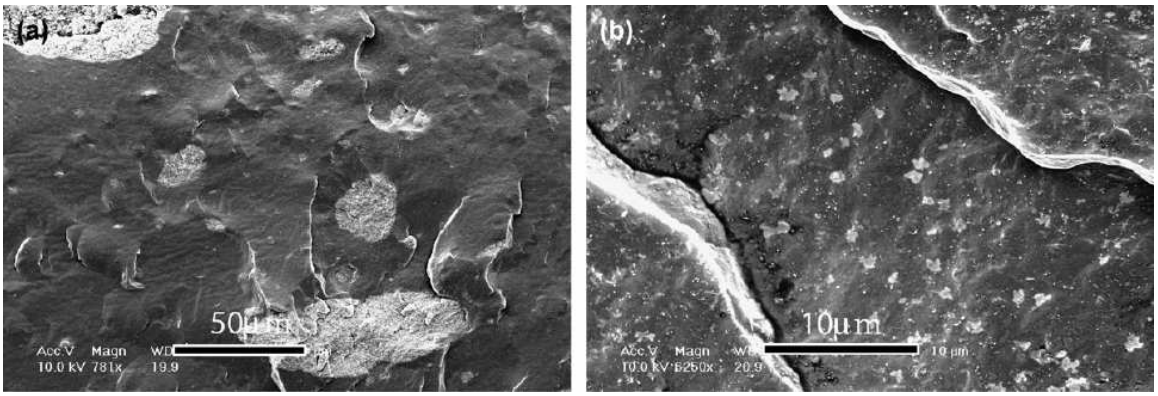

Figure 3-5. SEM images of the fracture surfaces of MWCNT/SBBS composite, produced at (a) 300 rpm, (b) 1000 rpm **[136]**.

Another challenge towards improving properties of the PNCs is achieving good and uniform nanotube dispersion. They are naturally insoluble and tend to agglomerate (or to cluster) together in the hosting matrix [137]. More importantly, they are prone to re-cluster soon after dispersed [138]. This difficulty can be attributed to various factors. One of the factors is the interaction between the nanotubes due to strong binding energy, i.e., Van der Waals forces, and their high surface areas [139]. In addition, high viscosity of the nanotube/resin mixture - as a result of nanotube addition – causes poor dispersion characteristic. It is reported in the literature that only a small amount of nanotube content in a matrix drastically increases the viscosity of the system [140]. Other aspects of the nanotube re-agglomeration may be because of the dynamic effects during curing process of the polymer nanocomposites. These effects can be listed as surface tension of the matrix [141], random movement of nanotube in the matrix [142], and static electricity of the nanotubes [143].

This dissertation considers dispersion in the form of nanotube agglomerations. A number of studies have indicated the presence of these clusters of SWCNT. Figure 3-6 (a) presents an SEM image of a PNC consisting of individual and agglomerated SWCNTs, taken by Loos et al. [144]. Seidel and Lagoudas [82] also examined the dispersion characteristics of the nanotubes. They used transmission electron microscope (TEM) to capture an image of CNT-polymer composite, shown in Figure 3-6 (b). The image shows the clustering of SWCNTs in the matrix. In both images, the nanotubes exhibit moderately good distribution, yet a poor dispersion. Li et al. [128] discovered the

existence of the SWCNT aggregates on fracture surface of a PNC, loaded with as low as one percent of nanotubes in weight.

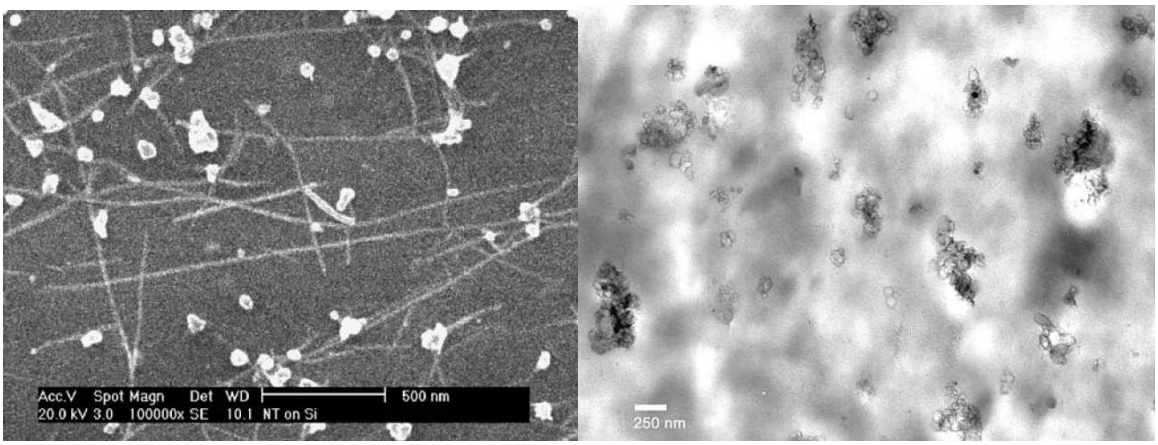

Figure 3-6. (a) Left - SEM image of SWCNTs (bright is individual or aggregate of CNTs) **[144]**. (b) Right - TEM image of SWCNTs (Dark regions are CNTs) **[82]**.

Heterogeneity in PNCs and generally in all composites also arises from the way the inclusions in the matrix are oriented. Their overall properties are vastly dependent on the nanotube orientation. In design and analysis, it is essential to control the nanotube orientation to maximize their capacity. While it is relatively effortless to fabricate PNCs with randomly oriented CNTs, it is rather challenging to produce orientation controlled PNCs. To that extent, PNCs have been fabricated in the literature with various nanotube orientations. Such production method has been developed by Park et al. [145]. They produced SWCNT reinforced polymer composites by high shear alignment. The degree of the alignment was controlled by the magnitude, frequency and the treatment time of the applied electric field.

Park et al. initially used optical microscopy for qualitative evaluation of the degree of alignment. Figure 3-7 (a) shows an optical micrograph of a SWCNT reinforced polymer

without applying an electric field. Reasonably uniform nanotube distribution is observed overall with agglomerates in few microns. CNTs are considered to be randomly oriented with no preferential alignment. On the other hand, a PNC prepared with an electric field is shown in Figure 3-7 (b). Black dots in the figure are aligned SWCNT agglomerates and bundles along the electric field direction. Similarly, individual nanotubes are also believed to be aligned.

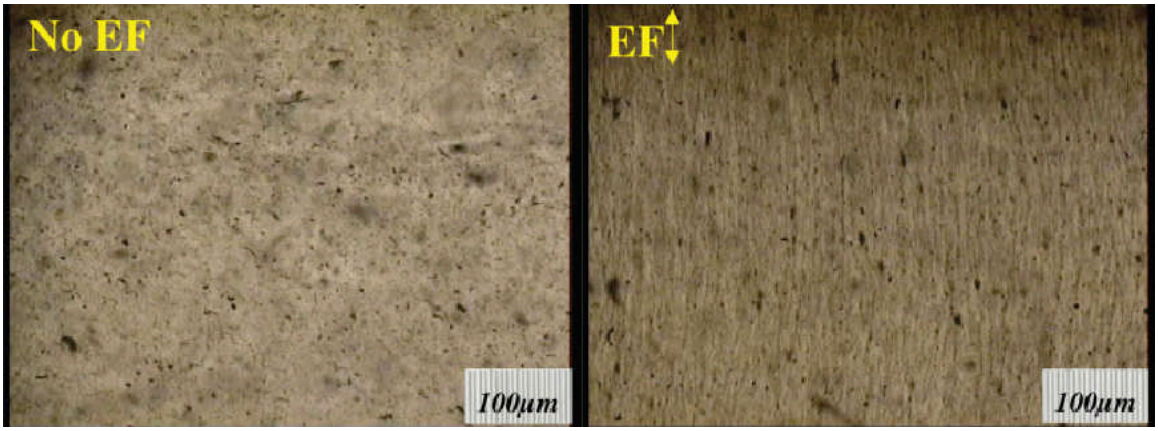

Figure 3-7. Optical micrographs of PNCs. (a) PNC cured without an electric field. CNTs are randomly oriented. (b) PNC cured with electric field. CNTs are aligned along the applied electric field **[145].**

More detailed micro-structures of the aligned SWCNTs were investigated with a high resolution scanning electron microscopy (HRSEM). Figure 3-8 (a) and (b) show the microtomed (cut for examination by microtome) surfaces of the SWCNTs aligned along the electric field, on different magnification scales. Clustered nanotubes observed in the images are aligned and are in various sizes. The images also provide evidence that the CNTs can be distributed in a heterogeneous fashion even if they are aligned.

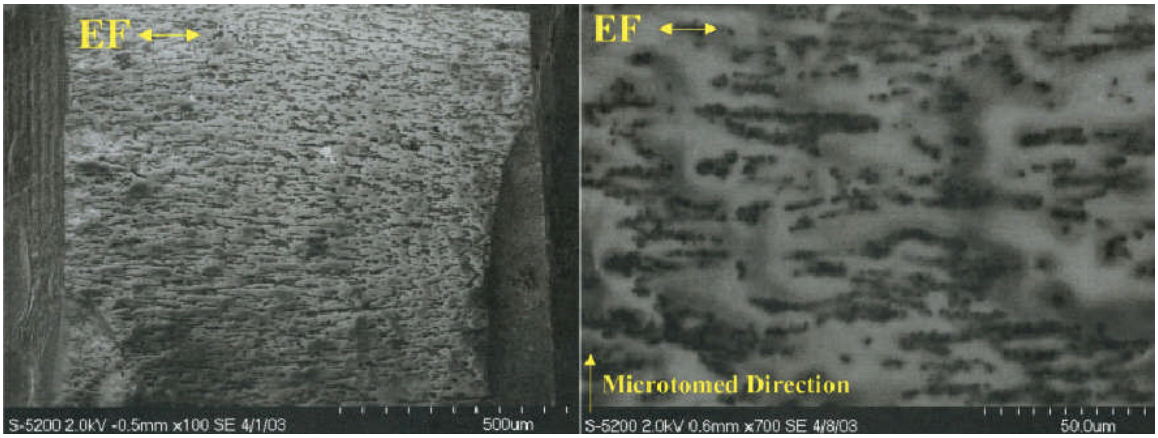

Figure 3-8. High resolution scanning electron micrographs of the aligned PNCs surfaces parallel to the electric field **[145]**.

As much as it is demanding to achieve good nanotube distribution, dispersion and alignment in polymers, it is almost impossible to reach defect free composites. Therefore, presence of voids in the final product is an unavoidable fact, causing further heterogeneity in PNCs. The voids are essentially formed due to the fabrication and processing induced defects, such as air trapping [146–148]. Existence of such voids reduces the performance of the overall nanocomposites, e.g. elastic and thermal properties [149]. The voids within composites can be found in various sizes and shapes (e.g., ellipsoidal or spherical), in the direction of the applied load or in the direction of inclusions [150], [151].

Polizos et al. [152] dispersed TiO2 nano-particles in an epoxy matrix at 3% weight concentration. The images in Figure 3-9 obtained by TEM exposed formation of nanotube agglomerates as well as existence of micro voids within the epoxy. Voids within a SWCNT-polymer composite are also observed in the work of Diez-Pascual et al. [153], shown in Figure 3-10.

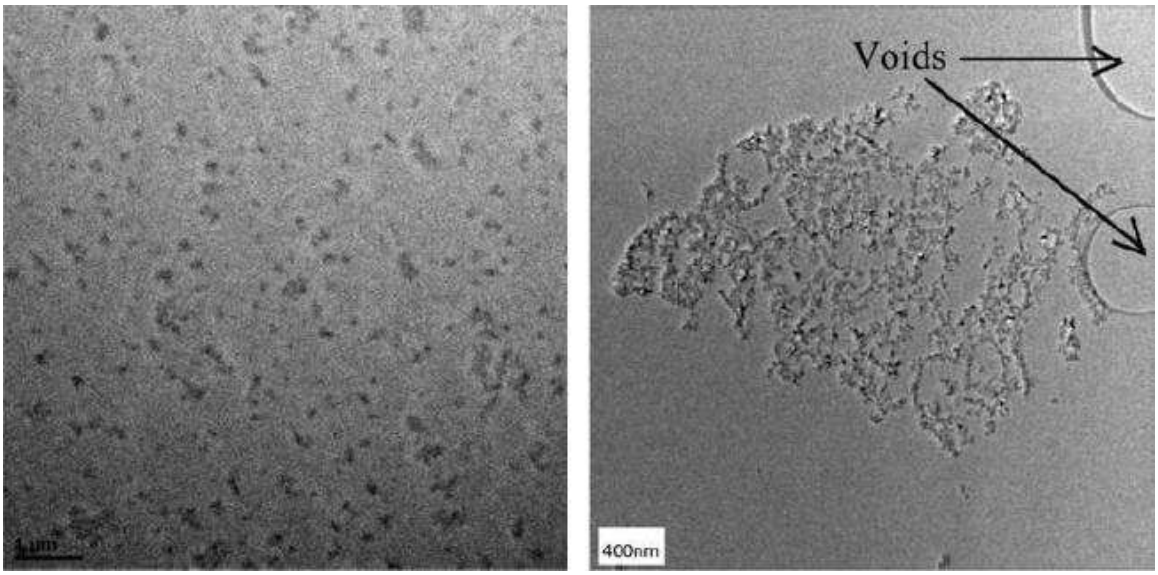

Figure 3-9. TEM images of TiO2-epoxy composites at 3 wt %at various magnifications.

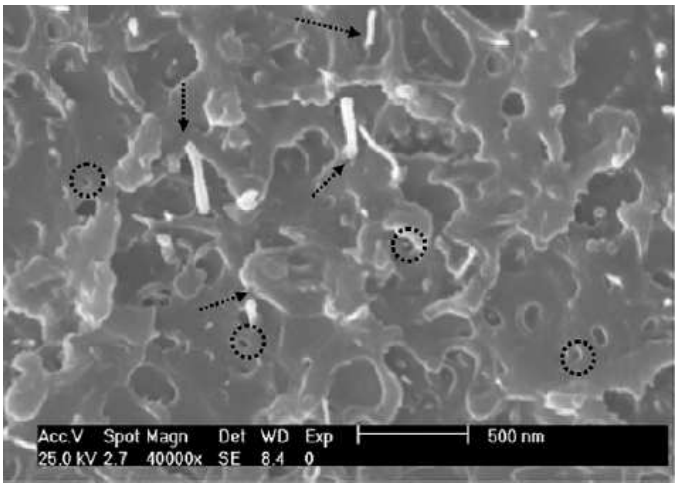

Figure 3-10. SEM image of SWCNT-polymer composite. The arrows show SWCNTs and the circles show voids.

Moreover, carbon nanotube samples include by-products and foreign particles regardless of the synthesis methods. Despite application of successful purification processes, polymer nanocomposites may still contain certain amount of impurities. These impurities contribute further to uncertainties and cause poor CNT dispersion in PNCs [95], [154]. Several examples of such impurities are named as metal catalyst particles, amorphous

carbon, buckyballs, and incomplete tubes. In the context of purification, common methods include thermal oxidation [155], acid treatment [156], ultra-sonication [157], micro-filtration [158], chromatography [159], and functionalization [160], [161]. These methods can be used in combination to achieve a higher degree of purification.

Experimentation and characterization of polymer nanocomposites (PNCs) provide evidence of the existence of heterogeneities in the PNC structure, e.g. SWCNT clusters, agglomerates, volume fraction, orientation, nano/micro voids and impurities. They induce certain spatial randomness which has not been taken into account in previous studies for determining the thermal conductivity of PNCs. The MCFEA developed in this dissertation aims to model the SWCNT distribution and dispersion in PNCs using information taken from the actual images of its nanostructure. The statistical data obtained are used to develop an appropriate random field model which is then incorporated in a finite element model.

3.3. Characterization of Randomness in PNCs

Successful application of the random field models into the proposed MCFEA depends on quantification of the spatial randomness in PNCs. In this context, the identification of SWCNT distribution, dispersion and orientation in polymer is important. Current fabrication and processing techniques can moderately ensure homogeneous distribution with almost perfectly randomly oriented SWCNTs [100–104]. However, their homogeneous dispersion in the polymer matrix is not easily achieved, and its effects on

the thermal conductivity of PNCs are unknown to a great extent. To simulate reliably the physical properties of the CNT-filled composites, it is necessary to understand the influence of CNT dispersion. It is therefore the aim of this dissertation to model the non-uniform dispersion and distribution of SWCNTs in a polymer nanocomposite using the data extracted from the actual nanostructure images, which is then used to define appropriate random field models.

Morphology and characterization studies of SWCNTs in PNCs reveal that the deficiency in spatial dispersion is caused by clustering, agglomeration, and bundling of SWCNTs due to their high aspect ratios and surface energies. On the other hand, the degree of distribution is considered to be solely dependent on the fabrication of PNCs. Analyses of actual images also exhibit similar visualization. Figure 3-11 (a) is an SEM image of SWCNTs in epoxy matrix, where the individual and entangled SWCNTs can clearly be identified, representing both poor distribution and poor dispersion [162]. Figure 3-11 (b) provides evidence of a good distribution and of a relatively better dispersion; such that the agglomerations of SWCNTs can, nonetheless, be detected in the polymer. One can notice the random local volume fractions and concentrations, resulting from the poor nanotube distribution, along with CNT clustering. Good-poor distribution and dispersion are represented by the constructed sketches shown in Figure 3-12.

The variations of the SWCNT volume fraction throughout the nanostructure affect the local material properties, and thus overall thermal behavior of PNCs [99], [163]. The proposed approach in this dissertation uses statistical information obtained via actual

images of random material fields. It is then used to generate random values of volume fraction which are assigned to the finite elements in the material region (MR) selected. Obviously, it is necessary to quantify this spatial distribution and dispersion of SWCNTs in the polymer.

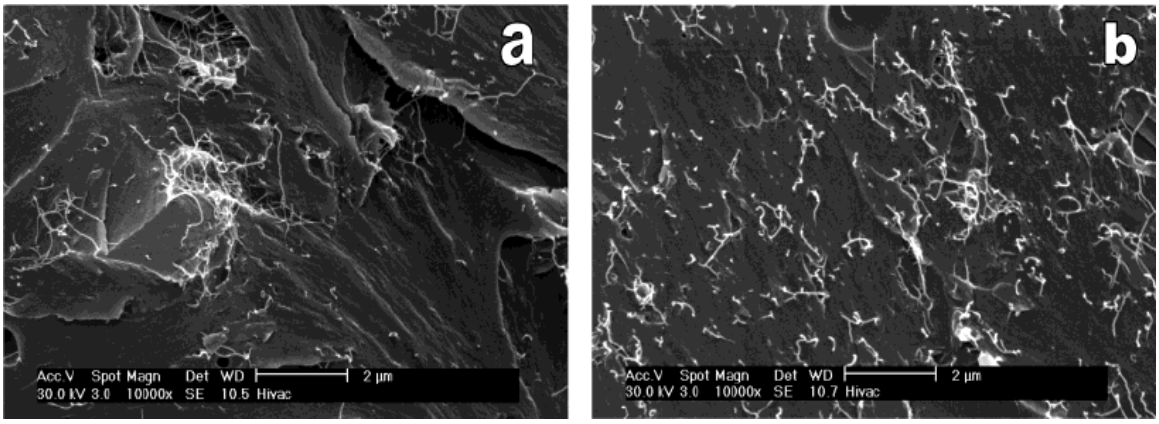

Figure 3-11. SEM images of PNC with 1 wt % SWCNT dispersed in epoxy, (a) poor distribution and poor dispersion, (b) good distribution and poor dispersion **[162]**.

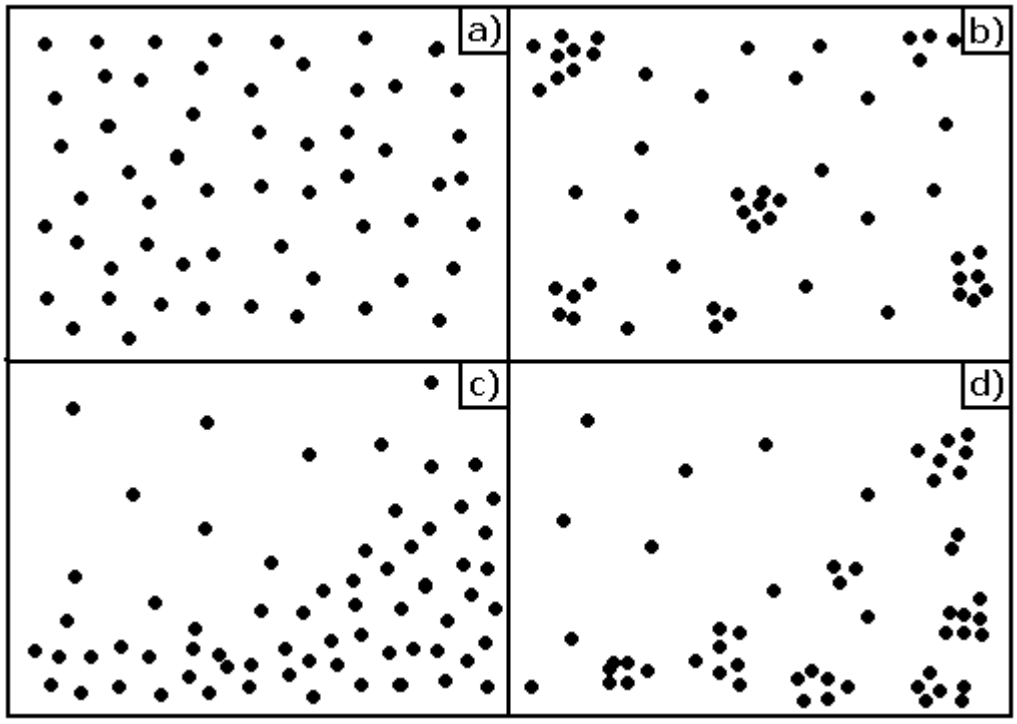

Figure 3-12. (a) Good distribution, good dispersion. (b) Good distribution, poor dispersion. (c) Poor distribution, good dispersion. (d) Poor distribution, poor dispersion.

Several studies have been performed on quantification and characterization of carbon nanotubes in a matrix. To this end, Ziegler et al. [164] conducted an analysis, identifying the length and size of over a thousand nanotubes. High quality AFM images were taken and the nanotubes were measured using the nanotube length analysis package of SIMAGIS® software (Figure 3-19). The program is capable of recognizing the SWCNTs in the image and tracing their lengths, simultaneously obtaining an average height as well. Histograms of individual and roped SWCNT length and diameter, and those of particle diameter were created, with appropriate distribution functions fitted. Taking advantage of their results, one can readily quantify the nanotube volume ratio locally and globally. Practical applications of this technique are presented in Section 3.4.

Traditional methods for characterization of composites with random heterogeneous nano/micro structures employ a homogenization or effective properties approach, and assume that the pertinent parameters are constant. These assumptions can be valid for bulk behavior of composite materials, yielding solely average or approximate values of the responses (e.g. stress, temperature). However, to capture the heterogeneous nano/micro structures in detail and to accurately simulate the physical behavior of the composites, one must account for the variations in the system parameters, such as inclusion distribution, dispersion as agglomeration, aspect ratio, orientation and voids.

Several research studies have incorporated the uncertainties into the properties and structures of composite materials. Fukunaga et al. [165] estimated the ultimate strength of hybrid laminates, taking into account the effect of scatter in lamina strength, relative fiber

volume fraction and stacking sequence. Engelstad and Reddy [166] studied metal matrix composites with various probabilistic distributions of constituent properties using Monte Carlo simulations. Smith [167] derived a formulation to approximate the failure probability in 2D composite material with randomly spaced fibers. Roberts and Knackstedt [168] developed rigorous bounds for effective properties of sample random fields, based on statistical correlation functions. Povirk [169] employed a finite element method to predict effective elastic properties of the composite, adopting representative volume elements for periodic microstructures that are statistically similar to more complex random microstructure.

Another approach to investigate the performance of nano/micro structures was proposed by Baxter and Graham [170]. Due to the inherent randomness in composite microstructure, the characterization required a significant amount of effort. In their method, instead of attempting to reconstruct and to describe a specific random microstructure, the material property field is associated with images of the real structures. Simulation of the material response was performed directly from this material property field. Digital images of the composite were obtained via computer aided tomography (CAT) scans which give detailed descriptions of the microstructure. Converting the CAT images into numeric data produced 2D material property fields (Figure 3-13). A local micromechanical analysis in conjunction with the moving window technique was then carried out to predict the material properties of small areas of images, generating spatially varying material property fields. Rather than characterizing the statistics of the microstructure, statistics can be numerically generated on these property fields, resulting

in generalizations potentially valid for classes of microstructure. The presence of a digital record nano/micro structure eliminates the requirement of a priori assumptions regarding random material properties.

The methodology was extended to three dimensions by Baxter et al. [171]. Furthermore, material property fields can be consistently developed from digital images of real microstructures and can be introduced into finite element models using regular grids. Their statistical characterization can provide the basis for simulations of additional material samples. In Figure 3-13 (a), a sample composite microstructure is shown, which was generated numerically by placing circular fibers randomly in 2D space following a uniform distribution. Figure 3-13 (b) shows a finite element model constructed for the sample microstructure shown in Figure 3-13 (a) [172]. It can be argued that the simulation is comparable to the actual image shown in Figure 3-3 (a). Three sequences of uniformly distributed random numbers were generated to simulate a digitized image of a particulate microstructure which is demonstrated in Figure 3-14 [171].

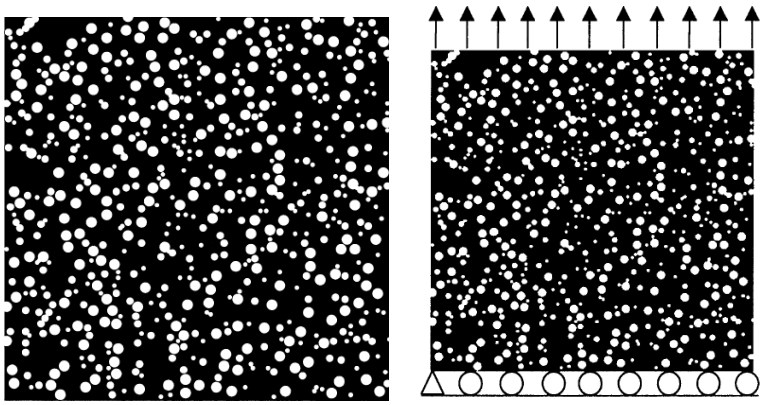

Figure 3-13. (a) Left – Cross section of a numerically generated unidirectional composite microstructure (white areas are fibers, dark represents matrix). (b) Right – Sample loading and boundary conditions on finite element model **[172]**.

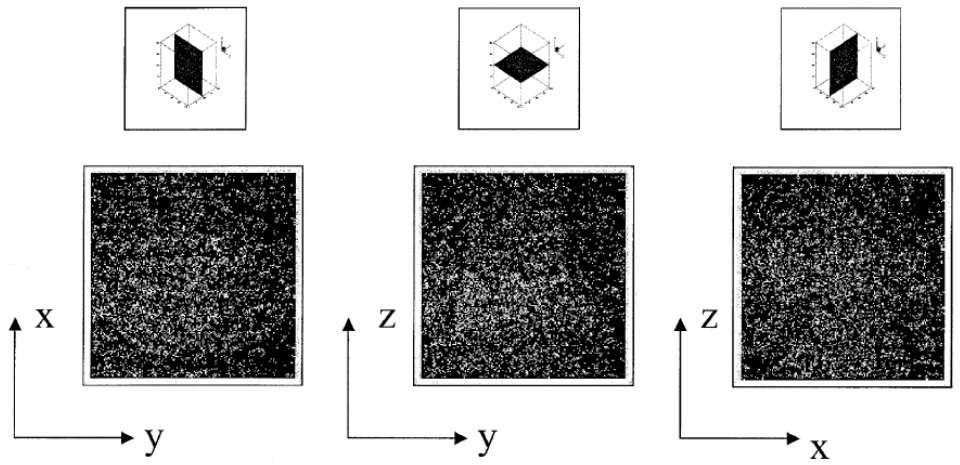

Figure 3-14. Orthogonal cross-sections of simulated microstructure. Black is aluminum matrix, white dots correspond to silicon carbide particles **[171]**.

Kashiwagi and his co-workers [163] followed a rather unique approach for characterization of nanotube dispersion. They prepared 0.5 wt % SWCNT filled PMMA samples. PMMA, (poly methyl methacrylate) is a light weight and shatter resistant transparent thermoplastic also known as Plexiglass^{TM}. The distribution of the SWCNTs in PNC was examined by optical microscopy to capture the global dispersion of the nanotubes, (Figure 3-15, Main Image). A laser scanning confocal microscope (SCM) was used to image the SWCNTs in the PMMA matrix over 100 images to obtain spatial statistics. Then, the same authors [173] reconstructed three-dimensional images using the data obtained (Figure 3-15 a-d). The optical images revealed regions of nanotube aggregation; the darker the region, the more nanotubes it contains. Figure 3-15 (a)-(d) were reconstructed with the same SWCNT content, but with different dispersion characteristics. These images show SWNT bundles and agglomerates; transparent areas correspond to the polymer. Figure 3-15 (d) shows the highest agglomeration ratio with numerous large agglomerates. It can be clearly deduced from their analysis that the amount of agglomeration increases as the nanotube content increases. The proposed

MCFEA takes advantage of this fact in Chapter 5, incorporating the SWCNT agglomerations in the determination of the overall thermal conductivity of PNC.

Similarly, the assessment of the voids and impurities existing in a PNC requires the knowledge of their overall volume fraction and size distribution. In this context, image analysis [164], ultrasonic c-scan [174], radiography [175] and optical microscopy [176] are amongst the available methods for the measurement of the void and impurity characteristics of the nanocomposites.

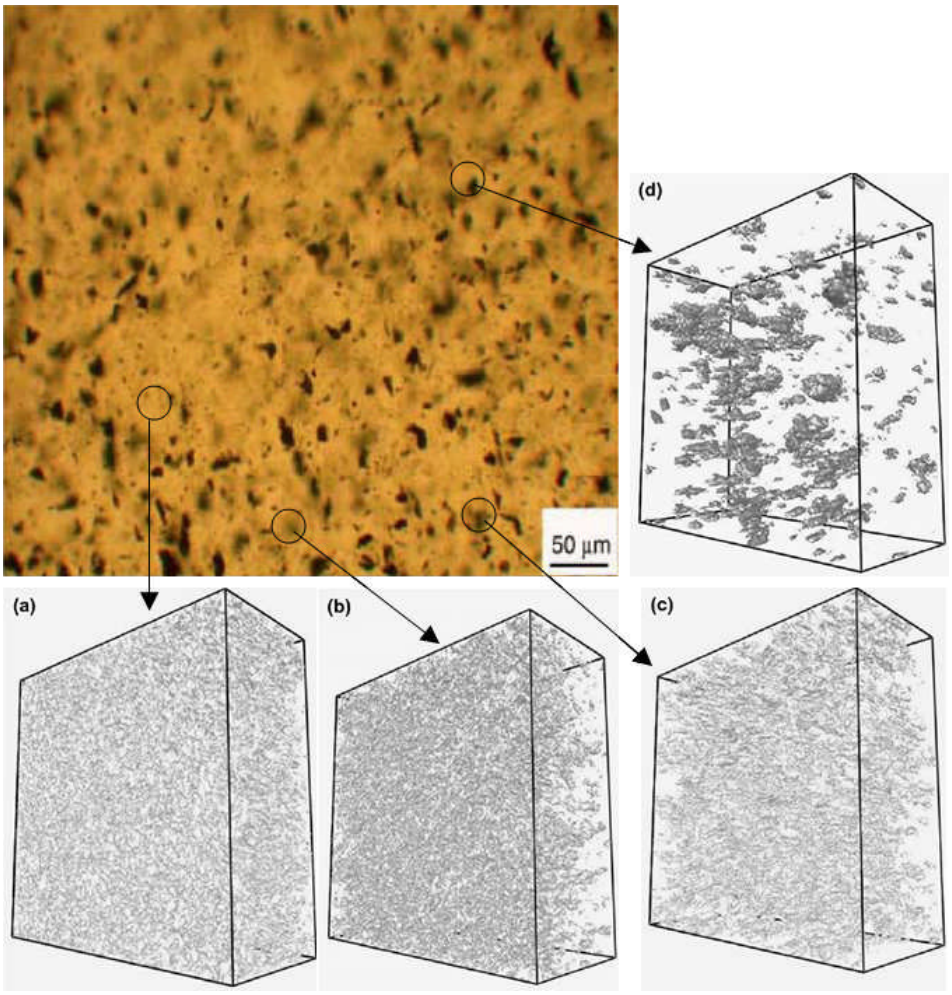

Figure 3-15. Main Image; Optical micrograph of 0.5 wt % SWCNT filled PMMA. Images (a) to (d); 3D reconstructed images of SWCNT-PMMA composite with increasing nanotube dispersion. Reconstructed from **[163]**, **[173]**.

As it can be seen in Figure 3-15, the carbon nanotubes are found to be distributed and dispersed in a rather random fashion, which causes random variation in local nanotube concentrations. The MCFEA developed in this dissertation is based on such local non-uniform SWCNT contents in the polymer, which result in variations in local thermal conductivity of the nanocomposite. Spatial statistics of the nanotube contents are then generated and assigned randomly to the finite elements (FEs).

A material region (MR) is assumed to represent the whole PNC (e.g., Figure 3-16-left shows an optical image of a PNC in micro-scale). The MR is then divided into FEs (Figure 3-16-right), where each FE represents the nano-scale formation (e.g., Figure 3-6-left, SEM image of a PNC). The following chapters delineate how the local SWCNT volume fractions are quantified and how the local and the overall thermal conductivities are computed based on the statistical information obtained from the image analyses.

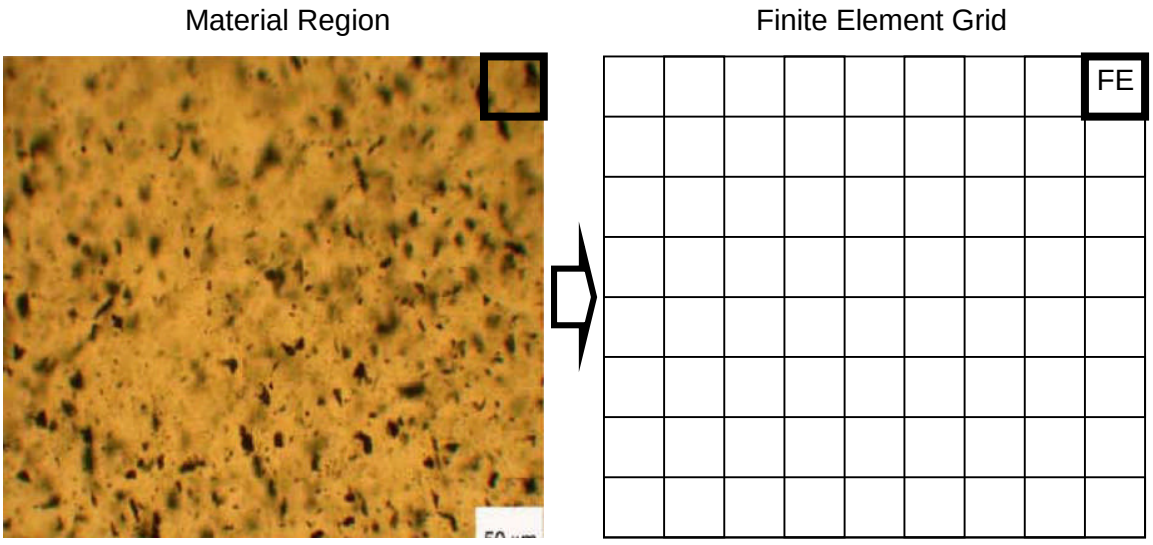

Figure 3-16. Local SWCNT concentrations in the actual image of a PNC, selected as material region, are assigned randomly to finite elements.

3.4. Statistical Representation of CNT Length and Diameter Distribution

It has been discussed in Section 3.3 that the spatial distribution of the SWCNTs, i.e., volume fraction, has a great influence on the thermal properties of PNCs. Statistical representation of such random nanostructures can then be established from the experimental images. Analyses from the actual images also report that nanotubes in a polymer exist in varying length and diameters as a result of CNT synthesis and PNC manufacturing [107], [144], [164], [177]. It is, therefore, necessary to have a quantitative description of the statistical information on the shape and size of SWCNTs, and to incorporate this data into the nanocomposite modeling.

To this extent, Wang et al. [107] made an attempt for accurate measurement and statistical characterization of the nanotube lengths. They quantified a large population of nanotubes dispersed in water. The Atomic Force Microscope (AFM) was used to image SWCNT dispersion, and the lengths were automatically traced and measured with the aid of the SIMAGIS® software package, shown in Figure 3-17. The quantified nanotube lengths extracted from the software analysis were plotted into a histogram, and an appropriate statistical distribution was fitted. They found that the histogram can be represented best with a Weibull distribution. Figure 3-18 shows the length histogram obtained from the measurement of 651 SWCNTs. In this regard, to demonstrate the reproducibility of such statistical data numerically, this dissertation applies a Weibull fitting with the shape and scale parameters, L=2.4 and k=162, respectively.

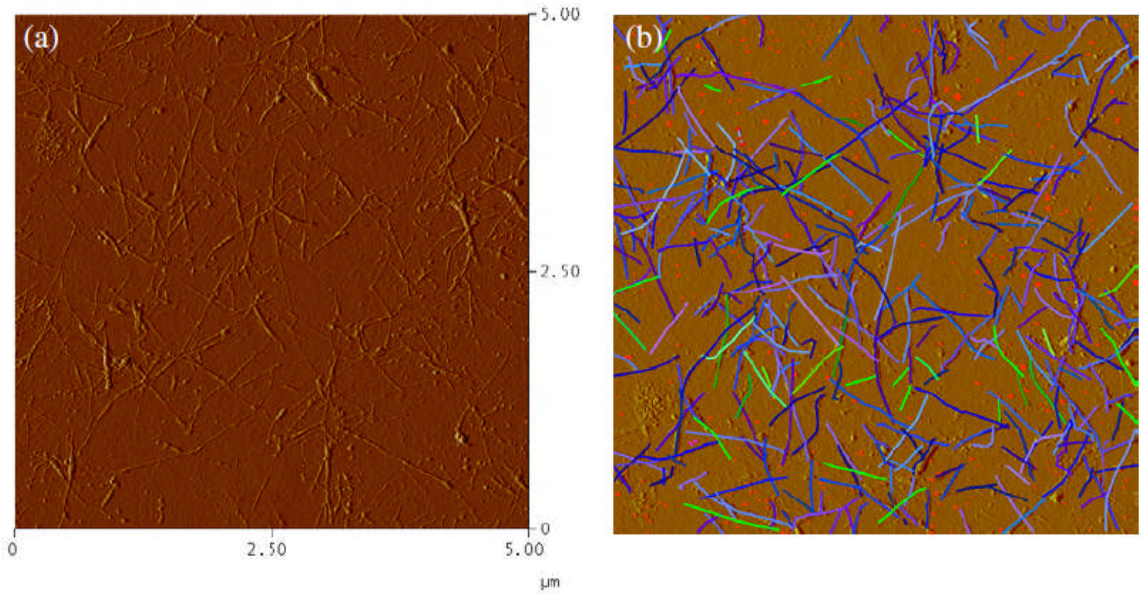

Figure 3-17. Measurement of SWCNT lengths. (a) AFM image. (b) Identified SWCNTs via SIMAGIS software **[107]**.

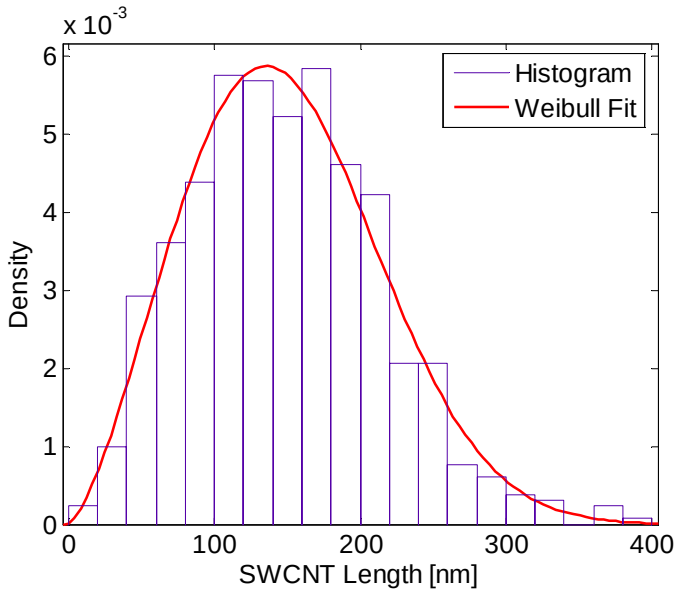

Figure 3-18. Reproduced histogram of dispersed SWCNT lengths with Weibull distribution fit.

A more extensive study was performed by Ziegler et al. [164]. They adopted an identical approach to analyze not only the nanotube lengths but the nanotube diameters, as well. Statistically accurate length and diameter measurements of nanotubes were acquired by

the SIMAGIS® image analysis program (Figure 3-19). After characterization of multiple AFM images of numerous samples, the nanotubes with lengths between 30 and 750 nanometers (nm), and with diameters between 0.5 and 2 nm were considered to be individual SWCNTs. Histogram of these individual SWCNT lengths was plotted, and fitted with a lognormal distribution with a mean of 170 nm and a standard deviation of 118 nm, as demonstrated in Figure 3-20 (a) [164]. Using this statistical information provided by these authors, a compatible histogram is numerically regenerated in this dissertation, conforming with the actual data. The MATLAB module *dfittool* was utilized to corroborate that the reproduced data in fact belong to a lognormal distribution, as shown in Figure 3-20 (b).

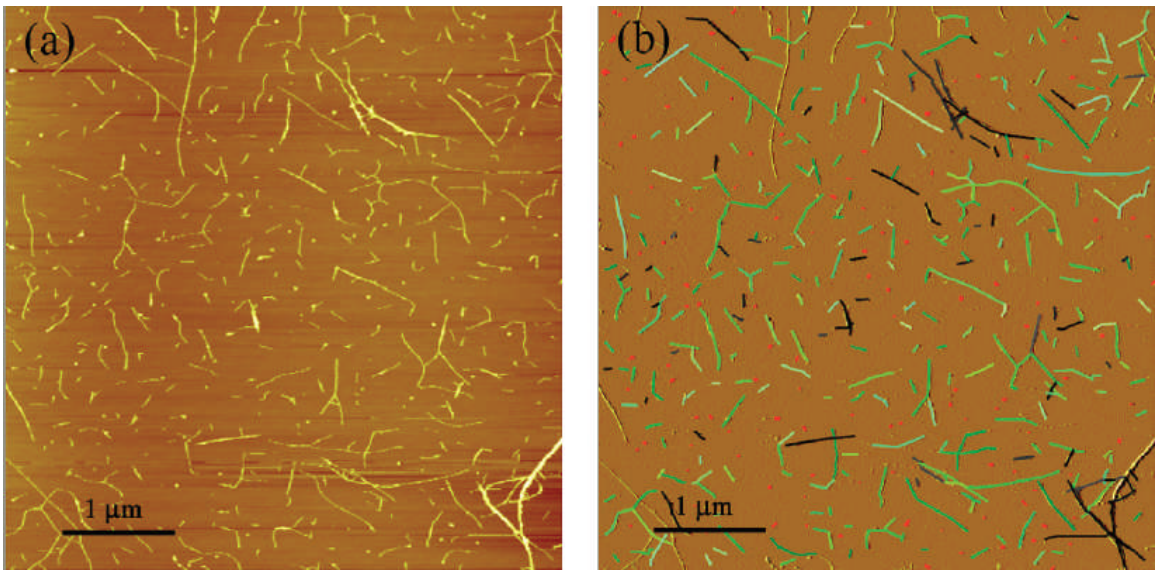

Figure 3-19. (a) AFM image of CNTs dispersed on a mica substrate. (b) CNTs measured by SIMAGIS image analyzer. Individual nanotubes are designated by a green color while the nanotube ropes are shown in black. Particles are also shown in red [164].

It is noted that, Ziegler and his co-workers provided a histogram regarding the SWCNT diameters, but no curve fitting (Figure 3-21 (a)). It is thus necessary to acquire the statistical distribution representing the diameter data to incorporate this information in the

proposed MCFEA. To this end, in Figure 3-21 (b) a diameter histogram is generated and fed into MATLAB. Employing the *dfittool* module, the lognormal distribution is selected to fit best the actual diameter data, which has a mean of 1.09 nm and a standard deviation of 0.3755.

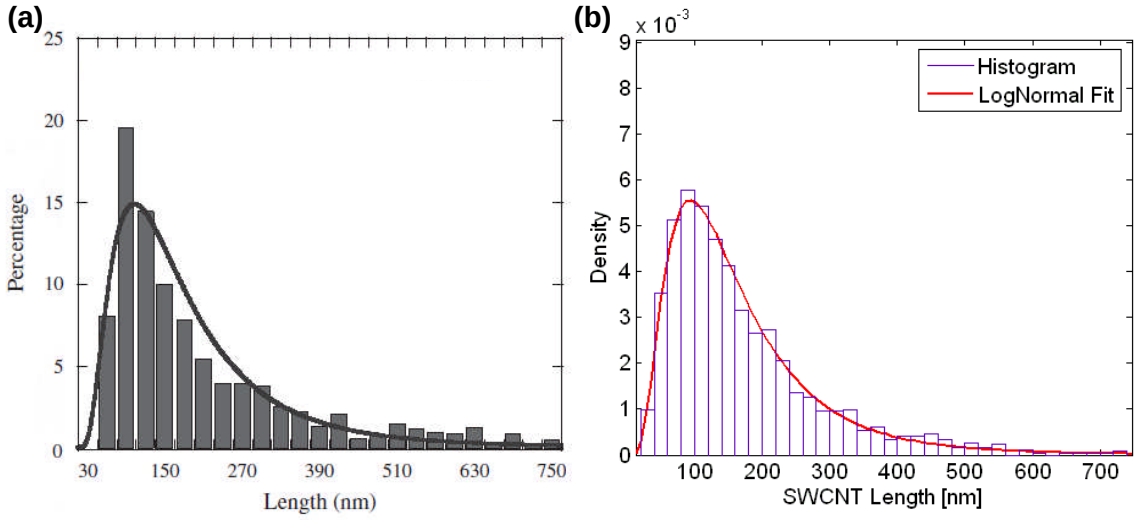

Figure 3-20. (a) Actual histogram of SWCNT lengths obtained from the AFM image shown in Figure 3-19 and lognormal fit **[164]**. (b)Digitally generated histogram of SWCNT lengths compared to the reported PDF.

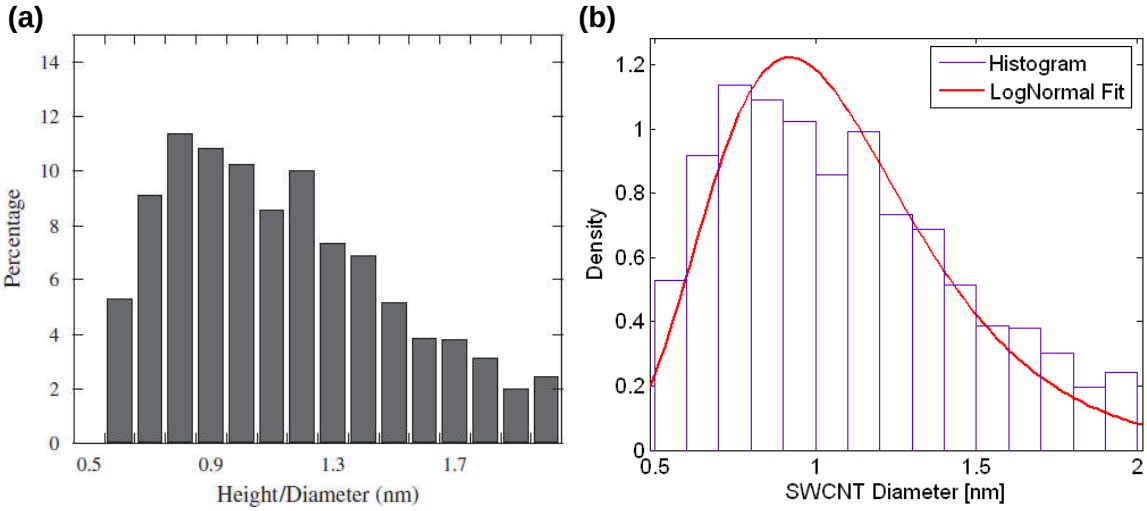

Figure 3-21. (a) Actual histogram of SWCNT diameters obtained from the AFM image shown in Figure 3-19 **[164]**. (b) Digitally generated histogram of SWCNT diameters and lognormal distribution fit.

The approach developed herein for determining the thermal conductivity of PNCs employs the Monte Carlo (MC) approach to integrate the randomness of inclusions. In this context, repetitive and consistent generation of random numbers is critical for producing realizations for the MC method. Random numbers defined as a random variable (RV) are numerically generated based on a specified statistical distribution, which is described in terms of the probability density function (PDF). The desired PDF of an RV can be produced from the inverse of its corresponding cumulative distribution function (CDF), which is called the inverse-transform method [178]. However, one must note that the inverse of CDF must be available for the utilization of the inverse-transform method.

After deciding on the PDF ($f(x)$) of the random variable, its corresponding CDF ($F(x)$) and the inverse of the CDF ($F^{-1}(x)$) is obtained. Given a random number u_i, drawn from the uniform distribution in the interval (0, 1), the target random number can be generated as $x_i = F^{-1}(u_i)$. For instance, to incorporate the SWCNT diameter distribution given in Figure 3-21 (b) into the proposed MCFEA, one must be able to generate random values of diameter that belong to a lognormal distribution. The PDF of a lognormal random variable *x* is given by the equation

$$f(x) = \frac{1}{x\sigma\sqrt{2\pi}} e^{-\frac{(\ln x - \mu)^2}{2\sigma^2}}, \qquad (3\text{-}2)$$

where μ and σ are the mean and standard deviation of the variable's natural logarithm, respectively. Clearly, the logarithm of the variable is normally distributed.

Integration of the PDF gives the CDF and takes the form

$$F(x) = \frac{1}{2} + \frac{1}{2} erf\left[\frac{\ln x - \mu}{\sigma\sqrt{2}}\right], \quad (3\text{-}3)$$

where *erf* is the error function, defined as

$$erf(x) = \frac{2}{\sqrt{\pi}} \int_0^x e^{-t^2} dt. \quad (3\text{-}4)$$

In equation (3-3), μ and σ can be obtained from the relationships of the expected value (mean), and the variance (square of standard deviation), of a lognormally distributed variable, *X*. Specifically,

$$E(X) = e^{\mu + \sigma^2/2}, \quad (3\text{-}5)$$

and

$$Var(X) = (e^{\sigma^2} - 1)e^{2\mu + \sigma^2}. \quad (3\text{-}6)$$

Furthermore, the expression for the random variable *x* can be given in terms of a uniformly distributed random variable *u* as

$$x = e^{\mu + \sigma\sqrt{2}\, erf^{-1}(2u-1)}. \quad (3\text{-}7)$$

Chapter 4

Monte Carlo Finite Element Approach

Large aspect ratios of single-walled carbon nanotubes (SWCNTs) in combination with their atomically smooth surfaces cause them to form agglomerates, bundles, and clusters in polymers during manufacturing of the polymer nanocomposites (PNCs) as discussed in Chapter 3. These entanglements and mixing procedure result in poor dispersion and distribution of SWCNTs within the matrix, which turn PNC into heterogeneous random media. Chapter 3 also discusses how such randomness at the nanoscale can be quantified and fed into the proposed Monte Carlo Finite Element Approach (MCFEA) to determine the thermal conductivity of PNCs at microscale. This dissertation relies on a homogenization technique to address the challenges in transition from the nanoscale to the microscale.

In this context, a micromechanics approach is adopted to model the effective thermal conductivity of CNT-reinforced composites. Specifically, the actual heterogeneous material structure, which consists of multiple phases, is replaced by an equivalent

homogeneous one with appropriate properties. The property of a composite calculated by homogenization is called the effective property, to distinguish it from those of the reinforcing fillers and that of the matrix. This MCFEA approximates the SWCNTs as ellipsoidal inclusions and computes the values for the local thermal conductivity of PNC at microscale with the equivalent inclusion method. Thus, these local values are introduced into the Monte Carlo finite element scheme to determine the overall effective thermal conductivity of the polymer nanocomposite. In the micromechanics modeling it is assumed that SWCNTs are straight with certain aspect ratios and with no defects. PNC contains merely SWCNTs without any residual particles created in nanotube synthesis. Perfect contact between the constituents is also assumed.

The analytical micromechanics technique is based on the modified Eshelby's equivalent inclusion method, first developed by Hatta and Taya [120], [179]. The essence of this modified method is that the domain includes an infinite number of ellipsoidal inhomogeneities and takes into account the interaction between them. In the adopted approach, the matrix is taken to contain randomly distributed individual SWCNTs as ellipsoidal inclusions with certain aspect ratios. The effects of the random distribution of SWCNTs due to nanotube characteristics, matrix-nanotube interaction and fabrication procedures on the thermal conductivity of PNC can then be determined.

This chapter of this dissertation presents the Monte Carlo Finite Element Approach (MCFEA) developed in the previous work for determining the thermal conductivity of polymer nanocomposites (PNCs). The PNCs considered here are composed of a polymer

with poor conductivity and single-walled carbon nanotubes (SWCNTs) as reinforcing fillers. Various models and techniques are utilized in the pursuit of capturing the thermal conductivity of PNC as realistic as possible, ranging from the nanoscale to the microscale.

4.1. Equivalent Inclusion Method for Thermal Conductivity

The analytical model described in this section is used to predict the effective thermal conductivity of a composite containing a matrix and a single ellipsoidal inhomogeneity, first developed by Eshelby [121] and known as Eshelby's equivalent inclusion method, then extended by Hatta and Taya to heat conduction problems [120].

Consider a single ellipsoidal inhomogeneity (domain Ω) with thermal conductivity $K^f \delta_{ij}$ embedded in an infinite homogeneous body D with thermal conductivity $K^m \delta_{ij}$ under uniform heat flux q_i^0 applied at far field as shown in Figure 4-1 (a), where δ_{ij} is the Kronecker's delta. Both the fiber and the matrix are assumed to be isotropic and perfectly bonded. Since the inclusion and the matrix have different thermal conductivities, the heat flux in the neighborhood of the inclusion becomes distorted.

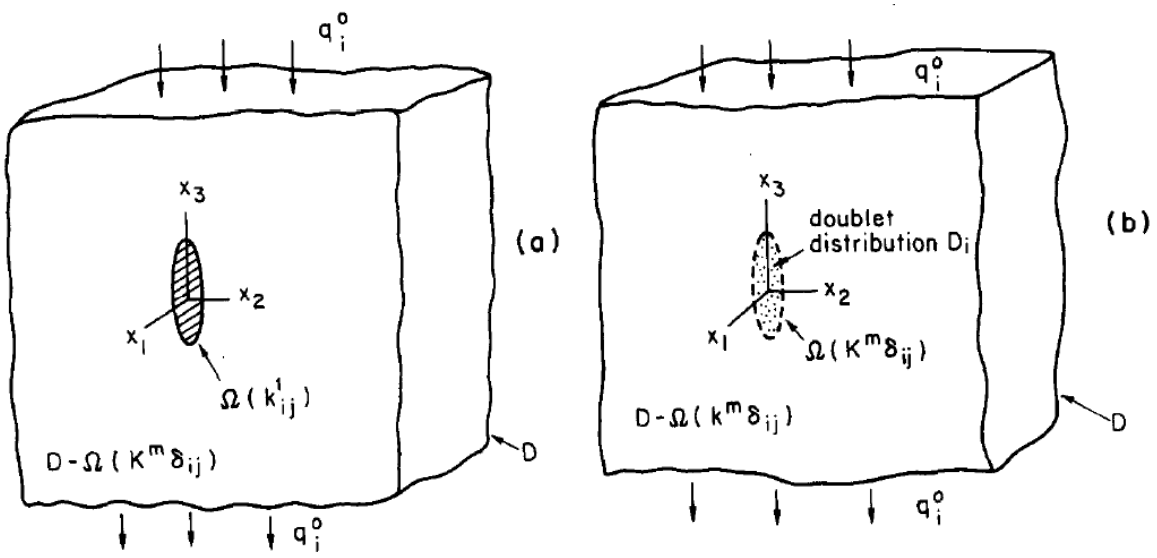

Figure 4-1. Theoretical Model. (a) Actual heterogeneous composite body D with a matrix and an ellipsoidal inclusion phase. (b) Homogenization of (a) by equivalent inclusion method [180].

Homogenization is done by introducing an equivalent inclusion Ω which has the same thermal conductivity as that of the matrix and a uniform doublet distribution of strength D_i as illustrated in Figure 4-1 (b), so that the total domain is treated as a homogeneous material. The equivalence between the actual inhomogeneity and fictitious equivalent inclusion in domain Ω, then, can be expressed in the form

$$K^f \delta_{ij}(T,_j^0 + T,_j^c) = K^m \delta_{ij}(T,_j^0 + T,_j^c - T,_j^*), \qquad (4\text{-}1)$$

where the comma followed by j denotes partial spatial derivative $\partial / \partial x_j$, the left-hand side equation represents the heat flux of the actual inhomogeneity (Figure 4-1 (a)) and the right-hand side is for the equivalent inclusion (Figure 4-1 (b)). The symbol $T,_j^0$ denotes the uniform thermal gradient, and is related to the far-field applied heat flux, q_i^0, by the equation

$$T,_i^0 = -q_i^0 / K^m \,. \qquad (4\text{-}2)$$

In equation (4-1), $T,_j^c$ is the constrained thermal gradient disturbed by the existence of the inhomogeneity. $T,_j^*$ is the transformation thermal gradient, known as "eigen thermal gradient" introduced by Lai [181]. The quantity $T,_j^*$, is proportional to the strength of the uniformly distributed doublet, has a constant value within domain Ω, but is zero outside. Analogous to well known Eshelby's elasticity problem [121], in the case that the matrix is infinitely extended and contains a single inclusion which has an ellipsoidal shape, the relation between $T,_j^c$ and $T,_j^*$ is expressed as

$$T,_j^c = S_{ij}\, T,_j^*, \qquad (4\text{-}3)$$

where S_{ij} is called "*S*" tensor and dependent solely on the shape of the ellipsoidal inhomogeneity, analogous to the Eshelby's tensor. Explicit expressions of S_{ij} for certain shapes of inclusions are given in references [180], [182].

When multiple ellipsoidal inhomogeneities are present in the body, the interaction among them becomes important. In this section, the formulation in the previous section for single inclusion is extended to multiple inclusions with thermal conductivities $K^f \delta_{ij}$ in a matrix (D - Ω) of conductivity $K^m \delta_{ij}$, under constant heat flux q_i^0 (Figure 4-2(a)). Again, they are assumed to be perfectly bonded and isotropic. To take into account the interaction among fillers, the average disturbance of the temperature gradient in the

matrix (so called “interaction term”) due to the presence of all of the inhomogeneities, $\tilde{T}_{,j}$ is introduced. It is defined as

$$\tilde{T}_{,j} = \frac{1}{V_{D-\Omega}} \int_{D-\Omega} (T^{t}_{,j} - T^{0}_{,j}) dv , \qquad (4\text{-}4)$$

where T^{t} is the total (actual) temperature and $V_{D-\Omega}$ is the volume of the matrix.

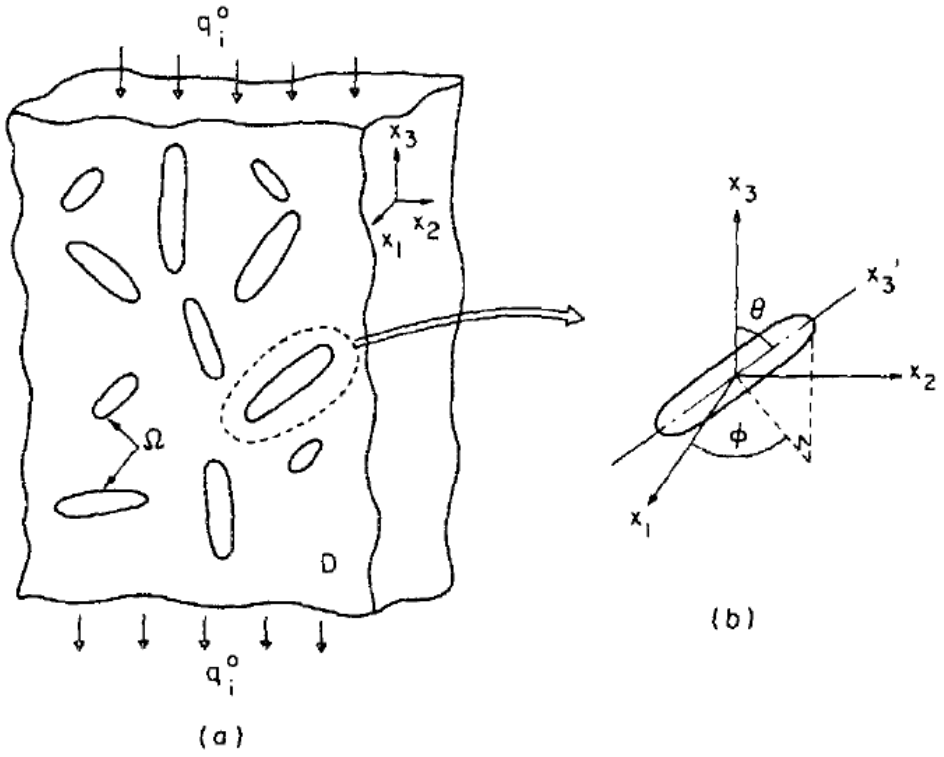

Figure 4-2. (a) A theoretical model for multiple inhomogeneities embedded in the matrix. (b) Relationship between the local (x_i') and global coordinate system (x_i) **[120]**.

Next, applying the equivalent inclusion method to a representative fiber yields

$$q_i^0 + q_i = K^f \delta_{ij} (T^{0}_{,j} + \tilde{T}_{,j} + T^{c}_{,j}) = K^m \delta_{ij} (T^{0}_{,j} + \tilde{T}_{,j} + T^{c}_{,j} - T^{*}_{,j}) , \qquad (4\text{-}5)$$

where q_i is the disturbance of the heat flux due to a representative inhomogeneity, which vanishes when integrated over the entire composite domain *D*, That is,

$$\int_D q_i dv = 0 . \qquad (4\text{-}6)$$

Combining equations (4-4) and (4-6), the interaction term $\tilde{T}_{,i}$ can be obtained as

$$\tilde{T}_{,i} = -\frac{1}{V_D}\int_\Omega (T_{,i}^{c} - T_{,i}^{*}) dv , \qquad (4\text{-}7)$$

where V_D is the volume of the entire composite domain *D*.

In the case of three dimensionally misoriented inclusion phases, the composite body is set on the global coordinates x_1, x_2 and x_3 and the orientation of a single inclusion is defined by angles θ and ϕ as shown in Figure 4-2 (b). The local coordinates of this inclusion are denoted by x_1', x_2' and x_3', where x_3' coincides with the longitudinal axis of the inclusion. Then, the equivalent inclusion method for that single fiber in local coordinates yields

$$q_i^0 ' + q_i ' = K^f \delta_{ij} (T_{,j}^{0} ' + \tilde{T}_{,j} ' + T_{,j}^{c} ') = K^m \delta_{ij} (T_{,j}^{0} ' + \tilde{T}_{,j} ' + T_{,j}^{c} ' - T_{,j}^{*} ') , \qquad (4\text{-}8)$$

and

$$T_{,j}^{c} ' = S_{ij} T_{,j}^{*} ' , \qquad (4\text{-}9)$$

where the entities with primes refer to the ones in local coordinate system. Due to the fact that the single fiber considered here is a representative fiber in the composite, equations (4-8) and (4-9) are applicable to any fiber in the matrix. Therefore, equations (4-8) and (4-9) can be recast in the form

$$T,_i^{*}{}' = (K^m - K^f)\delta_{ij}\, A_{jk}^{-1}(T,_k^{0}{}' + \tilde{T},_k{}'), \qquad (4\text{-}10)$$

where A_{jk}^{-1} is the inverse of A_{jk}, given by the equation

$$A_{jk} = (K^f - K^m)\delta_{jl}\, S_{lk} + K^m \delta_{jk}. \qquad (4\text{-}11)$$

Substituting equation (4-9) into (4-10) yields

$$T,_i^{c}{}' = S_{ij}(K^m - K^f)\delta_{jk}\, A_{kl}^{-1}(T,_l^{0}{}' + \tilde{T},_l{}'). \qquad (4\text{-}12)$$

Furthermore, the quantities in the local coordinate system need to be transformed into the composite's coordinate system (global). Assume y_i' and y_i are vectors in local and global axes, respectively. A transformation matrix is then introduced to map y_i' to y_i, such that

$$y_i = X_{ij}\, y_j{}', \qquad (4\text{-}13)$$

where the coordinate transformation matrix X_{ij} is given as

$$X_{ij} = \begin{bmatrix} \cos\theta\cos\phi & -\sin\phi & \sin\theta\cos\phi \\ \cos\theta\sin\phi & \cos\phi & \sin\theta\sin\phi \\ -\sin\theta & 0 & \cos\theta \end{bmatrix}. \qquad (4\text{-}14)$$

Thus, $T,_i^{*}$ and $T,_i^{c}$ can be expressed as

$$T,_i^{*} = X_{ij}(K^m - K^f)\delta_{jk}\, A_{kl}^{-1} X_{ln}^{-1}(T,_n^{0} + \tilde{T},_n), \qquad (4\text{-}15)$$

and

$$T,_i^c = X_{ij} S_{jk} (K^m - K^f) \delta_{kl} A_{ln}^{-1} X_{np}^{-1} (T,_p^0 + \tilde{T},_p), \qquad (4\text{-}16)$$

respectively, where X_{ln}^{-1} is the inverse of X_{ln}. The interaction term $\tilde{T},_i$, then can be evaluated by substituting equations (4-15) and (4-16) into equation (4-7), which eventually yields the solutions for $T,_i^*$ and $T,_i^c$.

Therefore, the effective thermal conductivity, K_{ij}, of the representative volume element which is the composite body in this case, can be found by the equation

$$K_{ij} \left\langle T,_j^t \right\rangle = K^m \delta_{ij} \left\langle T,_j^t \right\rangle + \frac{1}{V_D} (K^f - K^m) \delta_{ij} \int_\Omega T,_j^t \, dv, \qquad (4\text{-}17)$$

where

$$\left\langle T,_j^t \right\rangle = T,_j^0 + \frac{1}{V_D} \int_\Omega T,_j^* \, dv, \qquad (4\text{-}18)$$

$$T,_j^t = T,_j^0 + T,_j^c + \tilde{T},_j = T,_j^0 + S_{ij} T,_j^* - \frac{1}{V_D} \int_\Omega (T,_j^c - T,_j^*) \, dv, \qquad (4\text{-}19)$$

$$\left\langle T,_j^* \right\rangle_\Omega = \frac{1}{f V_D} \int_\Omega T,_j^* \, dv, \qquad (4\text{-}20)$$

and

$$\left\langle T,_j^c \right\rangle_\Omega = \frac{1}{f V_D} \int_\Omega T,_j^c \, dv. \qquad (4\text{-}21)$$

In equation (4-17), T^t is the total (actual) temperature, and $\langle \ \rangle$ denotes averaging over all possible orientations. In equations (4-20) and (4-21), f is the volume fraction of

the fibers. Consequently, based on equations (4-17) to (4-21) it can be concluded that to determine the effective thermal conductivity of the two-phase composite using equivalent inclusion method, one needs the thermal conductivity of the phases, the volume fraction of the inclusion, and "*S*" tensor which is based on fiber aspect ratio.

The proposed MCFEA employs the equivalent inclusion method in each finite element in the mesh. Each finite element contains certain amount of SWCNTs quantified by SWCNT volume fraction, studied in Sections 3.2 and 3.3. It is assigned randomly based on a chosen volume fraction distribution The PNC is considered to consist of a polymer, individual SWCNTs and agglomerations of SWCNTs as spherical inclusions which are composed of polymer and SWCNT with specific volume fraction. The equivalent inclusion approach in the MCFEA computes the thermal conductivity of the matrix composing of straight, randomly oriented, and perfectly bonded SWCNTs and polymer. The values for the thermal conductivity of the polymer, single-walled carbon nanotube and nanotube aspect ratio are determined based on experimental evidence, which is discussed later in this chapter.

4.2. Random Field Study

Chapter 3 provides an account of the uncertainties present inherently in the nanostructure of the PNCs. The random nature of the heterogeneous media has been characterized in terms of distribution and dispersion of the carbon nanotubes. It has been concluded that volume fraction of the SWCNTs in the polymer matrix can be treated as a random field

which quantifies the spatial randomness of the nanotubes dispersed in polymers. The random fields are then discretized as random variables that have specific probability density functions (PDFs). The selection of an appropriate statistical distribution is obviously critical. In this context, a number of PDFs are used to define volume fractions of the SWCNTs in the proposed model. The carbon nanotubes are assumed to be distributed throughout the polymer randomly conforming to that certain statistical distribution. Three distinct distributions used to quantify the uncertainty of the SWCNTs are Weibull, Lognormal and Uniform distributions given, respectively, by the expressions

$$f(x) = \frac{k}{L}\left(\frac{x}{L}\right)^{k-1} e^{-(x/L)^k}, \ for \ x \geq 0, \qquad (4\text{-}22)$$

$$f(x) = \frac{1}{x\sigma\sqrt{2\pi}} e^{-\frac{(\ln x - \mu)^2}{2\sigma^2}}, \ for \ x > 0, \qquad (4\text{-}23)$$

and

$$f(x) = \frac{1}{b-a}, \ for \ a \leq x \leq b. \qquad (4\text{-}24)$$

In equation (4-22), the k and L values represent Weibull parameters; in equation (4-23 **)**, μ and σ are the mean and standard deviation of the variable's natural logarithm, respectively; and the values a and b are the two boundaries of the uniform distribution in equation (4-24). Bearing in mind that for each realization, a set of random vectors is generated numerically based on the assigned statistical distribution. In the case of polymer nanocomposites, the random values in the vector set correspond to the local nanotube volume fraction values in each finite element. The mean values in all

distributions are always set equal to the global SWCNT volume fraction (vf) value of the nanocomposite.

Further, it is noted that the random values in each numerically generated vector are scaled accordingly, so that their mean value is always identical to the overall SWCNT volume fraction in the matrix. The standard deviations in the PDFs are selected such that no SWCNT volume fraction value can be negative or greater than 0.80 within a finite element conforming to the manufacturing constraints of the PNC.

Simulations are performed with a selected number of carbon nanotube volume fraction values with appropriate standard deviations in order to illustrate the effects of their heterogeneous distributions on the effective thermal conductivity of the PNCs. Figure 4-3 shows the probability density function of the Weibull distributions from which the local SWCNTs volume fractions are numerically generated. The PDFs are plotted for the mean volume percentage values of 5, 10 and 20. Further, in the MCFEA simulations numerous standard deviation (σ) values are used with each mean value so as to obtain the local vf values in various ranges. In Figure 4-3 the standard deviations used are equal to 0.02, 0.05 0.07; 0.05, 0.08 0.10; and 0.07, 0.10 0.13 for 0.05, 0.10 and 0.20 mean vf values, respectively.

In addition, Figure 4-4 and Figure 4-5 show the analogous PDFs of Log-normal and Uniform distributions with the same mean values. The Log-normal distributions are plotted with the σ values of 0.02, 0.05, 0.08; 0.05, 0.10, 0.15; and 0.05, 0.10, 0.15. The

standard deviation values selected for the Uniform distribution are based on the interval in which the random values are generated. Since the local SWCNT volume fraction value cannot be less then zero, the highest value it can possess is twice of the mean vf value.

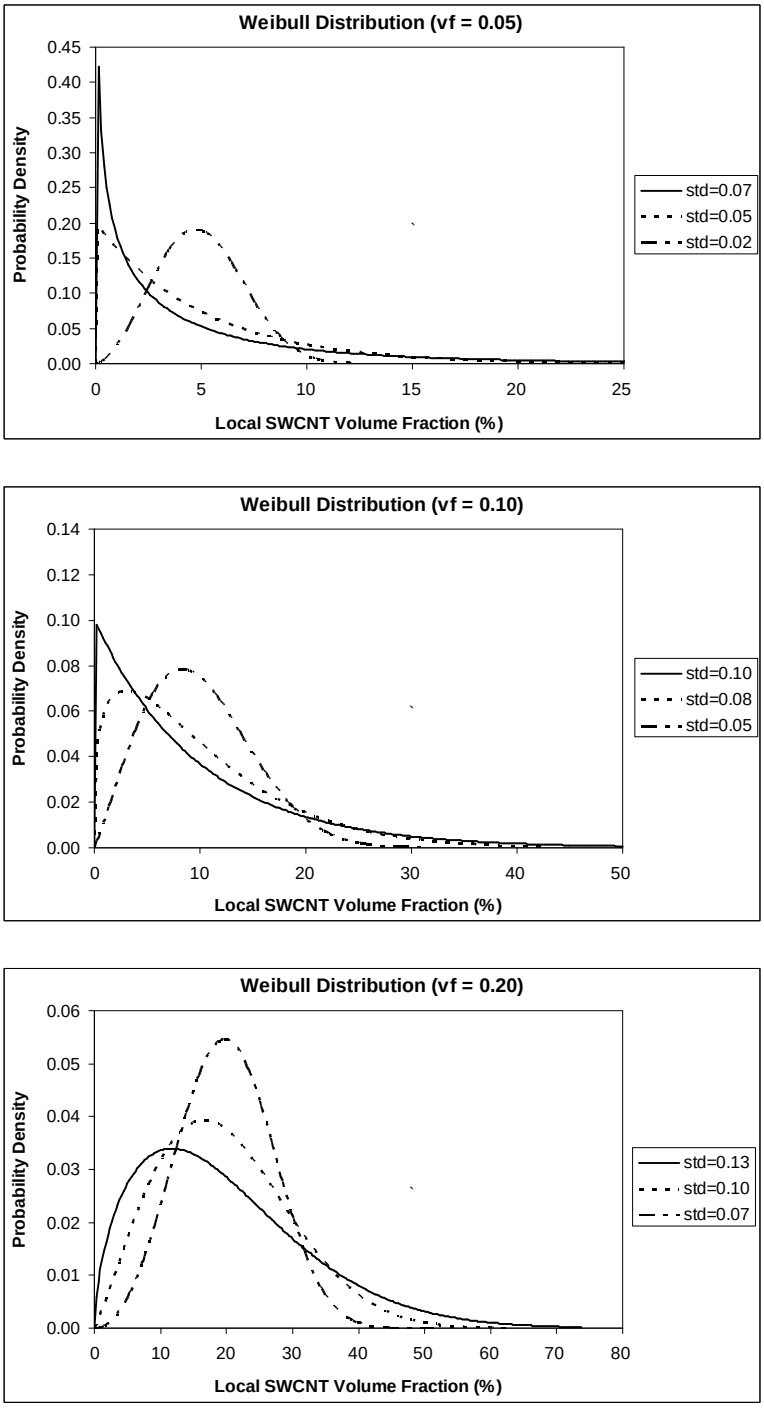

Figure 4-3. SWCNT volume fraction distribution produced by Weibull distribution for mean values of 0.05, 0.10 and 0.20 with various standard deviations.

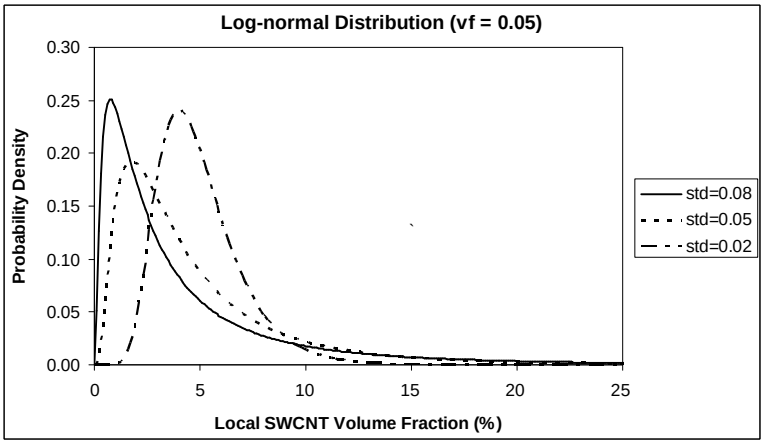

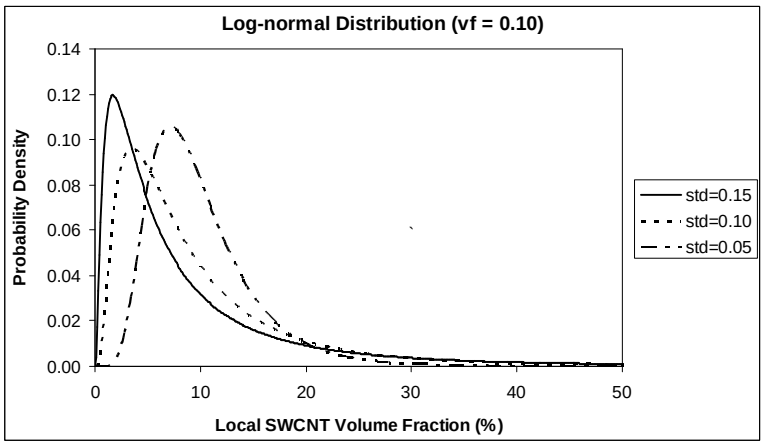

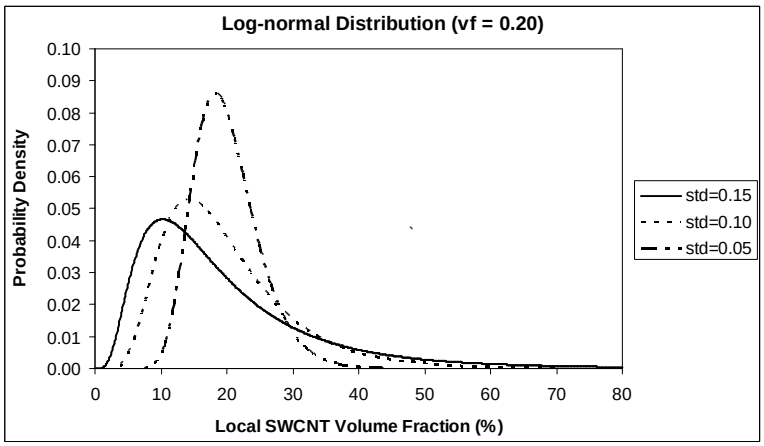

Figure 4-4. SWCNT volume fraction distribution produced by Log-normal distribution for mean values of 0.05, 0.10 and 0.20 with various standard deviations.

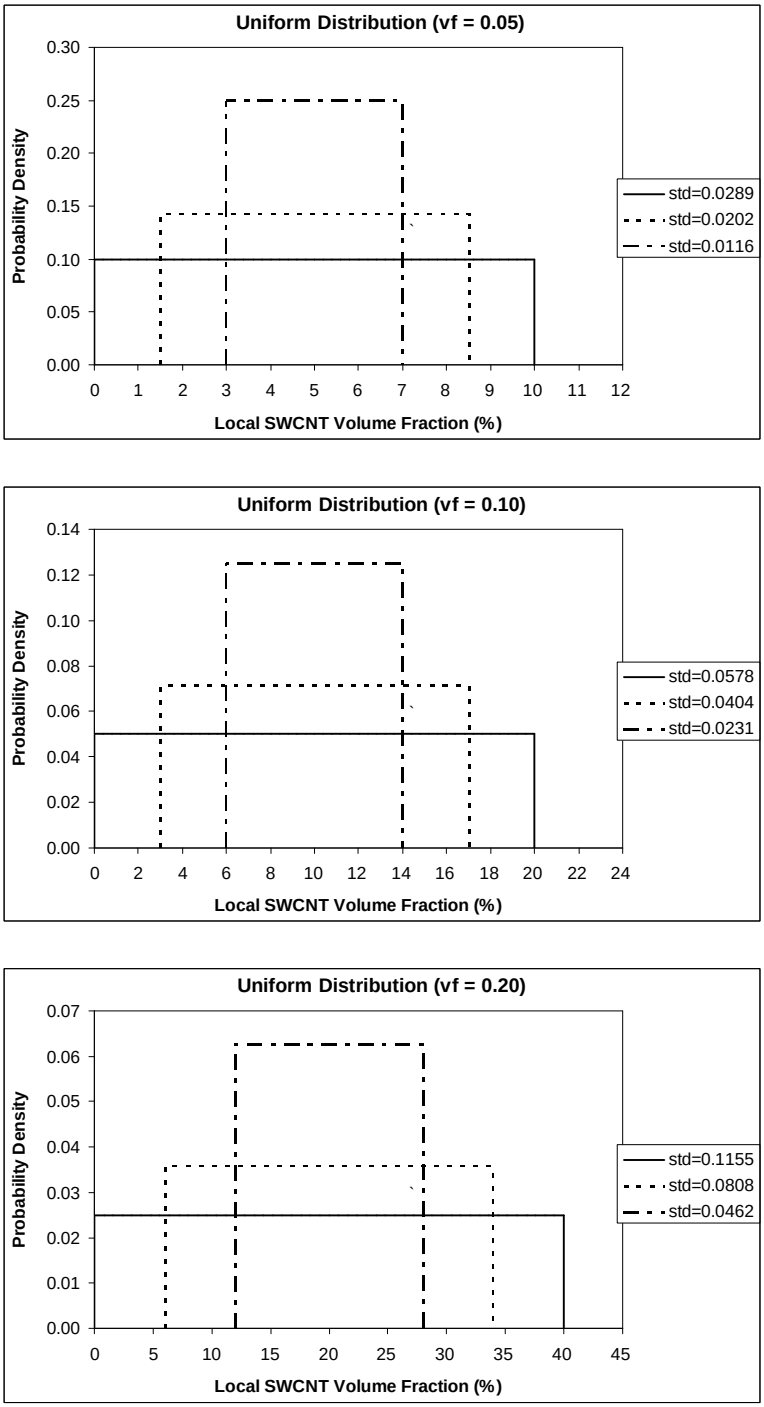

Figure 4-5. SWCNT volume fraction distribution produced by Uniform distribution for mean values of 0.05, 0.10 and 0.20 with various standard deviations.

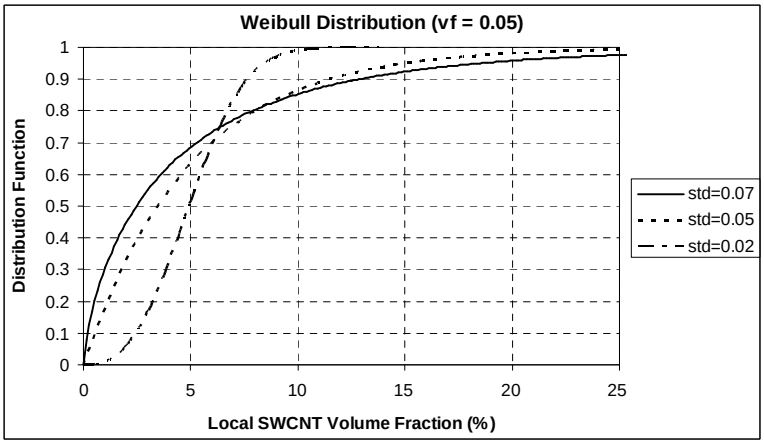

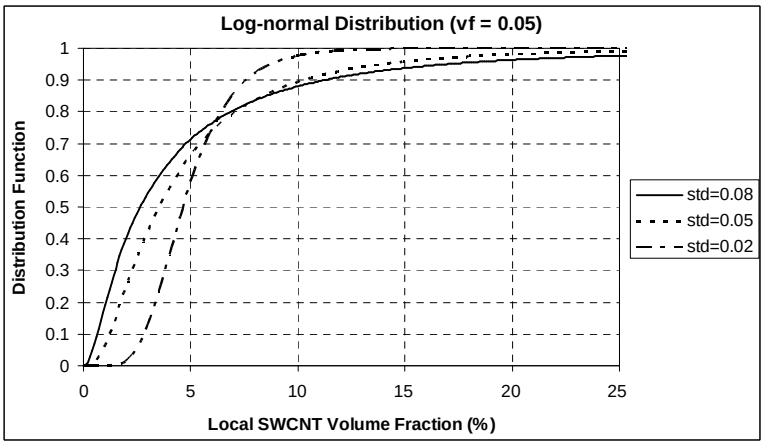

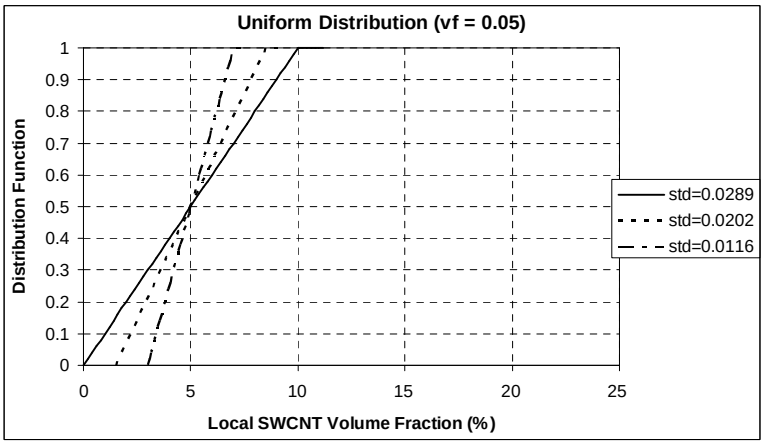

Figure 4-6. Cumulative distribution functions of SWCNTs obtained from Weibull, Log-normal and Uniform distributions for the mean value of 0.05 with the corresponding standard variations.

Particularly, in Figure 4-5 for the mean vf of 5%, the maximum local vf can be 10% denoting an interval from 0 to 10%, which then corresponds to a σ of 2.89%. Similarly, keeping the 5% volume percentage, for the intervals [1.5-8.5] and [3-7], the associated standard deviations are 2.02% and 1.16%, respectively.

The intervals used for the mean volume fractions of 0.10 are [0-20], [3-17] and [6-14], corresponding to the σ values of 0.0578, 0.0404 and 0.0231. Likewise, for the mean vf of 20%, the local SWCNT vf values are produced within the intervals of [0-40], [6-34] and [12-28] with standard deviations of 11.55%, 8.08% and 4.62%, respectively. Samples of the cumulative distribution functions (CDFs) of the statistical distributions used in the simulations are also given in Figure 4-6, for the mean SWCNT volume fraction of 5% with their corresponding standard deviations.

Figure 4-7, Figure 4-8 and Figure 4-9 show the histograms of random vector samples of the local SWCNT volume fractions. Each figure presents a single realization generated numerically based on the three probability density functions defined in Equations (4-22), (4-23) and (4-24). The samples have 400 elements representing a material region discretized by 400 finite elements, i.e. 20x20 grid. The graphs are plotted with mean nanotube volume fractions of 0.05, 0.10 and 0.20 and with various standard deviations. The influence of the standard deviation on the numerically computed values of the effective thermal conductivity of the polymer nanocomposites is also discussed later in this chapter.

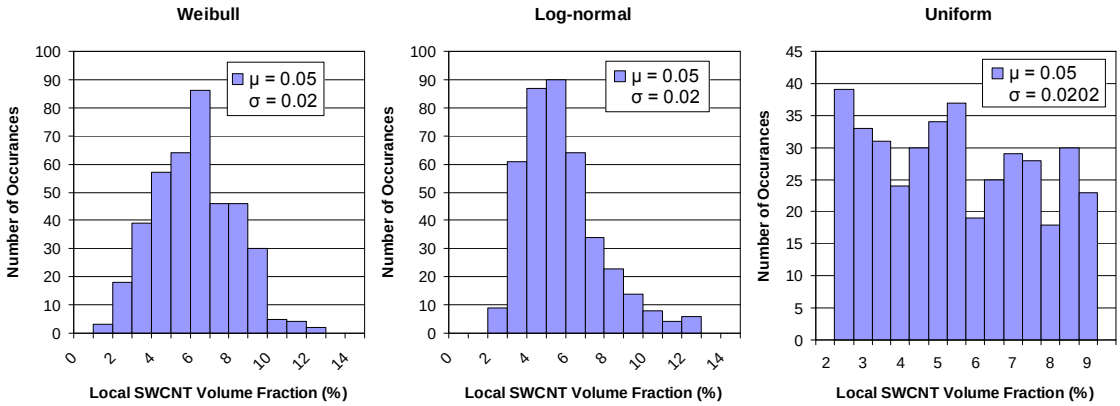

Figure 4-7. Samples of vectors of random values that have Weibull, Log-normal and Uniform distributions. The plots have the mean SWCNT volume percentages of 5% and the standard deviations of 2%.

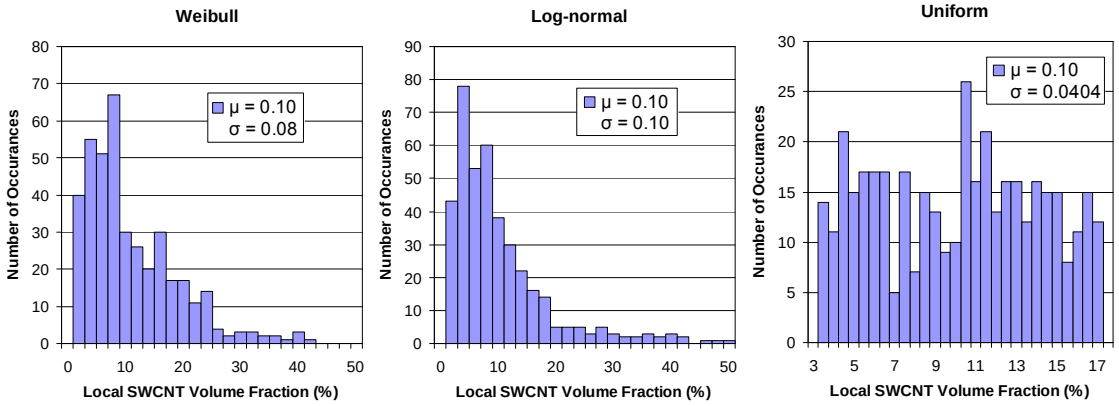

Figure 4-8. Samples of vectors of random values that have Weibull, Log-normal and Uniform distributions. The plots with μ = 0.10 and with σ = 0.08, 0.10, 0.0404, respectively.

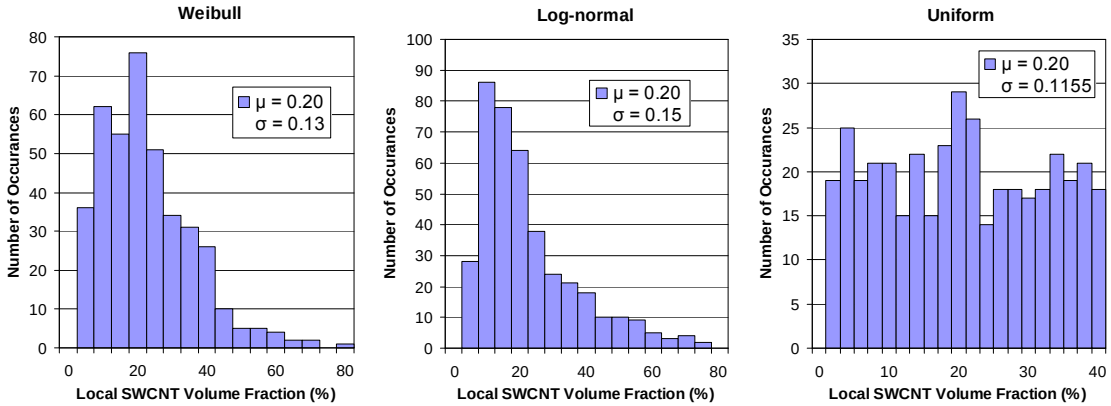

Figure 4-9. Samples of vectors of random values that have Weibull, Log-normal and Uniform distributions. The plots with μ = 0.20 and with σ = 0.13, 0.15, 0.1155, respectively.

4.3. Introducing Randomness into Finite Element Scheme

To proceed to the determination of the thermal conductivity of polymer nanocomposites, the 'Stochastic Finite Element Method' (SFEM) is adopted. This is a fundamentally deterministic finite element method that incorporates the inherent randomness in nanostructure such as nanotube distribution, dispersion, shape, size, orientation, with the description of corresponding random fields. Among the SFEM methods available in the literature to compute the response of the random media, the Monte Carlo (MC) simulation technique is adopted in the proposed model due to certain advantages.

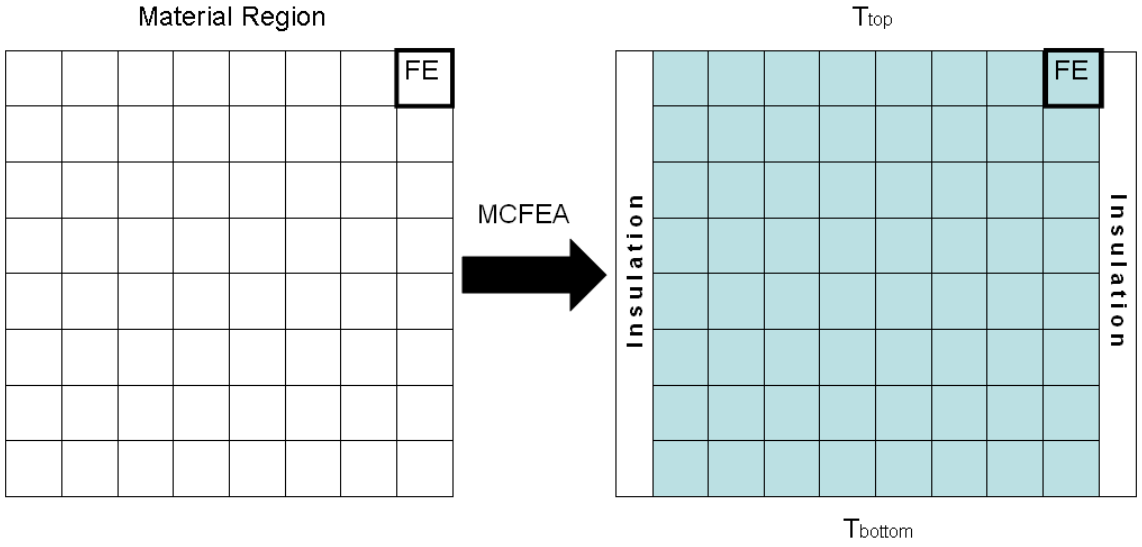

Figure 4-10. The finite element scheme used in the MCFEA to determine the effective thermal conductivity of PNC.

The MC analysis used in the proposed approach addresses the heterogeneous random media in the nanocomposites as the spatial distribution of the SWCNT in a polymer. Random vector sets for local SWCNT volume fractions are generated through the random

fields selected which correspond to the uncertainties in the PNC. Each random vector represents one realization, whose values are then assigned to all the finite elements in the two dimensional FE model, demonstrated in Figure 4-10. Subsequently, the local thermal conductivity of each finite element is calculated by the equivalent inclusion method (EIM), introduced in Section 4.1. One must bear in mind that the EIM assumes homogeneous distribution of the inclusions in the matrix material. It is thus important to select an appropriate finite element size. On one hand, to perform this micromechanics method in a finite element, the FE size must be sufficiently larger than the SWCNT size; similar to the demonstration in Figure 3-1. Considering the ordinary length of a single nanotube is in the vicinity of 150 nanometers, the FE size must be in microns. On the other hand, if the FE size is chosen too large, the distribution characteristics cannot be captured properly. For example, in case of a poor nanotube distribution, an excessively large FE size causes this spatial variation to be ignored by the proposed MCFEA.

Finite element method is employed to compute the overall thermal conductivity of the two dimensional problem for each realization of the random field. The heat transfer problem described in this dissertation refers to a steady state, one dimensional heat flow with defined top and bottom temperature boundary conditions. The matrix equation given in equation (4-25) is solved for the system to obtain the heat flow rate gradients, namely the heat flux vectors, and the element temperatures in each FE.

$$[M^e]\{\dot{T}^e\}+[K^e]\{T^e\}=f\ , \qquad (4\text{-}25)$$

where M and K are the capacitance (mass) and coefficient (conductivity) matrices, respectively. T is the element temperatures vector, $\dot{T}$ is equal to $\partial T/\partial t$, time derivative of the temperature, and f is the outside heat source (or sink). $\dot{T}$ and f are zero for steady state heat transfer with free response. Then, the effective thermal conductivity of the RVE, k_{RVE} for one realization can be obtained for the case of 1-D geometry between two end points at constant temperatures by the equation

$$\frac{\Delta Q}{\Delta t} = -k_{RVE} A \frac{\Delta T}{\Delta x}, \qquad (4\text{-}26)$$

where is A is the cross-sectional surface area which is the thickness t times the RVE width w, ΔT is the temperature difference between the boundaries, Δx is the length of the RVE, and $\Delta Q/\Delta t$ is the total heat flow rate.

To obtain the statistics of the effective thermal conductivity of the polymer nanocomposites using the proposed model, numerous samples of the SWCNT volume fraction distribution are generated. By repeating this process for a certain number of realizations, a collection of the effective RVE thermal conductivities is obtained. The results subsequently reveal the mean value and the standard deviation of the overall effective thermal conductivity of the carbon nanotube reinforced polymer.

Figure 4-11, Figure 4-12 and Figure 4-13 show random vector samples of the local SWCNT volume fractions used in the proposed approach, along with a realization of the nanotube volume fraction random field. The histograms of 100 values (10x10 grid) are

generated based on Weibull, Log-normal and Uniform distributions with mean volume fraction value of 0.05 with σ of 0.02. For each v_f realization, the local thermal conductivities are computed by the FE approach described in Figure 4-10. Furthermore, the second parts of the figures show sample histograms of the calculated local thermal conductivities. They also present samples of the spatial variation of the local thermal conductivities determined by the proposed MCFEA for 10 by 10 meshed grid. It is evident from the figures how the poor nanotube distribution causes non-uniform thermal conductivity throughout the composite.

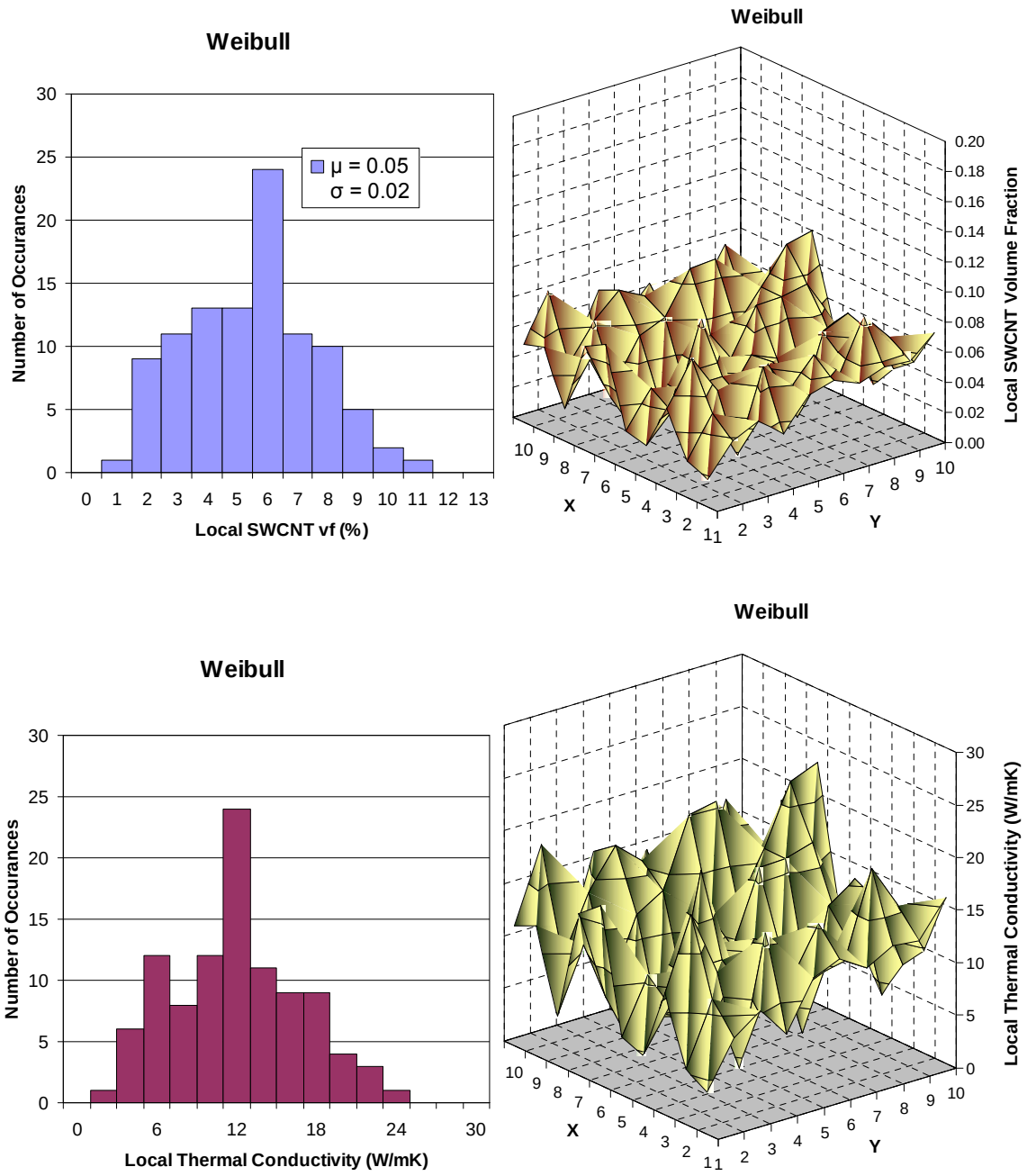

Figure 4-11. Top - Sample histogram and sample spatial variation of the local SWCNT volume fractions of 100 values, based on Weibull distribution, with a mean value of 0.05 and a standard deviation of 0.02. **Bottom -** Sample histogram and sample realization of the local thermal conductivity random field generated by the proposed MCFEA employing the corresponding SWCNT volume fraction values in the upper plots.

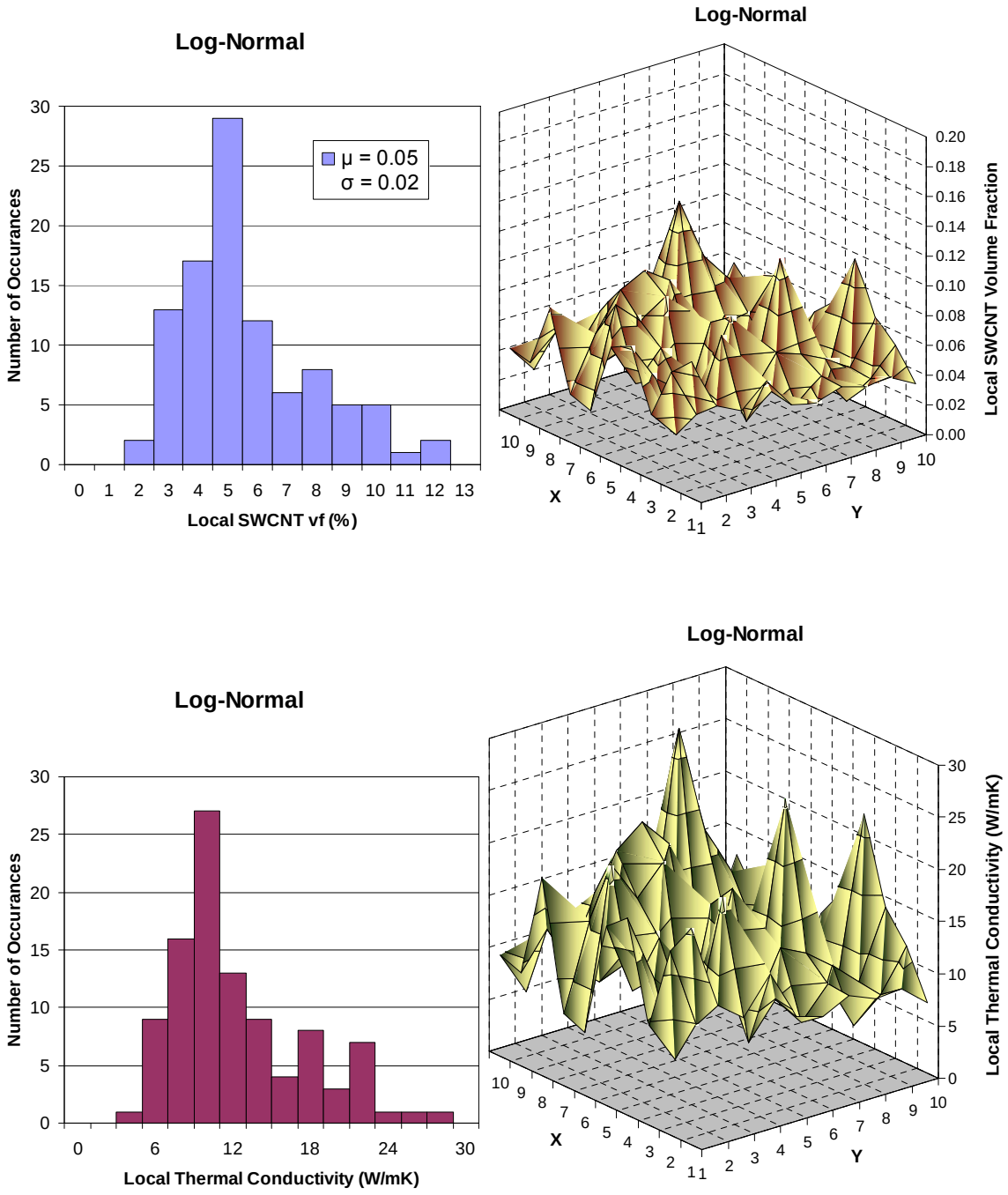

Figure 4-12. Top - Sample histogram and sample spatial variation of the local SWCNT volume fractions of 100 values, based on Log-Normal distribution, with a mean value of 0.05 and a standard deviation of 0.02. **Bottom -** Sample histogram and sample realization of the local thermal conductivity random field generated by the proposed MCFEA employing the corresponding SWCNT volume fraction values in the upper plots.

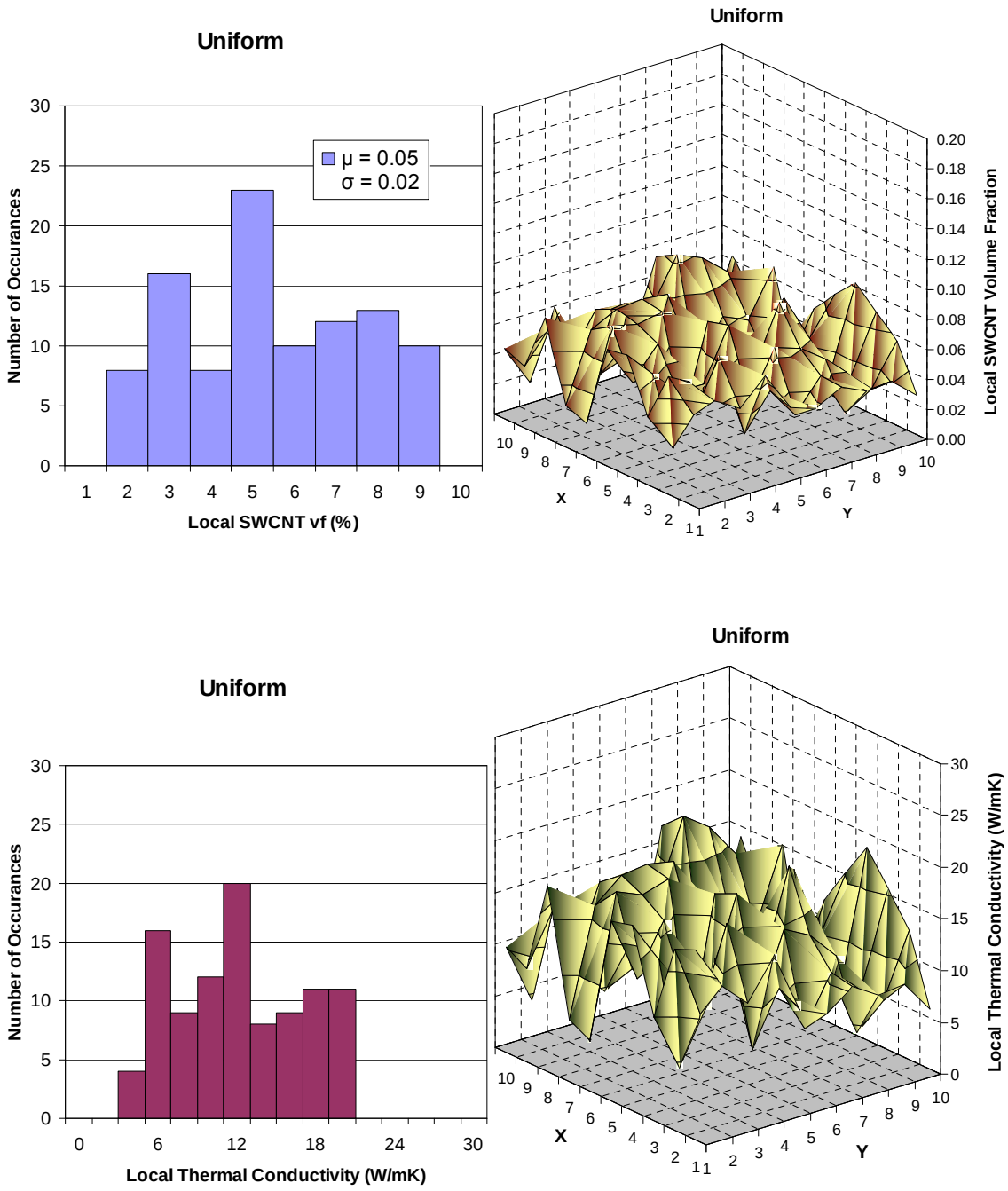

Figure 4-13. Top - Sample histogram and sample spatial variation of the local SWCNT volume fractions of 100 values, based on Uniform distribution, with a mean value of 0.05 and a standard deviation of 0.02. **Bottom -** Sample histogram and sample realization of the local thermal conductivity random field generated by the proposed MCFEA employing the corresponding SWCNT volume fraction values in the upper plots.

4.4. Sensitivity Analysis on Mesh Sizing and Constituent Properties

From an application point of view, the composite's heterogeneous thermal conductivity variation in the local level creates complexities in the design process to a considerable extent. Uncertainties and nonlinearities always give rise to intricate challenges for engineers. In this context, the Monte Carlo (MC) method offers a reasonable solution providing statistical information on the overall thermal conductivity of the structure. With a mean and a standard value, reliable designs with certain safety factors can be performed in the real case of applications.

In engineering and in computational modeling one of the most important factors to be considered is the feasibility. That is, obtaining the best accuracy in the shortest time. Since the main disadvantage of the MC simulations is their expensive computational time, it is important to carry out the investigations efficiently with regards to the effects of the SWCNT distribution on the overall thermal conductivity of the PNCs. Therefore, first an attempt is made to select the most appropriate number of Monte Carlo realizations to perform the simulations. Figure 4-14 shows how the effective thermal conductivity changes as the number of realizations used in the MC simulation increases. The variation of the effective thermal conductivity of PNC is plotted versus the MC samples number, ranging from 100 to 2000. Weibull PDF is used to assign the SWCNT volume fraction values to the finite elements, with mean volume fraction of 0.20 and standard deviation of 0.17. One can reliably claim that beyond 500 realizations, the K_{eff} converges to a constant value. It is, thus, decided on using 500 MC realizations in the MCFEA developed in this dissertation for preserving computational time.

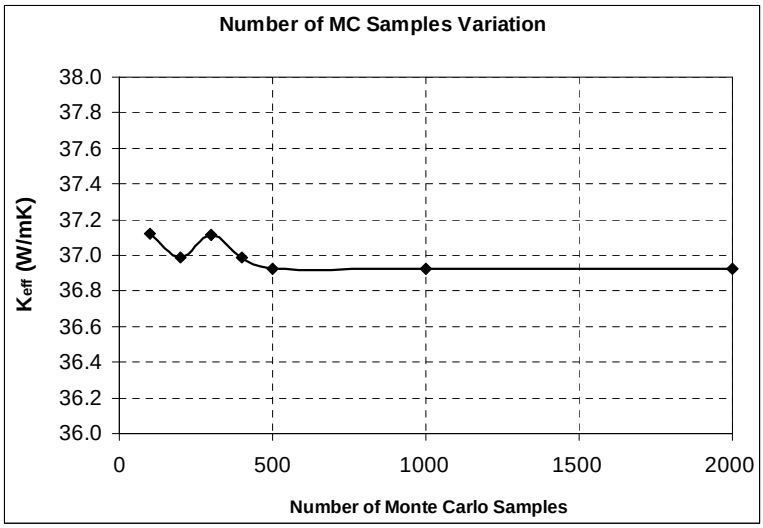

Figure 4-14. Variation of the effective thermal conductivity of PNC w.r.t. number of Monte Carlo samples.

Further, the PNC used in the simulations are considered to be composed of isotropic SWCNTs and epoxy matrix with thermal conductivities of 2000 W/mK and 0.188 W/mK at room temperature, respectively [183], [96]. The number of MC realizations is kept at 500, which provides high accuracy with reasonable computation time. Based on the statistical information reported in the literature, mean value of the ratio of the nanotube length to its diameter, aspect ratio (L/D) is chosen to be 150 [177], [164].

The methods described and developed in the previous chapters aim to take into consideration the distribution characteristics of the single-walled carbon nanotubes in a polymer matrix. However, there are no thorough image analyses or studies available in the literature, which statistically quantify the spatial variation of the local SWCNT content throughout the composite. The MCEFA developed in this dissertation proposes two factors to investigate the nanotube distribution characteristics. One aspect

investigates the effect of the carbon nanotube distribution in the matrix by using various mesh sizes in the material region as illustrated in Figure 4-10.

Mesh size, that is the number of finite elements in the model, can be considered as the number of images taken from the actual material. For this purpose, the mesh sizes of 1, 25, 100, 225, 400 and 625 elements are used in the simulations where 1 element refers to the regular the Hatta-Taya method. It is reminded that the Hatta-Taya method treats the material region as a single element where the inclusions are homogeneously distributed. The standard deviations of the calculated overall thermal conductivity values for each mesh size reveal the quality of the distribution.

The other aspect is the standard deviation of the SWCNT volume fraction values of the finite elements. In the MCFEA simulations, several values of the standard deviation are used with each vf probability distribution to observe the effect of the degree of the nanotube distribution. The standard deviation of the volume fraction of the finite elements depends on the scatter of the data and hence is an indicator of the quality of the distribution. A higher value of variance indicates a poor distribution, since it indicates a large scatter in the values of nanotube volume fraction in different parts of the nanocomposite; that is the finite elements in the material region.

Figure 4-15 shows the effective thermal conductivities of the polymer nanocomposite computed by the proposed MCFEA for the SWCNT volume fraction equal to 0.05. Both the mean conductivity values and their corresponding standard deviations are presented

for finite element models with different mesh sizes. Further, the three probability density functions are utilized for assigning the local volume fractions to the finite elements, which are Weibull, Log-normal and Uniform distributions. The plots in Figure 4-15 are presented for each PDF with three selected standard deviation values to observe the quality of the nanotube distribution.

It can be easily seen in the plots that for small mesh sizes especially below 100 finite elements where the FE size is much larger that the nanotube size, the standard deviation values of the estimated effective thermal conductivities are considerably high. The significance of this finding is that the SWCNTs have extremely poor distribution throughout the matrix material. However, this poor distribution takes place at a low frequency, which means that the nanotube content variation occurs over large portions in the material region. Due to this fact it is possible that the model is not able to capture the nanotube variation completely.

Moreover, in Figure 4-15 for each value of the SWCNT standard deviation (σ), the mean values of the effective thermal conductivities (ETCs) of the PNC decreases until 100 finite elements after which they stay constant. This implies that beyond 100 FE the effect of the mesh size diminishes and that the finite element size reaches its lower limit at which the micromechanics method can be applied. It is also observed that the σ values of the ETCs decrease as the mesh size increases. This result can be counterintuitive due to the fact that the degree of scatter is expected to increase with the number of FE. However, it actually indicates that the material region tends to possess homogeneous

nanotube distribution. Nevertheless, at the same time the SWCNT variation is incorporated more capably because more finite elements are included in the computations. This outcome is corroborated by Figure 4-18 where the coefficient of variation (CV) of the normalized effective thermal conductivity values computed by the MCFEA is plotted against the number of the finite elements. The CV is defined as the ratio of the standard deviation to the mean value. The figure shows that all CVs of the ETCs decrease as the number of FE increases and converge to their natural values. A physical interpretation of this result is that the better precision of the thermal conductivity estimation, the more data extracted from image analysis.

Furthermore, the mean values of the ETCs decrease as the standard deviations of the SWCNT volume fraction increase, and since the vf range expands with the rise of SWCNT σ values, their σ values of ETC increases. As it can be seen in Figure 4-15, Figure 4-16 and Figure 4-17, the ETC value computed by the Hatta-Taya method, which corresponds to the value of the single finite element has the highest estimates. This is the proof of non-linear relation between the SWCNT vf and the ETC even for the case of Uniform nanotube distribution. In addition to that in Weibull and Log-normal distributions, most of the vf values generated fall below the mean vf value, which result in much lower mean ETC values than the ones obtained by Uniform distribution.

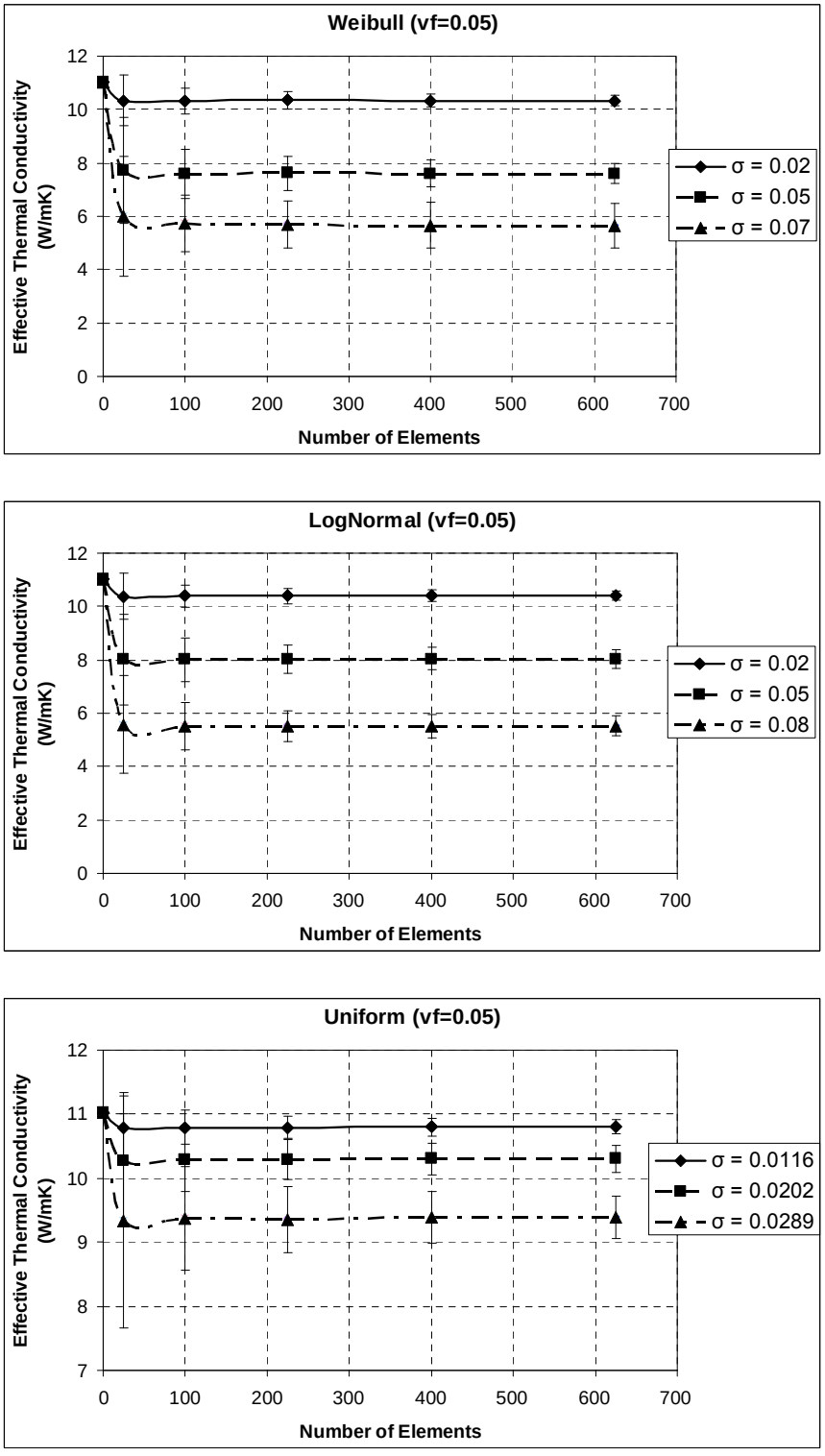

Figure 4-15. Variations of the effective thermal conductivities with plus and minus one standard deviation computed by the MCFEA w.r.t. the number of finite elements. Three different PDFs are used with 5% SWCNT vf with the selected standard deviations.

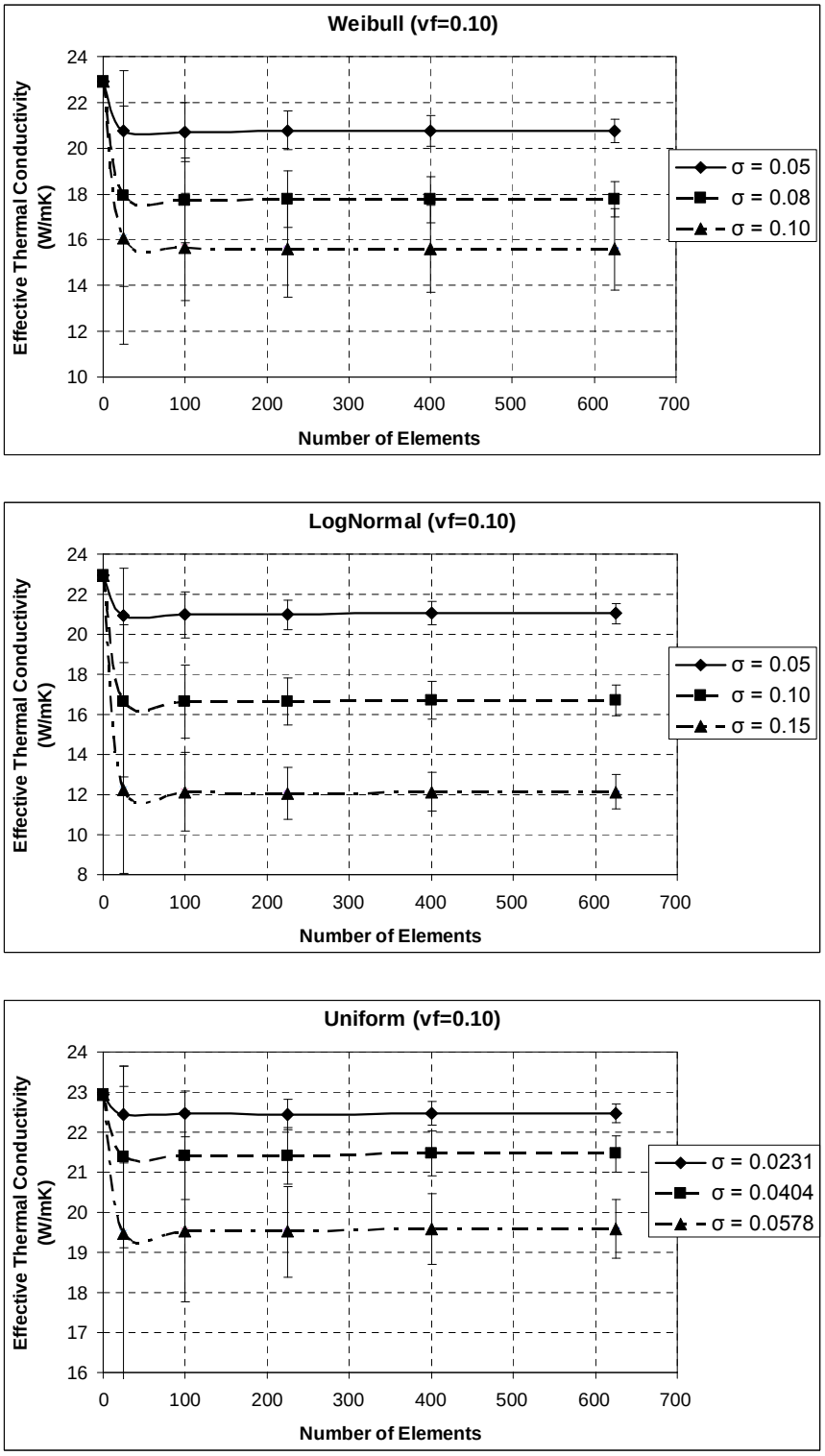

Figure 4-16. Variations of the effective thermal conductivities with plus and minus one standard deviation computed by the MCFEA w.r.t. the number of finite elements. Three different PDFs are used with 10% SWCNT vf with the selected standard deviations.

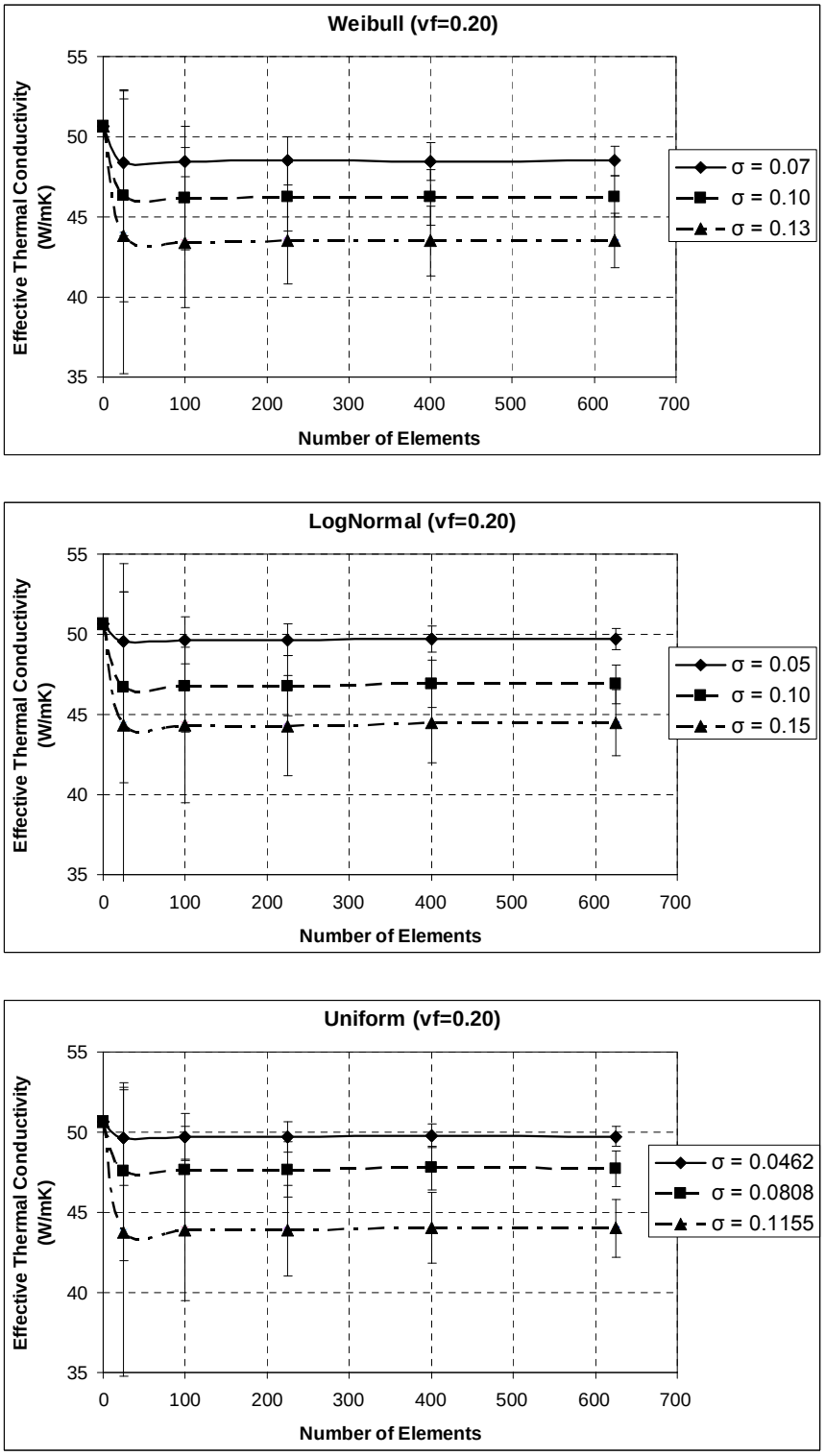

Figure 4-17. Variations of the effective thermal conductivities with plus and minus one standard deviation computed by the MCFEA w.r.t. the number of finite elements. Three different PDFs are used with 20% SWCNT vf with the selected standard deviations.

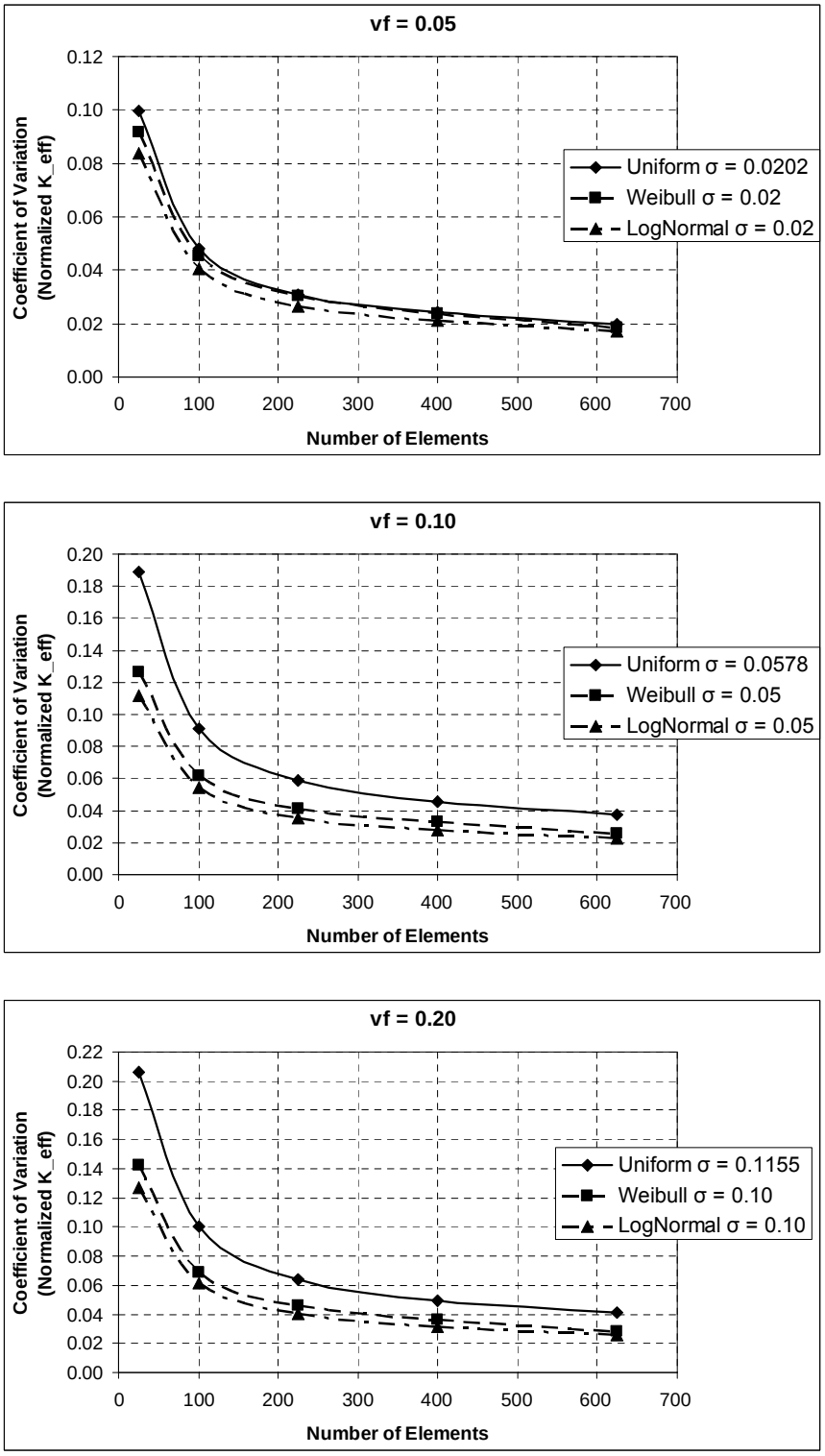

Figure 4-18. Coefficient of variation of the normalized effective thermal conductivity values computed by the MCFEA, shown in Figure 4-15, Figure 4-16 and Figure 4-17 versus the number of the finite elements. The plots are for 5, 10 and 20% SWCNT vf and for the three PDFs with chosen standard deviations.

As it can be inferred from Figure 4-18, the change in the coefficient of variation is minimized beyond the number of 400 finite elements. Figures also suggest that confidence interval can be increased when higher number of finite elements are used, vis-à-vis higher number of nanotube volume content data from image analysis. However, high FE number demands additional effort for obtaining data from the actual materials. Figure 4-18 hence suggests that reasonable accuracy can be achieved at 100 mesh size. As a result of this, fewer amounts of real data need to be collected and the simulation time can be kept moderately short.

The variation of the effective thermal conductivity of the PNC is plotted with respect to the SWCNT volume fractions, shown in Figure 4-19. The numerical results are generated by the proposed MCFEA using 500 Monte Carlo realizations and 100 finite elements, with nanotube aspect ratio of 150 [177], [164]. The graph presents a sample comparison of the mean ETC values produced by those three probability distributions and the one by the Hatta-Taya method. For each mean nanotube vf value, appropriate σ values are used. The results are plotted as a function of volume fraction up to 40% content for the sake of keeping the simulations within realistic limits.

One can deduce from the graph that the values obtained by the MCFEA are considerably lower than the one computed by the Hatta-Taya model, especially at low volume fraction values. Examining closely the value obtained by the model with Weibull distribution is found to be less than half of what the random Hatta-Taya gives for 5% nanotube volume content. This gives corroborating evidence of the influence of the randomness on the

thermal conductivity of PNCs, and shows that even a complex micromechanics model, such as the Hatta-Taya alone, cannot predict conclusively the values determined by experiments.

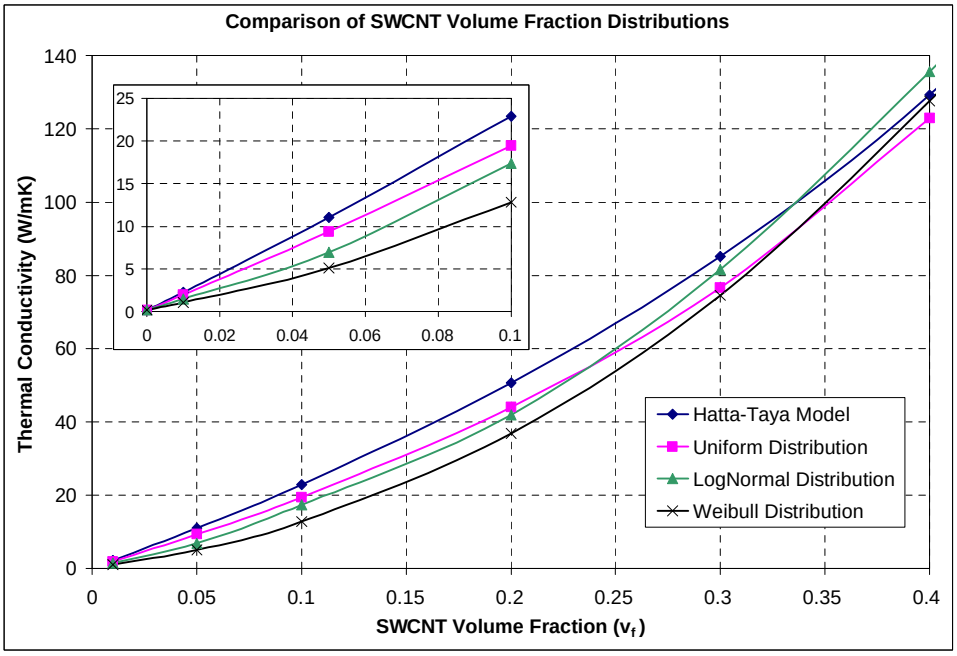

Figure 4-19. Effective thermal conductivity of PNC versus SWCNT volume fraction produced by Uniform, Log-normal and Weibull and with Hatta-Taya method.

The proposed model is also used to investigate how the aspect ratio of the single-walled carbon nanotubes affects the effective thermal conductivity of a PNC. Variation of the results computed with the Log-normal distribution for the aspect ratio values ranging from 50 to 2000 are presented in Figure 4-20. The nanotube volume fractions used are equal to 0.20, 0.10 and 0.05 with the standard deviations of 0.15, 0.15 and 0.08, respectively. It can be seen that the curve becomes flat after the value 1000, after which SWCNTs can be considered infinitely long. However, as mentioned previously, simulations are carried out for an aspect ratio value of 150 so as to conform to the experimental studies [177], [164].

Similarly, variations of the effective thermal conductivity of PNCs as a function of the thermal conductivity of the matrix and the SWCNT are also investigated as shown in Figure 4-21 and Figure 4-22, respectively. The nanotube volume fractions of 0.20, 0.10 and 0.05 with the corresponding standard deviation of 0.15, 0.15 and 0.08 are used in both graphs. In Figure 4-21 the thermal conductivity of the matrix is kept constant at 0.188 W/mK, equivalent to that of the epoxy resin. Likewise, the thermal conductivity of the SWCNTs is set at 2000 W/mK in Figure 4-22.

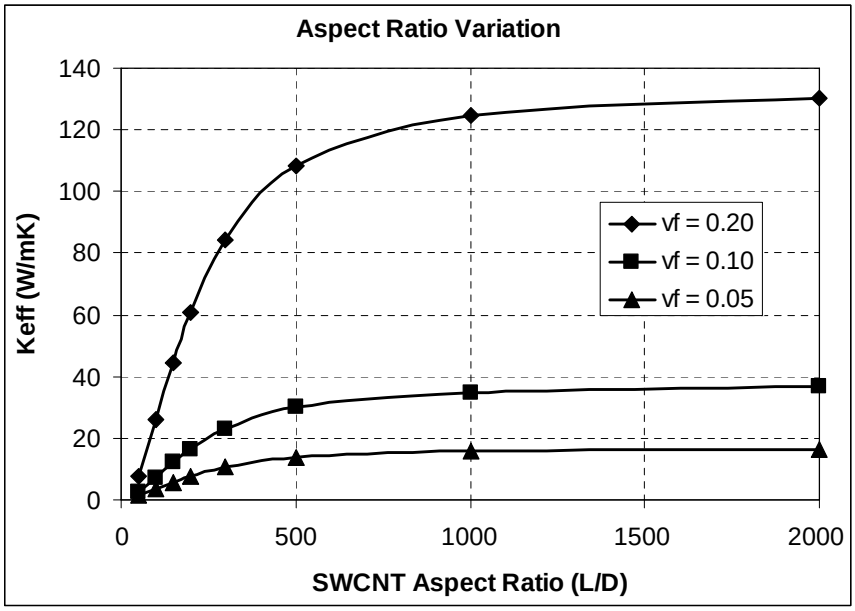

Figure 4-20. Variation of the effective thermal conductivity of PNC w.r.t. aspect ratio (L/D) of SWCNTs, with various content ratios.

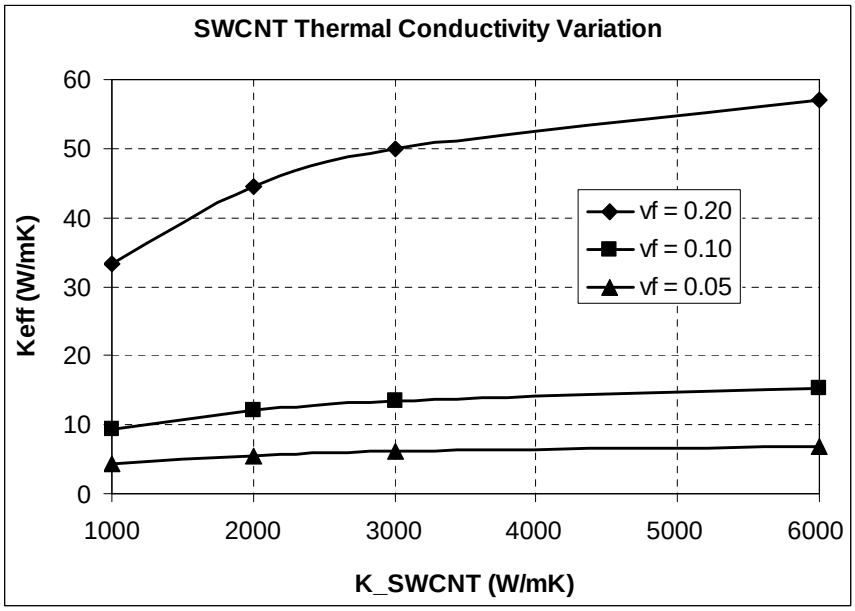

Figure 4-21. Variation of the effective conductivity of PNC w.r.t the thermal conductivity of SWCNT for the volume fractions of 0.20, 0.10 and 0.05. Log-normal distribution was employed for the nanotube volume fraction, keeping the matrix thermal conductivity at 0.188 W/mK.

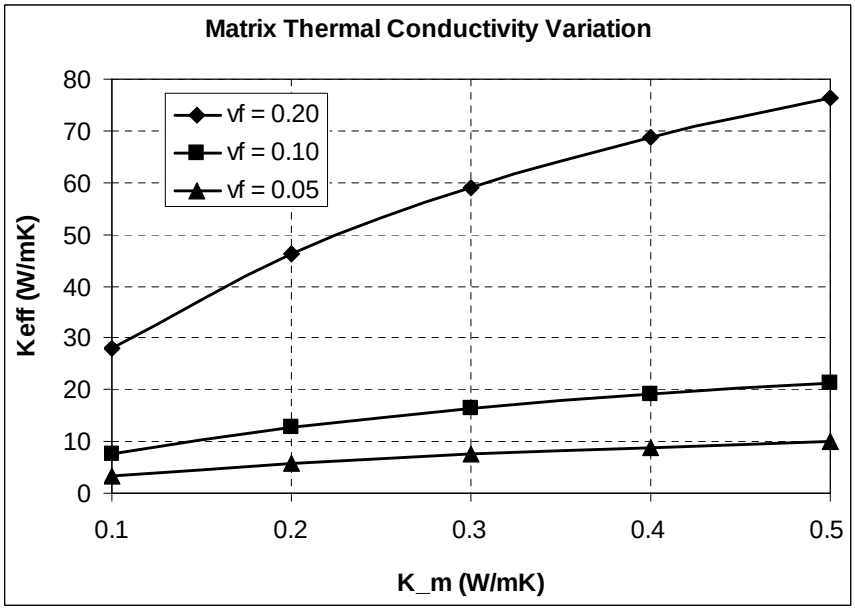

Figure 4-22. Variation of the effective conductivity of PNC w.r.t the thermal conductivity of the matrix for the volume fractions of 0.20, 0.10 and 0.05. Log-normal distribution was employed for the nanotube volume fraction, keeping the SWCNT thermal conductivity at 2000 W/mK

Chapter 5

Nanotube Dispersion on PNC Thermal Conductivity

It has been pointed out in Chapter 3 that the single-walled carbon nanotubes (SWCNTs) are present in the base matrix material not merely as individuals but also in forms of clusters and agglomerates. The morphological studies give evidences of the heterogeneity and the randomness in the distribution and dispersion of SWCNTs. The term distribution relates to the spatial variation of the nanotube forms and the dispersion refers to the agglomeration of the SWCNTs. The effect of the spatial randomness on the thermal conductivity of the polymer nanocomposites (PNCs) is presented in Chapter 4. The results produced by the proposed Monte Carlo Finite Element Approach (MCFEA) have been obtained exclusively for PNCs reinforced with individual SWCNTs to keep the focus solely on the spatial distribution. The local thermal conductivities of each finite element in the model are calculated by the equivalent inclusion method (EIM) introduced in the previous chapter. The EIM is a micromechanics method originally constructed for the case of single type inhomogeneities embedded in a matrix as illustrated in Figure 5-1.

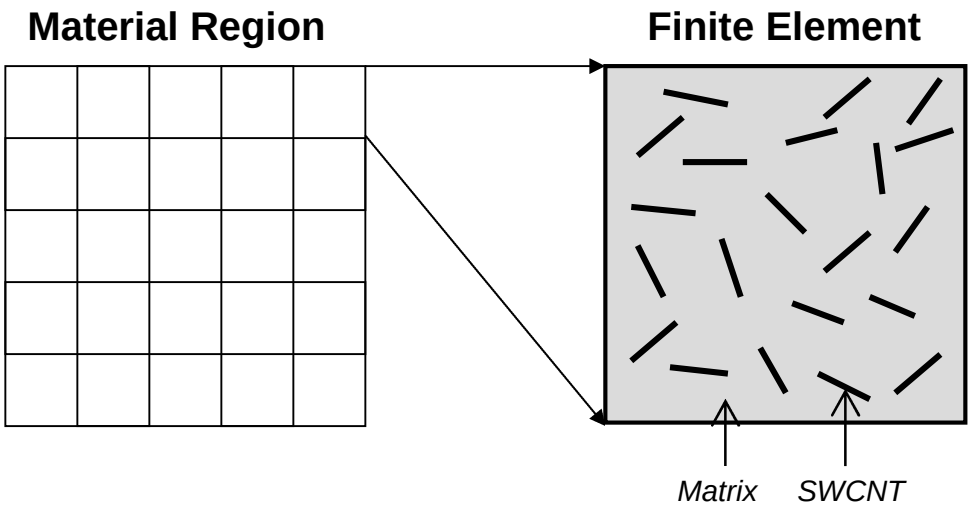

Figure 5-1. The material structure in a finite element used in Chapter 4, comprising matrix and individual SWCNTs.

It is, nevertheless, essential to account for the dispersion characteristics of SWCNTs to pragmatically determine the effective thermal conductivity of PNCs. To this end, the nanotube agglomerations are considered as an additional reinforcing phase in the matrix. It is the aim of this chapter to investigate the heat conduction of this new three-phase composite, wherein the reinforcements are the individual SWCNTs and the spherical nanotube agglomerates, as shown in Figure 5-2.

An effort is discussed to address the problem of CNT dispersion in Chapter 5. To this extent, two separate techniques are introduced to incorporate the nanotube agglomerates into the MCFEA developed in Chapter 4. The first one is a hybrid approach described in Section 5.1, which utilizes the 2-phase equivalent inclusion method presented in Section 4.1. The second technique expands the 2-phase EIM to the case of three phase one; the formulation is given in Section 5.2. The validity and the accuracy of these analytical approaches for the effective thermal conductivity (ETC) of the PNCs are examined in

Section 5.3 in the light of experimental measurements. The differences between the results predicted by these techniques and the experimental findings are discussed. It is also noted that both techniques make use of certain parameters pertinent to the nanotube agglomeration to account for the degree of dispersion. The influence of the agglomeration parameters on the ETC of PNCs are studied and discussed in Section 5.4.

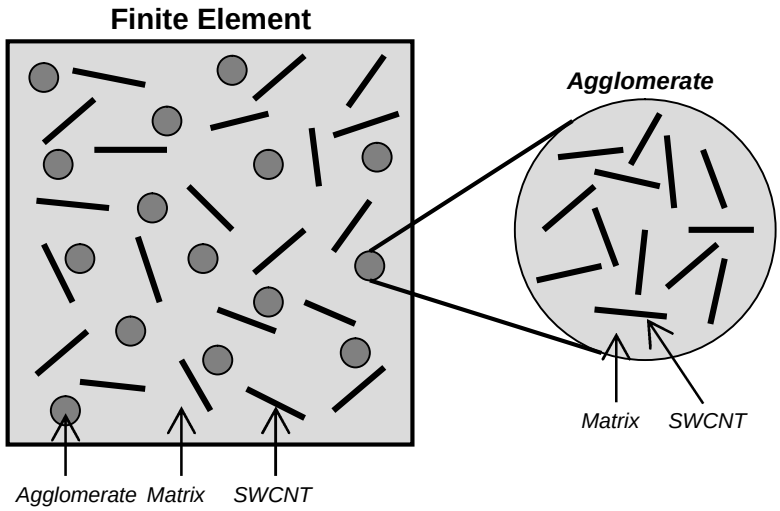

Figure 5-2. Schematic showing the multiple inhomogeneities embedded in the matrix in a finite element, comprising matrix, individual SWCNTs and spherical nanotube agglomerates.

5.1. Two-Phase Hybrid Model

A vast number of studies in literature have reported clearly that in order to achieve the desired properties of the polymer nanocomposites, it is important to have homogeneous SWCNT dispersion in the matrix. As stated in Chapter 3, there are numerous amounts of nanotube concentrated regions present throughout the material. The evidence has been provided on the existence of SWCNT bundles, agglomerates and clusters based on the actual image analysis of the polymer nanocomposites. To this end, there exists no model

in the literature for determining the thermal conductivity of PNC that does consider the influence of nanotube agglomeration. Nevertheless, Shi et al. [122] introduced a novel micromechanics model to investigate the effective elastic stiffness of PNCs, accounting for the effects of the extensively observed agglomeration of the SWCNTs. Spanos and Kontsos [123] also utilized this approach in their multiscale stochastic finite element method to predict the mechanical properties of PNCs with structural heterogeneities. They performed the local homogenization using the 2-phase EIM via a hybrid approach.

In this section, a similar approach is followed in the case of local thermal conductivity homogenization within a finite element. Each finite element of the coupon is considered to include a certain amount of SWCNTs by volume in their domain. The carbon nanotubes are regarded to exist in the body in two forms; individual SWCNTs, and nanotube agglomerates. These agglomerates as inclusions are assumed to have spherical shapes; containing highly concentrated, randomly distributed, straight SWCNTs, and a polymer as a matrix material. The individual SWCNTs in the matrix are also assumed to be straight, randomly oriented, and homogeneously dispersed. This matrix that is reinforced only with the individual SWCNTs is to be referred as the ‘hybrid matrix’ as of this point. Then, the spherical agglomerates are, as well, considered to be randomly distributed in this hybrid matrix. The structure of the composite domain, which is represented as the finite element (FE) is shown in Figure 5-3. The amount of SWCNTs in the agglomerates and in the hybrid matrix varies, depending on the degree of agglomeration. The 2-phase EIM is applied to each stage of the calculations. This

procedure is explained in depth in Section 4.1. The following formulation develops the necessary agglomeration parameters used in the hybrid model.

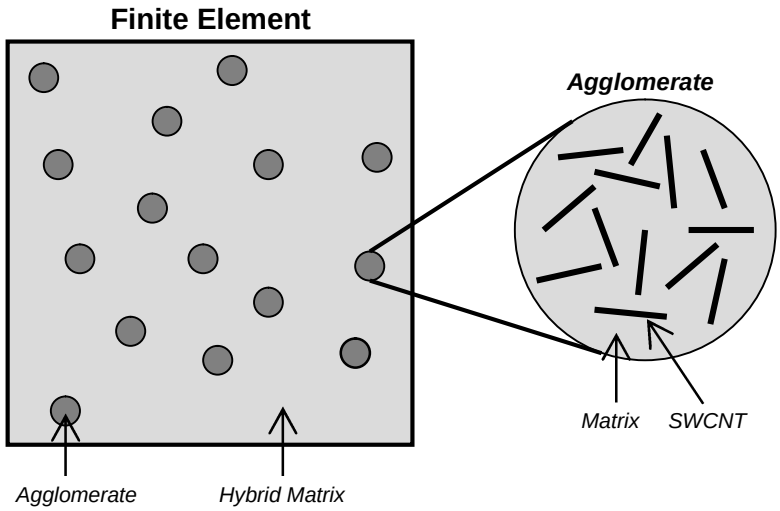

Figure 5-3. The material structure in a finite element used in the MSFEA, comprising a hybrid matrix and spherical inclusions.

Consider the total volume of the finite element, V^{FE} is composed of the volume of the hybrid matrix, V_{hybrid}^{FE} and the volume occupied by the agglomerates, $V_{agglomerates}^{FE}$, such that

$$V^{FE} = V_{hybrid}^{FE} + V_{agglomerates}^{FE}. \qquad (5\text{-}1)$$

From equation (5-1), the volume fraction of the spherical agglomerates in each FE can be introduced and the agglomeration index, ξ, given by the equation

$$\xi = \frac{V_{agglomerates}^{FE}}{V^{FE}}. \qquad (5\text{-}2)$$

One can conclude that as ξ approaches to 1, the entire volume of the FE becomes filled more with the spherical agglomerates and since nanotubes are homogeneously dispersed in the agglomerates, they become more homogeneously dispersed in the FE.

Furthermore, the total volume of the single-walled carbon nanotubes, V^{NT} in the finite element can be divided as

$$V^{NT} = V_{hybrid}^{NT} + V_{agglomerates}^{NT}, \qquad (5\text{-}3)$$

where V_{hybrid}^{NT} and $V_{agglomerates}^{NT}$ are the volumes of SWCNT dispersed in the modified matrix and in the spherical agglomerations, respectively. From equation (5-3), the dispersion index, ζ can be defined by the equation

$$\zeta = \frac{V_{agglomerates}^{NT}}{V^{NT}}. \qquad (5\text{-}4)$$

The parameter ζ denotes the volume ratio of the SWCNTs dispersed in the spherical agglomerates in the total volume of the SWCNTs. Equation suggests that when ζ is equal to 1, all the nanotubes are located in the spheres. Further, in the case of $\zeta > \xi$, the spatial dispersion of CNTs is more heterogeneous in the PNC and when $\zeta = \xi$, all nanotubes are uniformly dispersed.

It is worth defining the local volume fraction of the SWCNTs in each FE, υ_{SWCNT}^{FE}, since it is one of the most crucial input parameters in the proposed approach, expressed in equation (5-5).

$$\upsilon_{SWCNT}^{FE} = \frac{V^{NT}}{V^{FE}}. \qquad (5\text{-}5)$$

Moreover, due to the fact that the FE as a domain consists of spherical agglomerations embedded in a hybrid matrix, the volume fractions of SWCNTs in the agglomerates and in the hybrid matrix become essential in the analysis of the thermal conductivity of the PNC. Equations (5-6) and (5-7) give the expressions for the SWCNT volume fraction in the agglomerates and in the hybrid matrix, respectively. That is,

$$\upsilon f2 = \frac{V_{agglomerates}^{NT}}{V_{agglomerates}^{FE}} = \upsilon_{SWCNT}^{FE}\frac{\zeta}{\xi}, \qquad (5\text{-}6)$$

and

$$\upsilon f1 = \frac{V_{hybrid}^{NT}}{V_{hybrid}^{FE}} = \upsilon_{SWCNT}^{FE}\frac{1-\zeta}{1-\xi}. \qquad (5\text{-}7)$$

Several researches have reported that number of agglomerates in a nanocomposite increases as the number of nanotubes in the composite increases [128], [184], [185]. That is, when υ_{SWCNT}^{FE} increases, ξ increases, however the relation between two has not been established yet. Further, another issue to be considered is that whether there is a threshold υ_{SWCNT}^{FE}, at which the agglomerations begin to form, which is to be referred as 'agglomeration threshold' (agg_th) in this disseration.

In the literature, even though experimental analyses have shown the existence of nanotube agglomerates, a small number of studies have quantified the CNT volume fraction within an agglomerate [186]. In the course of investigating the effects of the agglomeration and dispersion of SWCNTs in polymers on thermal conductivity of PNCs, the proposed MCFEA takes into account the nanotube volume fraction threshold value, ‘agg_th’ and minimum nanotube volume fraction in the agglomerates, ‘vf2_min’. The significance of vf2_min is that the nanotube volume fraction within an agglomerate never drops below a certain value, and increases linearly towards the value of one as the total nanotube volume fraction increases in the finite element. The parametric studies are carried out over these two variables in the following sections.

5.2. Multi-Phase Model

This section focuses on improving the micromechanics homogenization model to predict the average thermal conductivity of the finite element, shown previously in Figure 5-2. The extension of the 2-phase EIM to the case of multiphase composites is introduced, which effectively called as 3-phase EIM. The significance of the 3-phase EIM model lies in its strength of simultaneously taking into account the interaction between the multiple phases. The phases are considered to be ellipsoidal in shape, thus they can be used to approximate a wide range of nano/micro structural geometries. In the case of SWCNT agglomeration, there exist two separate reinforcing phases embedded in the matrix; one being the individual SWCNTs, and the other being the agglomerates, which are compound of the matrix and extremely high concentration of SWCNTs.

Figure 5-4 represents a unit volume element with domain D, consisting of a matrix and N types of reinforcing spherical inclusions whose domains are denoted by Ω_n (n = 1 → N). Thermal conductivities of the matrix and the phases are assumed to be isotropic and are given by $K^m\delta_{ij}$ and $K^n\delta_{ij}$, respectively.

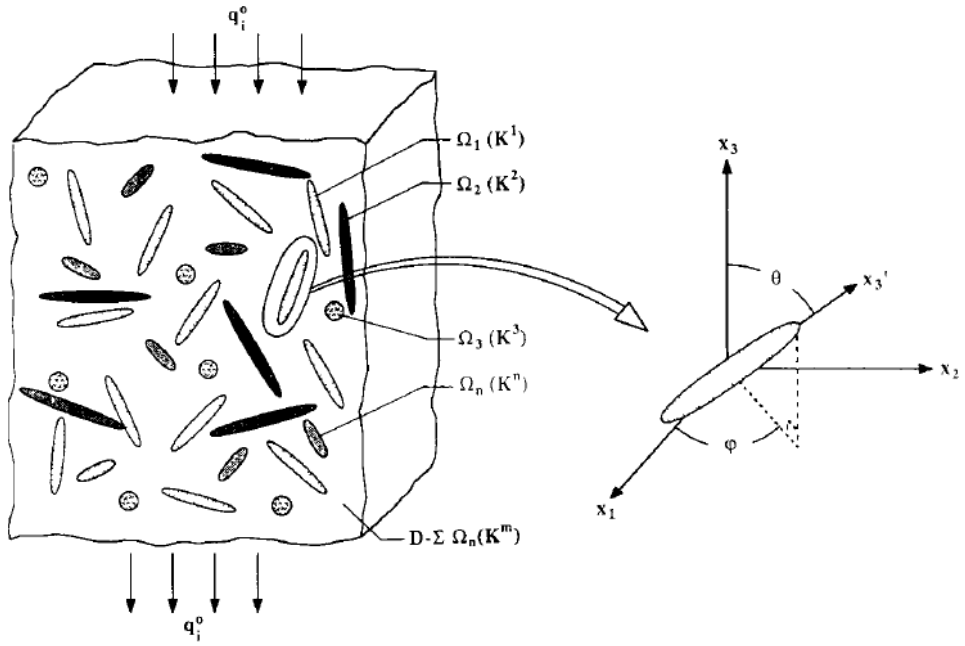

Figure 5-4. The analytical model for multiphase composite containing N types of mis-oriented fibers embedded in the matrix and definition of the coordinate system used [187].

The effective thermal conductivity of the composite, K_{ij}, is defined by the equation

$$\left\langle q_i^t \right\rangle = -K_{ij} \left\langle T,_j^t \right\rangle, \qquad (5\text{-}8)$$

where q_i^t and $T,_j^t$ are the total (uniform + disturbance) heat flux and temperature gradient respectively, and $\langle\ \rangle$ denotes averaging over the entire domain D. The composite is assumed to be statistically homogeneous, and thus the volume average over a suitable representative volume can be used in place of an entire structure. The quantities

in equation (5-8) can be expressed in terms of their volume averages over the N phases as

$$\left\langle q_i^t \right\rangle = \left[1 - \sum_{n=1}^{N} f_n \right] \left\langle q_i^t \right\rangle_m + \sum_{n=1}^{N} f_n \left\langle q_i^t \right\rangle_n , \qquad (5\text{-}9)$$

and

$$\left\langle T,_i^t \right\rangle = \left[1 - \sum_{n=1}^{N} f_n \right] \left\langle T,_i^t \right\rangle_m + \sum_{n=1}^{N} f_n \left\langle T,_i^t \right\rangle_n , \qquad (5\text{-}10)$$

where $f_n \langle . \rangle_n = \frac{1}{V_D} \int_{\Omega_n} . \, dV$, V_D is the volume of the entire composite, f_n is the volume fraction of the n-th phase (n = 1 → N), and the subscripts m and n refer to the matrix and the n-th phase inclusion, respectively. By expressing the heat flux in each domain in terms of the corresponding thermal conductivity and gradient through Fourier's law of conduction, the effective thermal conductivity of the composite can be recast in the form

$$K_{ij} \left\langle T,_i^t \right\rangle = K^m \delta_{ij} \left\langle T,_i^t \right\rangle + \sum_{n=1}^{N} (K^n - K^m) \delta_{ij} \frac{1}{V_D} \int_{\Omega_n} T,_i^t \, dV , \qquad (5\text{-}11)$$

where $T,_i^t$ is the total thermal gradient.

To determine the quantities in equation (5-11), the equivalent inclusion method (EIM) for steady state heat conduction, explained in the previous chapter, is extended to multiphase composites with mis-oriented inclusions. The EIM is applied in local coordinates to a representative fiber of each type yields the N equations as

$$\begin{aligned} q_i^{0\,\prime} + q_i^{n\,\prime} &= K^f \delta_{ij} (T,_j^{0\,\prime} + \tilde{T},_j{}' + T,_j^{cn\,\prime}) \\ &= K^m \delta_{ij} (T,_j^{0\,\prime} + \tilde{T},_j{}' + T,_j^{cn\,\prime} - T,_j^{*n\,\prime}) \qquad in \Omega_n, \quad n = 1 \to N. \end{aligned} \qquad (5\text{-}12)$$

The first right-hand side term of equation (5-12) represents the heat flux in the actual inhomogeneity while the second one represents the heat flux in the equivalent inclusion. The relation between the thermal gradient disturbed by the existence of a single inhomogeneity $T_{,j}^{cn}{}'$ and the fictitious 'eigen thermal gradient' $T_{,j}^{*n}{}'$ is expressed as

$$T_{,j}^{cn}{}' = S_{ij}^{n} T_{,j}^{*n}{}', \qquad (5\text{-}13)$$

where S_{ij}^{n} are functions of the inclusion geometry. The S_{ij}^{n} expressions for various ellipsoidal inclusions are given in Appendix A.

Equations (5-12) and (5-13) can be rearranged to solve for $T_{,j}^{*n}{}'$ and $T_{,j}^{cn}{}'$ which then can be transformed to global coordinates by the use of second order transformation tensor X_{ij}^{n}, given by equation (4-14), and its inverse $X_{ij}^{n^{-1}}$. This yields

$$T_{,i}^{*n} = X_{ij}^{n}(K^{m} - K^{n})\delta_{jk} A_{kl}^{n^{-1}} X_{ln}^{n^{-1}}(T_{,n}^{0} + \tilde{T}_{,n}), \qquad (5\text{-}14)$$

and

$$T_{,i}^{cn} = X_{ij}^{n}(K^{m} - K^{n})\delta_{jp} S_{pk} A_{kl}^{n^{-1}} X_{ln}^{n^{-1}}(T_{,n}^{0} + \tilde{T}_{,n}), \qquad (5\text{-}15)$$

where

$$A_{jk}^{n} = (K^{n} - K^{m})\delta_{jl} S_{lk}^{n} + K^{m}\delta_{jk}. \qquad (5\text{-}16)$$

The average disturbance of temperature gradient in the matrix is defined by

$$\tilde{T}_{,i} = -\sum_{n=1}^{N} \frac{1}{V_D} \int_{\Omega_n} (T_{,i}^{cn} - T_{,i}^{*n}) dv \qquad (5\text{-}17)$$

The volume average of the total temperature gradient over each phase of the composite (matrix and inclusions, respectively) can be expressed as

$$\left\langle T_{,i}^{\,t} \right\rangle_m = T_{,i}^{\,0} + \tilde{T}_{,i}\,, \tag{5-18}$$

and

$$\left\langle T_{,i}^{\,t} \right\rangle_n = T_{,i}^{\,0} + \tilde{T}_{,i} + T_{,i}^{*n}\,. \tag{5-19}$$

The volume average of the total temperature gradient over the entire composite is then obtained as

$$\left\langle T_{,i}^{\,t} \right\rangle = \left[1 - \sum_{n=1}^{N} f_n\right]\left\langle T_{,i}^{\,t} \right\rangle_m + \sum_{n=1}^{N} f_n \left\langle T_{,i}^{\,t} \right\rangle_n = T_{,i}^{\,0} + \sum_{n=1}^{N} \frac{1}{V_D}\int_{\Omega_n} T_{,i}^{*n}\, dv\,. \tag{5-20}$$

The volume average of the quantities $T_{,i}^{cn}$ and $T_{,i}^{*n}$ can be evaluated over all possible orientations with the use of equation (5-17) and can be recast in the form

$$\left\langle T_{,i}^{*n} \right\rangle_{\Omega_n} = \frac{1}{f_n V_D}\int_{\Omega_n} T_{,i}^{*n}\, dv = Q_i^{*n}(T_{,i}^{\,0} + \tilde{T}_{,i})\,, \tag{5-21}$$

and

$$\left\langle T_{,i}^{cn} \right\rangle_{\Omega_n} = \frac{1}{f_n V_D}\int_{\Omega_n} T_{,i}^{cn}\, dv = Q_i^{cn}(T_{,i}^{\,0} + \tilde{T}_{,i})\,. \tag{5-22}$$

Further, substituting equations (5-21) and (5-22) into equation (5-17) yields

$$\frac{1}{V_D}\int_{\Omega_n} T_{,i}^{*n} dv = f_n \frac{Q_i^{*n}}{1 - \sum^{N} f_n (Q_i^{*n} - Q_i^{cn})} T_{,i}^{\,0}\,, \tag{5-23}$$

and

$$\frac{1}{V_D}\int_{\Omega_n} T_{,i}^{cn}\,dv = f_n \frac{Q_i^{cn}}{1-\sum^{N} f_n (Q_i^{*n} - Q_i^{cn})} T_{,i}^{0} \,. \qquad (5\text{-}24)$$

The quantities Q_i^{*n} and Q_i^{cn} are dependent on the assumed distribution functions of the inhomogeneities in the composite. In the special case of an isotropic ellipsoidal inclusion ($S_{11} = S_{22} \neq S_{33}$) with completely random distributions, the expressions are given by the equations

$$Q_i^{*n} = \frac{K^m - K^n}{3}\left[\frac{2}{(K^n - K^m)S_{11} + K^m} + \frac{1}{(K^n - K^m)S_{33} + K^m}\right], \qquad (5\text{-}25)$$

and

$$Q_i^{cn} = \frac{K^m - K^n}{3}\left[\frac{2S_{11}}{(K^n - K^m)S_{11} + K^m} + \frac{S_{33}}{(K^n - K^m)S_{33} + K^m}\right]. \qquad (5\text{-}26)$$

Therefore, the effective thermal conductivity of the composite, K_{ij} can be computed from the equation (5-11), (5-23) and (5-24). Considering all N types of inhomogeneities are isotropic, K_{ij} can be found by the equation

$$K_{ii} = K^m + \sum_{n=1}^{N} f_n (K^n - K^m) \frac{1 + Q_i^{cn}}{1 + \sum^{N} f_m Q_i^{cm}} \,. \qquad (5\text{-}27)$$

For the case in which carbon nanotubes form agglomerations, the composite comprises three phases; matrix as the base material and two reinforcing phases, that is individual nanotubes and nanotube agglomerates. Therefore, in equation (5-27), K^m, K^1 and K^2 denote the thermal conductivities of the matrix, the individual SWCNTs, and the

agglomerates, respectively. and the quantities f_1 and f_2 are the volume fractions of the individual SWCNTs and the agglomerates, respectively. The degree of the nanotube dispersion is determined by the agglomeration parameters, agg_th and vf2_min, introduced in Section 5.1.

5.3. Comparison of Homogenization Models

In the preceding two sections, two distinct analytical micromechanics approaches have been introduced for modeling the agglomeration of single-walled carbon nanotubes (SWCNTs) in the polymer nanocomposites (PNCs). This section of the dissertation makes a comparison of these two techniques in the pursuit of capturing the effective thermal conductivity of PNCs utilizing the proposed Monte Carlo Finite Element Approach (MCFEA). Their benefits and weaknesses are discussed, and the discrepancy between the models is shown. Limitations of the two-parameter agglomeration model are highlighted.

Section 5.1 introduces a two parameter agglomeration model based on the work of Shi et al. [122] to account for the dispersion of the nanotubes. Their micromechanics model investigates the effective elastic stiffness of PNC, taking into account the effects of the observed agglomeration of the SWCNTs. The model was also adopted by Spanos and Kontsos [123] and was utilized in their multiscale stochastic finite element method to determine the mechanical properties of PNCs.

The micromechanics model presented in Section 5.1 employs the two-parameter agglomeration approach in conjunction with the Hatta-Taya 2-phase equivalent inclusion method (EIM) to calculate the thermal conductivity of a finite element with a certain local SWCNT content. The detailed formulation of the 2- phase EIM is explained in Section 4.1. For simplicity, the combination of these methods henceforth is to be called the “hybrid approach”. The model assumes that the SWCNTs are present in two forms within the matrix, one as individual nanotubes with certain aspect ratios, and the other as spherical agglomerates which contain high concentration of nanotubes. The 2-phase EIM scheme is used to compute the thermal conductivity of the agglomerates, then the same scheme is used to calculate the thermal conductivity of the so-called “hybrid matrix” which is composed of the individual CNTs and the neat matrix. Finally, the 2-phase EIM is again utilized to obtain the final thermal conductivity of a finite element (FE). Subsequently, the MCFEA, explained in Chapter 4, is employed to acquire the effective thermal conductivity of the composite.

The second method described in Section 5.2 is the extension of the equivalent inclusion method (EIM) in steady state heat conduction, first developed for misoriented single reinforcing phase by Hatta and Taya [120]. The same authors then extended the EIM for multiphase composites but only the case for aligned fibers. Dunn et al. [187] gives inside on the use of the equivalent inclusion method to consider multiple reinforcing phases, each in unique ellipsoidal shapes and with random distributions. In the case of the problem described here, two separate reinforcing phases exist in the matrix; that is the individual ellipsoidal SWCNTs and the spherical agglomeration. Since the

nanocomposite is composed of three phases, to make a distinction this method is to be addressed as the “3-phase EIM” hereafter. The thermal conductivity of the spherical agglomerations is obtained by the use of the 2-phase EIM.

The superiority of the 3-phase EIM approach over the hybrid approach relates to the fact that the 3-phase EIM takes into account the interaction between the reinforcing phases and regards the entire composite as one. In juxtaposition, the hybrid approach isolates the reinforcing phases and treats them separately which causes the phases to lose the communication and leads to inaccuracy. One can argue that the only limiting aspect of the 3-phase EIM is its more complicated analytical derivation. However, in terms of numerical computational time, it requires much fewer coding lines and subroutines, which result in lesser computational time.

It is also noted that both of the agglomeration models proposed in Sections 5.1 and 5.2 assume that the SWCNTs are straight with large aspect ratios. Both the individual SWCNTs and the spherical agglomerates are poorly distributed and poorly dispersed within the matrix. Moreover, both the inclusions are assumed to be perfectly bonded with the polymer matrix. Figure 5-5 and Figure 5-6 show the schematics of the methodologies regarding the assumed nano-structural formation in a finite element, by the hybrid approach and 3-phase EIM approach, respectively.

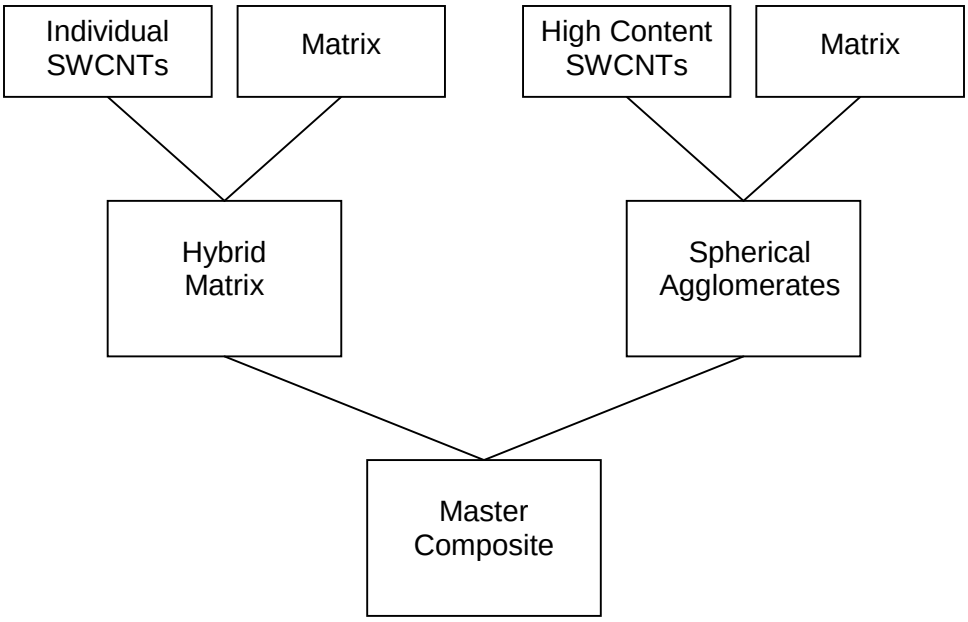

Figure 5-5. Schematic representation of the nano-structural formation in the 'Hybrid Approach'.

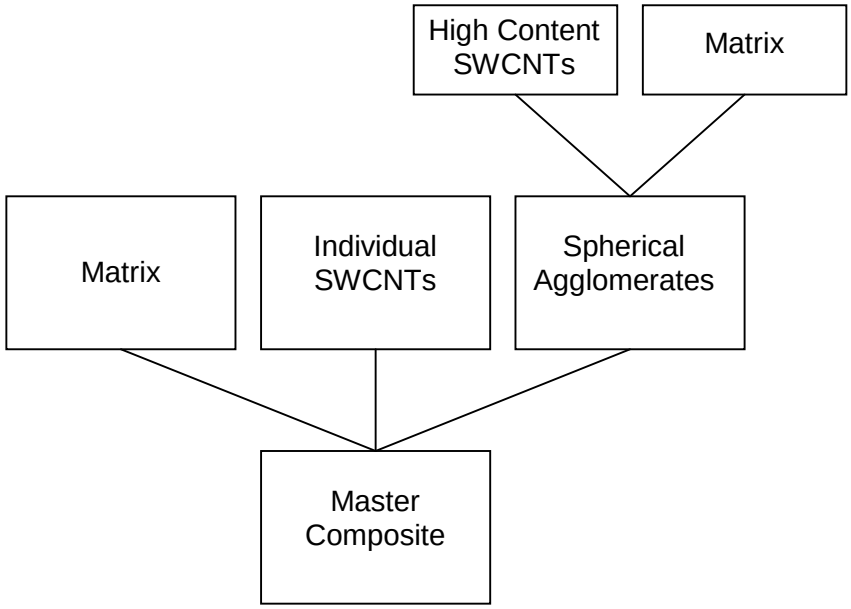

Figure 5-6. Schematic representation of the nano-structural formation in the '3-phase EIM'.

The comparison of the hybrid approach and 3-phase EIM is shown in Figure 5-7 alongside the results obtained by the well-known Hatta-Taya method and by MCFEA with no agglomeration developed in the previous work. The variation of the effective

thermal conductivities of the composite are plotted with respect to the mean single-walled carbon nanotube volume fraction in the composite up to 40 percent in volume to keep the simulation within reasonable limits. The variations are plotted using 500 Monte Carlo realizations and 400 finite elements with SWCNT aspect ratio of 150. The agglomeration parameters agg_th and vf2_min are chosen as 0.2 and 0.7, respectively.

One can readily notice the discrepancy between the two agglomeration models especially for the nanotube volume fraction over 10 percent. Close examination reveals that this disparity is due to the difference in the methodology that the two models follow, particularly the calculation of the volume fractions of the individual SWCNTs within the matrix.

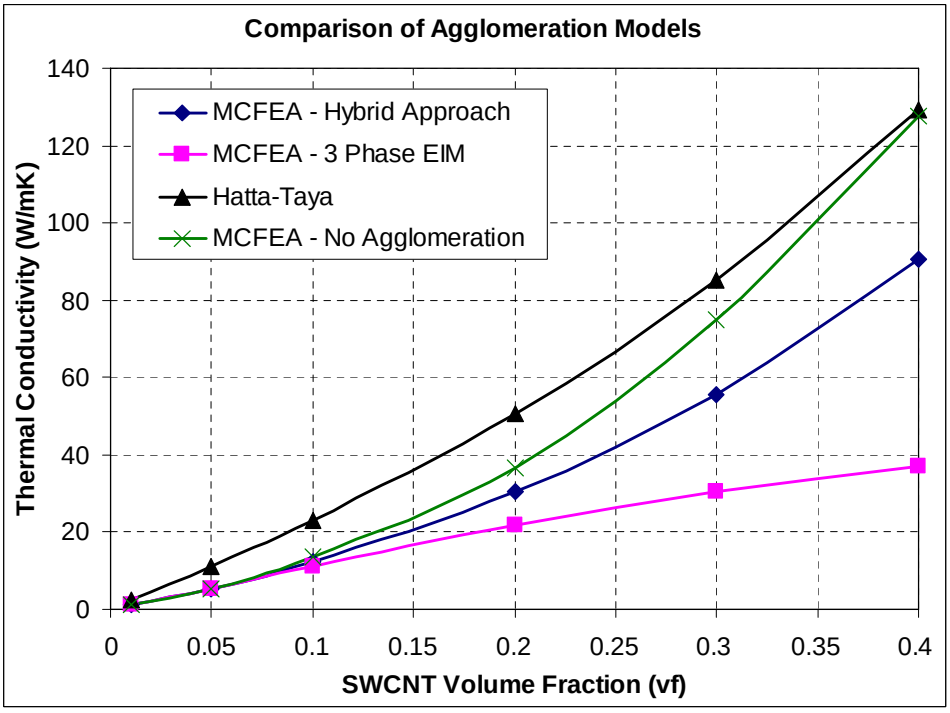

Figure 5-7. Comparison of the hybrid approach and 3-phase EIM

In the hybrid approach, the spherical agglomerations are mixed into a so-called hybrid matrix which has higher thermal conductivity than a neat polymer. It is due to the fact that the hybrid matrix is already a composite itself, reinforced with SWCNTs. On the other hand, in 3-phase equivalent inclusion method, the agglomerates and the individual SWCNTs are added as two separate phases directly into the matrix with poor thermal conductivity. While the volume fraction of the spherical inclusions (vf2) is identically defined, the volume fraction of the individual nanotubes (vf1) has different expressions.

$$vf1\big|_{hybrid} \equiv f1 = \frac{V^{NT} - V^{NT}_{agglomerates}}{V^{FE} - V^{FE}_{agglomerates}}, \qquad (5\text{-}28)$$

and

$$vf1\big|_{3phEIM} \equiv f1 = \frac{V^{NT} - V^{NT}_{agglomerates}}{V^{FE}}. \qquad (5\text{-}29)$$

The equations give the expressions for vf1s that each model uses in their formulation, the hybrid approach and the 3-phase EIM, respectively. Note that the equation (5-28) is practically the same as equation (5-7) in Section 5.1.Since the hybrid approach isolates the reinforcing phases, in the expression (5-28) to calculate the volume fraction of SWCNTs in the matrix, the volume of the individual nanotubes present in the matrix is divided by the volume of the matrix only, which excludes the volume of the spherical inclusions from the total finite element volume. At this point, it is convenient to remind that the MCFEA proposed in this dissertation assumes that the agglomeration content in a material region, i.e., a finite element, increases as the local SWCNT content increases. This causes a reduction of the effective matrix volume and results in a relative increase in

the volume fraction of the individual SWCNTs in the matrix. However, the 3-phase EIM considers the system as a whole when computing the volume fractions of each inclusion.

Figure 5-8 shows the corresponding variations in vf1 values in the FE. The values are plotted against the local nanotube volume fractions up to the physical limit of 0.8. It can be deduced from the graph that the divergence begins at early local nanotube volume fractions (vf), and increases greatly for the higher vfs. The significance of this deviation emerges in the calculation of the local thermal conductivity of the finite element. Since the 3-phase EIM uses the pristine matrix as the base material, its thermal conductivity remains constant during the computations. However, the hybrid approach uses the already nanotube reinforced hybrid matrix. The effective thermal conductivity of the hybrid matrix is presented in Figure 5-9.

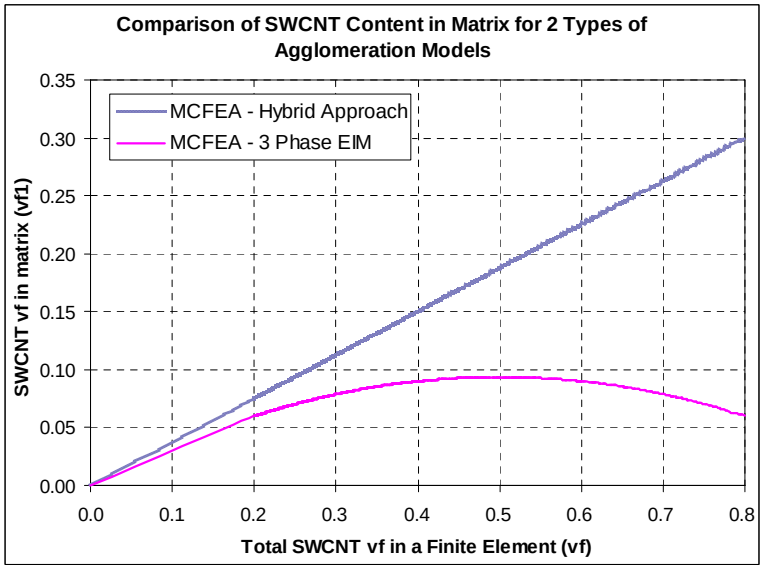

Figure 5-8. Variation of the individual SWCNT volume fraction in the matrix w.r.t the local nanotube volume fraction in a finite element used in the agglomeration models.

Figure 5-9 provides useful evidence as to why the effective thermal conductivity of the composite in Figure 5-7 obtained by the hybrid approach deviates from the one obtained by the 3-phase EIM. Experimental measurements show that the behavior of the thermal conductivity of SWCNT composites follows a similar trend with the ones predicted by the MCFEA with 3-phase equivalent inclusion method. To illustrate this tendency, the experimental values measured by Xu et al. [97] are presented in Figure 5-10. Even though the measured values fall considerably below the computed ones, the similarity of the behavior of the two curves is indisputable. Based on this fact, the 3-phase EIM is chosen as the preferred micromechanics technique in the MCFEA developed in this dissertation. The discrepancy between the computed and the experimental thermal conductivity values of the composites is discussed in the following sections.

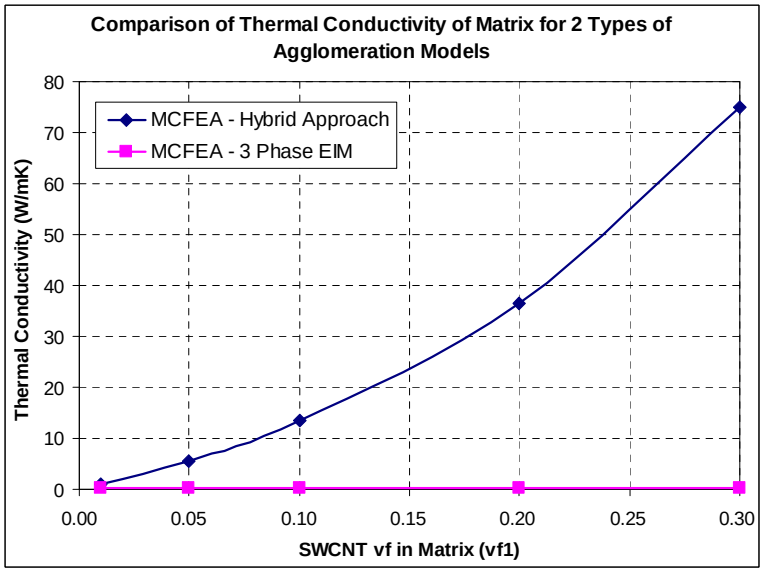

Figure 5-9. The effective thermal conductivity of the hybrid matrix used in the hybrid approach. The thermal conductivity of the matrix used in 3-phase EIM remains at the value of the neat epoxy, 0.188 W/mK (square dots).

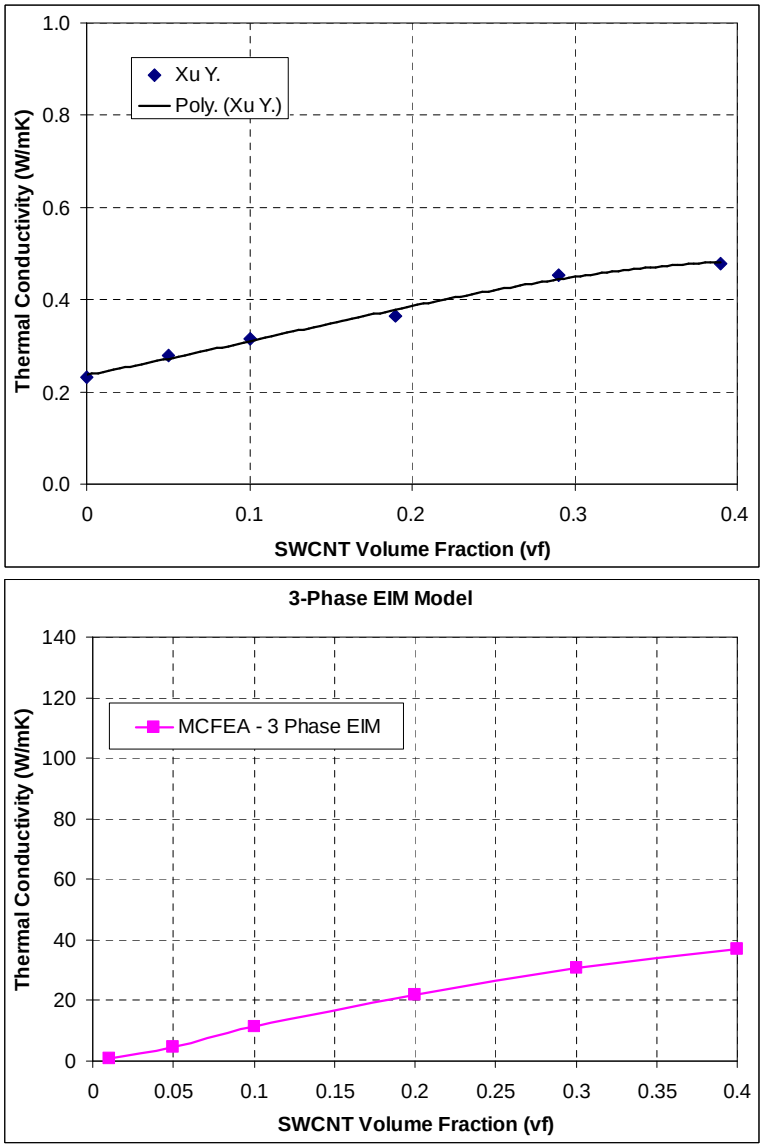

Figure 5-10. Tendancies of the thermal conductivity of SWCNT-composites; **Top** – experimentally measured at room temperature by Xu et al., [97], **Bottom** – results by MCFEA via 3-phase EIM.

5.4. Management of Dispersion Parameters

Previous sections in this chapter describe the methods used to include the nanotube agglomerates into the proposed Monte Carlo Finite Element Approach (MCFEA) to account for the distribution characteristics. However, quantification of the quality of the dispersion of the single-walled carbon nanotubes (SWCNTs) is essential in the polymer nanocomposites (PNCs). To this end, this section studies the influences of the agglomeration parameters used in the methods on the effective thermal conductivity of the PNCs. In particular, two parameters are considered, who are discussed in depth in Section 5.1. The first one is related to a threshold SWCNT volume fraction value below which the carbon nanotubes are dispersed well and they exist in the matrix as individuals. When the nanotube concentration reaches a certain level, they begin to form agglomerates. That threshold value is henceforth named as the “agglomeration threshold” value, which is denoted as “agg_th” in this dissertation. The second parameter relates to the SWCNT concentration within the agglomerates. It has been reported in the literature that when the nanotubes form clusters or agglomerates, the nanotube concentration in the agglomerates can vary from 60% to 90% depending on the surface quality of the carbon nanotubes and the overall SWCNT volume fraction of the PNC [188], [189]. Therefore one must take into account the minimum nanotube volume fraction in the agglomerates; which is denoted as “vf2_min”, where vf2 is the total SWCNT volume fraction in the agglomerates. The significance of vf2_min is that the nanotube volume fraction within an agglomerate never drops below a certain value, and increases linearly towards the value of one as the total nanotube volume fraction increases in the finite element. It is noted

that the nanotube agglomerates are assumed to be in spherical shape. Subsequently, extensive parametric studies are carried out over the influence of these two variables.

The effect of the agglomeration threshold (agg_th) on the effective thermal conductivity (ETC) of the polymer nanocomposite (PNC) is shown in Figure 5-11. The ETC variations are plotted for various values of the minimum SWCNT vf in agglomerates, vf2_min based on Weibull local nanotube volume fraction distribution. It can be deduced that the ETC value decreases as agg_th decreases. It is due to the fact that at low thresholds, higher amount of nanotubes form into spherical clusters, which have much poorer thermal conductivity than an individual SWCNT. One can further notice that the ETC values converge to the one with no agglomeration vis-à-vis perfect nanotube dispersion.

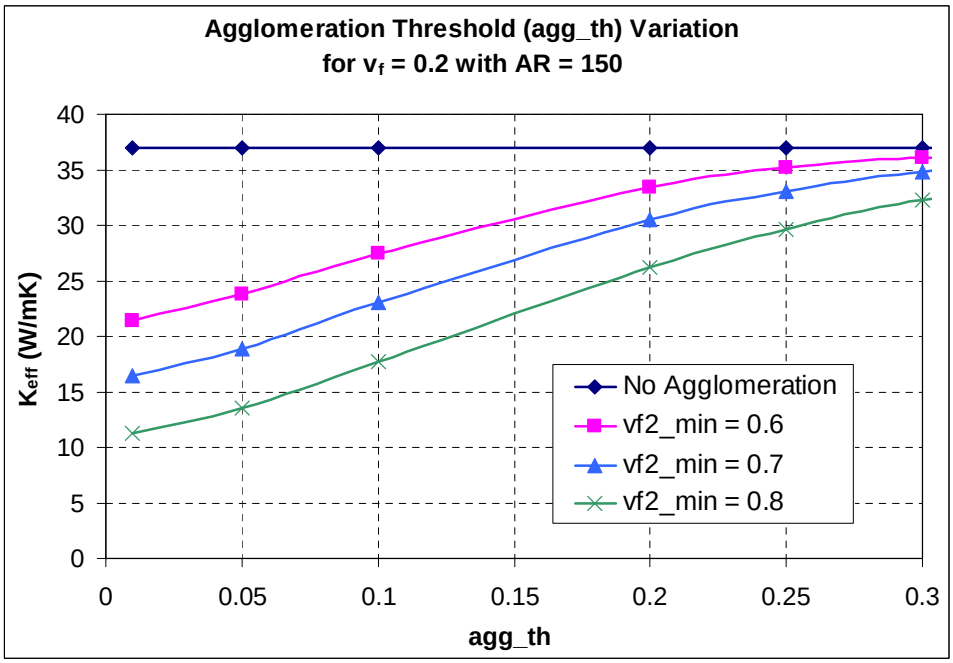

Figure 5-11. Variation of the effective thermal conductivity of PNC w.r.t. the agglomeration threshold agg_th, for various values of the minimum SWCNT vf in agglomerates vf2_min, based on Weibull local nanotube vf distribution.

Figure 5-12 shows the variation of the effective thermal conductivity with respect to the minimum SWCNT volume fraction in agglomerates, vf2_min. The results are produced using Weibull distribution under different agglomeration thresholds (agg_th). It can be seen that the ETC values decrease vastly as vf2_min increases. Since there are more nanotubes present within the agglomerates, the number of individual SWCNT is reduced in the matrix, which effectively results in poor ETC of the PNCs. To this extent, the effect of poor dispersion on the thermal conductivity of a PNC with 5 percent SWCNT loading is investigated.

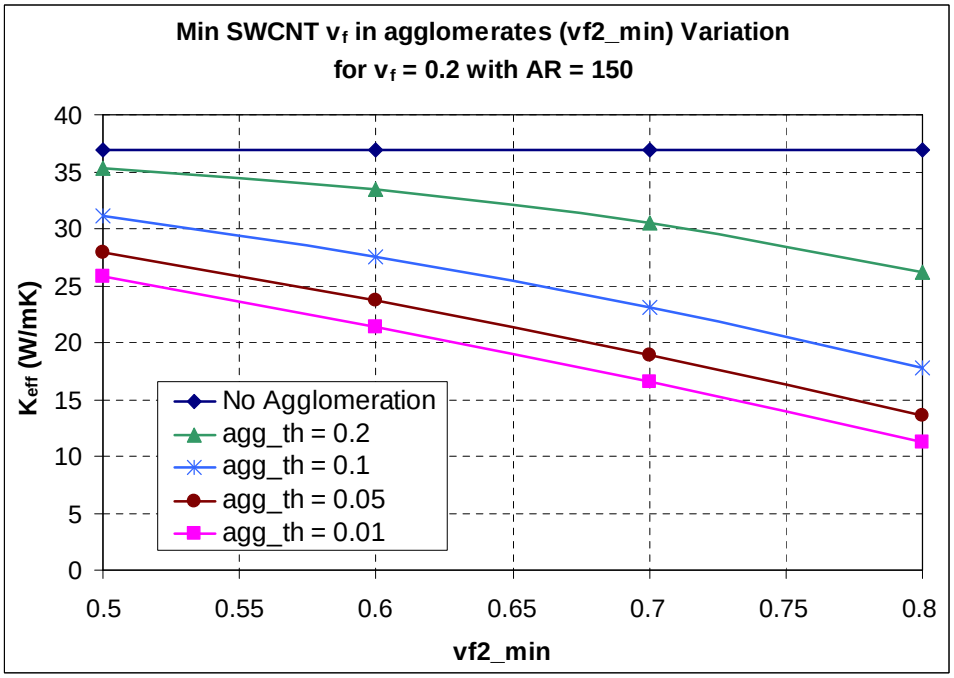

Figure 5-12. Variation of the effective thermal conductivity of PNC w.r.t. the minimum SWCNT vf in agglomerates vf2_min, for various values of the agglomeration threshold agg_th, based on Weibull local nanotube vf distribution.

Sample simulations are generated with the three nanotube volume distributions mentioned a priori, with various standard deviations, given in Figure 5-13. The agglomeration parameters are used agg_th = 0.01, vf2_min = 0.7.

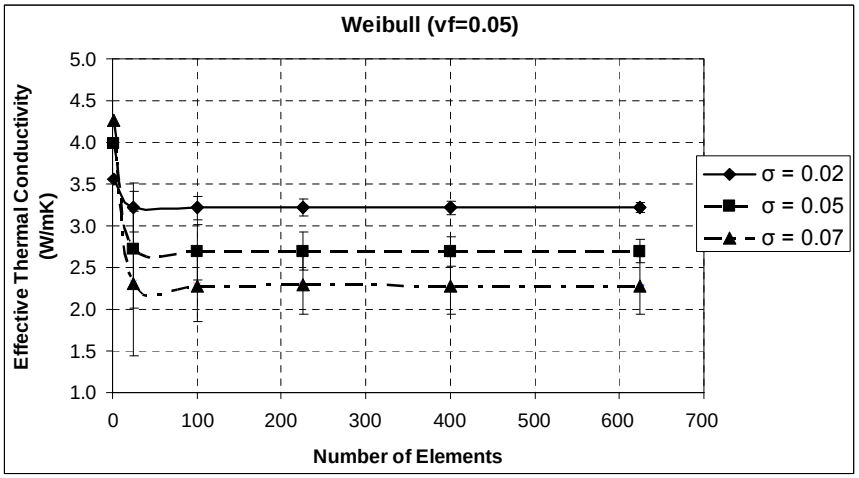

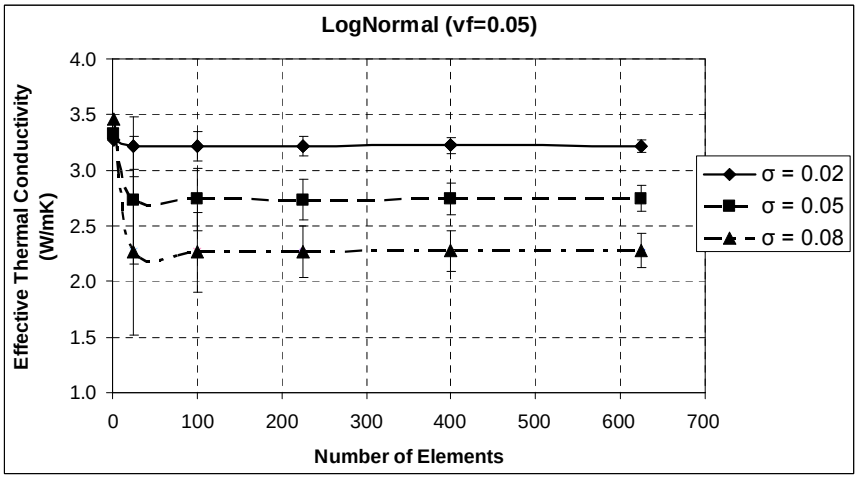

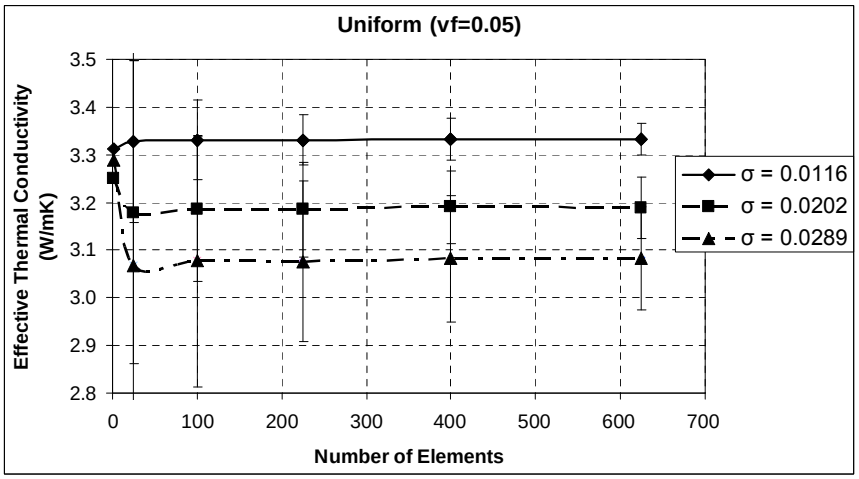

Figure 5-13. Variations of the effective thermal conductivities with plus and minus one standard deviation computed by the MCFEA w.r.t. the number of finite elements. Three different PDFs are used with 5% SWCNT vf with the selected standard deviations. The agglomeration parameters are agg_th = 0.01, vf2_min = 0.7.

The plots presented in Figure 5-13 are to be compared with the ones given in Figure 4-15 in Section 4.4. It is observed that the mean values are approximately three times reduced compared to the ones computed without taken into account the existence of the agglomerates.

Delving into the dispersion characterization of polymer nanocomposites, it is deemed useful to provide some information on the behavior of the agglomeration parameters introduced in the MCFEA developed in this dissertation. Derivation of these parameters is given in Section 5.1 in detail. In Figure 5-14 and Figure 5-15, the influence of the parameters pertaining to the dispersion of nanotubes is discussed.

As more agglomerates form, the fewer amounts of individual SWCNTs are left in the polymer matrix. It is known that agglomerates have poor thermal conductivity, thus the majority of the enhancement results from the individually dispersed nanotubes. Naturally, the individual nanotube volume fraction in the matrix (vf1) is dependent on the agglomeration parameters used in the analysis. Figure 5-14-(a) shows the vf1 variation with respect to the total nanotube content in a finite element. The threshold parameter (agg_th) is kept as 0.2, implying that CNTs are perfectly dispersed throughout the FE until the CNT content in a FE is 20 percent. After that threshold, the agglomerates form with high nanotube concentration. As discussed previously, minimum nanotube vf in an agglomerate (vf2_min) can be as low as 60 percent. Influence of the vf2_min (i.e., 0.6, 0.7, 0.8) is also shown in Figure 5-14-(a). If the agglomerates are assumed to contain higher CNT content, the number of individual CNTs in the pristine polymer reduces.

a)

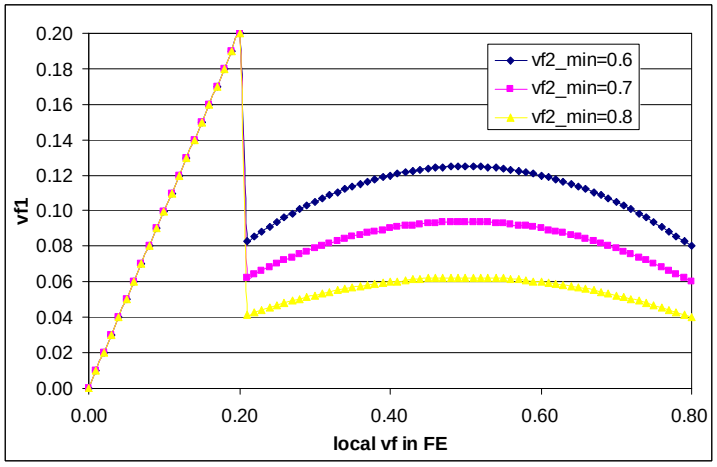

b)

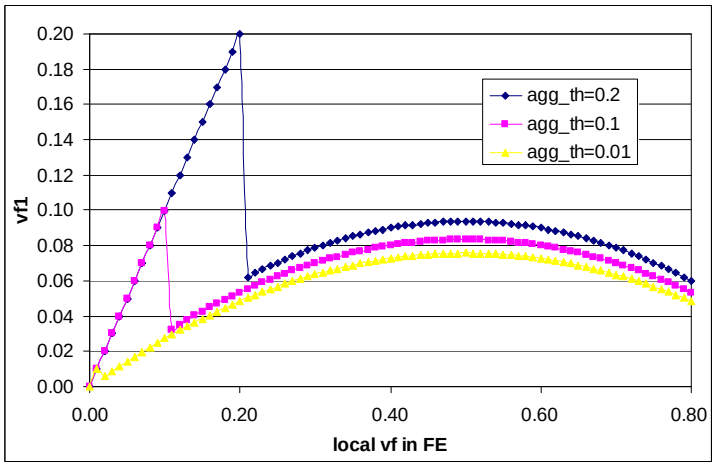

c)

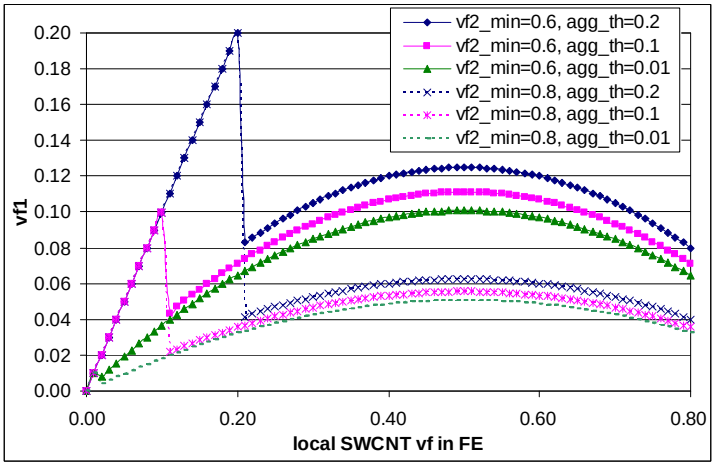

Figure 5-14. Effects of the agglomeration parameters agg_th and vf2_min on the individual SWCNT vf in the matrix (vf1) in a finite element.

a)

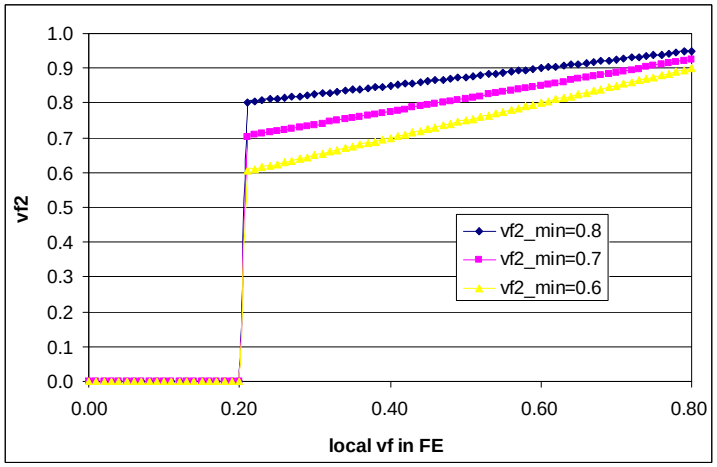

b)

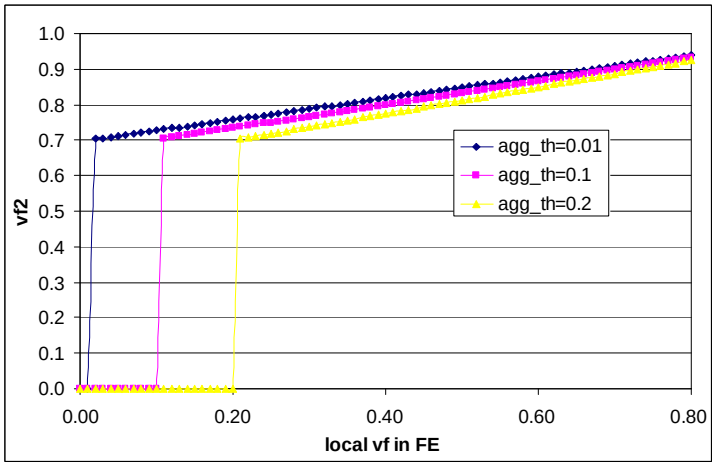

c)

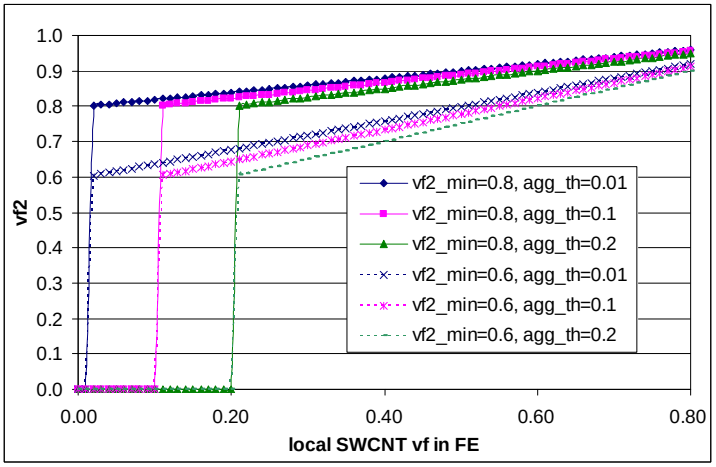

Figure 5-15. Effects of the agglomeration parameters agg_th and vf2_min on the SWCNT vf in the spherical agglomerates (vf2) in a finite element.

Similarly, Figure 5-14-b shows the vf1 versus local vf variation. The vf2_min value is kept constant at 0.7, meaning the agglomerates have at least 70 percent SWCNT ratio. Samples are generated with various threshold parameters, i.e. agg_th = 0.01, 0.1, 0.2. Additional examples are provided in Figure 5-14-c. Herein, an assumption is made for the nanotube volume fraction in the agglomerates (vf2) such that, as the CNT content increases in a finite element (local vf), vf2 also increases gradually, making the agglomerates denser. The maximum overall CNT vf in a FE is limited at 80 percent. In this context, a number of cases have been simulated and the results are presented in Figure 5-15. As it can clearly be seen from the figures, until the SWCNT volume fraction reaches the given agglomeration threshold value, vf2 stays zero. Immediately after nanotubes form, vf2 assumes the value of the prescribed vf2_min, and continues climbing. Theoretically, if the over all nanotube content in a FE is hundred percent, vf2 also becomes one.

Figure 5-16, Figure 5-17 and Figure 5-18 present the numerically computed mean values of the effective thermal conductivity of polymer nanocomposites, produced with various agglomeration parameters. The thermal conductivity values of the SWCNTs and the epoxy polymer are 2000 W/mK and 0.188 W/mK, respectively. For comparison, the figures also contain the resultant mean value of a PNC with perfect CNT dispersion, vis-à-vis no agglomeration. Further, the results obtained by the Hatta-Taya method are included, which assumes both perfect CNT dispersion and distribution. The MCFEA used for the analysis employs Weibull distribution for the nanotube volume fraction for all the cases stated.

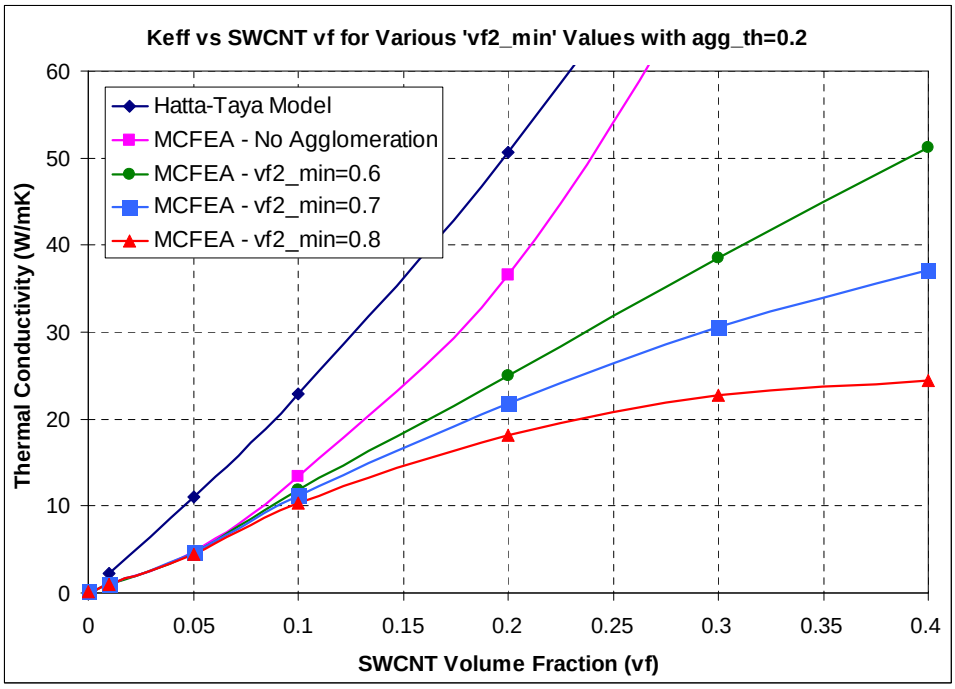

Figure 5-16. Effect of vf2_min on the effective thermal conductivity of PNC, produced by the MCFEA, based on Weibull distribution with agg_th = 0.2.

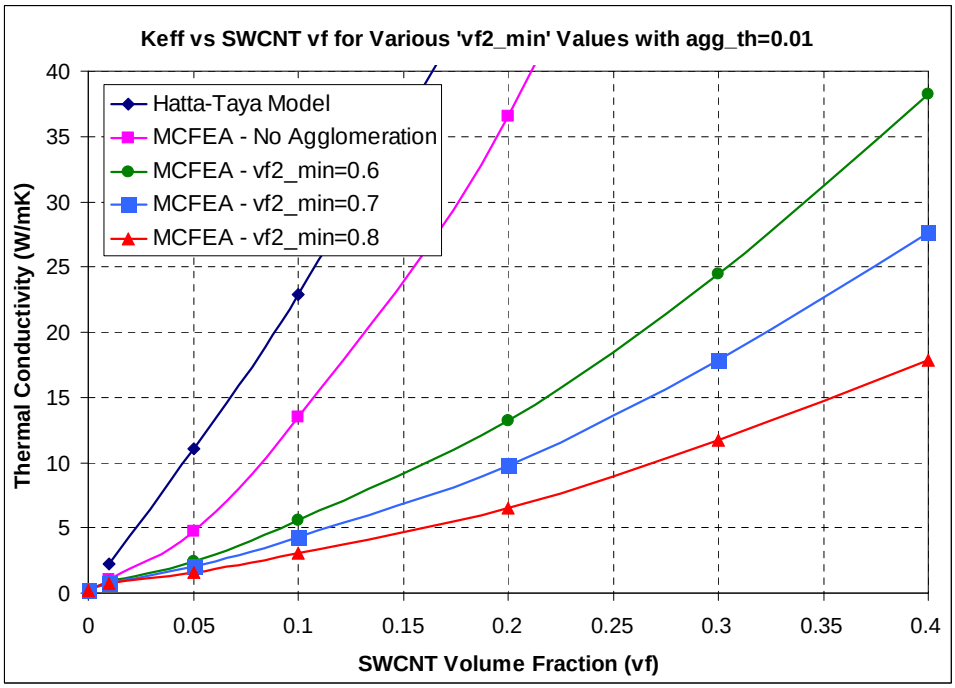

Figure 5-17. Effect of vf2_min on the effective thermal conductivity of PNC, produced by the MCFEA, based on Weibull distribution with agg_th = 0.01.

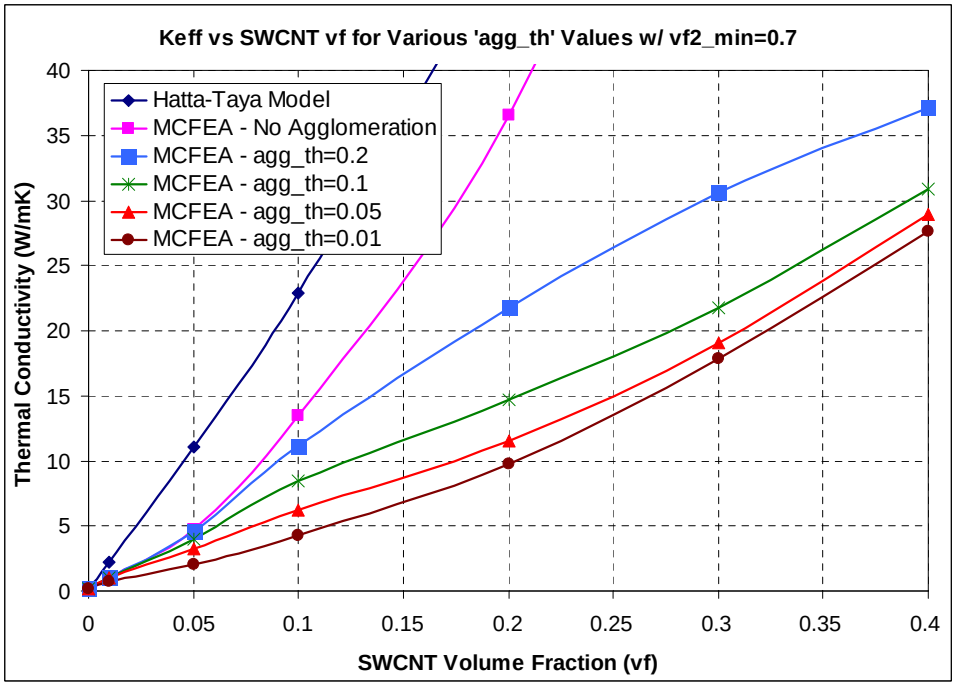

Figure 5-18. Effect of agg_th on the effective thermal conductivity of PNC, produced by the MCFEA, based on Weibull distribution with vf2_min = 0.7.

Chapter 6

Characterization of PNC Thermal Conductivity

The Monte Carlo Finite Element Approach (MCFEA) is proposed in this dissertation with the intention of providing a broad engineering applicability for simulating the thermal conductivity of polymer nanocomposites (PNCs). However, as the model involves a large number of variables, the robustness of the MCFEA is best demonstrated via comparison with the results of the pertinent experiments. In other words, the proposed approach must be able to replicate the experiments with a reasonable degree of accuracy, yet not requiring extensive amount of parameter calibration. Having presented and developed the theoretical and numerical bases in previous chapters, the reliability of the MCFEA is assessed in this chapter. Adequate modeling parameters are modified such that they are in agreement with the material properties, structures and the manufacturing methods used in each experiment. The polymer nanocomposites are, in essence, manufactured by mixing nanotubes in a polymer matrix. In this process nanotubes are first quantified by their weight percentage. Subsequently, the volume fraction is

calculated by converting the weight fraction w_f to the volume fraction v_f, specifically from the work of Pipes et al. [190].

$$v_f = \frac{w_f \rho_p}{w_f \rho_p + (1 - w_f)\rho_{NT}}, \quad (6\text{-}1)$$

where the indices "*p*" and "*NT*" denote polymer and nanotube, respectively, while ρ is the mass density. In the literature, while most researchers report the nanotube volume fraction value, a number of studies present the nanotube content as the weight percentage. However, w_f alone is not sufficient to calculate v_f values. To this end, the CNT mass density is also needed, which is defined by the total mass of carbon atoms in the nanotube. Therefore, the SWCNT density can be calculated by the equation

$$\rho_{NT} = \frac{4 N M_w}{\pi N_A d^2}, \quad (6\text{-}2)$$

where M_w is the atomic weight of carbon, N_A is the Avogadro's number, d is the diameter of the SWCNT, and N is the number of the carbon atoms per unit length given by the equation

$$N = \frac{4\Lambda}{3b}, \quad (6\text{-}3)$$

where

$$\Lambda = \sqrt{n^2 + nm + m^2}\ . \quad (6\text{-}4)$$

Further, the dependence of the nanotube diameter, d to the parameter Λ is expressed as

$$\Lambda = (d - v)\frac{\pi}{b\sqrt{3}}, \qquad (6\text{-}5)$$

where v is the measured equilibrium standoff distance between the nanotube and the adjacent medium, which is in the vicinity of 0.34 nm, as measured by Gao et al. [191]. In equation (6-3), b is the bond length between two carbon atoms, which is equal to 0.142 nm in case of SWCNT, and the parameters n and m denote the chiral vector of the SWCNT. The SWCNT mass density as a function of its diameter is shown in Figure 6-1.

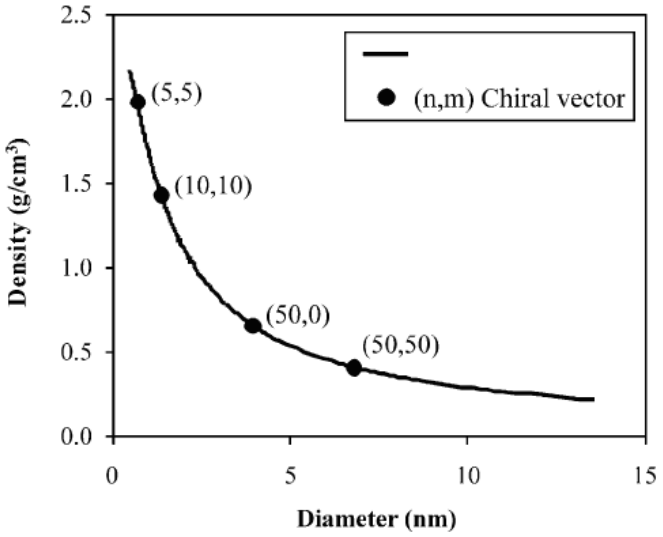

Figure 6-1. Variation of SWCNT density as a function of diameter. Reproduced from [190].

In the cases where only w_f is provided, the proposed MCFEA considers the reported weight fraction value as the expected value for the statistical distribution. Thus, the nanotube volume fraction of each finite element is computed using the weight fraction in conjunction with the corresponding SWCNT diameter based on the diameter distribution as presented in Section 3.4. Randomly assigned values of d are plugged in Equation (6-5) below, which is then used in Equation (6-3).

Similarly, variations of effective thermal conductivity of PNC as a function of thermal conductivity of matrix and SWCNT are also examined, as shown in Figure 6-2 and Figure 6-3, respectively.

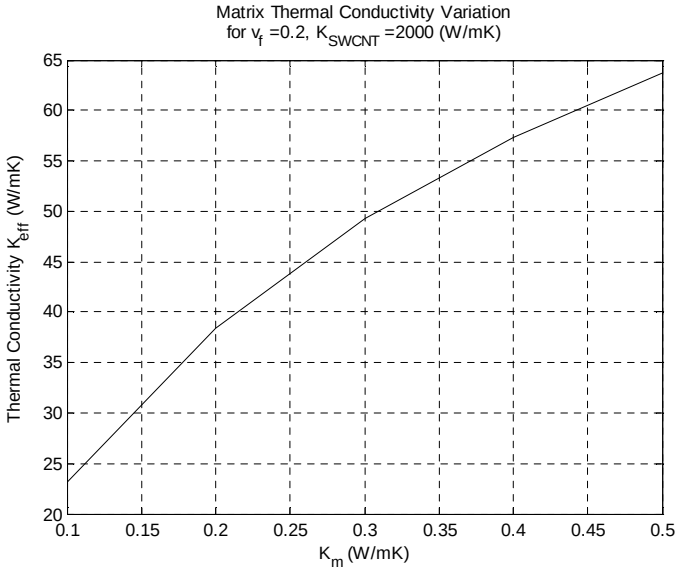

Figure 6-2. Variation of effective thermal conductivity of PNC w.r.t. thermal conductivity of matrix. Weibull NT v_f distribution is employed.

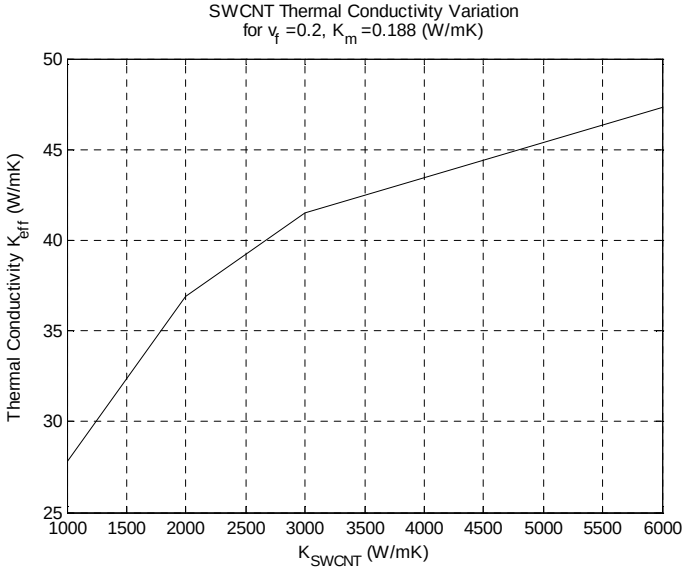

Figure 6-3. Variation of effective thermal conductivity of PNC w.r.t. thermal conductivity of SWCNT. Weibull NT v_f distribution is employed.

6.1. Interface Thermal Resistance

The preliminary simulations in Chapter 5 reveal that the enhancements observed by the experimental studies are significantly lower than the numerical simulation results. These unexpectedly low thermal conductivities are attributed to the thermal interface resistance R_K, which results from the weak van der Waals forces acting between the nanotube and the polymer matrix. Hence, poor thermal coupling exists, leading to significantly high thermal interfacial resistance. This phenomenon has been observed by numerous experimental studies on PNC thermal conductivity [93–98], [186]. Xue [117] developed a simple model that takes into account this thermal resistance. They provided an equivalent thermal conductivity for the nanotube, K_{NT}^{eq}, expressed as

$$K_{NT}^{eq} = \frac{K_{NT}}{1+\frac{2R_K K_{NT}}{L}} \ , \qquad (6\text{-}6)$$

where K_{NT} is the thermal conductivity of SWCNT, L is nanotube length and R_K is thermal interface resistance. Figure 6-4 shows the effect of the interfacial thermal resistance on the resultant thermal conductivity of nanotubes; such that an increase in R_K decreases K_{NT}^{eq} drastically. The data are plotted keeping the SWCNT thermal conductivity at 2000 W/mK, and the length of SWCNT at 165 nm, chosen out of L/D=150 and d=1.09 nm as reported in Section 3.4.

The interfacial thermal resistance between a SWCNT and epoxy was measured experimentally by Bryning et al. [114] for two kinds of composites processed with different methods. The outcomes show R_K = 0.24±0.13x10^{-8} m^{2}K/W and R_K = 2.6±0.9x10^{-8} m^{2}K/W for DMF-processed and surfactant-processed PNCs, resulting in K_{NT}^{eq} values, ranging from 25 to 75 W/mK, and 2 to 5 W/mK, respectively.

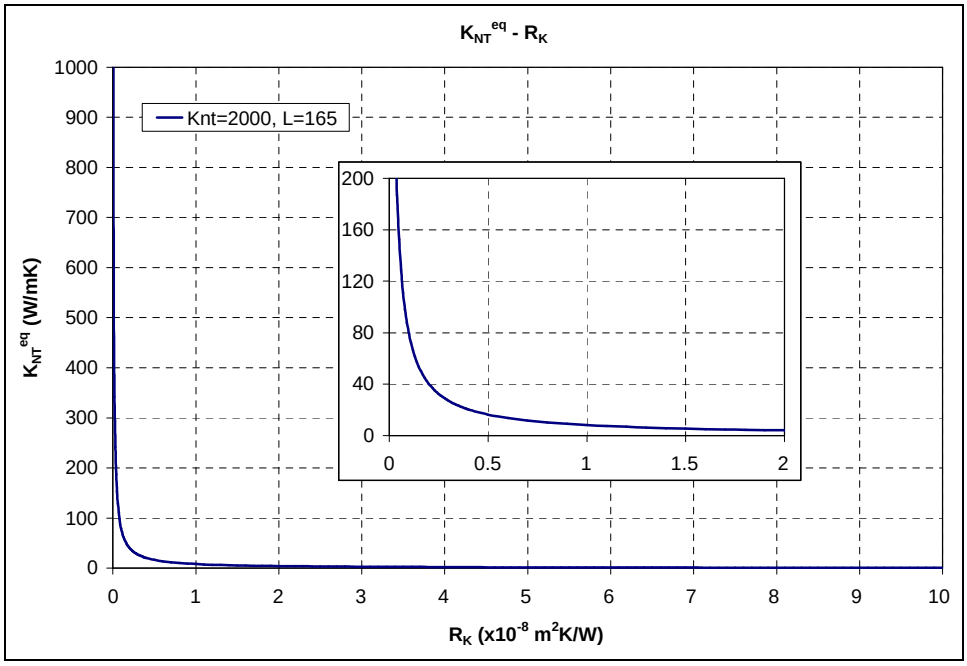

Figure 6-4. Effect of the interface thermal resistance on the equivalent thermal conductivity of SWCNT. Nanotube thermal conductivity and length are kept constant at 2000 W/mK and 165 nm, respectively.

The variation of K_{NT}^{eq} as a function of nanotube length is shown in Figure 6-5 (a) for the two R_K values, with K_{NT} = 2000 W/mK. The results have near linear tendency and discrepancy between the slopes is evident. However, the effect of the SWCNT thermal conductivity on K_{NT}^{eq} is insignificant, almost invariant; it is shown in Figure 6-5 (b) for R_K = 0.24±0.13x10^{-8} m^{2}K/W and L = 165 nm.

Based on the interface thermal resistance stated by Bryning et al. [114], the equivalent thermal conductivity of SWCNT can be estimated – ranging from the values as low as 2 W/mK to 75 W/mK. To that end, in each experimental comparison, the K_{NT}^{eq} value used in the MCFEA is estimated, conforming to the interface resistance value provided by the corresponding experimental work.

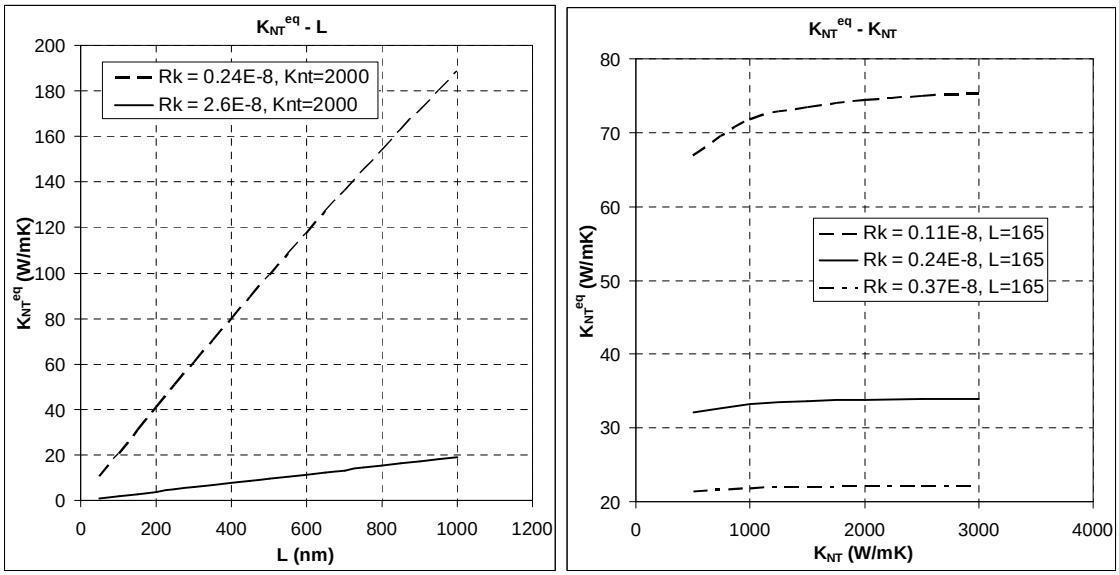

Figure 6-5. Effect of (a) the length, and (b) thermal conductivity of SWCNT on the equivalent thermal conductivity of SWCNT.

6.2. Effect of Voids

Polymer nanocomposites manufactured by any practical processing methods do not entirely emerge free of defects. It has been observed in the literature that composites materials, both with brittle or ductile matrices, suffer from substantial porosity, voids, and nano/micro cracking due to the manufacturing methods, handling, thermal cycling, and loading, as stated in Section 3.2 [149], [192–194]. Especially the presence of voids, even

at low volume fractions, has been found to degrade the properties of composites [195]. Further, studies have shown that the composite properties are affected by the void fraction, size, shape and distribution [150], [196].

In pursuit of capturing the uncertainties in the nanotube reinforced polymer composites, it is important to take into consideration the pre-existing voids in the structure, besides the distribution and the dispersion characteristics. Similarly, the voids may form progressively at the reinforcement and the matrix interface during the life of the structure [98]. This section focuses on pre-existing voids in the polymer. In particular, the MCFEA is expanded by incorporating a certain level of nano/micro voids into the micromechanics model. The assumption here is that the polymer nanocomposite consists of four phases – matrix, individual SWCNTs, spherical agglomerates, and nano voids.

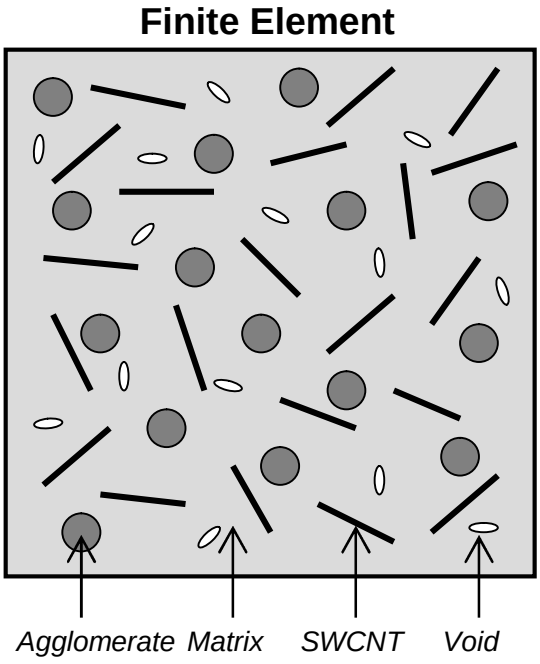

Figure 6-6. The material structure in a finite element used in the MCFEA comprising matrix, individual SWCNTs, spherical agglomerates and penny shaped voids.

The voids have insignificant thermal conductivity value, which are thus approximated to be zero. Figure 6-6 shows the finite element (FE) used by the proposed MCFEA. The homogenization within a FE is performed by extending the 3-phase Eshelby's equivalent inclusion method to capture 4-phase problem at hand. The spatial randomness is introduced by Weibull distribution with given dispersion parameters.

First, the effect of the void shape on thermal conductivity has been investigated. It is known that depending on the fracture mechanism and/or manufacturing methods of the nanocomposites, the defects in the polymer can be formed in various shapes, namely spherical and penny shapes. Figure 6-7 shows the reduction in thermal conductivity of the matrix, that is epoxy with Km = 0.188 W/mK, by introducing different defect shapes. It is observed that the penny shape voids causes greater decrease in the ETC due to their high aspect ratios. Nonetheless, throughout the rest of the analysis, the voids are assumed to adopt spherical shapes for the purpose of conservatism and consistency.

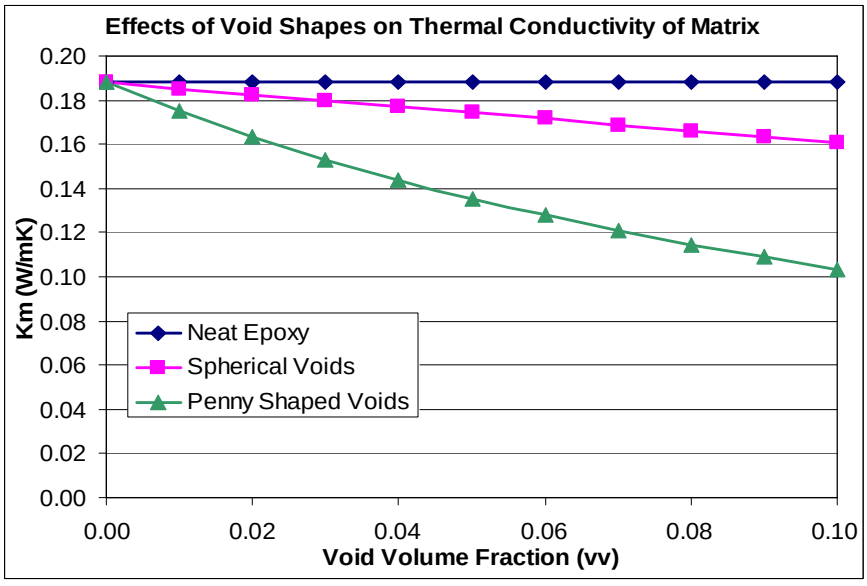

Figure 6-7. Effect of the shape of the defects on the thermal conductivity of the matrix. Spherical and penny-shaped voids are compared.

Figure 6-8 and Figure 6-9 show comparison of the models developed in this dissertation on the effective thermal conductivity (ETC) of PNC. The voids are considered to be penny shaped randomly distributed cracks in the model, with an aspect ratio of 30, and with a volume fraction of 10%. Simulations were carried out for two different agglomeration threshold parameters, i.e., agg_th=0.01 and agg_th=0.2. For both the cases, it is observed that the existence of 10% voids within the composite reduces the ETC approximately by half. To this end, the influence of the degree of the defects has also been examined for 0, 1, 5 and 10 percent void content, shown in Figure 6-10.

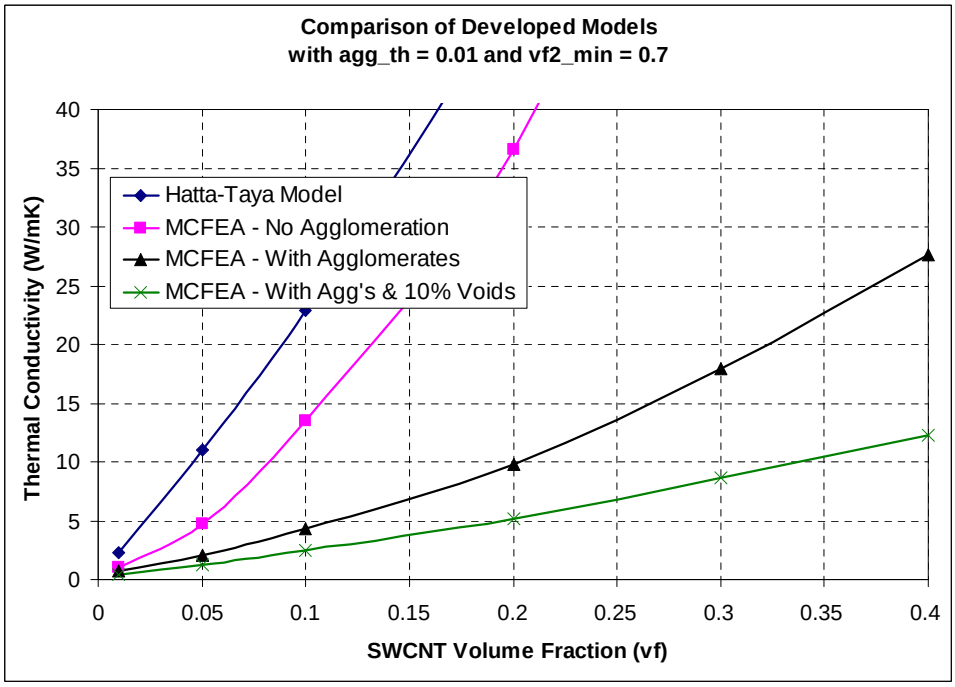

Figure 6-8. Effect of voids on the effective thermal conductivity of PNC, produced by the MCFEA, based on Weibull distribution with agg_th = 0.01 and vf2_min = 0.7.

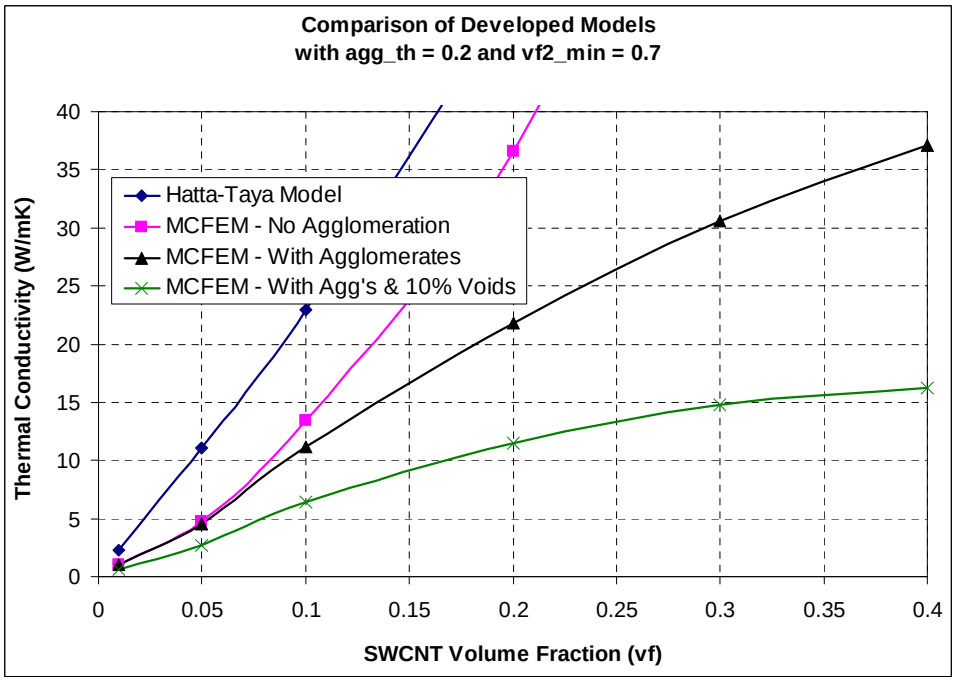

Figure 6-9. Effect of voids on the effective thermal conductivity of PNC, produced by the MCFEA, based on Weibull distribution with agg_th = 0.2 and vf2_min = 0.7.

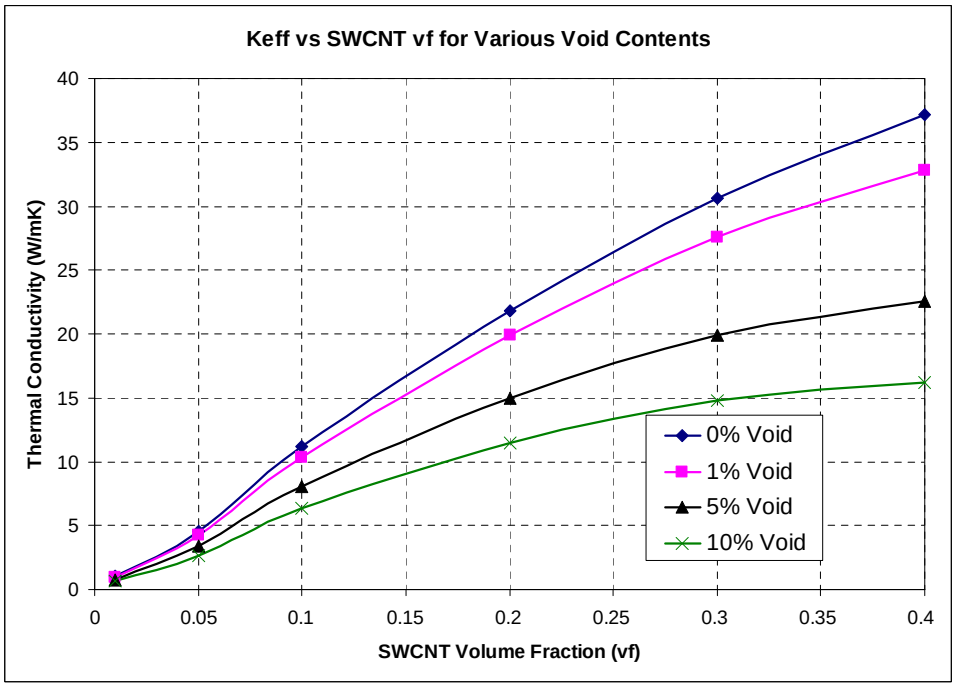

Figure 6-10. Effect of void content on the effective thermal conductivity of PNC, produced by the MCFEA, based on Weibull distribution with agg_th = 0.2 and vf2_min = 0.7.

Sensitivity analysis has been performed to determine the impact of the void content in a PNC in detail. Void volume fractions up to 10 percent with 1 percent increments are

included in nanocomposites with two different SWCNT volume fractions for given dispersion parameters (agg_th and vf2_min), as shown below in Figure 6-11.

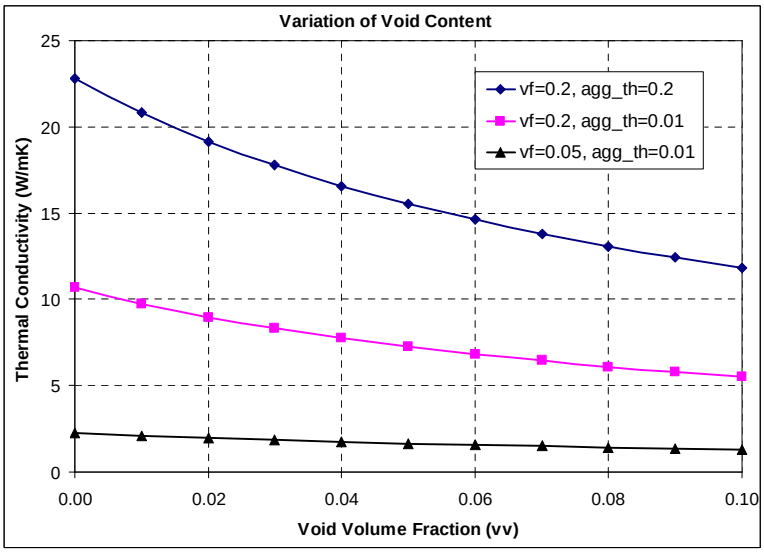

Figure 6-11. Sample variations of ETC w.r.t. void content, with vf2_min=0.7.

6.3. Experimental Data Comparison

To assess the quality and consistency of the MCFEA developed in this dissertation, experimental comparison of the numerical simulations is essential. In this section, experimental data reported in several pertinent studies in the literature are compared with the values derived using the MCFEA. For each comparison, appropriate assumptions are made based on the experimental characteristics pertaining to manufacturing, treatment and processing of the nanocomposites. Following are the detailed comparisons of the numerical results derived by the MCFEA with the data obtained from relevant independent experimental studies.

Effect of Impurities

The effect of SWCNT purity on the thermal conductivity of polymer nanocomposites was studied, utilizing raw and purified nanotubes by Yu et al. [95]. The purified SWCNTs were produced via acid treatment followed by high speed centrifugation, which removed most of the impurities. Tests were conducted with nanotube content up to 9 percent in weight in epoxy with K_m=0.201 W/mK. Thermal conductivity values determined by the proposed MCFEA are compared to the experimental data. Performance of the MCFEA is also assessed via exhibiting the results obtained by the Hatta-Taya method and the MCFEA with no agglomerates.

The authors reported that the nanotubes are not surface processed; hence the SWCNTs possess poor dispersion characteristics. As a result, the agglomeration threshold parameter (agg_th) is assumed to be 0.01, which means that nanotubes begin forming clusters at 1 percent volume content within a material region, namely a finite element. The minimum nanotube content in an agglomerate (vf2_min) is assumed to be 0.6 based on the work presented by Keblinski [186]. Further, the thermal interface resistance is taken as 0.11×10^{-8} m^2K/W yielding an effective thermal conductivity of SWCNT of 75 W/mK, lower limit value reported by Bryning et al. [114] in Section 6.1. Weight fraction quantities are converted to volume fractions; thus they can be assigned in the model developed in this dissertation.

Figure 6-12(a) compares the results with standard deviations from this study to that obtained by the No-Agglomeration-MCFEA, which assumes uniform dispersion yet, only

poor distribution. The results from the novel approach are given in Figure 6-12(b) with standard deviation of plus/minus one. It can be clearly seen that the proposed approach meets the experimental data with a greater accuracy. Figure 6-12(c) shows the mean value results of all the compared methods.

Figure 6-13 presents the sample probability density functions of the Weibull distributions that are used to generate the random SWCNT weight fraction (wfr) values. The values are then employed by the MCFEA for the comparison given in Figure 6-12. The plots correspond to the wfr mean values equaling to 1, 2.4, 4.8, 7 and 9 percent. Horizontal axis shows the total values of the SWCNT wfr in percentage, and vertical axis is the overall number of wfr generated.

In the paper of Yu et al., the nanocomposites prepared with raw nanotubes have 60 percent of purity. This indicates that 40 percent of the carbon content are impurities existing in the structures. The authors state that these impurities are mostly composed of amorphous carbon (a-C). Thermal conductivity of a-C is significantly lower than SWCNTs. Marques and Lacerda [197] report that thermal conductivity values of a-C can vary from 0.3 to 10 W/mK. In this regard, better estimation was suggested by Hurler et al. [198] after studying micro films made up of a-C. They found that most samples have a thermal conductivity of approximately 1 W/mK. The other variables are kept constant. In the analysis, 40 percent of the SWCNTs were replaced by the amorphous carbon.

Figure 6-14 (a) and (b) show the results of the MCFEA with pure nanotubes, and the MCFEA containing impurities, along with their standard deviations, respectively. The mean values of the MCFEAs are compared in Figure 6-14(c), including that of the Hatta-Taya method. A significant degree of agreement between the measured results with the values calculated by the proposed MCFEA is noted. Particularly, the MCFEA that accounts for impurities exhibits the strength of the developed model in capturing the thermal conductivity of multi-phase nanocomposites.

Similarly, Figure 6-15 presents the sample probability density functions of the Weibull distributions that are used to generate the random SWCNT weight fraction (wfr) values. The values are then employed by the MCFEA for the comparison given in Figure 6-14. The plots correspond to the wfr mean values equaling to 0.5, 1, 2, 3.9 and 4.8 percent. Horizontal axis shows the total values of the SWCNT wfr in percentage, and vertical axis is the overall number of wfr generated.

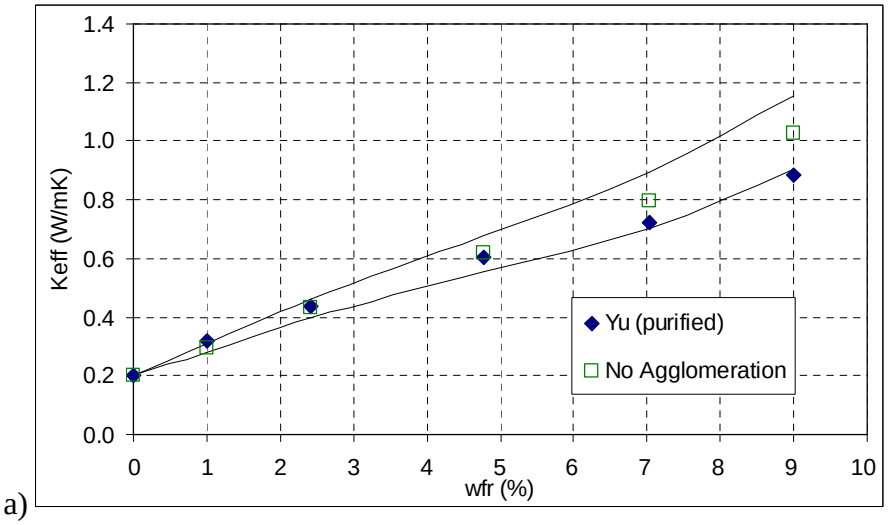

a)

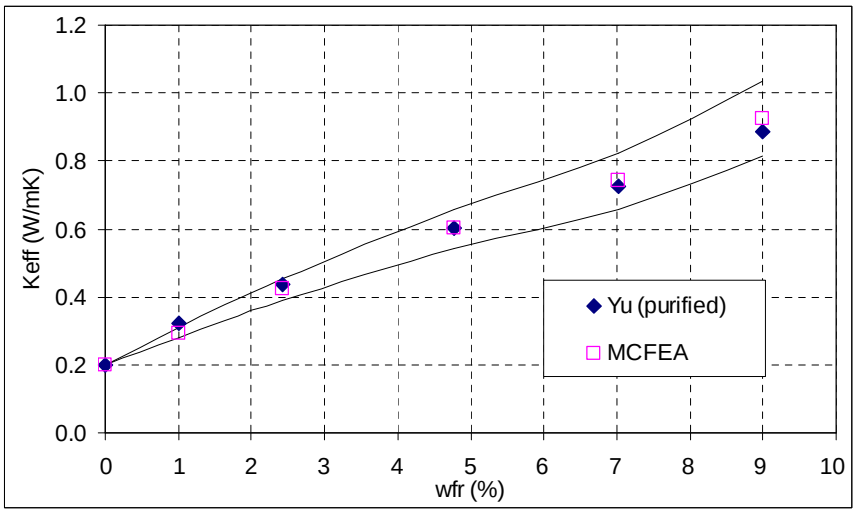

b)

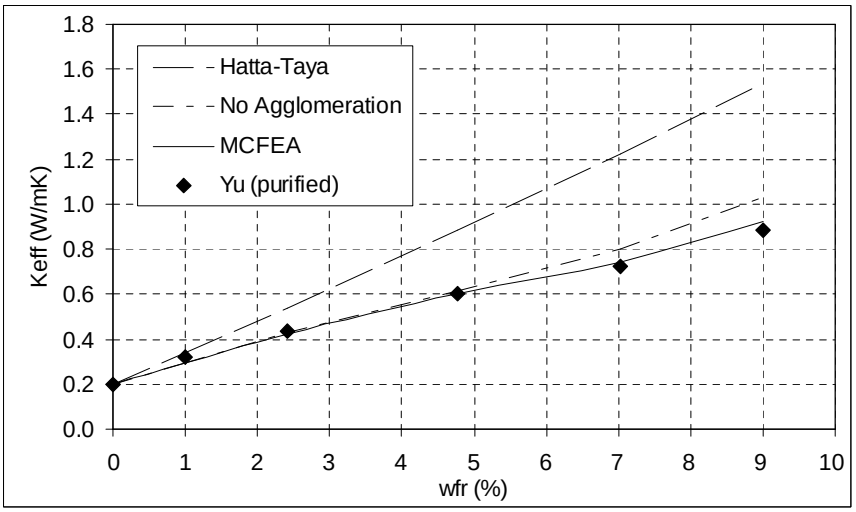

c)

Figure 6-12. Thermal conductivity of PNC as a function of SWCNT weight fraction of purified nanotubes in comparison with the values computed by the MCFEA.

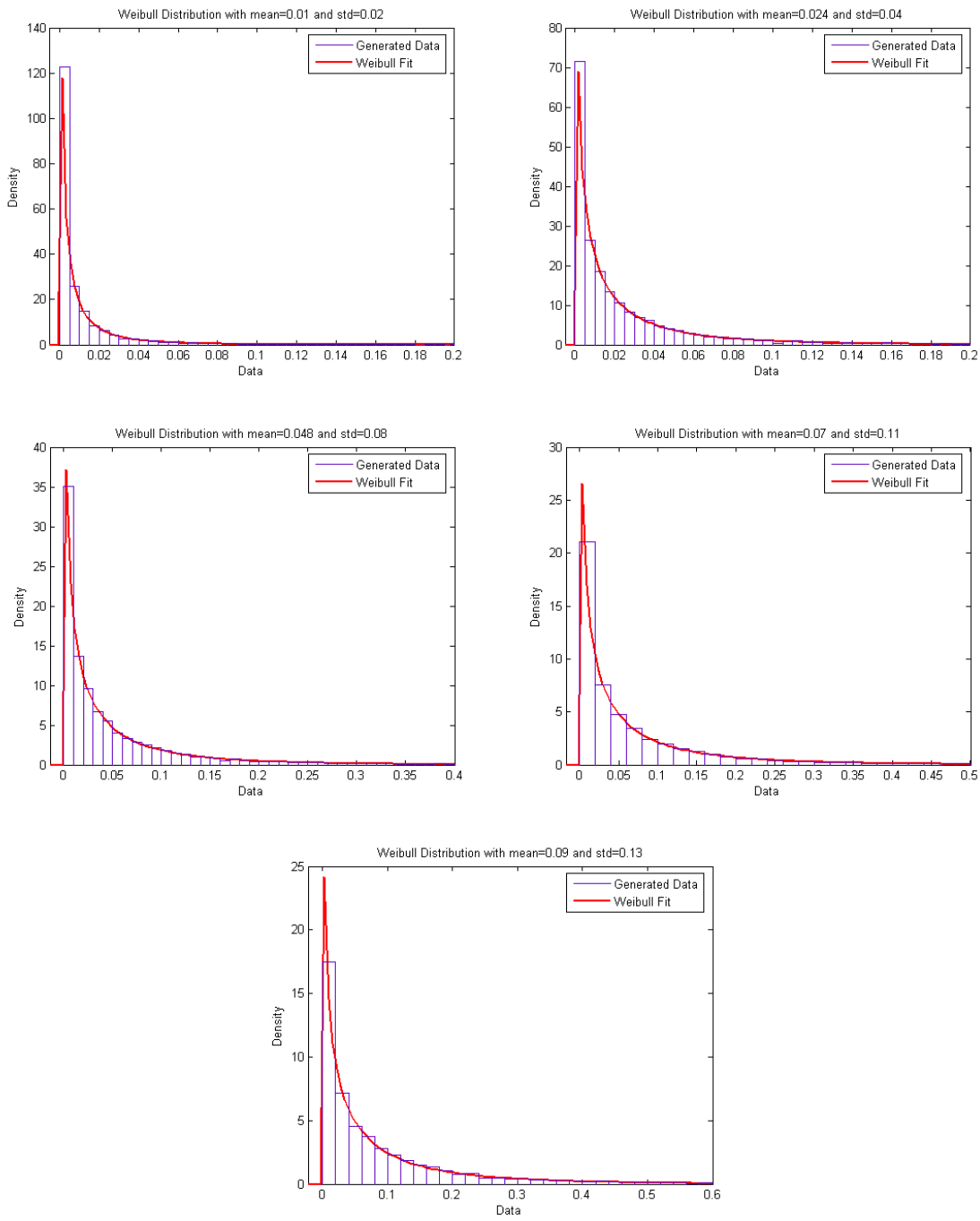

Figure 6-13. Weibull pdf of the computed values used in the comparison (purified SWCNT). Plots correspond to the SWCNT weight fraction (wfr) equaling to 1, 2.4, 4.8, 7 and 9 percent. Horizontal axis shows wfr in percentage, and vertical axis is the overall number of wfr generated.

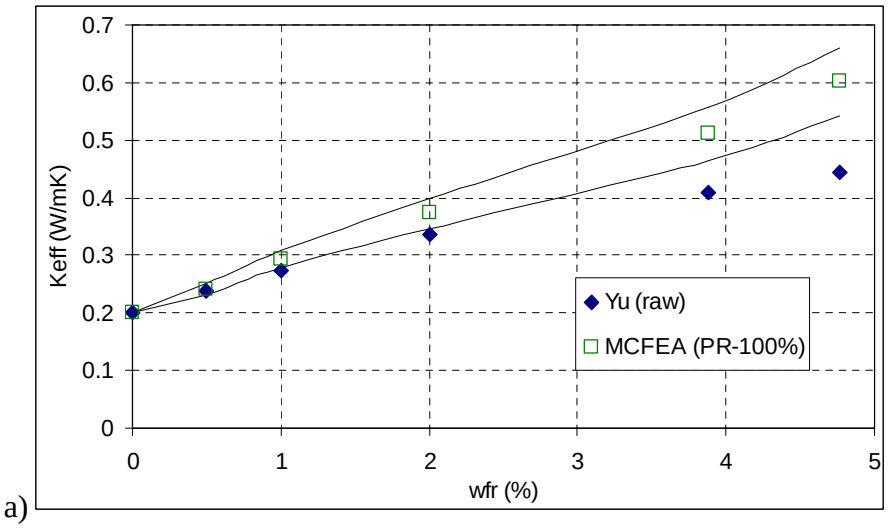

a)

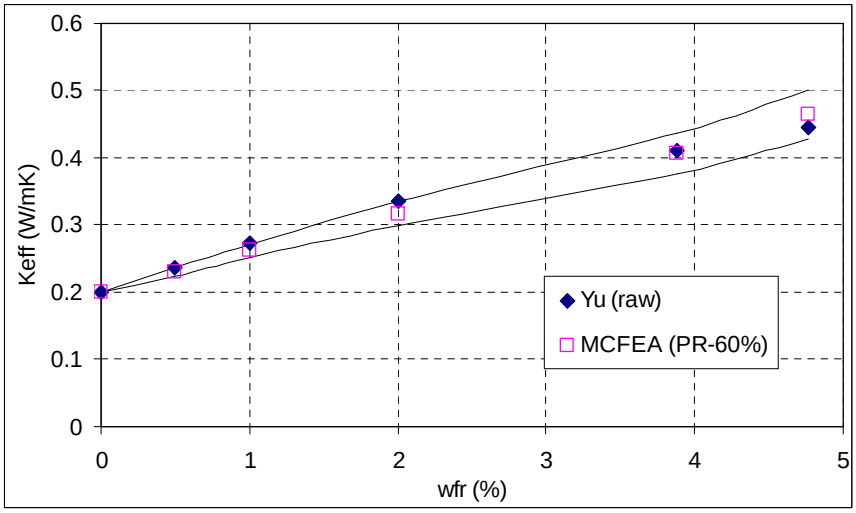

b)

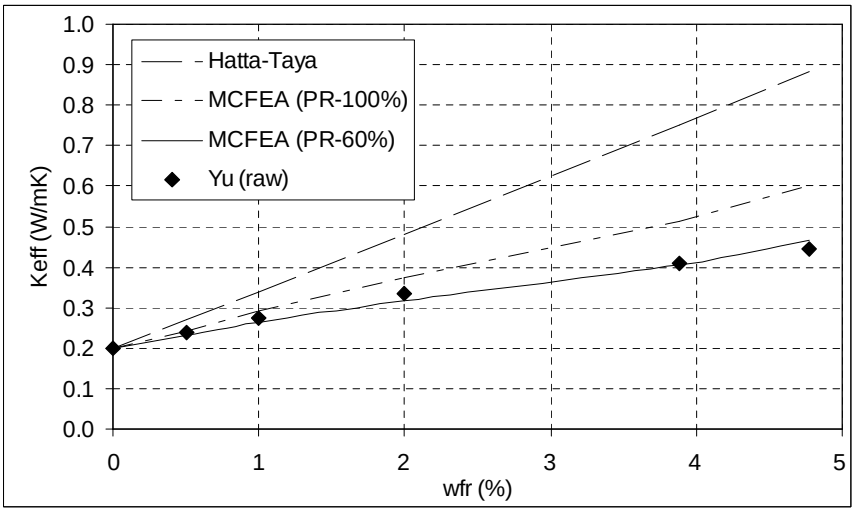

c)

Figure 6-14. Thermal conductivity of PNC as a function of SWCNT weight fraction of raw nanotubes in comparison with the values computed by the MCFEA.

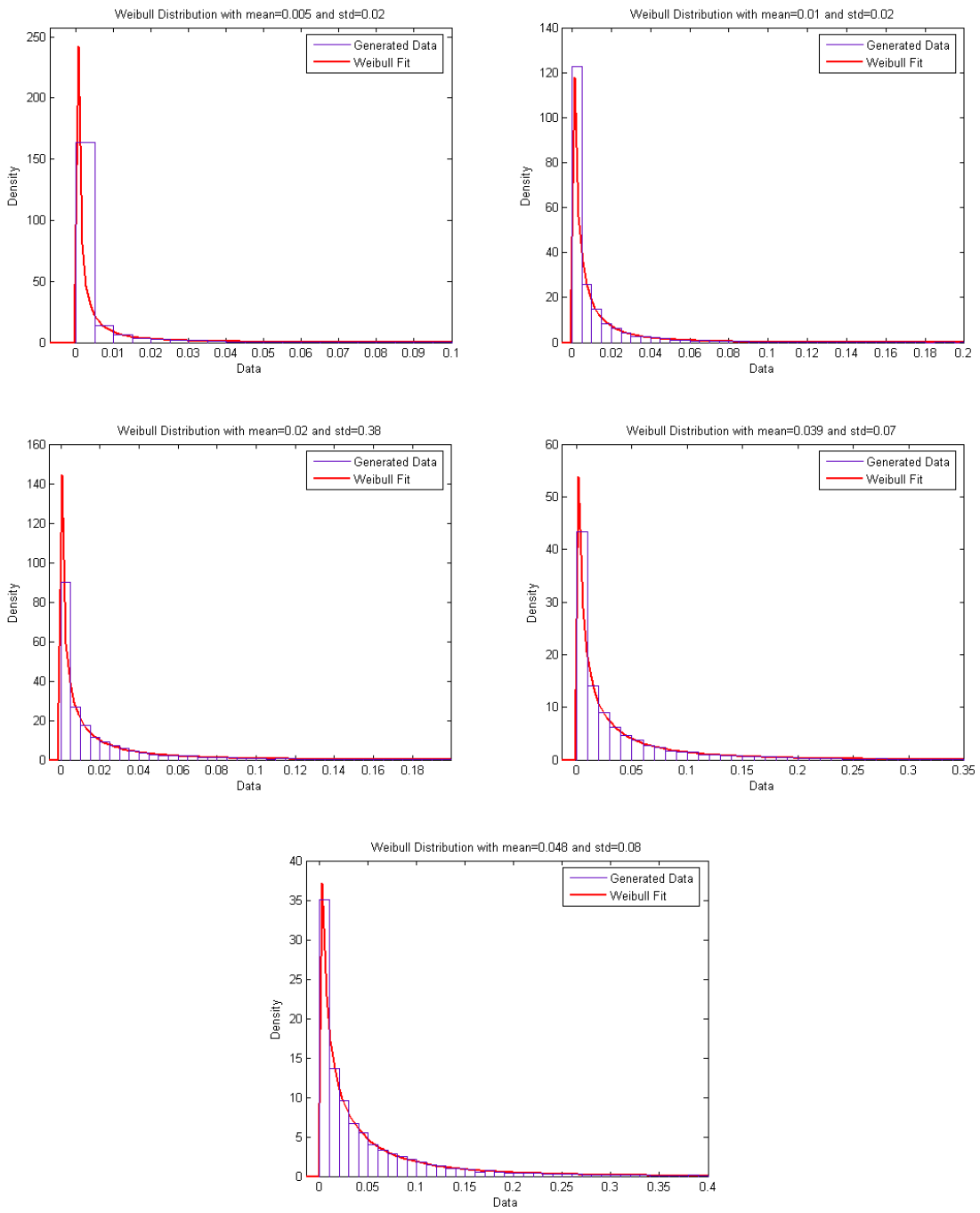

Figure 6-15. Weibull pdf of the computed values used in the comparison (raw SWCNT). Plots correspond to the SWCNT weight fraction (wfr) equal to 0.5, 1, 2, 3.9 and 4.8 percent. Horizontal axis shows wfr in percentage, and vertical axis is the overall number of wfr generated.

Degree of Polymer Crystallinity

Haggenmueller et al. [93] measured the effective thermal conductivity of SWCNT reinforced composites in terms of nanotube loading utilizing low density polyethylene (LDPE) and high-density polyethylene (HDPE). They investigated the degree of polyethylene (PE) crystallinity. Experiments were conducted for PNC samples prepared with SWCNT weight fractions (w_f) of 0.01 and 0.30 in LDPE, and 0.01, 0.05, 0.10, 0.30 in HDPE. They measured the thermal conductivity values reaching 1.8 and 3.5 W/mK for 30 percent loading, respectively. The authors found that the average length and diameter of the SWCNTs used in their experiments are 445 and 3 nm, respectively.

The proposed MCFEA is first compared to the measured values acquired from PNCs with LDPE. The LDPE has an experimental thermal conductivity of 0.26 W/mK and density of 0.92 g/cm^3. In the model, the agglomeration parameters used are kept as the previous comparison; agg_th = 0.01 and vf2_min = 0.6. In their work, Haggenmueller et al. emphasizes strong influence of the thermal resistance (R_K) between the nanotube and the polymer. They suggest utilizing the finding of Bryning et al. [114] for quantifying the interfacial resistance value. They estimated the effective thermal conductivity of SWCNT as 32 W/mK (R_K = 0.7x10^{-8} m^{2}K/W), which is used as an input in the following comparison.

The comparison of the results computed by the developed model shown in Figure 6-16 (a) offers a high degree of agreement, achieved by the introduction of poor dispersion via agglomerates along with poor nanotube distribution. Figure 6-16 (b) shows that without

the agglomerate effects, there is nearly 50 percent discrepancy between the computed and the measured results. The quality of the matching with respect to a number of numerical models is emphasized and their corresponding mean values are plotted in Figure 6-16 (c).

Further, numerical evidence to assess this achieved level of compatibility of the MCFEA, comparison is performed for the HDPE based PNC. The HDPE has a measured thermal conductivity of 0.5 W/mK and a density of 0.96 g/cm^3. It is noticed in the authors' study that the thermal conductivity measured for HDPE is considerably greater than that of LDPE. Notably, this disparity is attributed to the high crystallinity characteristics of HDPE. The authors hypothesize that the HDPE matrix reduces the interfacial thermal resistance relative to the LDPE. PE is found to nucleate on the SWCNT in the melt state and thereby locally increasing the PE crystallinity at the interface. In a HDPE matrix, PE crystallites are more likely to span between SWCNTs, especially at higher nanotube loadings.

In accordance with the above evidence, a reduced thermal resistance (R_K = 0.37x10^{-8} m^{2}K/W) is defined in the model per Bryning et al. [114], yielding 58 W/mK of SWCNT thermal conductivity. Figure 6-17 is the evidence of the superiority of the MCFEA compared to the Hatta-Taya and the No-Agglomeration-MCFEA. Note that for both comparisons, the conversion from weight to volume nanotube fraction is performed using equation (6-1), mentioned above.

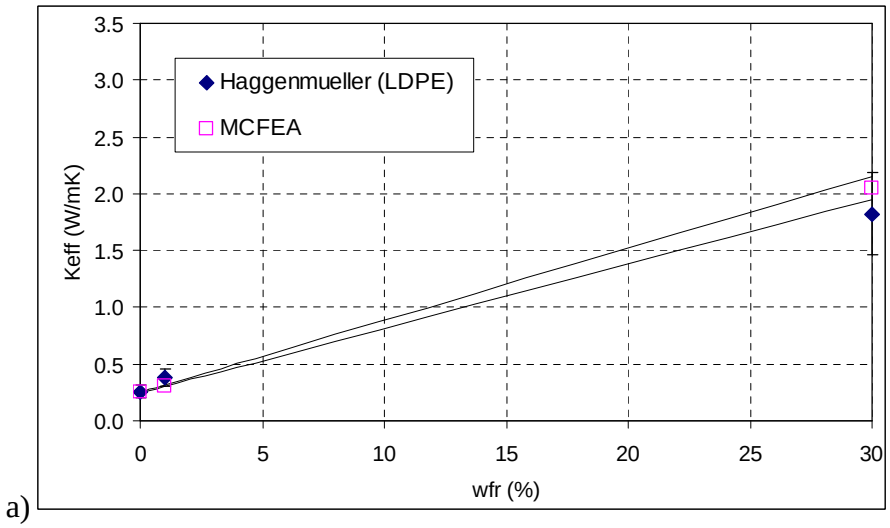

a)

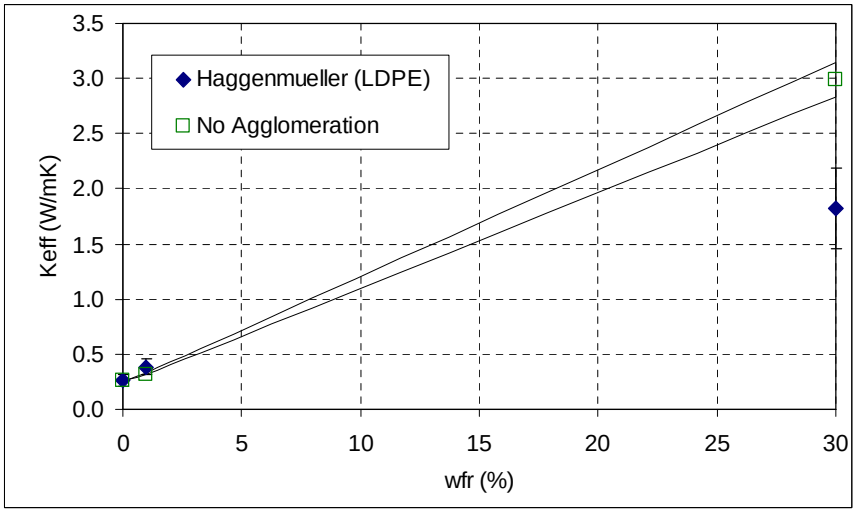

b)

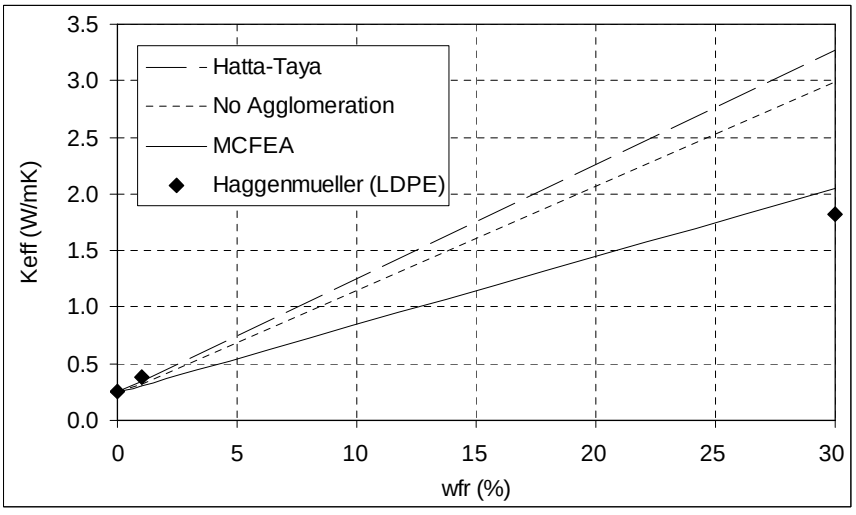

c)

Figure 6-16. The proposed MCFEA compared with Hatta-Taya model and the experimental values measured for SWCNT-LDPE composites. Plots (a) and (b) include the corresponding standard deviations, (c) is plotted with the mean values of the results.

a)

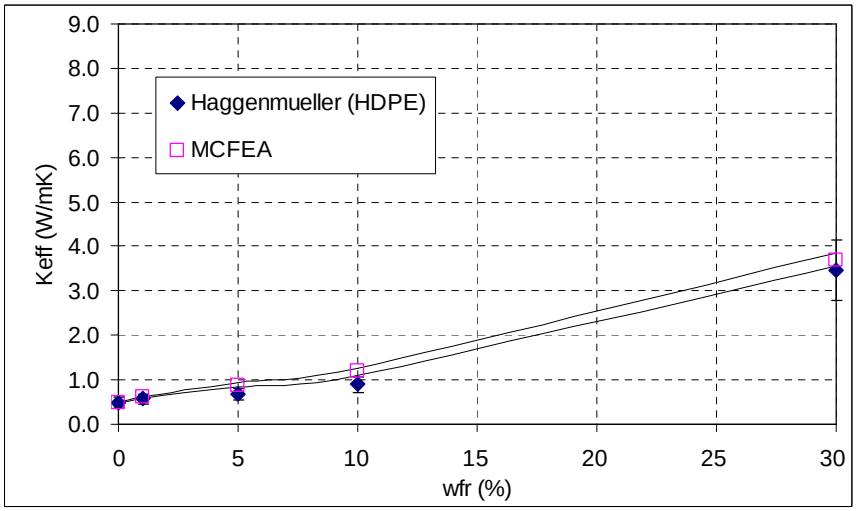

b)

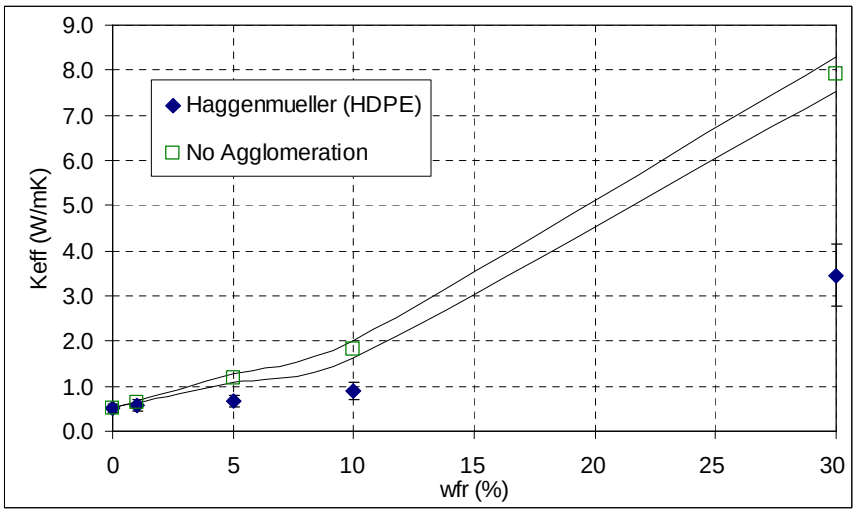

c)

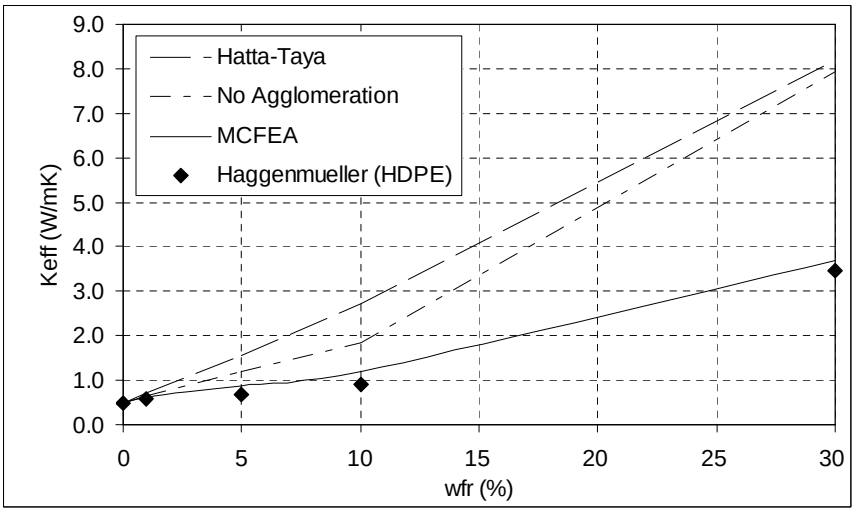

Figure 6-17. The proposed MCFEA compared with Hatta-Taya model and the experimental values measured for SWCNT-HDPE composites. Plots (a) and (b) include the corresponding standard deviations, (c) is plotted with the mean values of the results.

Effect of Voids

Xu et al. [97] conducted experiments to predict the thermal properties of SWCNT-PVDF composites up to 49% nanotube loading. Thermal conductivity of PVDF was measured as 0.233 W/mK. The samples used in the experiments are produced with aqueous surfactant solution. Therefore, significantly low measured conductivities are expected based on the work of Bryning et al. [114]. They reported that R_K of surfactant-processed SWCNT-polymer composite is approximately 2.6×10^{-8} m^2K/W, which corresponds to an equivalent NT thermal conductivity of 3.2 W/mK. The experimental results and the mean values calculated by the MCFEA are shown in Figure 6-18(a).

It is seen by examining the results that the discrepancy between the numerical and the experimental values increases after 10 percent nanotube loading. This unexpected pattern is attributed to the large number of junctions among SWCNTs by Xu et al. Such incompatibilities result in high concentration stress points and are followed by debonding of the interface, particularly voids, as suggested by Hatta et al. [192]. They demonstrated that volume fraction (vf) of such voids can reach as high as 12 percent. In that regard, the effect of the voids is accounted for by introducing voids into the MCFEA. The voids are assumed to have zero thermal conductivity value, and to exist at 10 percent of the local SWCNT vf. The generated results are plotted in Figure 6-18(b). The MCFEA with voids gives enhanced compatibility with the experimental findings. Figure 6-18(c) compares the mean values of the numerous methods considered in the analysis. Figure 6-19 shows the pdf of Weibull distributions used to numerically generate the random vf values, compared to the corresponding experimental results.

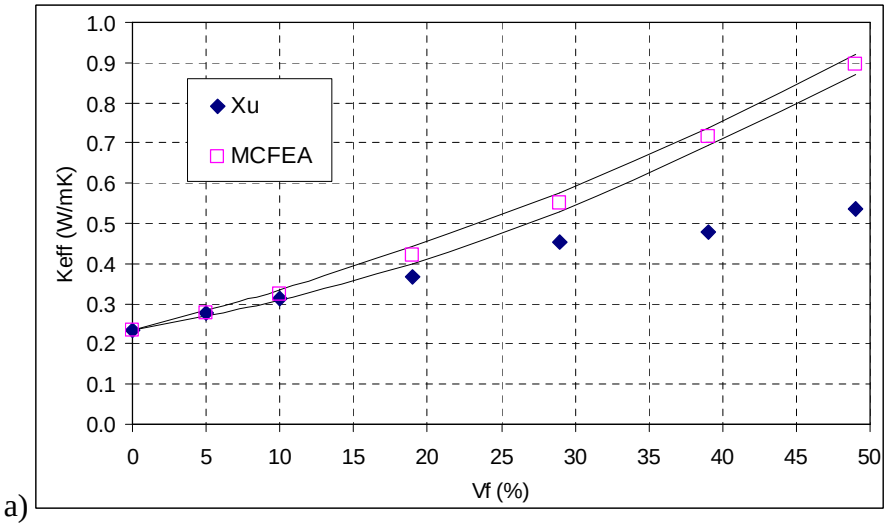

a)

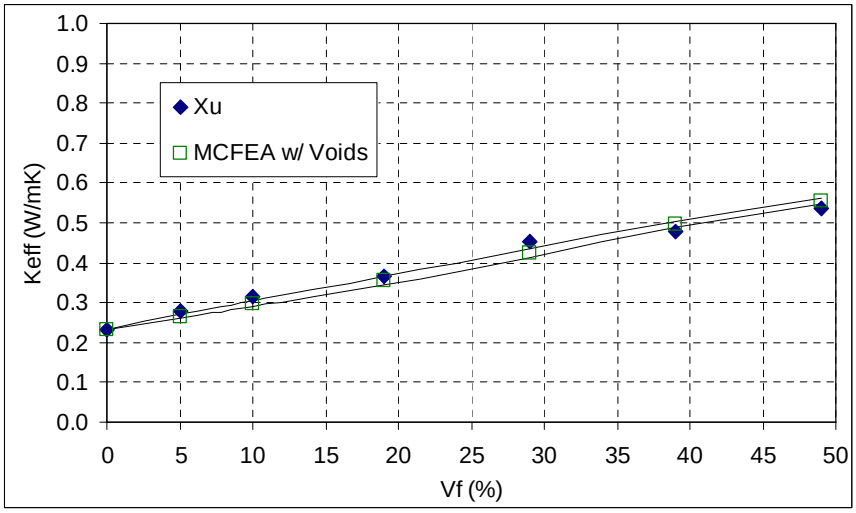

b)

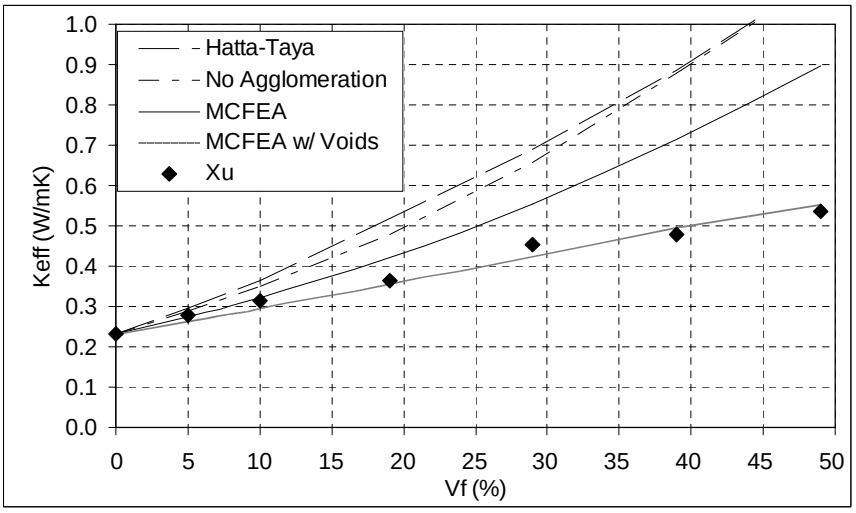

c)

Figure 6-18. The proposed MCFEA compared with the experimental values measured for SWCNT-PVDF composites. Plots (a) and (b) include the corresponding standard deviations, (c) is plotted with the mean values of the results.

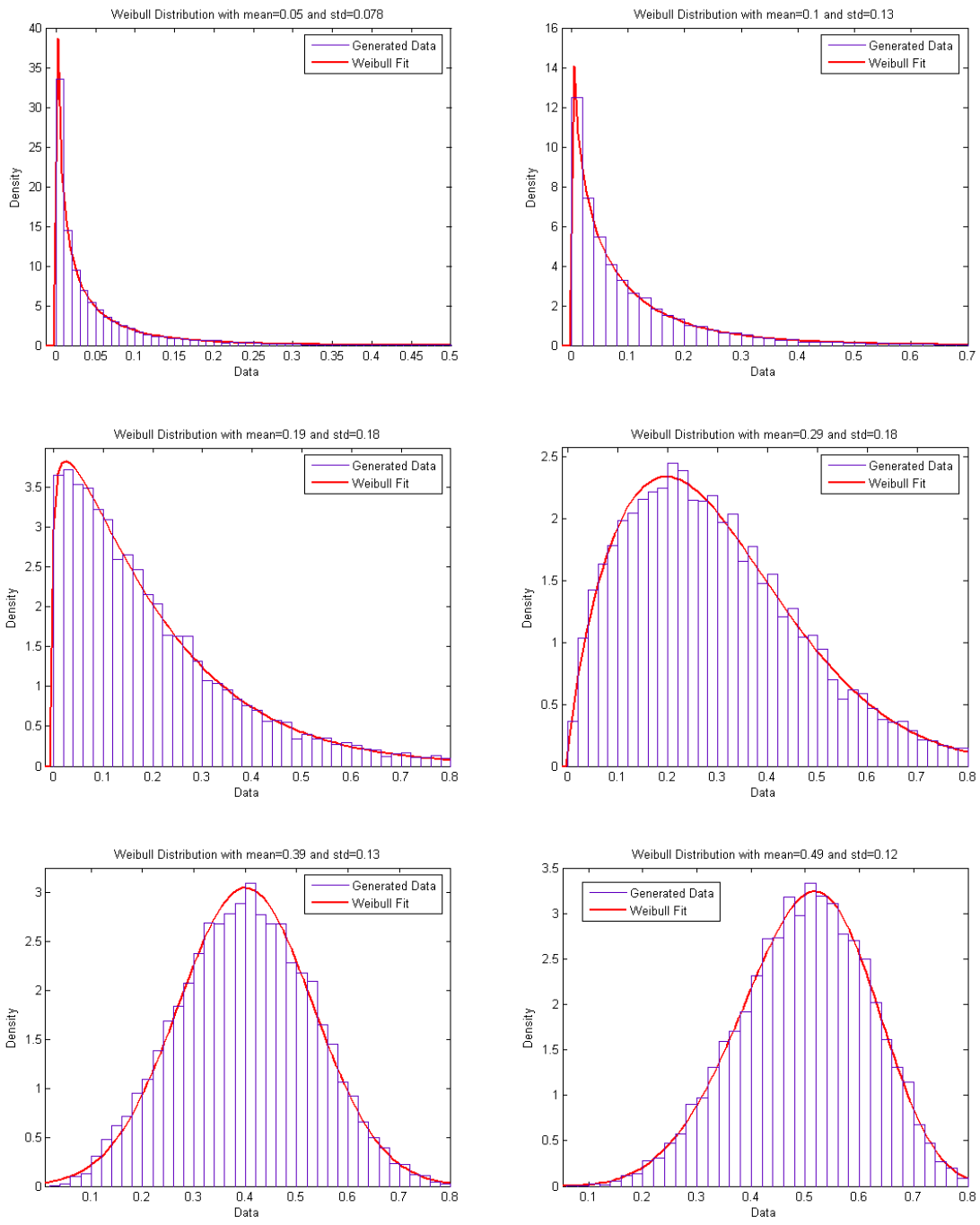

Figure 6-19. Weibull pdf of the computed values used in the comparison. Plots correspond to the SWCNT volume fraction (vf) equal to 5, 10, 19, 29, 39 and 49 percent. Horizontal axis shows the total values of the SWCNT vf in percentage, and vertical axis is the overall number of vf generated.

Networks of SWCNTs

Du et al. [96] presented a particular fabrication method for SWCNT reinforced PNCs. Heterogeneous distribution of nanotubes were created by coagulation method, which possesses an interconnected SWCNT-rich phase within an epoxy matrix. First, a freestanding nanotube framework was prepared by removing the polymer matrix from SWCNT-PMMA (poly methyl methacrylate) composite by nitrogen gasification, and then epoxy resin was infiltrated and cured (Figure 6-20). They produced nanocomposites with loadings reaching 7 percent in weight and measured their thermal conductivities.

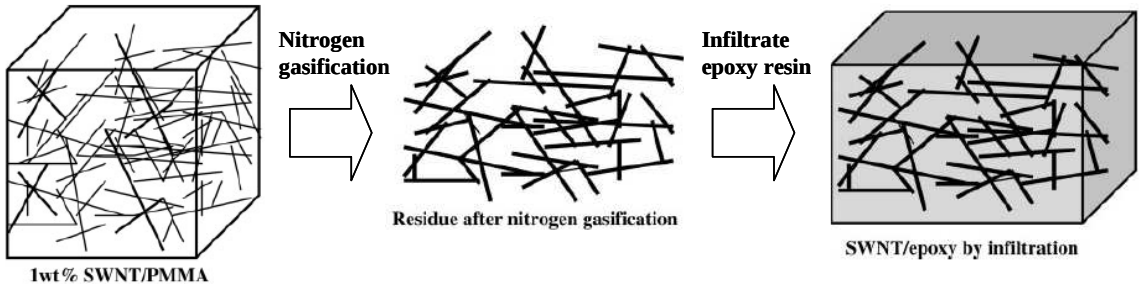

Figure 6-20. Schematic of the coagulation method. Reproduced from [96].

The thermal conductivity of the pure epoxy used is 0.18 W/mK as found in the study of the same authors. Further, the conductivity of the SWCNT is given in the vicinity of 30 W/mK in their paper. This value was corroborated by the work of Hone et al.[183]. They fabricated high purity, densely packed SWCNT mat formations and achieved an effective thermal conductivity of 35 W/mK. It is also noticed that this value exactly corresponds to the aforementioned mean value of the thermal conductivity (with $R_K = 0.24 \times 10^{-8}$ m^2K/W), measured by Bryning et al. [114]. Hence, 35 W/mK of SWCNT is used in the MCFEA in this comparison.

The numerical results from the simulations are compared to their experimental results. For the sake of consistency, the agglomeration parameters used are again kept constant; agg_th = 0.01 and vf2_min = 0.6. In their results, Du et al. present the measured values with 15 percent accuracy, which is shown with the error bars in the following figures.

Figure 6-21(a) shows a comparison between the experimental values to the No-Agglomeration-MCFEA with the standard deviation of plus/minus one, which does not consider the dispersion effects, i.e., no agglomerations. The results from the novel approach are given in Figure 6-21(b) with plus/minus one sigma. It is found that the proposed approach falls in the range of the experimental data with a greater accuracy. Figure 6-21(c) plots the mean value results of all the compared methods, including Hatta-Taya's. Examining these numerical results, the trend obtained by the MCFEA yields a satisfactory enhancement.

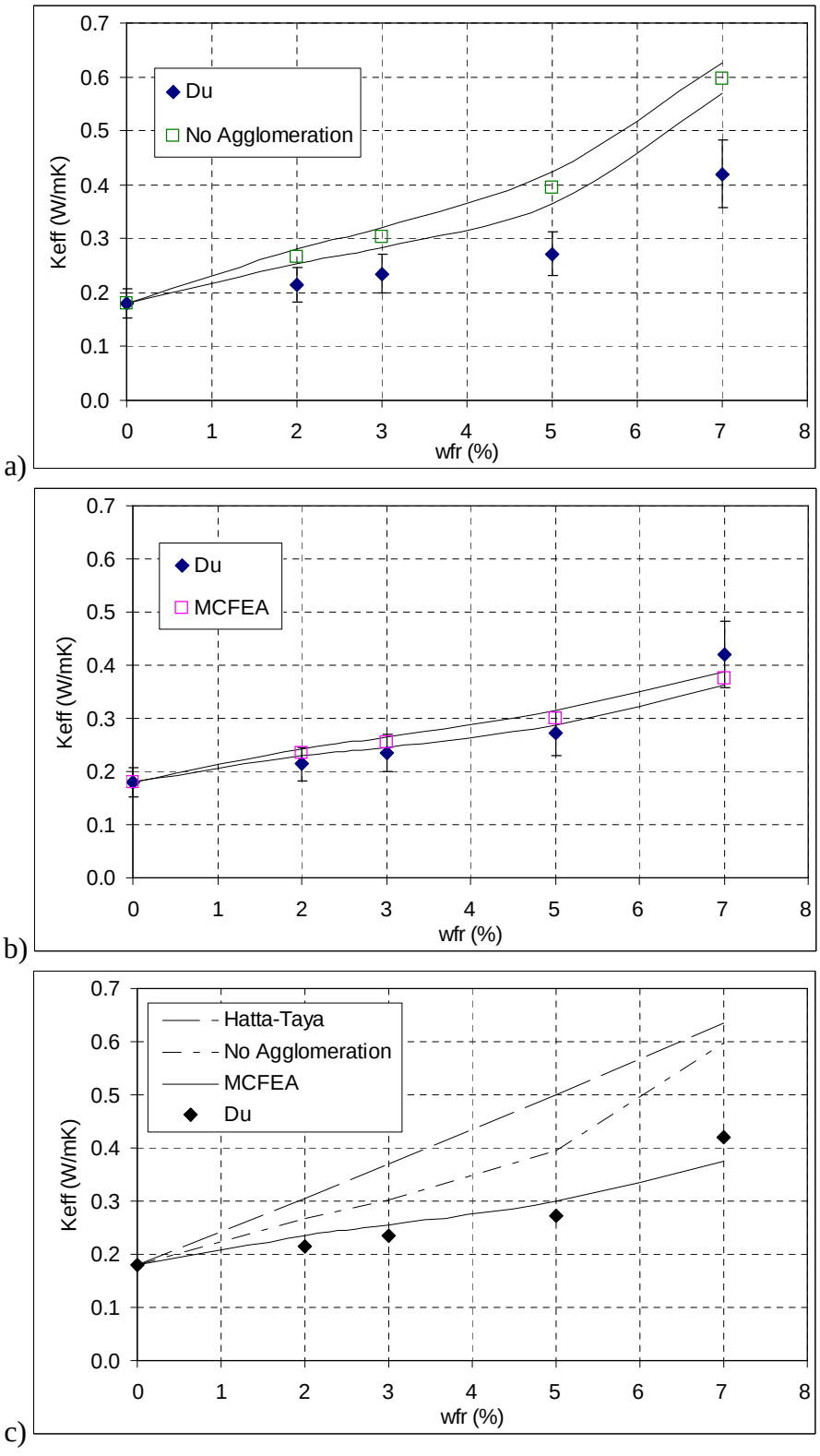

Figure 6-21. The proposed MCFEA compared with the experimental values measured for SWCNT-epoxy composites. Plots (a) and (b) include the corresponding standard deviations, (c) is plotted with the mean values of the results.

Without the Effect of Agglomeration

Liu et al. [98] studied the thermal conductivity of a PNC by introducing CNTs into a silicone elastomer. They tested samples with nanotube loadings of 0.8, 2.3 and 3.8 weight percent. The CNTs used are purified and grown by chemical vapor deposition. While highlighting the difficulty in nanotube dispersion in the matrix, they reported no notable CNT agglomerates. They added that the CNTs were distributed individually in random orientation. To this end, a comparison is performed between numerically computed values by the proposed MCFEA and the experimentally measured values. The agglomeration parameters used are agg_th = 0.01 and vf2_min = 0.6. Further, the thermal conductivity of the nanotubes is assumed to be 75 W/mK, in accord with the work of Bryning et al. [114]. Liu et al. reported that value for the silicone elastomer as 1.1 W/mK.

Figure 6-22(a) compares the measured values to the computed ones by the MCFEA with nanotube agglomerates. Figure 6-22(b) presents the results of the No-Agglomeration-MCFEA, which does not consider the dispersion effects but only poor distribution. The comparisons are given for a standard deviation of plus/minus one. In view of the numerical evidence, it can be concluded that the proposed approach without the effect of the agglomerates meets the experimental findings with a greater accuracy. Further, this conclusion supports the author's statement on the nanotube dispersion – no notable agglomeration observed. Figure 6-22(c) shows the mean values computed by all the numerical methods, including Hatta-Taya's. Conclusively, the No-Agglomeration-MCFEA yields more acceptable results in agreement with the experimental information.

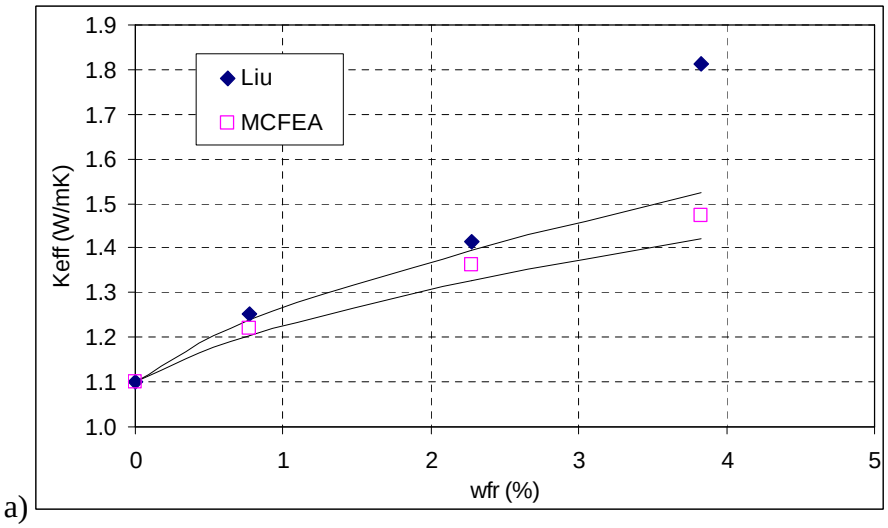

a)

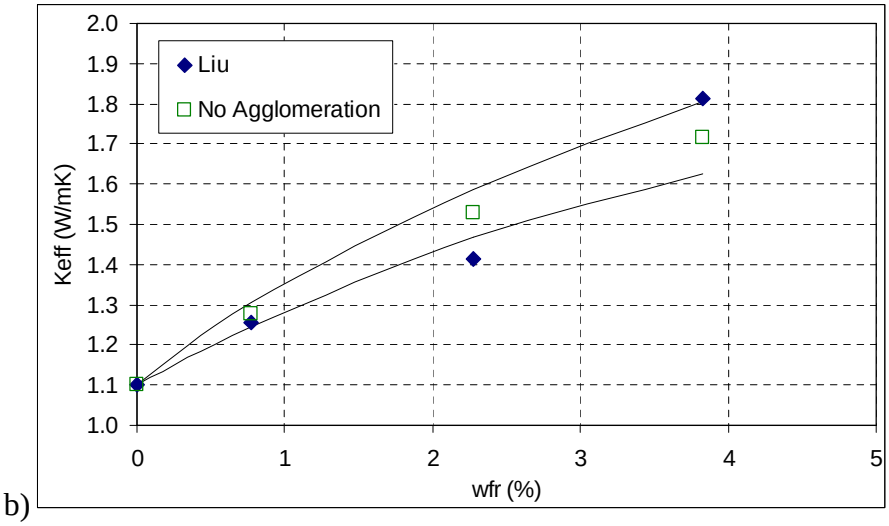

b)

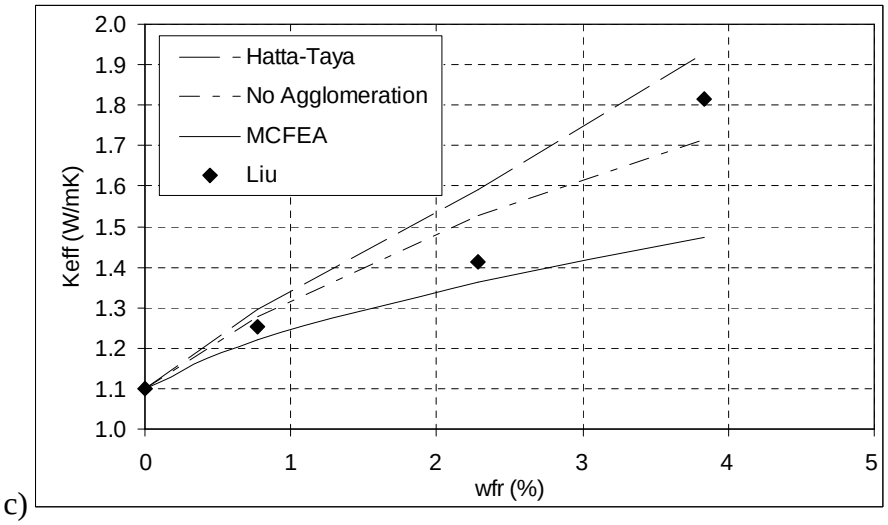

c)

Figure 6-22. The proposed MCFEA compared with the experimental values measured for SWCNT-silicone elastomer composites. Plots (a) and (b) include the corresponding standard deviations, (c) is plotted with the mean values of the results.

6.4. PNCs with Aligned SWCNTs

Thermal conductivity of polymer nanocomposites is directly linked to the orientation of the nanotubes. It has been shown that PNCs with randomly oriented SWCNTs fail to reveal the full potential of the thermal conductivity of the nanotubes. The potential of the carbon nanotubes can be exploited to the highest degree when they are uniaxially aligned, due to their large aspect ratios. Therefore, it is of great interest to investigate the properties of PNCs with aligned SWCNTs. Nanoscale dimensions make it more challenging to achieve desired nanotube alignment in polymers, compared to the randomly oriented ones. Nonetheless, several production techniques can be applied to align the SWCNTs, such as using magnetic or electric field. In addition, only a few attempts have been made to model the aligned PNCs [145], [199–205].

In this regard, this section expands the MCFEA developed in the previous chapters, and attempts to predict the effective thermal conductivity of polymer composites reinforced with aligned SWCNTs. Specifically, the Hatta-Taya method, used in each finite element for homogenization, is modified to implement the nanotube alignment [180]. The SWCNTs is assumed to be perfectly aligned in the direction of the heat flux (Figure 6-23).

The average disturbance of temperature gradient in the matrix defined by equation (5-17) in Section 5.2 is recast to account for the perfectly aligned inclusions as

$$\tilde{T}_{,i} = -\sum_{n=1}^{N} f_i (T_{,i}^{cn} - T_{,i}^{*n}) . \qquad (6\text{-}7)$$

The quantity Q_i^{cn} is related to the assumed distribution functions of the inhomogeneities in the composite. For perfect alignment with isotropic ellipsoidal inclusions ($S_{11} = S_{22} \neq S_{33}$), the overall composite becomes transversely isotropic. Hence, the term given by the equation (5-26) can be expressed as

$$Q_1^{cn} = Q_2^{cn} = \frac{(K^m - K^n) S_{11}}{(K^n - K^m) S_{11} + K^m}, \qquad (6\text{-}8)$$

and

$$Q_3^{cn} = \frac{(K^m - K^n) S_{33}}{(K^n - K^m) S_{33} + K^m} . \qquad (6\text{-}9)$$

Note that the subscript 3 represents the longitudinal direction, the subscripts 1 and 2 are in transverse directions. Finally, the effective thermal conductivity of the composites with aligned inclusions, K_{ij} can be computed by the equation (5-27).

For simplicity and comparison reasons, the aligned PNCs studied in this dissertation have good dispersion characteristics; that is no nanotube agglomerations are considered (Figure 6-23). However, the spatial randomness in nanotube distribution is taken into account in the MCFEA by assuming Weibull distribution throughout the composite.

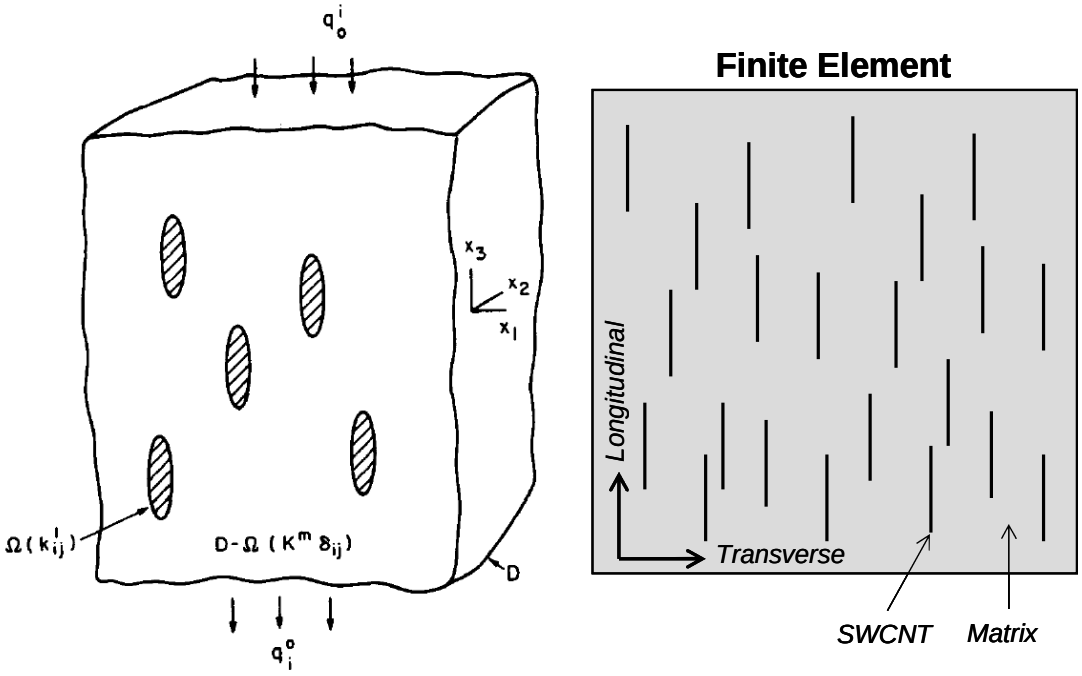

Figure 6-23. Left – A theoretical model for perfectly aligned inclusions embedded in the matrix **[180]**. Right – Schematic showing a finite element, comprising matrix and aligned individual SWCNTs.

The simulations are performed for SWCNTs with an aspect ratio of 150. As discussed in Section 6.1, the interfacial thermal resistance is also taken into consideration. The thermal conductivity (K) of the SWCNTs is therefore assumed to be 75 W/mK. The polymer is chosen to be epoxy with K=0.2 W/mK.

First, the results are obtained for the composite with randomly oriented SWCNTs for comparison purposes. The details on such PNCs are discussed and analyzed in previous sections. Figure 6-24 shows the variation of K_{eff} of the PNC with respect to SWCNT volume ratio; evaluated by the Hatta-Taya method, and by the MCFEA with corresponding standard deviations. Figure 6-25 shows the change in K_{eff} for the PNCs with aligned SWCNTs. The plotted results are for the longitudinal direction in which the nanotubes are aligned. It is noticed that the values obtained by the Hatta-Taya method

behaves almost linearly with the SWCNT volume fraction. This is attributed to the high aspect ratio of the nanotubes. Their effect is more pronounced in the direction of the alignment, which is not observed for the randomly oriented nanotubes. When the nanotube aspect ratio is high, the behavior of the Hatta-Taya model converges to that of simple rule of mixture. However, the reduction in the resultant values can still be observed due to the random spatial distribution. In summary, the thermal conductivity of the PNC is improved when the SWCNTs are aligned.

Figure 6-26 and Figure 6-27 make direct comparisons of the effective conductivities between the PNCs with randomly oriented and aligned SWCNTs. The results show the K_{eff} behaviors, produced by the Hatta-Taya method and the proposed MCFEA, respectively. In the figures, the suffixes LL and TT represent the longitudinal and transverse directions, respectively.

It can be seen that the values are greatly improved for the PNC with aligned SWCNTs in the longitudinal direction. The increase is approximately twice of the random SWCNT case. However, no substantial enhancement is observed in the transverse direction. This can be attributed to the fact that the aspect ratio of the nanotubes in transverse direction has considerably low value. Even though the SWCNTs are assumed to be isotropic, the final composite becomes transversely isotropic because of the nanotube alignment with high aspect ratios. This suggests that the isotropic nanotube assumption is reasonable.

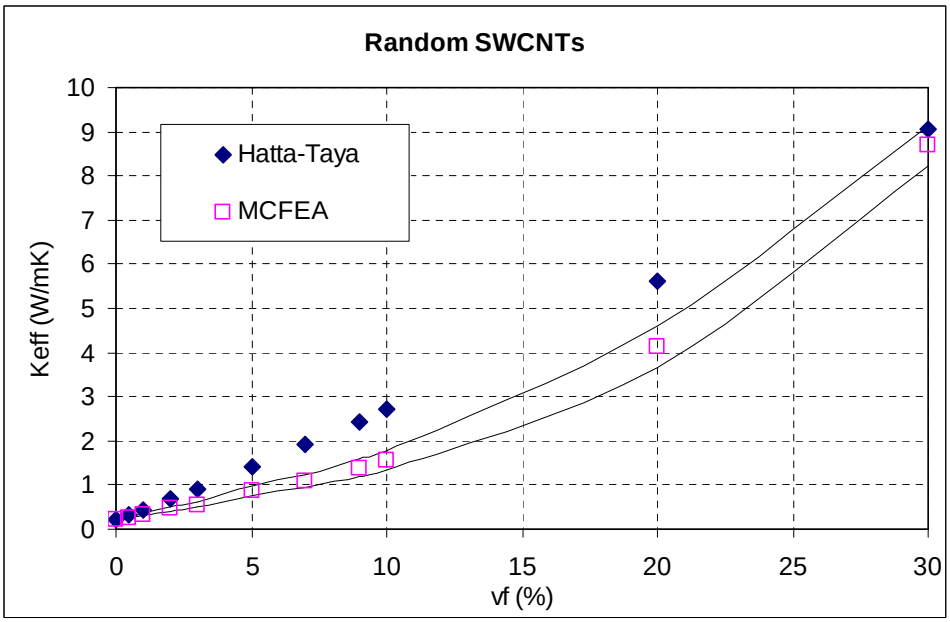

Figure 6-24. The proposed MCFEA compared with Hatta-Taya method. SWCNTs are randomly distributed in polymer. Solid lines are the corresponding standard deviation of the MCFEA.

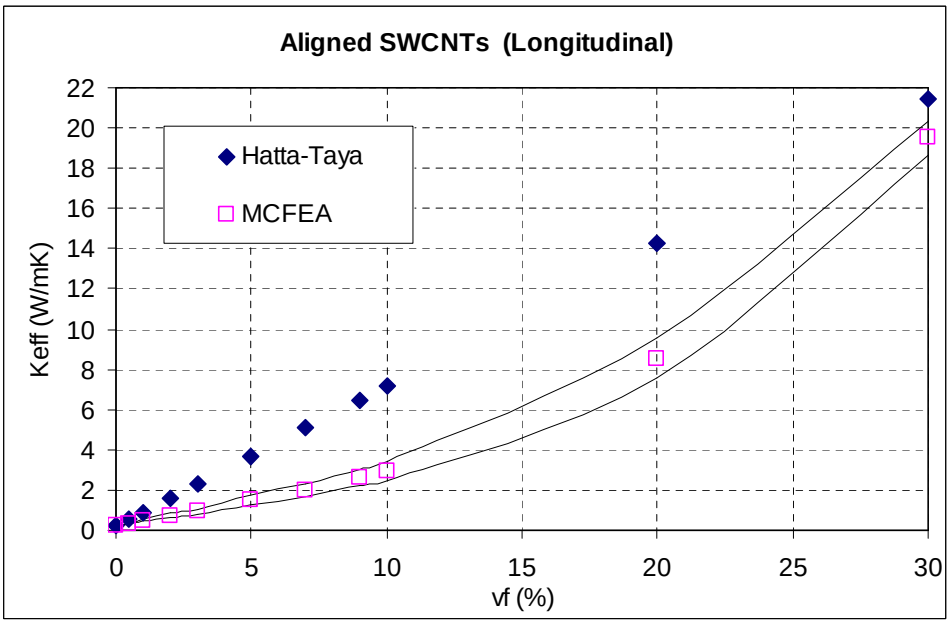

Figure 6-25. The proposed MCFEA compared with Hatta-Taya method. SWCNTs are aligned along the length but distributed randomly in polymer. Solid lines are the corresponding standard deviation of the MCFEA.

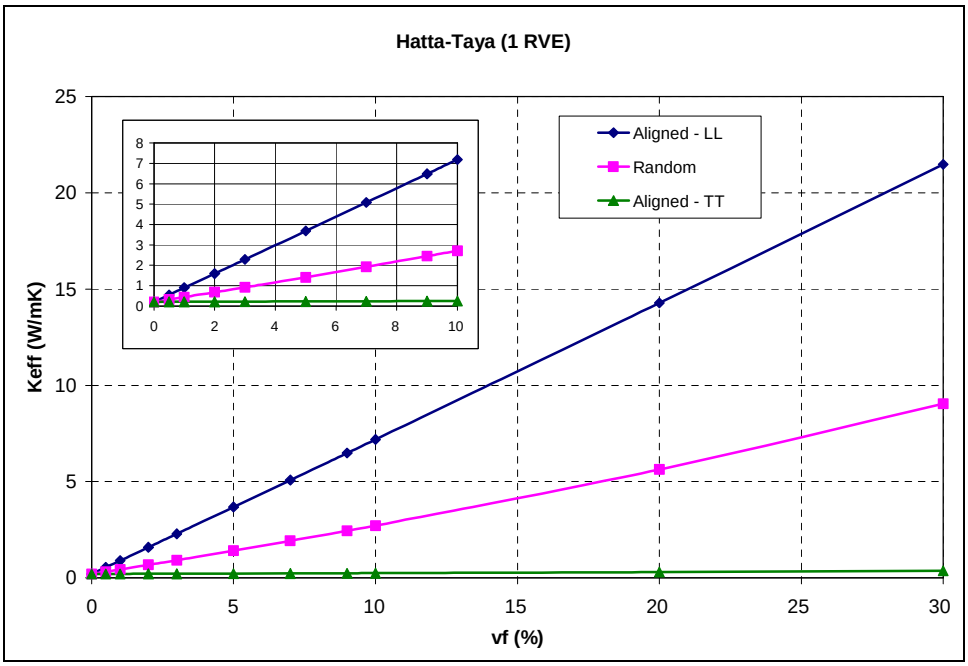

Figure 6-26. Comparison of randomly distributed and aligned PNCs, produced by Hatta-Taya method.

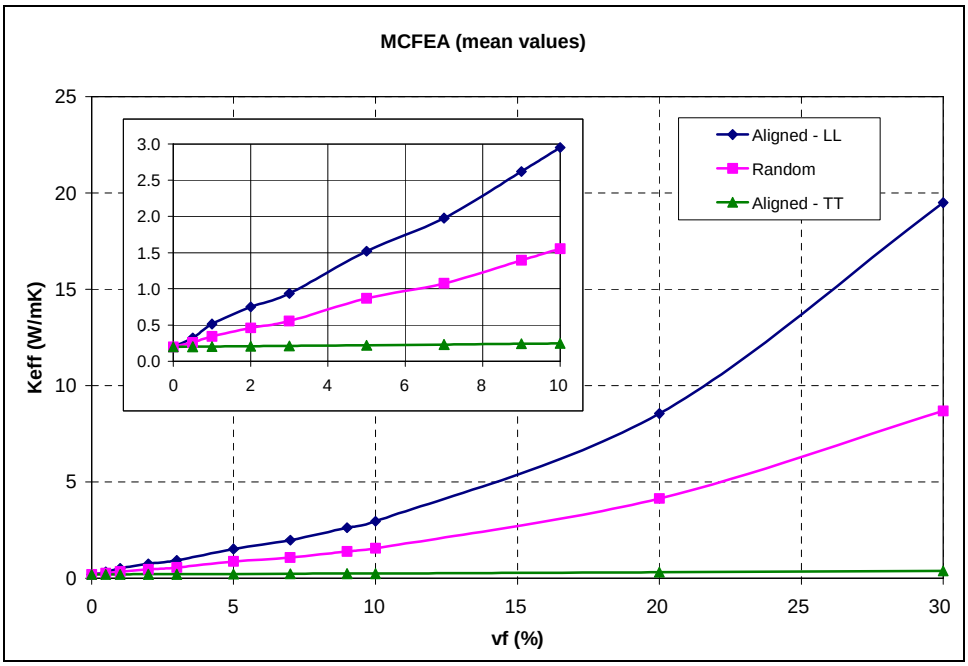

Figure 6-27. Comparison of randomly distributed and aligned PNCs, produced by the proposed MCFEA.

Chapter 7

Behavior of PNCs in Thermal Cycling

Having superior thermal properties over conventional materials, polymer nanocomposites are quite appealing as micro components in thermal and electrical applications. These components are typically subjected to large repetitive temperature variations. The stresses and strains induced by such temperature cycling cause thermal fatigue damage in PNCs. This damage is defined as gradual property degradation, which results from voids existing in PNCs. Consecutively, the progressive fatigue damage is considered to accumulate as the void content increases due to thermal cyclic loading. This chapter proposes a novel approach for simulating the long-term performance of PNCs. Temperature cycling is applied to a constrained polymer coupon containing SWCNTs and pre-existing voids. A Weibull-based model is adopted for the gradual progress of the void content. PNC properties are calculated in each thermal cycle by homogenization methods. Degradation of the PNC properties and the consequent PNC life are determined. Extensive parametric studies are performed. Pertinent theoretical and numerical backgrounds are also provided.

7.1. Thermal Fatigue and Failure Criteria

Increased use of polymer based composites reinforced with carbon nanotubes (PNCs) has prompted extensive research in estimating their properties, such as mechanical and thermal. The majority of the efforts have been devoted to predict their properties in constant equilibrium or static conditions. However, their long term behavior has been much less investigated. This chapter focuses on the long term performance of the PNCs.

Fatigue

During their time of service, most engineering materials are subjected to cyclic or alternating loads. Cyclic loading causes damage and material degradation in a cumulative manner - phenomenon known as fatigue. When this progressive damage accumulation occurs due to large temperature variations and repetitive thermal loading, it is called thermal fatigue. Continuously regenerated stresses and strains are induced by this thermal cycling. Their quantities are less than the values required to fracture the material in a monotonic load testing. Nonetheless, they can exert substantial influence on the material properties in long-term exposure.

The mechanism of fatigue for metals is relatively well established. However, it is extremely complicated for polymer composites due to their inherent inhomogeneities and anisotropy. The complexity in damage process increases even further for the PNCs due to their nanoscales. In general, fatigue response of composites includes progressive change in the state of the material, the interactions of their constituents, and the changes in their properties, e.g., elastic modulus and thermal conductivity. Therefore, understanding the

damage mechanisms, remaining properties, and expected life is crucial if the composite materials are to satisfy long-term performance requirements. In this regard, this chapter attempts to estimate the life and performance of PNCs under thermal fatigue loading.

Failure Criteria

Fatigue life of materials is associated with the premature failure or damage of a component under repeated mechanical or thermal loading. Catastrophic failure takes place when the amount of damage exceeds a critical value. For instance, assuming cyclic loading is applied to a polymer composite used as a structural member. It yields an alternating stress, which is lower than its ultimate strength. The fatigue damage growth then leads to deterioration in strength of the composite. Finally, the failure is considered to occur as the material loses its load carrying capacity, and subsequently the residual strength equals the applied load. This failure process is shown in Figure 7-1 [206].

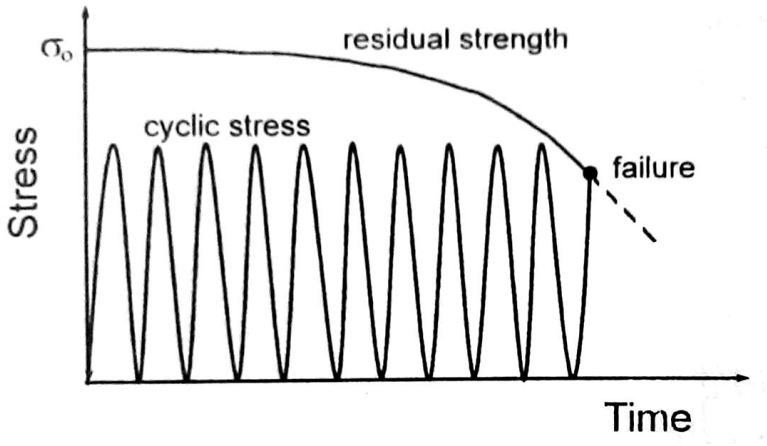

Figure 7-1. Degradation of composite strength. Failure occurs when residual stress meets cyclic stress.

As presented in the above example, strength is one of the well-known failure criteria used in engineering applications. However, the strength-based failure criteria suffer from a number of weaknesses. The assessment of the remaining strength is solely dependent on destructive testing. Therefore, an extensive and costly experimental characterization is required to predict the strength degradation. Further, when the slowly accumulated damage reaches near the fracture point, the composites can undergo sudden failure. This phenomenon results in inaccuracy in the measurements [207], [208].

Depending on the design specifications, various other fatigue damage or failure criteria can be enforced to define the life of the polymer composites. Each application requires a distinct failure criterion, or a combination of such criteria. The fatigue criteria may involve the degradation of the mechanical or thermal properties of PNCs, such as elastic modulus, coefficient of thermal expansion (CTE) and thermal conductivity. In other words, if any selected property falls below a specified value, the component is considered to be failed or damaged. In particular, stiffness-based fatigue criteria are useful for monitoring the structural property degradation of the composite materials, as they can be tracked by non-destructive testing (NDT). The response of the material reveals the changes in stiffness associated with the fatigue damage [209]. In case of thermal fatigue, assessment of degradation in CTE may also be critical, as the induced thermal strains affect the displacement-controlled composite designs. Similarly, the damage criteria can be on thermal conductivity basis. The deterioration of the conductivity results in poorer heat removal from a composite, whose performance is reduced by overheating. All of the mentioned criteria are eventually used to predict the remaining life of the composite.

Note that, the assumed failure criterion must be the most critical mechanism and it must have more influence over the component than any other criteria. In other words, the material must be pronounced as failed, first by that assumed criterion.

7.2. Damage Mechanism and Evolution

Whether it is metal or composite, the fatigue damage process can generally be divided into two major phases – initiation and propagation. For metals, the initiation portion includes the development and the early growth of a small crack, which then propagates until the failure. Most of the fatigue life is spent in the initiation of a single dominant crack [210]. On the contrary, the heterogeneity of the reinforced polymer composites leads to a mixture of damage modes. The damage initiation starts with matrix cracking and/or micro voids; followed by interfacial debonding between the matrix and the inclusion, and breakage of the reinforcement. Further, if the composite is laminated, it can evolve from delamination between the plies. The progressive development of damage can emerge from the increase of initial damage, or from the initiation of new damage types [207], [211]. In this context, characterization of the damage mechanism is highly essential in the development of fatigue models for composites, particularly for PNCs.

Proper experimental observation of the damage progression is a key element in modeling the fatigue life of composites. For instance, Stinchcomb and Bakis [209] investigated the fatigue behavior of a fiber reinforced composite under cyclic loading. Figure 7-2 shows the change in stiffness with respect to number of cycles, under tension-tension loading.

Three distinct damage stages can clearly be identified. Stage I is characterized by the initial decrease in stiffness induced primarily by matrix cracking. Stage II is the intermediate stiffness reduction period caused by further matrix cracking, crack couplings, and internal delaminations. Finally, in Stage III, growth of the previous damages and fiber breakages result in rapid decrease in stiffness of the composite.

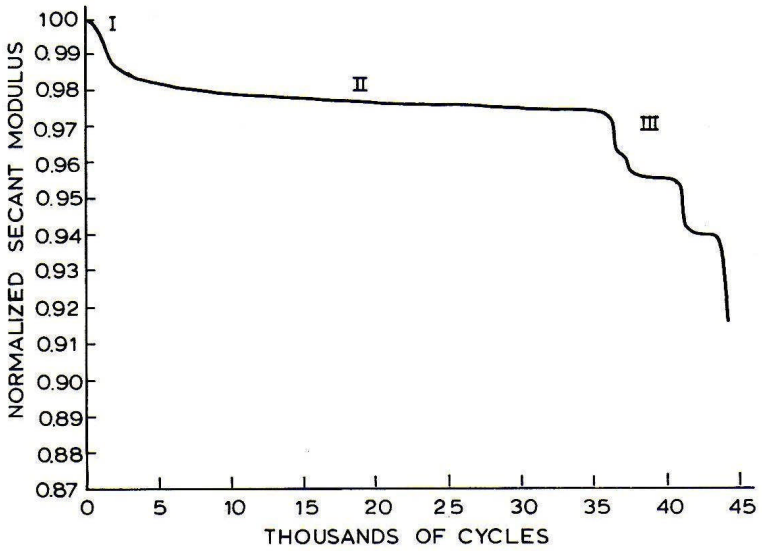

Figure 7-2. Stages of stiffness reduction during fatigue life.

Another study done by the same authors investigates the influence of the load level on the stiffness change of composites, shown in Figure 7-3. The composites were subjected to completely reversed tension-compression loadings. High degree of similarities in the fatigue behavior was observed for both tensile and compressive loading. Low stress level yields to long life and high stress level results in short composite life. Further, regardless of the life, both loadings show similar behaviors over their fatigue life.

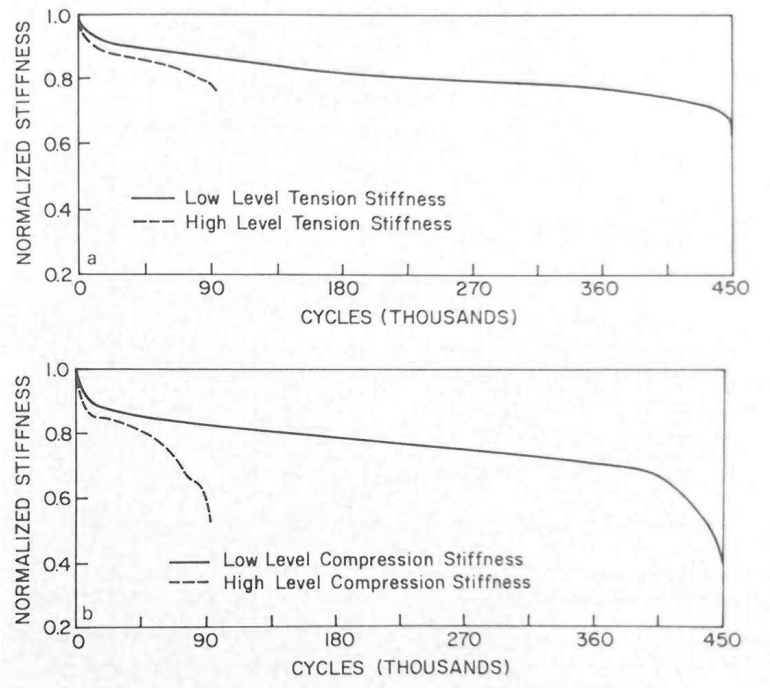

Figure 7-3. Effects of fatigue loading on stiffness change, for tensile and compressive loadings.

Matrix Cracking

Notice that Stage I of both experimental studies cover approximately ten percent of the over all fatigue life of the composite. This phenomenon has been emphasized by several other researchers, as well. Hansen [212] investigated the fatigue damage development of glass fiber reinforced composites. Figure 7-4 shows the experimentally measured stiffness reduction. The author divides the damage evolution into two phases. Phase I is referred as the development of micro-cracking part, which occupies approximately 20 percent of the total fatigue life. Stiffness degradation only occurs due to micro cracks or voids during Phase I, and continues until they become saturated. Followed by Phase II, the stiffness reduction is further assumed to take place because of other damage mechanisms, such as crack interactions and fiber breakage.

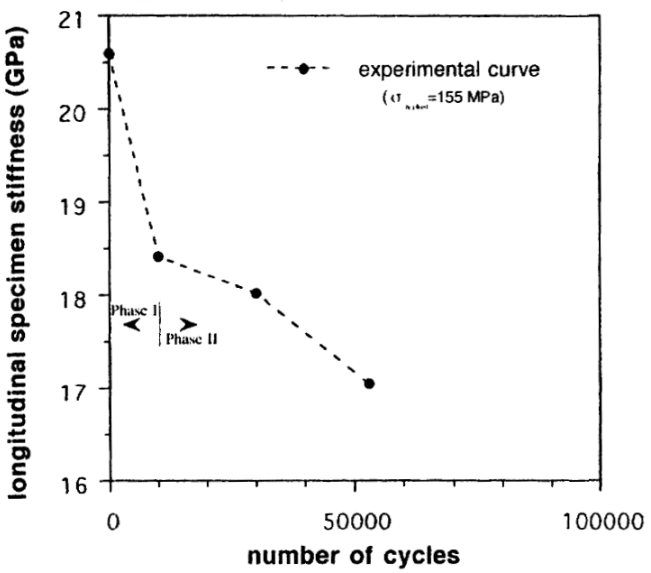

Figure 7-4. Experimentally measured modulus change in fatigue. Reproduced from Hansen [212].

Naik et al. [213] conducted fatigue experiments in an attempt to characterize the stiffness loss progression. Figure 7-5 shows the deterioration in normalized stiffness plotted on a semi-log scale. Region I of the curve is dominated by the evolution of matrix cracking, which corresponds to nearly 15 percent of the entire life.

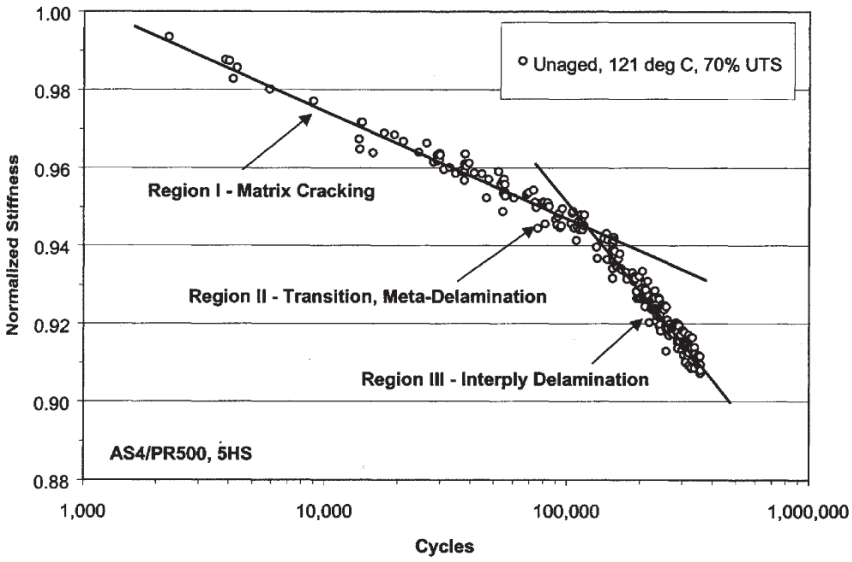

Figure 7-5. Experimentally measured stiffness loss in fatigue [213].

As pertinent literature studies show, formation of micro cracks/voids dominates the initial stage of the fatigue damage. The micro defects thereby cover the first 10 to 20 percent of the total life of the polymer composites. The transition point between the first and the second stages is controlled by a phenomenon known as characteristic damage state (CDS). In the course of cycling loading, the pre-existing cracks or voids increase in number fairly fast. The rate of this increase eventually slows down and reaches a constant value. This saturation level provides an upper limit for micro-cracking, and is called CDS. The CDS is governed by the properties of the matrix and the environmental conditions. The damage progressing after the CDS is believed to emerge from other damage mechanisms [211]. The schematic of the mentioned damage stages during fatigue life of a composite is represented in Figure 7-6.

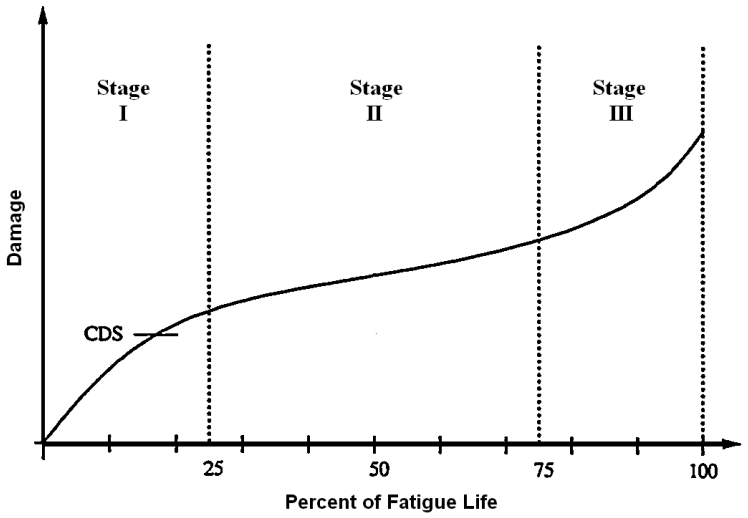

Figure 7-6. Damage progression during fatigue life of a composite. Reproduced from Reinsnider [211].

In engineering practice, codes and regulations impose strict safety design factors, particularly on structures that are subjected to fatigue loadings. For instance, Det Norske Veritas (DNV) is one of the well recognized foundations, servicing for maritime and oil

industries. The code DNV-OS-F101 recommends a safety factor of 10, for the design of structural members against fatigue [214]. This procedure has motivated the focus, in this chapter, on the investigation of the Stage I damage evolution that solely involves matrix cracking and void nucleation.

Damage Evolution

As the nature of the damage evolution, new cracks and voids are formed at each cyclic loading. The local stresses that create the micro defects permanently yield the matrix locally around them. This leads to the change in local stress distribution, and the damage thus remains localized in a comparatively small volume. As a result, the structure keeps its integrity and the certain portion of the load-carrying capacity. Consequently, composite materials have potentially greater resistance against fatigue than other common materials. The energy, which is fed into the system during cycling loading, is distributed by the formation of micro cracks/voids. This phenomenon especially holds for brittle matrices in which a great number of cracks form and grow, improving the fatigue behavior due to energy dissipation. Tough matrices fail under high stress or strain and the crack formation is fairly complex. This causes shear stress concentration on fiber-matrix interface which leads to debonding, slippage and fiber breakage. This damage mechanism is more dangerous than high micro crack formations in brittle matrix [215–217].

Stress concentrations and large strains are generated locally in the vicinity of the existing defects, which comprise inclusions, pre-existing cracks and cavities. They yield inelastic behavior at micro level, even though the polymer composite behaves elastically under

cyclic loading. Eventually, voids are nucleated and arrested due to local plastic deformations [188]. This behavior is shown in Figure 7-7. The schematic represents the formation of micro cracks and voids under tensile and compressive loading.

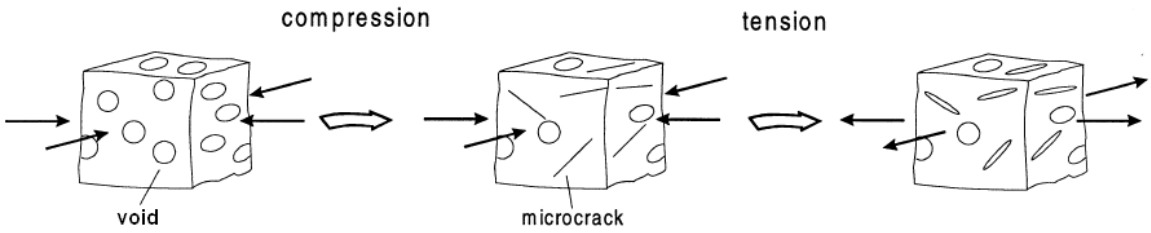

Figure 7-7. Development of micro voids and cracks under tensile and compressive loading.

The influence of micro voids are more pronounced in particle reinforced polymer composites. Unlike continuous fiber composites, tremendous amount of micro or nano inclusions exist in particle composites. The importance, thus, stems from the fact that each inclusion can potentially act as a crack originator. The cracks are initiated at the inclusion tips or at abrupt kinks, due to local stress concentrations. The local stresses stem from the differences between the properties of the matrix and the inclusion; e.g., elastic modulus and coefficient of thermal expansion. After a crack nucleates, it is confined as voids in the vicinity of the source because of local plastic deformation. In the event of fatigue, the number of voids increases at each load cycle. Micro cracking occurs both in tensile and compressive fatigue. The crack/void initiation and growth behave essentially in similar manner. In case of compressive loading, the cracks are also nucleated by local tensile stresses. Further, it can be said that the number of confined voids are higher in compression than in tension, due to the nature of loading [218].

Fu et al. [219] investigated the effect of temperature on matrix cracking. Figure 7-8 shows the crack/voids development in a particle reinforced composite as the change in temperature increased. Thermal mis-match between the phases causes local stress concentrations, thus leading crack nucleation on and in the vicinity of the inclusions.

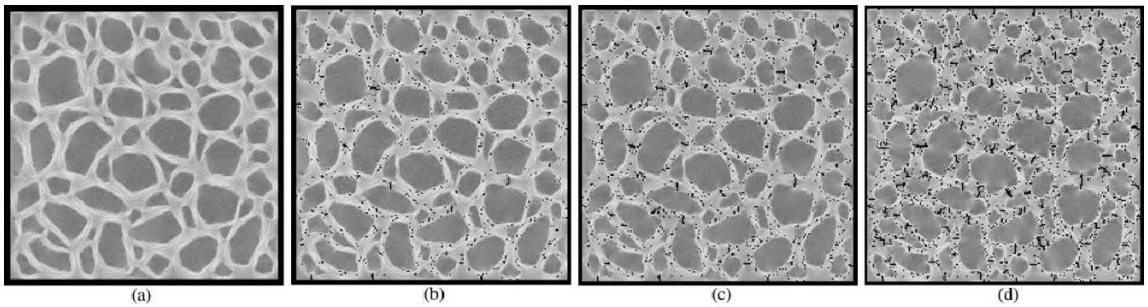

Figure 7-8. Development of micro voids and cracks induced by thermal stress.
(a) ΔT=20 °C; (b) ΔT=260 °C; (c) ΔT=320 °C; (d) ΔT=620 °C. Reproduced from [219].

Manjunatha et al. [220] studied the fatigue induce of nanoparticle-reinforced epoxy. Figure 7-9 (a) is the SEM image of the neat epoxy, revealing a void-free fracture surface. The smooth surface is the indication of a brittle failure mechanism. Figure 7-9 (a) and (b) show the fatigue fracture surfaces of the reinforced epoxy in various magnifications. The rough surface gives evidence on the ductile failure, which is accordance with the energy dissipation during fatigue damage progress. Nano-scale voids are observed in the vicinity of the nanoparticles. It is noticed that the number of voids increased during fatigue loading. They plastically deformed the epoxy and became arrested. The authors reported that the fatigue void growth rate of the particle reinforced epoxy is over an order of magnitude lower than that of neat epoxy.

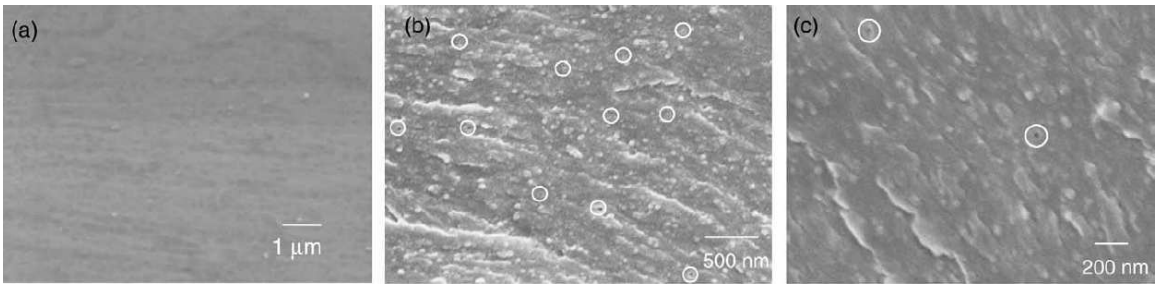

Figure 7-9. High resolution SEM images of the fatigue fracture.

Long and Zhou [221] performed thermal fatigue experiments on particle reinforced metal matrix composite (PMMC). They found that fatigue damage takes place in the form of voids and debonding at the matrix/inclusion interface.

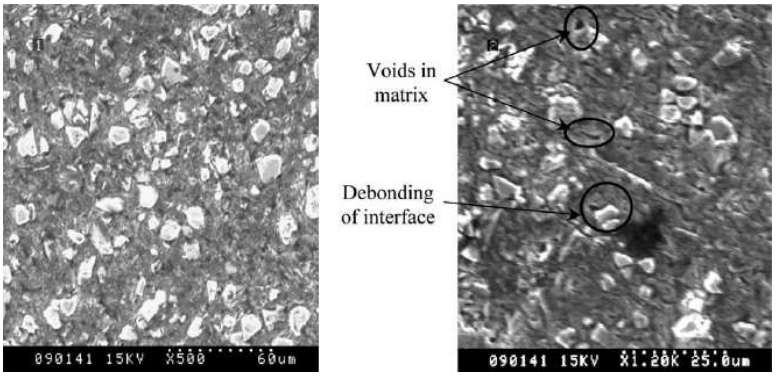

Figure 7-10. SEM images of PMMC before and after thermal loading. Reproduced from [221].

Polymer nanocomposites (PNC) have been receiving considerable attention from scientists and engineers in thermal applications, such as micro components [49], [50]. A few examples may include integrated circuits; e.g., central processing unit (CPU), chipset and graphic card. These parts are especially susceptible to temporary malfunction or permanent failure due to overheating, which is generated by computers. To this end, continuous heat removal is important to keep such components within allowable operating temperature limits during their service lives. Additionally, their structural

integrity must be sustained under the continuous thermal stresses and strains, during heating and cooling periods. In this respect, the thermal conductivity and the coefficient of thermal expansion (CTE) of the PNCs must be designed and controlled with great care. This consideration is motivated by the fact that while low CTE is associated with reduced stress or strain, higher conductivity promotes greater heat removal.

It has been shown previously in this dissertation that the existence of manufacturing induced voids decrease the properties of PNCs. When a PNC component is constrained, the increase in temperature induces internal compressive stress. The number of voids is known to grow, as this thermal stress is increased. Subsequently, the void content gradually increases with cyclic loading, as the number of thermal cycles increase. Fatigue causes progressive degradation of the properties of polymer nanocomposites. This chapter investigates the thermal fatigue behavior and damage progression, as the PNC is subjected to thermal cycling.

7.3. Fatigue Analysis Methods

Throughout their fatigue life, reinforced polymer composites experience rather complex damage developments. Mechanisms, such as matrix cracking, particle/matrix debonding, and fiber fracture, demand more elaborate fatigue models. Naturally composite materials are inhomogeneous. They may contain constituents which have distributions, properties and responses highly distinctive from each other. Further, anisotropy of composites makes the determination fatigue response and failure resistance quite complex and

challenging. To this end, proper anticipation of the property degradation and life of components made from such materials is required. This section proposes a micromechanics-based damage accumulation model to understand the long-term behavior of polymer nanocomposites in temperature cycling.

Before scientists and engineers developed analytical methods for predicting the fatigue life, they used basic empirical approaches for presenting experimental fatigue data. The most important one is the S-N diagram where constant cyclic stress amplitude, S is applied to a specimen. The number of loading cycles, N is counted until the specimen fails [222], [223]. S-N curves are obtained by conducting a number of experiments on samples of a material called coupons. Sinusoidal loads are applied to coupons by the machine while counting the number of cycles. Millions of cycles may be required to achieve fracture. In certain times coupon may not fail at specified number of cycles. Therefore, to prevent infinite cycling, tests are terminated at a limiting number of cycles, which is commonly 10^6 or 10^7. Each fatigue test is conducted with a different stress range, which in turn generates a point on the plot. Then, the S-N curve is created by the best line of these points.

In certain materials, such as steel, the S-N curve flattens out as the number of cycles increase (curve A in Figure 7-11). That stress value is referred as endurance limit at which failure does not occur no matter how long the material is tested. However, for materials like aluminum there is no endurance limit, and the coupon fails eventually (curve B in Figure 7-11). S-N diagrams can also be successfully applied to composite

systems. Yet, it is noted that the data obtain in composite fatigue experiments may be more scattered due to the natural randomness of composites.

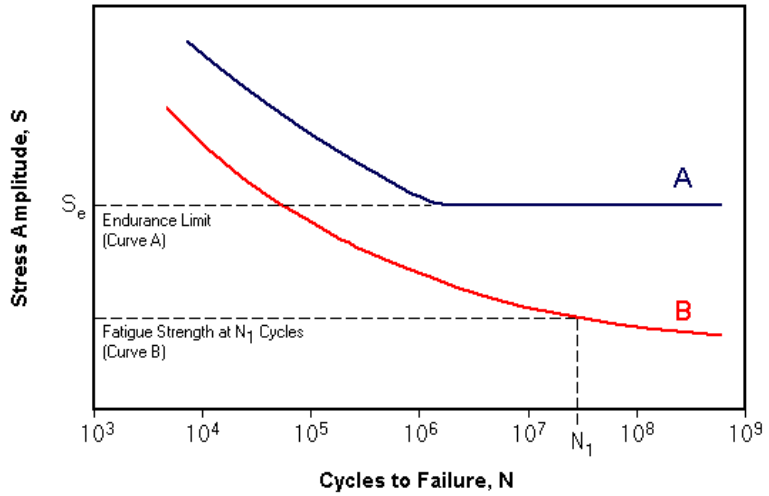

Figure 7-11. Basic S-N behavior of two distinct materials – (A) Steel, (B) Aluminum.

Heterogeneous structure and complex damage mechanics of composites demand more elaborate and complete models to understand their fatigue response. Representation of the damage stages, remaining properties, and expected life is vital for long-term performance and design of the composite materials, particularly for nanotube reinforced composites. Further, as a result of the complex nature of the composites, it is difficult to predict their behavior by detailed fracture mechanics methods. Therefore, in pursuit of predicting the life of composites in cycling loading, continuum damage mechanics models have emerged to be preferable due to their practical application in composite damage analysis [207], [224–226].

Continuum damage mechanics (CDM) focuses on the overall response of the composite by damage degradation, rather than internal fracture mechanics. In this regards, the composite is treated as a homogenous body. The damage is defined as a variable, which

is a measure of the degradation of the component. By the help of experimental observations, the evolution of the damage can be associated with the macroscopic properties of the composites, such as elastic modulus. This phenomenological CDM model was first proposed by Kachanov [227], and has been extensively used for modeling creep and fatigue damage by several researchers [224], [228–230]. Its practical use comes from the fact that it does not involve complex fracture or crack propagation theories. It only seeks to establish a relation between the composite properties and the level of damage. Further, phenomenological CDM models are particularly suited especially for Stage I damage state, where the predominant damage mechanism is homogenously distributed micro voids or cracks. However, lack of micro-structural information, including morphology and evolution, and strong experimental dependence impose limitations on the use of these phenomenological CDM models for an accurate prediction of the damage progression.

The general approach in CDM is to define a scalar variable, D ranging from 0 to 1, which describes the overall damage of a component. As the material undergoes a cyclic loading, the damage D changes from 0 (undamaged) to 1 (failure). Experimental observations are required to make a correlation between the damage and the material properties. The most common way is the measurement of elastic modulus, as it can be achieved by non-destructive techniques. A simple damage parameter, D can be presented in terms of stiffness as

$$D = 1 - \frac{\bar{E}}{E}, \qquad (7\text{-}1)$$

where $\bar{E}$ is the effective elastic modulus of the material, and E is the elastic modulus of the undamaged material. Failure is defined when D reaches the critical damage. The concept of failure depends on the specified failure criterion.

Efforts have been devoted to the development of detailed models for evaluating the macroscopic damage of composites. In this regard, micromechanical methods are incorporated into the continuum damage mechanics (CDM) models to account for the micro-structure. The model utilizes the concept of a representative volume element (RVE), whose behavior is assumed to describe the whole composite system. The damage is directly characterized by correlating it with internal state variables within an RVE. These damage variables are represented by discrete internal entities, such as defects, voids, cracks. Consequently, the micromechanics homogenization is employed to obtain the degraded properties of the RVE with the damage variables and the constituents of the composite. While a relatively superior accuracy can be achieved by the micromechanics techniques, characterization of the damage parameter variations is still based on experimental observations on the microscale. Therefore, the relationship between the internal damage variable and the overall damage of the component can be established through the micromechanical model. On that account, numerous researchers have adopted this approach. Nemat-Nasser and Hori [218] evaluated macroscopic damage by averaging over the micro structural parameters. Choi and Tamma [231], [232] predicted macroscopic damage as stiffness degradation by averaging micromechanical variables. Araki and Sato [233] took into account the distribution of micro voids and cracks into the micromechanical damage model for determining the macroscopic material properties.

Fan et al. [234] further studied the elastic properties of a composite material, considering the effect of void geometry as damage parameter.

Regarding to the variables associated with damage accumulation, both phenomenological and micromechanics based continuum damage mechanics models rely on statistical representation, which is characterized by the experimental analysis. Sun et al. [235], [236] used the transverse strength of laminated composites as the damage variable to calculate fatigue failure probability. Berthelot et al. [237] evaluated the fatigue life of a composite by calculating the strain energy in conjunction with a strength distribution. Wilkinson et al. [188] related the micro void density to the fatigue life, based on strain energy density of the composite. In contrast, cumulative fatigue damage accumulation performed by Wu and Li [238] represented the damage variable as micro flaw size. The change in the number of flaws is associated with the cumulative damage. Due to their unique nano-scale dimensions, void nucleation and evolution can be most conveniently founded on strain energy based approaches. This is as a consequence of the difficulty of extracting the individual stress/strain information of the nano-scaled inclusions. Further, strain energy based models involve the dependence on the volume fraction of the inclusions – both nanotubes and voids. This aspect facilitates the use of homogenization methods, such as Eshelby-based, for determining the overall composite properties, and particularly the influence of voids [239].

7.4. Proposed Micromechanics-Based Damage Evolution Model

This chapter attempts to develop an alternative model for the purpose of predicting the property degradation of polymer nanocomposites during thermal cycling, in conjunction with their life. The proposed model utilizes a micromechanics based continuum damage model for determining the thermal fatigue damage accumulation. On microscale, the fatigue damage parameter is characterized in terms of micro void content as void volume fraction. It is worth noting that the effects of voids on the PNC properties have been studied in Chapter 6. The results establish substantial evidence such that the presence of the voids deteriorates the thermal conductivity value of the PNCs.

The proposed damage model incorporates the progression of the void content by means of a statistical approach, as the damage mechanism. The micro voids are assumed to pre-exist within the PNC at a certain volume fraction. Further, the voids are considered to increase in number during fatigue loading, following a random or a deterministic pattern. In reality, this pattern can be obtained by experimental observation, which is then based on statistical distribution. In fatigue damage modeling of composites, using Weibull distribution to represent the damage variable is one of the most well recognized approaches. Such approaches have been adopted by several researchers. Wu and Li [238], and Kabir et al. [240] represented the damage mechanism of short fiber reinforced composites by Weibull distribution function to estimate the cumulative damage. Sun and co-workers [235], [236] assigned a Weibull distribution to define the transverse strength

of composite laminates. Wilkinson et al. [188] used the Weibull function to relate the microvoid density to the number of fatigue cycles.

In this chapter, evolution of the void volume fraction is assumed to abide with Weibull-based function. The function relates the void volume fraction (*vvoid*) at each fatigue cycle to the void fraction value at material failure (*vvfail*). The Weibull-based equation then calculates the new *vvoid* at each cycle through the use of parameters and variables, which are associated with the effective properties of the PNC.

$$vvoid = vvfail\,\frac{\sigma_0}{E_0}\left(\frac{\eta}{\eta_0}\right)^{\beta-1}\exp\left[-\left(\frac{\eta}{\eta_0}\right)^{\beta}\right], \qquad (7\text{-}2)$$

where

$$\eta = \frac{1}{2}\frac{\sigma^2}{E} \quad \text{and} \quad \eta_0 = \frac{1}{2}\frac{\sigma_0^2}{E_0}. \qquad (7\text{-}3)$$

In equation (7-3), η is the average strain energy of the nanocomposite, where E is the effective elastic modulus and σ is the average stress in the PNC, computed at each thermal cycle. The parameters with 0 subscriptions denote the initial values, representing the undamaged state of the composite. β is the shape parameter, pertinent to the shape of the distribution. The damage parameter *vvoid* is then fed into the micromechanical methods for the calculation of the effective properties of the PNC on the macroscale, at each thermal cycle. The parameter *vvfail* is determined beforehand in accordance with the failure criterion that is defined per the design specifications.

The proposed damage evaluation model takes advantage of Eshelby's equivalent inclusion method (EIM) based micromechanics homogenization techniques. They have proven to be an exceedingly efficient tool for determining the effective properties. Previous chapters demonstrated the practical use of the Hatta-Taya model for predicting the thermal conductivity of polymer nanocomposites. Similarly, in this chapter the same model is utilized in the thermal fatigue problem. Detailed information and broad parametric study on the Hatta-Taya model are provided in Chapters 4 and 5.

In pursuing a solution for the thermal fatigue problem, the proposed model incorporates the average stress and effective stiffness of the PNC. The PNC system simulated in this work is considered to be constrained. When its temperature is raised, the stress in the material increases. The coefficient of thermal expansion (CTE) describes how this thermal stress is related to the change in temperature and the elastic modulus of the PNC. Basically, this relation can be described by the equation

$$\sigma_{thermal} = E\alpha\Delta T\,, \qquad (7\text{-}4)$$

where E is the effective elastic modulus, α is the effective CTE and ΔT is the temperature change.

In the context of estimation of those PNC effective properties, the proposed model employs the well-known Mori-Tanaka (MT) approach. The Mori-Tanaka's method has been used by various researchers for PNCs [82], [123], [241], [242]. Briefly, the MT model considers a composite which contains randomly oriented, identically shaped

ellipsoidal inclusions. The average stress, $\bar{\sigma}$ and strain, $\bar{\varepsilon}$ in the composite can be represented through the stiffness tensor, L , given by the generalized equation

$$\bar{\sigma} = L\bar{\varepsilon}\,, \tag{7-5}$$

In a similar manner, the average stress and strain in the inclusion and the matrix phases can be expressed as

$$\bar{\sigma}_r = L_r\bar{\varepsilon}_r \quad \text{and} \quad \bar{\sigma}_0 = L_0\bar{\varepsilon}_0\,, \tag{7-6}$$

where the subscriptions *r* and *0* denote the inclusion and matrix phase, respectively. Then the average stress of the inclusion is recast by applying the Eshelby's equivalent inclusion principle as

$$\bar{\sigma}_r = L_r\left(\bar{\varepsilon}_0 + \varepsilon_r^C\right) = L_0\left(\bar{\varepsilon}_0 + \varepsilon_r^C - \varepsilon_r^*\right), \tag{7-7}$$

where ε_r^* is the equivalent transformation strain, standing for the misfit strain. ε_r^C denotes the constrained strain that is reached at equilibrium between the matrix and the inclusion. Figure 7-12 shows the Eshelby's approach by visualizing the problem [239].

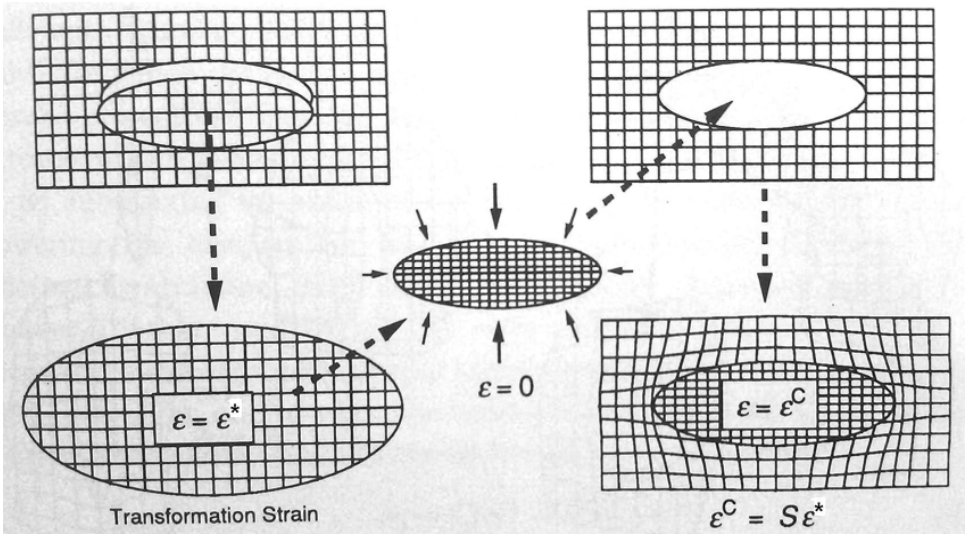

Figure 7-12. Eshelby's natural shape mis-match representation between the inclusion and the matrix. Reproduced from [239].

Eshelby showed that ε_r^C can be obtained from ε_r^* through Eshelby's tensor 'S', given in equation (7-8). The tensor S is calculated in terms of the aspect ratio of the inclusion and the Poisson's ratio of the matrix. Further details on the Eshelby's approach can be found in Mura [243].

$$\varepsilon_r^C = S_r \varepsilon_r^* . \qquad (7\text{-}8)$$

Subsequently, the average strain in the matrix can be derived from the internal stress balance equation in the composite.

$$\bar{\varepsilon}_0 = -\sum c_r \left\{ \varepsilon_r^C - \varepsilon_r^* \right\} . \qquad (7\text{-}9)$$

Eventually, Mori-Tanaka [244] develops the equation for the effective stiffness of the composite as

$$L = \left(c_0 L_0 + \sum_{r=1}^{n} c_r \left\{ L_r A_r \right\} \right) \left(c_0 I + \sum_{r=1}^{n} c_r \left\{ A_r \right\} \right)^{-1} , \qquad (7\text{-}10)$$

where

$$A_r = \left[I + S_r L_0^{-1} \left(L_r - L_0 \right) \right]^{-1} . \qquad (7\text{-}11)$$

In the above expressions, c_0 and c_r represent the volume fraction of the matrix and the inclusion, respectively. The curly brackets denote averaging over all possible inclusion orientations.

In regard to the effective CTE of composites, the Eshelby's method can be modified by introducing a thermal mis-fit strain as

$$\varepsilon_r^T = (\alpha_r - \alpha_0)\Delta T \,. \qquad (7\text{-}12)$$

Then, equation (7-7) can be recast as

$$L_r\left(\bar{\varepsilon}_0 + \varepsilon_r^C - \varepsilon_r^T\right) = L_0\left(\bar{\varepsilon}_0 + \varepsilon_r^C - \varepsilon_r^*\right). \qquad (7\text{-}13)$$

The final expression for the effective CTE ($\bar{\alpha}$) is given as

$$\bar{\alpha} = \alpha_0 + \sum_{r=1}^{n} c_r \left\{A_r^{-1} L_r\right\}(\alpha_r - \alpha_0)/\Delta T \,, \qquad (7\text{-}14)$$

where

$$A_r = (L_r - L_0)\left[c_0 S_r + \sum_{r=1}^{m} c_r\right] + L_0 \,. \qquad (7\text{-}15)$$

The values obtained from the equations (7-10) and (7-14) are plugged into equation (7-2) to update the void volume fraction at each thermal cycle. The new *vvoid* is then used to calculate the new PNC properties. The simulation is carried out until the degraded properties of the system meet the design failure criteria. The final property values are the remaining properties of the PNC, and the last cycle of the simulation denotes its expected life. The following section describes the application of the proposed model in detail and presents extensive parametric study.

7.5. Assessment of Thermal Fatigue Damage

The practical application and effectiveness of the previously developed damage evolution model for polymer nanocomposites subjected to thermal cycling are assessed in this section. Specifically, degradation of PNC properties during thermal fatigue as a result of increasing void volume fraction is studied. Computer simulations have been executed with the intention of concentrating on the adverse effects of void accumulation, vis-à-vis abandoning the statistical aspects of the problem. In this respect, the PNC is assumed to comprise a base matrix, individual SWCNTs and pre-existing micro/nano voids, with homogeneous distributions and perfectly random orientations.

In the course of simulating the thermal fatigue behavior, the PNC is modeled in the form of a square coupon with proper boundary conditions. The coupon is longitudinally restrained at the top and bottom ends, and it is alternately heated and cooled. The change in temperature (ΔT) is kept constant and assumed to be uniformly applied throughout the specimen. When heated, the coupon experiences compressive stress within, associated with its effective properties – CTE and elastic modulus – along with the applied temperature difference (equation (7-4)). The magnitudes of these PNC properties are determined by using the Mori-Tanaka homogenization method, described in Section 7.4. Similarly, the average strain energy within the coupon is then evaluated by using the average thermal stress and the effective stiffness (equation (7-3)). Subsequently, the proposed Weibull-based damage evolution equation is used to compute the void volume fraction (*vvoid*) within the coupon (equation (7-2)). At each thermal cycle, the updated

vvoid value is used to determine all these properties and parameters. Conclusively, the effective thermal conductivity of the coupon is independently calculated by applying the Hatta-Taya homogenization method. Similar to the previous chapters, the sides of the coupon are assumed to be thermally insulated allowing 1-D heat transfer. Figure 7-13 shows the structure of the PNC coupon and the corresponding boundary conditions used in the simulations.

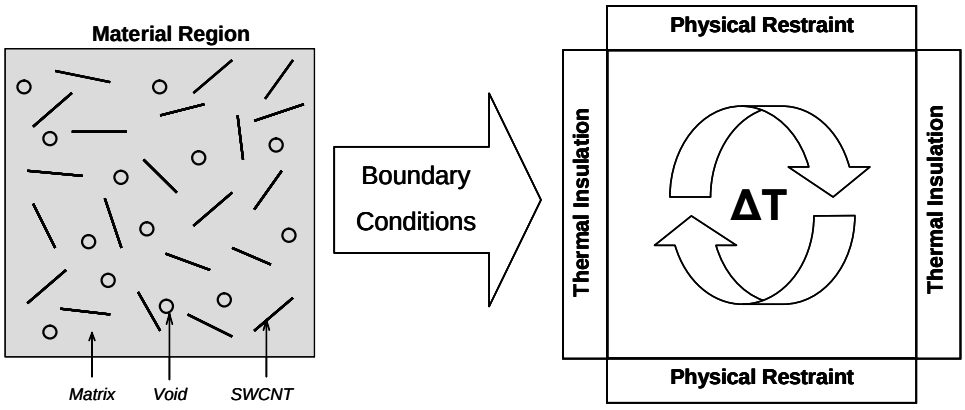

Figure 7-13. Schematics of the micromechanics model and the appropriate boundary conditions.

The polymer nanocomposite is modeled as a three-phase media; consisting of a neat matrix, individual SWCNTs and spherical voids. The voids are assumed to be individually distributed and spherical in shape. The SWCNTs are considered to be isotropic regarding their thermal conductivity and expansion coefficient, yet transversely isotropic in regard to the mechanical properties.

Epoxy polymer is chosen as the polymer matrix, because of its wide range of applications in engineering. Table 7-1 summarizes the properties of the epoxy used in the micro-mechanics homogenization methods. The CTE value of the epoxy is from Takahashi et

al. [245], and the thermal conductivity is from UL IDES database [246]. The isotropic elastic properties are provided from the study of Zhu et al. [247].

Table 7-1. Properties of Epoxy

Thermal	K (W/mK)	0.2
	CTE (1e-6/K)	60
Mechanical	E (GPa)	2.026
	ν	0.3

Table 7-2 presents the SWCNT properties used in the Hatta-Taya and Mori-Tanaka methods for calculating the effective properties of the PNC. The selected thermal conductivity value is consistent with the ones used in the previous chapters, which takes into account the interface thermal resistance. In the simulations, the CTE is treated as a modeling parameter, rather than a single-value property. In literature, both experimental and numerical studies conducted by scientists predicted the CTE of a SWCNT ranging from –10 to +10e-6 1/K [65], [248], [249]. The effect of nanotube CTE is investigated in the parametric study. As the SWCNT is assumed to be transversely isotropic in terms of mechanical properties, the five elastic parameters are obtained from the work by Seidel and Lagoudas [82].

Table 7-2. Properties of SWCNT

Thermal	K (W/mK)	75
	CTE (1e-6/K)	-10 to +10
Mechanical	E_{11} (GPa)	704
	E_{22} (GPa)	345
	μ_{12} (GPa)	227
	ν_{12}	0.14
	ν_{23}	0.3764

In Table 7-1, K is thermal conductivity; CTE is coefficient of thermal expansion; E is elastic modulus and ν is Poisson's ratio. Further, in Table 7-2, E_{11} and E_{22} represent the longitudinal and transverse moduli, respectively; μ_{12} is the Poisson's ratio in longitudinal plane; ν_{12} and ν_{23} are the shear moduli in longitudinal and transverse plane, respectively.

The void properties are assumed to have insignificant values equaling to zero. In regards to the aspect ratios of the inclusions, the voids are regarded as spherical in shape, thus having an aspect ratio of 1. Similarly, the aspect ratio of the SWCNTs is taken as 150 in accordance with Chapter 4.

Parametric Study and Sample Application

Initially, a polymer nanocomposite (PNC) coupon is considered, which is composed of epoxy matrix, individual SWCNTs with content (*vf*) of 5 percent, and a void volume fraction (*vvoid*) of 10 percent of the nanotubes (i.e., 0.5 percent). An alternating temperature change (ΔT) of 40 degrees is applied to the PNC. In addition, the Weibull shape parameter (β) in equation (7-2) is assumed to be equal to 15. However, it is again emphasized here that the value of beta directly relies on experimental observations. The parameters *vf*, ΔT and β are treated as variables in the subsequent portions, and their effects are assessed in this parametric study.

In regards to predicting the thermal fatigue life of PNCs, first the failure criterion must be defined. The simulations performed in this section focus on the elastic modulus degradation for the purpose of estimating the thermal fatigue life. Specifically, 10 percent

reduction in PNC stiffness is considered to be the determining factor. In accord with the evidence presented in Section 7.2, 10 percent reduction corresponds to the characteristic damage state (CDS). As previously stated, the CDS is governed by the matrix crack/void development, which is the focus of the proposed damage model. To this end, the simulations are terminated when the effective PNC modulus reduces to 90 percent of its undamaged value.

Then, the development of the void volume fraction is characterized, as outlined by equation (7-2). Figure 7-14 shows the progression of the void content during the thermal cycling of the sample PNC. In particular, plot (a) shows the *vvoid* values computed at each cycle, which have a diminishing behavior in time. Plot (b) gives the cumulative void volume fraction with respect to the number of cycles. The resultant cumulative *vvoid* curve converges to a constant value in agreement with the saturation level of the voids, as explained in Section 7.2.

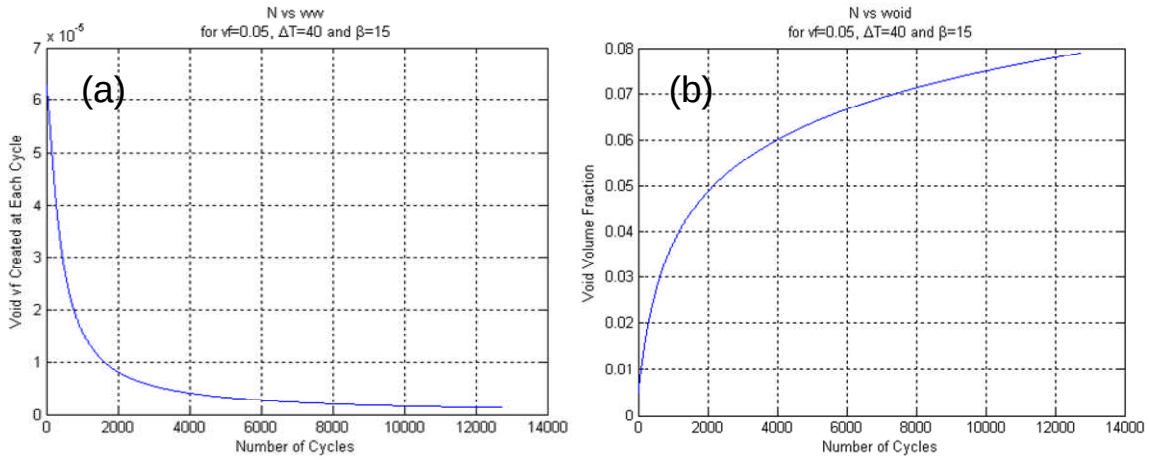

Figure 7-14. (a) Void volume fraction created in each thermal cycle. **(b)** Cumulative void volume fraction change during thermal cycling.

Special importance is placed on the cumulative void content within the composite, since it can be quantified from experiments via non-destructive testing, as explained in Section 7.1. Notably, the data obtained from these tests is subsequently used to calibrate the modeling parameters.

Further, in equation (7-2) the *vvoid* evolution is also dependent on the average strain energy ratio of the PNC. The ratio is arithmetically expressed as the division of the strain energy at each cycle to the initial strain energy. Their quantities are calculated per equation (7-3). Figure 7-15 shows the variation of strain energy (η) ratio with respect to the *vvoid* per cycle and to the cumulative void volume fraction. It is seen that η ratio decreases in time as a result of increasing cumulative *vvoid*. Given that the voids within the PNC result in reduction in the elastic modulus, and consequently lower stress as well as lower strain energy.

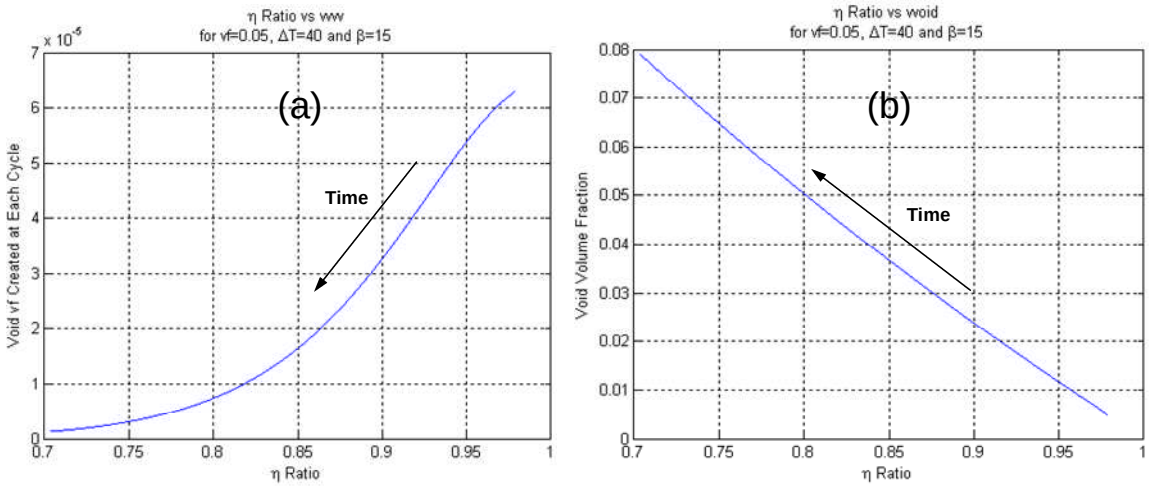

Figure 7-15. (a) Void volume fraction created per strain energy ratio (η/η_o). **(b)** Change in cumulative void volume fraction w.r.t. strain energy ratio (η/η_o).

In the context of the thermal fatigue life of PNCs, numerical simulations have been conducted with the aim of determining the influence of the several variables used in the model. In the parametric studies, three values are set a priori for each variable, while keeping the others constant. They are listed as Weibull parameter (β), volume fraction of SWCNT (*vf*), temperature change (ΔT), and CTE of SWCNT (CTEnt). Figure 7-16 shows the estimated lives of the PNCs, obtained by the developed damage model. The results produced for each parameter are shown in the sub-plots, with their pre-assigned values. In the plots, the base values of the parameters, used as constants in the model, are β = 15, *vf* = 0.05, ΔT = 40 deg, and CTEnt = 0 1/K. The thermal fatigue lives are represented in terms of number of thermal cycles. The PNC is considered to become damaged, conforming to the a priori set failure criterion, as previously described.

In Figure 7-16 plot (a), the fatigue lives are given per Weibull shape parameter (β) values of 10, 15, and 20. The results show an exponential improvement with increasing β values. This is well expected, as higher β values lead to lower *vvoid* amount created at each cycle. It is due to the fact that the strain energy ratio is less than one in equation (7-2). Plot (b) shows the effect of SWCNT content (*vf*) on the thermal fatigue life. The simulations have been conducted for PNCs with *vf* values of 1, 5 and 10 percent. Even though the life has an increasing tendency, its rate is declining. The corresponding void content has a prominent influence on this matter, as discussed in Section 6.2. In short, higher *vvoid* are created at higher *vf* and consequently leading greater property degradation. Specifically, the rate of life improvement is 26.5% per unit *vf* between 1 and 5% *vf*; 8.3% from 5 to 10% *vf*.

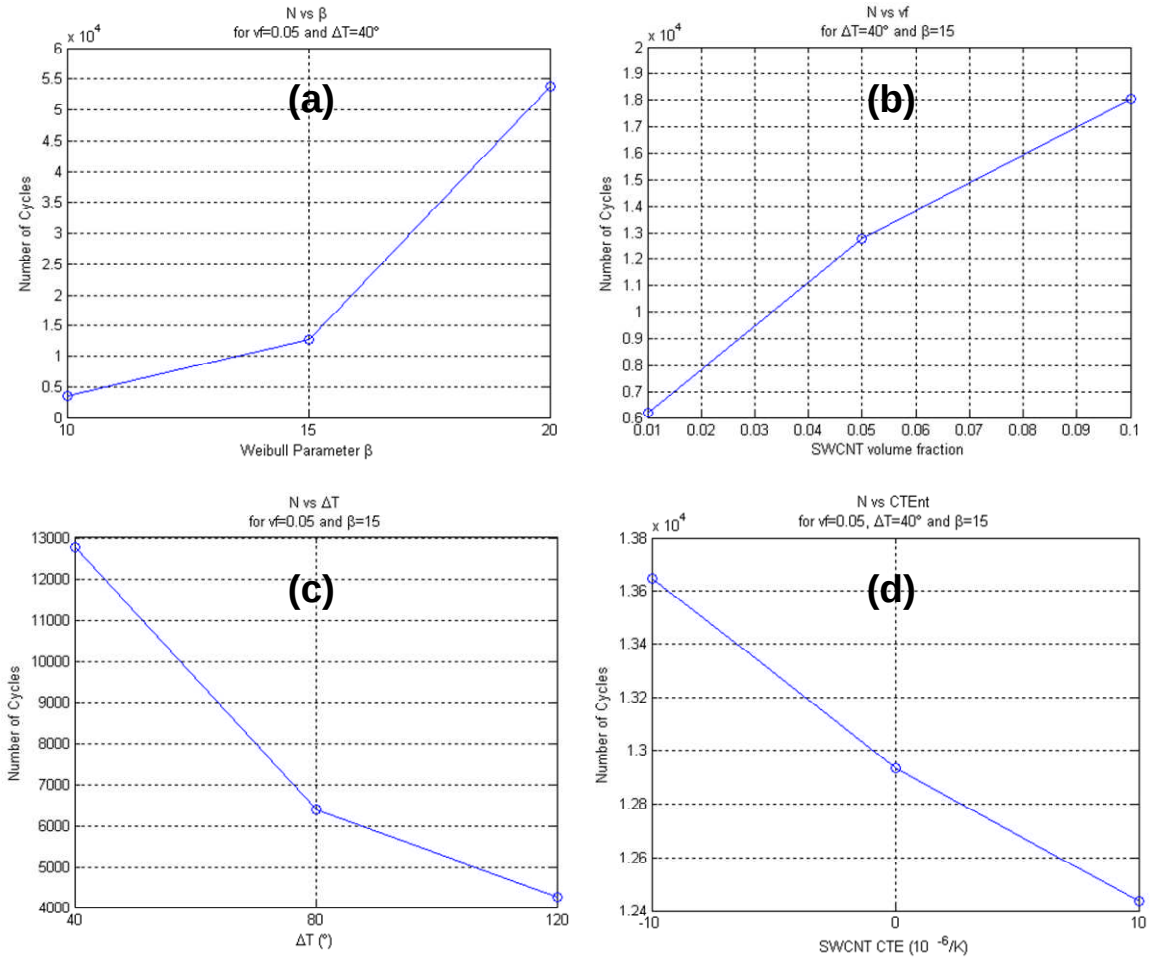

Figure 7-16. Change in PNC life (Nmax) w.r.t.; **(a)** Weibull parameter, beta values, **(b)** SWCNT volume fraction, vf values, **(c)** Temperature change, ΔT values, **(d)** SWCNT CTE values.

Plot (c) presents the PNC lives obtained for the temperature changes of 40, 80 and 120 degrees. A lessening exponential behavior is observed. As described previously, the thermal stress within the composite has a linear relation with ΔT; hence a greater amount of voids are created when larger ΔT is applied. Further, the diminishing rate is mainly attributed to the strain energy change, which is squarely proportional to the stress. In plot (d), the influence of CTE of SWCNTs is shown, using the values -10, 0 and 10 e-6 1/K. The PNC life drops with increasing CTEnt values. This tendency is expected as the lower CTEnt value results in a reduced average PNC stress, and thus a lower amount of voids

generated. It is also observed that the resultant trend is almost linear; nevertheless the amount of reduction is rather insignificant.

While Figure 7-16 solely provides the thermal fatigue lives of the PNCs, it does not offer any suggestion on the degradation behaviors of their properties. Appendices give details on the variations of the thermal (K and CTE) and elastic (E and ν) properties with respect to the number of thermal cycles. The influence of the modeling parameters (i.e., β , *vf*, ΔT, CTEnt) on each property is also presented. Notably, the property deteriorations follow similar fashions for each modeling parameter. Plots are given both on semi-logarithmic and linear scales with the purpose of enhanced assessment. Particularly, Appendices A, B, C and D provide the evolutions of the effective elastic modulus, Poisson's ratio, coefficient of thermal expansion, and thermal conductivity, respectively. As discussed earlier, the PNCs are assumed to be failed when their elastic modulus loss is 10 percent. At the material failure, 4 percent reduction in Poisson's ratio can be observed. Similarly, the effective CTE loss is approximately 11 percent. Lastly, the thermal conductivity decreases by nearly 5 percent.

Examining the plots on semi-log scale, the trend of the decay in the properties can be interpreted. As β being the shape parameter, it affects the rate of degradation. Specifically, a higher β value suggests a steeper slope of the curve, hence a lower thermal fatigue life. Regarding the impact of SWCNT *vf*, a rather non-linear fashion is observed; yet a consistent pattern can possibly be construed. To this end, a comparison of the normalized results reveals that rate of degradation rises with the *vf* values.

Conversely, an increase in ΔT merely causes the curve to shift down. A similar behavior is noticed in the variation of CTEnt parameter. The numerical evidence on the elastic modulus indicates that the influence of CTEnt on the PNC life is insignificant. As a consequence, it has not been studied for the other properties.

The proposed damage model calculates and updates the parameters and the properties at each thermal cycle until the failure criterion is satisfied, as described in Section 7.4. Depending on the simulation, various time steps (*dt*) are employed to optimize the numerical calculation time. Figure 7-17 investigates the influence of the time step on the effective elastic modulus degradation. The reference values are computed by *dt* equaling to 1. To this end, *dt* values of 3 and 10 are compared. The results computed by *dt* of 10 converges the reference line after 100 cycles; while a higher precision is attained as low as 10 cycles by using *dt* of 3. To conclude, the majority of the simulations are performed with *dt* of 1 in this chapter.

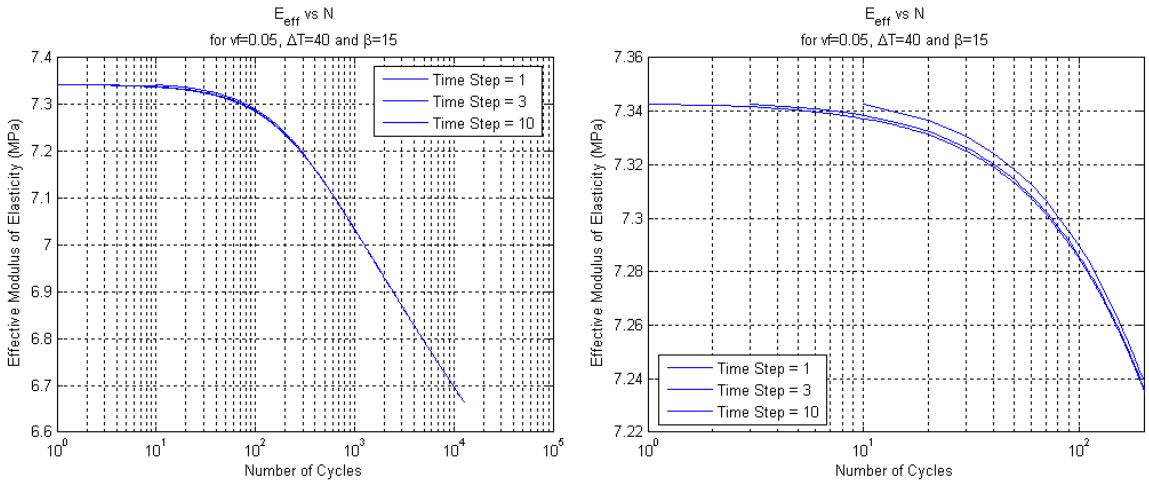

Figure 7-17. Effect of time step (dt) on the elastic modulus (E) w.r.t. number of thermal cycles (N) on a semi-log scale. Right plot shows the details of first 200 cycles.

Engineering design places special importance on the stress-strain behavior of a material. In this context, Figure 7-18 shows the progression of the secant modulus of a PNC, which can also be considered as the instantaneous elastic modulus change. The presented values are extracted at various thermal cycles. The results are for a PNC with 5% SWCNT vf in 40 degrees of temperature difference.

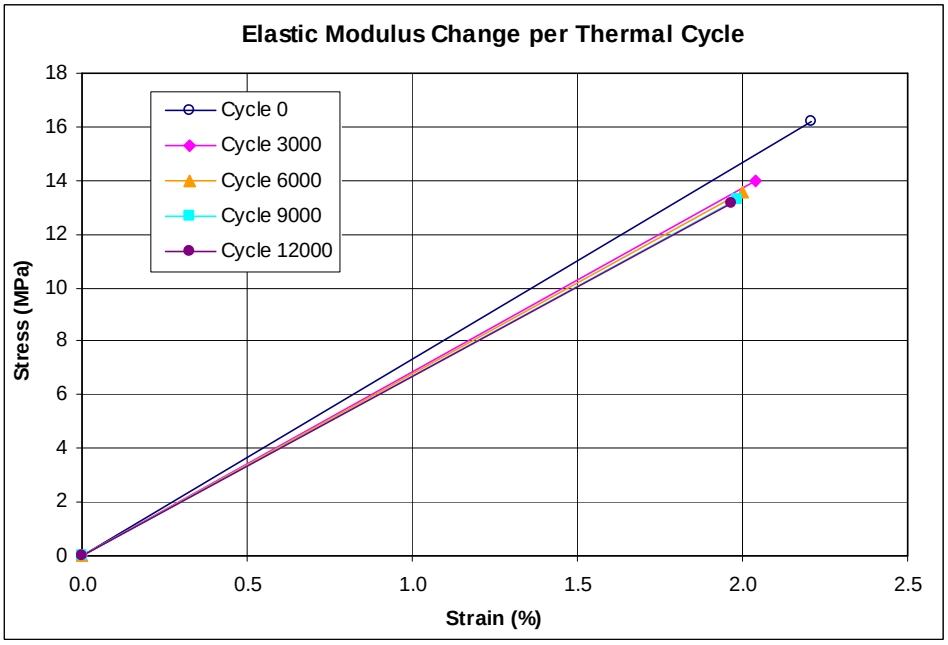

Figure 7-18. Change in thermal cyclic stress-strain behavior as damage develops.

An essential part of a computational modeling demands an adequate experimental evaluation for the assessment of its accuracy and precision. In this regard, an attempt is made to investigate the performance of the proposed fatigue damage evolution model. However, the literature provides no work pertinent to the thermal fatigue of the carbon nanotube reinforced polymer composites. To this end, the following comparisons are presented in an effort to illustrate the similarities of the trends between the experimental findings found in the literature and the numerical results computed in this chapter.

The major aspects of the problem addressed are degradation in the elastic modulus and growth of the void content. For the purpose of comparing their behavior, two sets of experimental studies are considered. Manjunatha et al. [220], performed tensile fatigue tests on epoxy polymer composites reinforced with well-dispersed silica nanoparticles. Berthelot et al. [237], analyzed the progressive development of transverse cracking in composite laminates subjected to uniaxial fatigue loadings.

Figure 7-19 and Figure 7-20 show the evolution of the elastic moduli with respect to the number of fatigue cycles, on linear and semi-log scale, respectively. The results obtained from the simulations suggest strong resemblance with the experiments. Further, the characteristic damage state (CDS) can be identified in Figure 7-19. It is noted that both numerically generated values represent the same simulation results, but on different scales. Similarly, compatible behaviors are attained in terms of the progression of the void content, shown in Figure 7-21 and Figure 7-22.

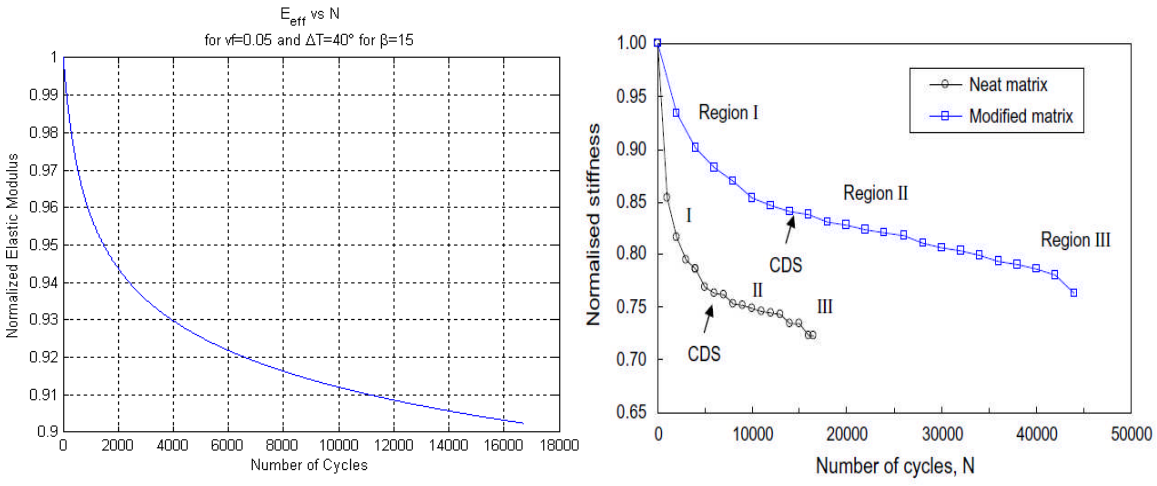

Figure 7-19. Comparison of stiffness degradation trends between the modeled sample PNC (left) and the experimentally obtained GFRPs with various matrices (right) [220].

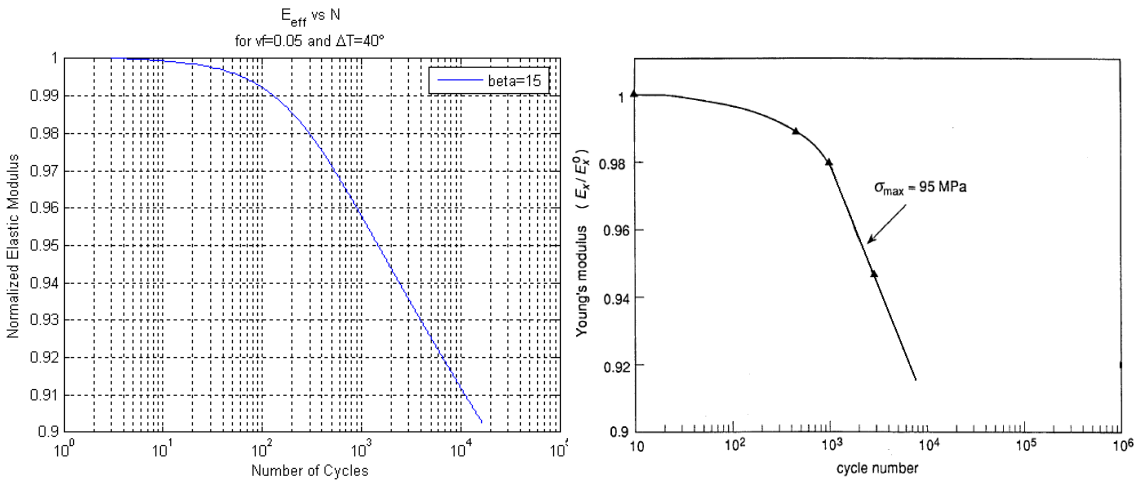

Figure 7-20. Comparison of stiffness degradation trends between the modeled sample PNC (left) and the modeled silica nanocomposite (right). Reproduced from [237].

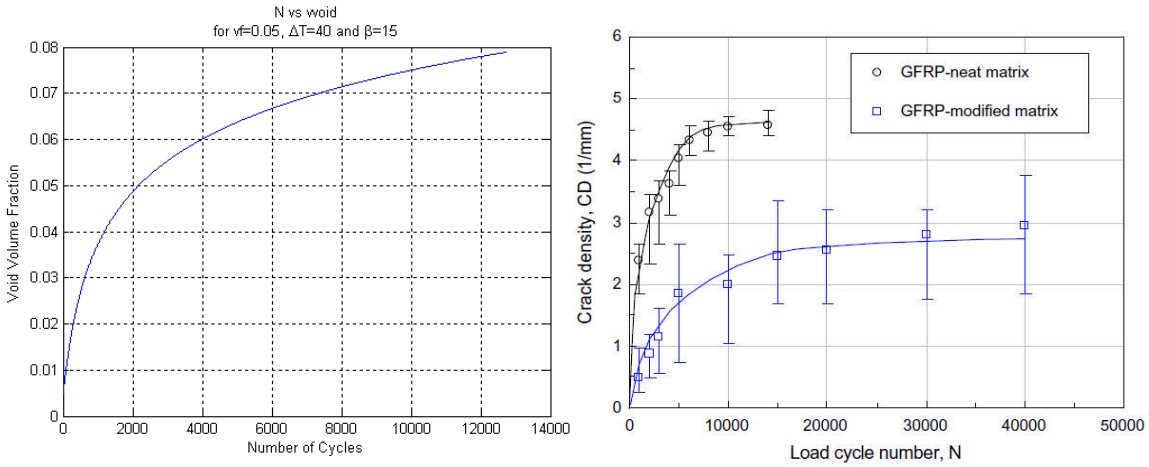

Figure 7-21. Comparison of void/crack density trends between the modeled sample PNC (left) and experimentally obtained GFRPs with various matrices (right) [220].

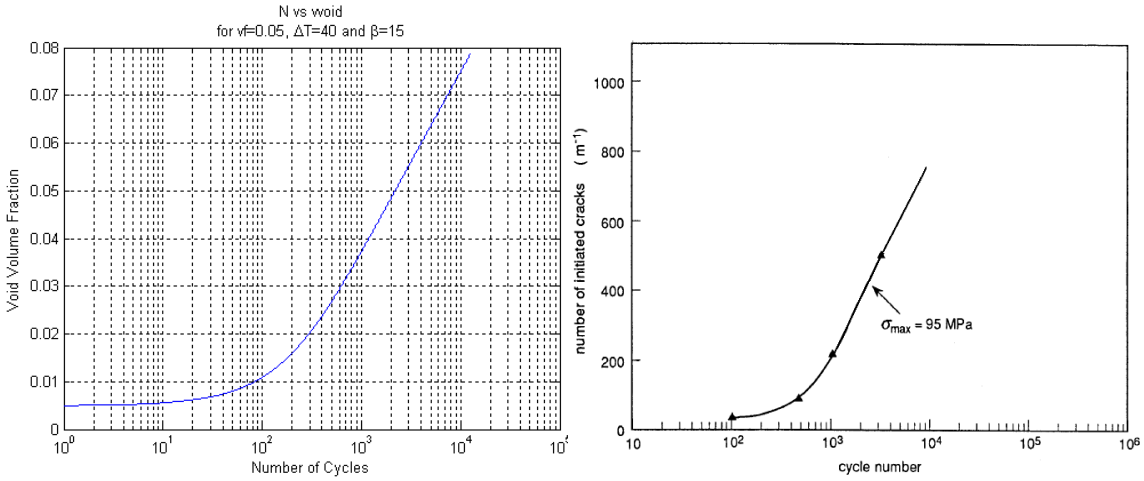

Figure 7-22. Comparison of void/crack density trends between the modeled sample PNC (left) and the modeled silica nanocomposite (right). Reproduced from [237].

Chapter 8

Concluding Remarks

A novel approach to determine the effective thermal conductivity of polymer nanocomposites (PNC) has been presented in this dissertation. The PNC has been considered to consist of randomly distributed and dispersed isotropic single-walled carbon nanotubes (SWCNT), SWCNT agglomerates and a polymer matrix. Evidence in the literature has demonstrated the notion that the thermal conductivity of PNC observed from the experimental findings and the estimations made by currently available models differs significantly. This discrepancy has been attributed to the inherent heterogeneity of the PNC, which is caused by various uncertainties, such as SWCNT dispersion, spatial distribution, size and shape. Thus, the proposed model is based on a statistical homogenization approach that captures the randomness in the nanocomposites. The characterization of the randomness in the nanostructure relies on the PNC structures obtained from actual images. In this context, the PNC has been treated as a random heterogeneous medium and its structure has been defined as a material region (MR) as a representative volume element (RVE) that has been discretized by a number of finite

elements (FEs). Random material fields have been generated that correspond to non-uniform nanotube content throughout the matrix. Local SWCNT volume fractions have been produced from appropriately selected random variables that have specific probability density functions (PDFs), i.e., uniform, normal and Weibull. A set of generated volume fraction values has been considered as one realization and assigned to each FE in the MR. The finite element method has been utilized to determine the overall thermal conductivity of the PNC in conjunction with a Monte Carlo scheme to assess the statistical information of the response. Numerous realizations of the SWCNT volume fraction have been generated to account for the variations in the distribution of the nanotubes in the polymer.

Experiments and image analyses reveal that carbon nanotubes (CNTs) exist in a non-homogeneous manner in polymers. Therefore, the proposed model assumed that a finite element is composed of a polymer, randomly distributed and dispersed individual SWCNTs and spherical agglomerates made of SWCNTs. In local level, the homogenization has been performed by the equivalent inclusion method (EIM) to determine the thermal conductivity of each FE that contains certain amount of randomly assigned SWCNT volume. Depending on the composite manufacturing, nanotubes can be present as individuals up to a certain volume and the rest forms agglomerates.

PNCs have been first modeled by the more basic hybrid approach using two-phase EIM. The individual nanotubes and the pristine matrix combination have been treated as a hybrid matrix with an improved thermal conductivity, and then the agglomerates have

been introduced into that hybrid matrix. At each stage, two-phase EIM has been employed. However, there is a strong need for a more accurate and effective technique for more realistic modeling of the PNCs. In this regard, a multi-phased EIM has been derived which can incorporate all three inclusions once with a higher efficiency. SWCNTs have been assumed to be straight, randomly distributed and oriented. The equivalent inclusion method based on the well known Hatta-Taya method, has been applied to individual SWCNTs and the polymer to determine the thermal conductivity of a finite element.

Further, the experimental studies and image analyses in the literature have proven the existence of nano/macro void inclusions within particle reinforced composites. The existence of voids originates from the current processing and manufacturing methods. It has been shown that their existence in the matrix has a lowering effect in the thermal conductivity of a polymer composite. The proposed approach in this dissertation has also investigated the impact of the voids in the PNCs by the use of the developed multi-phase equivalent inclusion method.

Furthermore, it has been shown that the undesired constituents existing in the composite besides nanotubes can impair the thermal conductivity enhancement of a nanocomposite. Provided that proper information on nanotube processing and the level of such impurities is available, the proposed approach is capable of incorporating the impurities into the model. To this end, the MCFEA has been employed to simulate such experimental studies. The results were sound and in excellent accord with the experimental findings.

The results derived by the Monte Carlo Finite Element Approach (MCFEA) capture the influence of the spatial randomness in the PNC structure, and provide statistical information of its effective thermal conductivity. Non-uniform nanotube distribution, dispersion and size effects have also been captured by the proposed model. Variations of certain parameters used in the model pertaining thermal conductivity of the constituents, SWCNT volume fraction, size, aspect ratio and their effects on the overall effective thermal conductivity of the PNC have been presented.

Next, to assess the accuracy of the proposed MCFEA, data obtained from experimental studies have been compared with present analytical techniques and with the numerical results derived by the new approach. In the comparison of the experimentally measured data with the values computed by the developed model, the interfacial thermal resistance between the polymer and SWCNT has also been considered. This high resistance appears to be a critical element in limiting the utility of nanotubes for enhancing the PNC thermal properties.

Collectively, the effective thermal conductivity values determined by the MCFEA in this dissertation have been found in good agreement with the currently available experimental data reported in the literature. Further, the approach provides valuable information on the influence of the randomness and heterogeneity in the PNC structure on the overall effective thermal conductivity of SWCNT reinforced polymers.

Lastly, this dissertation has taken an initiative in modeling the thermal cycling behavior of polymer nanocomposites. In the literature, it is known that the thermal and mechanical properties of polymer composites are impacted under thermal cyclic loading, caused by the thermally induced stresses and strains. This dissertation has focused on the first stage composite fatigue damage which is dominated by void/crack propagation. The PNCs have been assumed to contain an initial void content, which then gradually increase when subjected to alternating temperature change. A Weibull-based damage accumulation model has been adopted for the gradual void content evolution. Further, the PNC was pronounced as failed when a certain failure criterion is reached.

To estimate the properties of PNCs reduced by the presence of voids, micromechanics based homogenization methods have been used. Specifically, the Hatta-Taya method developed previously has been used to compute their thermal conductivity, and the Mori-Tanaka method has been developed for the elastic modulus, Poisson's ratio, and coefficient of thermal expansion. The PNC has been assumed to consist of matrix, individual SWCNTs, and voids. In the developed fatigue model, the PNC properties are re-calculated in each thermal cycle by the homogenization methods until the failure criterion is reached. Finally, the degradation of the PNC properties and the life has been estimated. The experimental comparisons have shown compatible behavior in terms of the progression of the void content and the PNC life. The proposed damage accumulation approach can serve for predicting the property degradations in PNCs and their life under thermal fatigue. It, therefore, provides a bridge between the micromechanics and the cumulative damage at macro level.

A further extension of the proposed approach may include the impact of temperature dependent nanotube thermal conductivity, and introducing the randomness in nanotube dispersion and distribution into the thermal fatigue problem of polymer nanocomposites.

References

[1] H. W. Kroto, J. R. Heath, S. C. O'Brien, R. F. Curl, and R. E. Smalley, "C60: Buckminsterfullerene," *, Published online: 14 November 1985; | doi:10.1038/318162a0,* vol. 318, no. 6042, pp. 162–163, Nov. 1985.

[2] G. von Helden, M. T. Hsu, N. Gotts, and M. T. Bowers, "Carbon cluster cations with up to 84 atoms: structures, formation mechanism, and reactivity," *J. Phys. Chem.*, vol. 97, no. 31, pp. 8182–8192, 1993.

[3] M. Terrones, "Science and Technology of the Twenty-First Century: Synthesis, Properties, and Applications of Carbon Nanotubes.," *Annual Review of Materials Research*, vol. 33, no. 1, pp. 419–501, 2003.

[4] S. Iijima, "Helical microtubules of graphitic carbon," *Nature*, vol. 354, no. 6348, pp. 56–58, Nov. 1991.

[5] E. V. Barrera, "Key Methods for Developing Single-Wall Nanotube Composite," *JOM*, vol. 52, no. 11, pp. 38–42, Nov. 2000.

[6] J. D. Kim, *Incorporation of Carbon Nanotubes in Epoxy Polymer Composites*. Houston, Tex.: , 2006.

[7] S. Berber, Y.-K. Kwon, and D. Tomanek, "Unusually High Thermal Conductivity of Carbon Nanotubes," *Phys. Rev. Lett.*, vol. 84, no. 20, p. 4613, May 2000.

[8] M. J. Biercuk, M. C. Llaguno, M. Radosavljevic, J. K. Hyun, A. T. Johnson, and J. E. Fischer, "Carbon nanotube composites for thermal management," *Appl. Phys. Lett.*, vol. 80, no. 15, pp. 2767–2769, Apr. 2002.

[9] A. G. Rinzler and J. H. Hafner, "Unraveling nanotubes: Field emission from an atomic wire.," *Science*, vol. 269, no. 5230, p. 1550, 1995.

[10] W. A. de Heer and A. Chatelain, "A carbon nanotube field-emission electron source.," *Science*, vol. 270, no. 5239, p. 1179, Nov. 1995.

[11] A. C. Dillon, K. M. Jones, T. A. Bekkedahl, C. H. Kiang, D. S. Bethune, and M. J. Heben, "Storage of hydrogen in single-walled carbon nanotubes," *Nature*, vol. 386, no. 6623, pp. 377–379, Mar. 1997.

[12] S. J. Tans, M. H. Devoret, H. Dai, A. Thess, R. E. Smalley, L. J. Geerligs, and C. Dekker, "Individual single-wall carbon nanotubes as quantum wires," *Nature*, vol. 386, no. 6624, pp. 474–477, Apr. 1997.

[13] A. P. Graham, G. S. Duesberg, W. Hoenlein, F. Kreupl, M. Liebau, R. Martin, B. Rajasekharan, W. Pamler, R. Seidel, W. Steinhoegl, and E. Unger, "How do carbon nanotubes fit into the semiconductor roadmap?," *Applied Physics A: Materials Science & Processing*, vol. 80, no. 6, pp. 1141–1151, Mar. 2005.

[14] K. Hata, D. N. Futaba, K. Mizuno, T. Namai, M. Yumura, and S. Iijima, "Water-Assisted Highly Efficient Synthesis of Impurity-Free Single-Walled Carbon Nanotubes," *Science*, vol. 306, no. 5700, pp. 1362–1364, Nov. 2004.

[15] Y. Saito, T. Yoshikawa, S. Bandow, M. Tomita, and T. Hayashi, "Interlayer spacings in carbon nanotubes," *Phys. Rev. B*, vol. 48, no. 3, pp. 1907–1909, Jul. 1993.

[16] C.-H. Kiang, M. Endo, P. M. Ajayan, G. Dresselhaus, and M. S. Dresselhaus, "Size Effects in Carbon Nanotubes," *Phys. Rev. Lett.*, vol. 81, no. 9, pp. 1869–1872, 1998.

[17] S. L. Mayo, B. D. Olafson, and W. A. Goddard, "Dreiding: a generic force field for molecular simulations," *J. Phys. Chem.*, vol. 94, no. 26, pp. 8897–8909, 1990.

[18] L. F. Su, J. N. Wang, F. Yu, Z. M. Sheng, H. Chang, and C. Pak, "Continuous production of single-wall carbon nanotubes by spray pyrolysis of alcohol with dissolved ferrocene," *Chemical Physics Letters*, vol. 420, no. 4–6, pp. 421–425, Mar. 2006.

[19] T. Spires and R. M. J. Brown, "High Resolution TEM Observations of Single-Walled Carbon Nanotubes," *Department of Botany, The University of Texas at Austin, Austin,Tx.*, Aug. 1996.

[20] V. G. Hadjiev, M. N. Iliev, S. Arepalli, P. Nikolaev, and B. S. Files, "Raman scattering test of single-wall carbon nanotube composites," *Applied Physics Letters*, vol. 78, no. 21, pp. 3193–3195, May 2001.

[21] M. S. Dresselhaus, G. Dresselhaus, and P. C. Eklund, *Science of Fullerenes and Carbon Nanotubes*. Academic Press, San Diego, 1996.

[22] Y. Ohno, S. Kishimoto, T. Mizutani, T. Okazaki, and H. Shinohara, "Chirality assignment of individual single-walled carbon nanotubes in carbon nanotube field-effect transistors by micro-photocurrent spectroscopy," *Applied Physics Letters*, vol. 84, no. 8, pp. 1368–1370, Feb. 2004.

[23] L. C. Venema, J. W. G. Wildöer, H. L. J. T. Tuinstra, C. Dekker, A. G. Rinzler, and R. E. Smalley, "Length control of individual carbon nanotubes by nanostructuring with a scanning tunneling microscope," *Applied Physics Letters*, vol. 71, no. 18, pp. 2629–2631, Nov. 1997.

[24] Y. Ando and X. Zhao, "Synthesis of Carbon Nanotubes by Arc-Discharge Method," *New Diamond and Frontier Carbon Technology*, vol. 16, no. 3, pp. 123–37, 2006.

[25] S. Iijima and T. Ichihashi, "Single-shell carbon nanotubes of 1-nm diameter," *Nature*, vol. 363, no. 6430, pp. 603–605, Jun. 1993.

[26] D. S. Bethune, C. H. Klang, M. S. de Vries, G. Gorman, R. Savoy, J. Vazquez, and R. Beyers, "Cobalt-catalysed growth of carbon nanotubes with single-atomic-layer walls," *Nature*, vol. 363, no. 6430, pp. 605–607, Jun. 1993.

[27] C. Journet, W. K. Maser, P. Bernier, A. Loiseau, M. L. de la Chapelle, S. Lefrant, P. Deniard, R. Lee, and J. E. Fischer, "Large-scale production of single-walled carbon nanotubes by the electric-arc technique," *Nature*, vol. 388, no. 6644, pp. 756–758, 1997.

[28] X. Zhao, S. Inoue, M. Jinno, T. Suzuki, and Y. Ando, "Macroscopic oriented web of single-wall carbon nanotubes," *Chemical Physics Letters*, vol. 373, no. 3–4, pp. 266–271, May 2003.

[29] Y. Guo, T. Okazaki, T. Kadoya, T. Suzuki, and Y. Ando, "Spectroscopic study during single-wall carbon nanotubes production by Ar, H2, and H2-Ar DC arc discharge," *Diamond and Related Materials*, vol. 14, no. 3–7, pp. 887–890, 2005.

[30] Y. Ando, X. Zhao, S. Inoue, T. Suzuki, and T. Kadoya, "Mass production of high-quality single-wall carbon nanotubes by H2-N2 arc discharge," *Diamond and Related Materials*, vol. 14, no. 3–7, pp. 729–732, 2005.

[31] T. W. Ebbesen and P. M. Ajayan, "Large-scale synthesis of carbon nanotubes," *Nature*, vol. 358, no. 6383, pp. 220–222, Jul. 1992.

[32] T. Guo, P. Nikolaev, A. Thess, D. T. Colbert, and R. E. Smalley, "Catalytic growth of single-walled manotubes by laser vaporization," *Chemical Physics Letters*, vol. 243, no. 1–2, pp. 49–54, Sep. 1995.

[33] T. Guo, P. Nikolaev, A. G. Rinzler, D. Tomanek, D. T. Colbert, and R. E. Smalley, "Self-Assembly of Tubular Fullerenes," *Journal of Physical Chemistry*, vol. 99, no. 27, pp. 10694–10697, 1995.

[34] A. G. Rinzler, J. Liu, H. Dai, P. Nikolaev, C. B. Huffman, F. J. Rodríguez-Macías, P. J. Boul, A. H. Lu, D. Heymann, D. T. Colbert, R. S. Lee, J. E. Fischer, A. M. Rao, P. C. Eklund, and R. E. Smalley, "Large-scale purification of single-wall

carbon nanotubes: process, product, and characterization.," *Applied Physics A: Materials Science & Processing*, vol. 67, no. 1, p. 29, 1998.

[35] B. Yakobson and R. E. Smalley, "Fullerene Nanotubes: C1,000,000 and Beyond," *American Scientist*, vol. 85, pp. 324–332, 1997.

[36] Z. F. Ren, Z. P. Huang, J. W. Xu, J. H. Wang, P. Bush, M. P. Siegal, and P. N. Provencio, "Synthesis of Large Arrays of Well-Aligned Carbon Nanotubes on Glass.," *Science*, vol. 282, no. 5391, p. 1105, Nov. 1998.

[37] H. M. Cheng, F. Li, G. Su, H. Y. Pan, L. L. He, X. Sun, and M. S. Dresselhaus, "Large-scale and low-cost synthesis of single-walled carbon nanotubes by the catalytic pyrolysis of hydrocarbons.," *Applied Physics Letters*, vol. 72, no. 25, Jun. 1998.

[38] Z. P. Huang, J. W. Xu, Z. F. Ren, J. H. Wang, M. P. Siegal, and P. N. Provencio, "Growth of highly oriented carbon nanotubes by plasma-enhanced hot filament chemical vapor deposition.," *Applied Physics Letters*, vol. 73, no. 26, p. 3845, Dec. 1998.

[39] C. Bower, W. Zhu, S. Jin, and O. Zhou, "Plasma-induced alignment of carbon nanotubes.," *Applied Physics Letters*, vol. 77, no. 6, 2000.

[40] P. Nikolaev, M. J. Bronikowski, R. K. Bradley, F. Rohmund, D. T. Colbert, K. A. Smith, and R. E. Smalley, "Gas-phase catalytic growth of single-walled carbon nanotubes from carbon monoxide," *Chemical Physics Letters*, vol. 313, no. 1–2, pp. 91–97, Nov. 1999.

[41] E. Joselevich, H. Dai, J. Liu, K. Hata, and A. H. Windle, "Carbon Nanotube Synthesis and Organization," in *Carbon Nanotubes*, vol. 111, Berlin, Heidelberg: Springer Berlin Heidelberg, pp. 101–164.

[42] R. E. Smalley and B. I. Yakobson, "The future of the fullerenes," *Solid State Communications*, vol. 107, no. 11, pp. 597–606, Aug. 1998.

[43] B. Q. Wei, R. Vajtai, and P. M. Ajayan, "Reliability and current carrying capacity of carbon nanotubes.," *Applied Physics Letters*, vol. 79, no. 8, p. p1172 –, 2001.

[44] S. Frank, P. Poncharal, Z. L. Wang, and W. A. de Heer, "Carbon nanotube quantum resistors.," *Science*, vol. 280, no. 5370, p. 1744, Jun. 1998.

[45] A. Christou, *Electromigration and electronic device degradation*. Wiley, 1994.

[46] P. L. McEuen, M. S. Fuhrer, and H. Park, "Single-walled carbon nanotube electronics," *IEEE Transactions on Nanotechnology*, vol. 1, no. 1, pp. 78 –85, Mar. 2002.

[47] B. G. Yacobi, *Semiconductor Materials: An Introduction to Basic Principles*. Springer, 2003.

[48] S. J. Tans, A. R. M. Verschueren, and C. Dekker, "Room-temperature transistor based on a single carbon nanotube," *Nature*, vol. 393, no. 6680, pp. 49–52, May 1998.

[49] R. Martel, T. Schmidt, H. R. Shea, T. Hertel, and P. Avouris, "Single- and multi-wall carbon nanotube field-effect transistors.," *Applied Physics Letters*, vol. 73, no. 17, Oct. 1998.

[50] K. Kordas, G. Toth, P. Moilanen, M. Kumpumaki, J. Vahakangas, A. Uusimaki, R. Vajtai, and P. M. Ajayan, "Chip cooling with integrated carbon nanotube microfin architectures," *Applied Physics Letters*, vol. 90, no. 12, pp. 123105–123105–3, Mar. 2007.

[51] B. T. Kelly, *Physics of Graphite*, 1st ed. Springer, 1981.

[52] D. R. Lide, *CRC handbook of chemistry and physics: a ready-reference book of chemical and physical data*. CRC Press, 2004.

[53] Dresselhaus, Dresselhaus, and Sugihara, *Graphite fibers and filaments*. Berlin: Springer, 1988.

[54] J. Heremans, I. Rahim, and M. S. Dresselhaus, "Thermal conductivity and Raman spectra of carbon fibers," *Phys. Rev. B*, vol. 32, no. 10, pp. 6742–6747, Nov. 1985.

[55] L. Wei, P. Kuo, R. Thomas, T. Anthony, and W. Banholzer, "Thermal conductivity of isotopically modified single crystal diamond," *Physical Review Letters*, vol. 70, no. 24, pp. 3764–3767, Jun. 1993.

[56] J. Che, T. Cagin, and W. A. G. III, "Thermal conductivity of carbon nanotubes," *Nanotechnology*, vol. 11, no. 2, pp. 65–69, 2000.

[57] E. Pop, D. Mann, Q. Wang, K. Goodson, and H. Dai, "Thermal Conductance of an Individual Single-Wall Carbon Nanotube above Room Temperature," *cond-mat/0512624*, Dec. 2005.

[58] P. Kim, L. Shi, A. Majumdar, and P. L. McEuen, "Thermal Transport Measurements of Individual Multiwalled Nanotubes," *Phys. Rev. Lett.*, vol. 87, no. 21, p. 215502, Oct. 2001.

[59] J. Hone, M. C. Llaguno, M. J. Biercuk, A. T. Johnson, B. Batlogg, Z. Benes, and J. E. Fischer, "Thermal properties of carbon nanotubes and nanotube-based materials.," *Applied Physics A: Materials Science & Processing*, vol. 74, no. 3, p. 339, 2002.

[60] J. Hone, M. C. Llaguno, N. M. Nemes, A. T. Johnson, J. E. Fischer, D. A. Walters, M. J. Casavant, J. Schmidt, and R. E. Smalley, "Electrical and thermal transport properties of magnetically aligned single wall carbon nanotube films," *Appl. Phys. Lett.*, vol. 77, no. 5, pp. 666–668, Jul. 2000.

[61] M. Fujii, X. Zhang, H. Xie, H. Ago, K. Takahashi, T. Ikuta, H. Abe, and T. Shimizu, "Measuring the thermal conductivity of a single carbon nanotube," *Phys. Rev. Lett.*, vol. 95, no. 6, p. 065502, Aug. 2005.

[62] Y. Yosida, "High-temperature shrinkage of single-walled carbon nanotube bundles up to 1600 K," *Journal of Applied Physics*, vol. 87, no. 7, pp. 3338–3341, Apr. 2000.

[63] Y. Maniwa, R. Fujiwara, H. Kira, H. Tou, H. Kataura, S. Suzuki, Y. Achiba, E. Nishibori, M. Takata, M. Sakata, A. Fujiwara, and H. Suematsu, "Thermal expansion of single-walled carbon nanotube (SWNT) bundles: X-ray diffraction studies," *Phys. Rev. B*, vol. 64, no. 24, p. 241402, Nov. 2001.

[64] Y.-K. Kwon, S. Berber, and D. Tománek, "Thermal contraction of carbon fullerenes and nanotubes," *Phys. Rev. Lett*, vol. 92, no. 1, p. 015901, Jan. 2004.

[65] H. Jiang, B. Liu, Y. Huang, and K. C. Hwang, "Thermal Expansion of Single Wall Carbon Nanotubes," *J. Eng. Mater. Technol.*, vol. 126, no. 3, pp. 265–270, Jul. 2004.

[66] C. Lee, X. Wei, J. W. Kysar, and J. Hone, "Measurement of the Elastic Properties and Intrinsic Strength of Monolayer Graphene," *Science*, vol. 321, no. 5887, pp. 385–388, Jul. 2008.

[67] H.-S. P. Wong and D. Akinwande, *Carbon Nanotube and Graphene Device Physics*. Cambridge University Press, 2010.

[68] M. M. J. Treacy, T. W. Ebbesen, and J. M. Gibson, "Exceptionally high Young's modulus observed for individual carbon nanotubes," *Nature*, vol. 381, no. 6584, p. 678, Jun. 1996.

[69] A. Krishnan, E. Dujardin, T. W. Ebbesen, P. N. Yianilos, and M. M. J. Treacy, "Young's modulus of single-walled nanotubes," *Phys. Rev. B*, vol. 58, no. 20, p. 14013, Nov. 1998.

[70] J.-P. Salvetat, G. A. D. Briggs, J.-M. Bonard, R. R. Bacsa, A. J. Kulik, T. St□ckli, N. A. Burnham, and L. Forr□, "Elastic and Shear Moduli of Single-Walled Carbon Nanotube Ropes," *Phys. Rev. Lett.*, vol. 82, no. 5, p. 944, Feb. 1999.

[71] M.-F. Yu, B. S. Files, S. Arepalli, and R. S. Ruoff, "Tensile Loading of Ropes of Single Wall Carbon Nanotubes and their Mechanical Properties," *Phys. Rev. Lett.*, vol. 84, no. 24, p. 5552, Jun. 2000.

[72] O. Lourie and H. D. Wagner, “Evaluation of Young’s modulus of carbon nanotubes by micro-Raman spectroscopy,” *J. Mater. Res.*, vol. 13, no. 9, pp. 2418–2422, 1998.

[73] E. Wong, P. Sheehan, and C. Lieber, “Nanobeam mechanics: Elasticity, strength, and toughness of nanorods and nanotubes,” *Science*, vol. 277, no. 5334, p. 1971, Sep. 1997.

[74] M.-F. Yu, O. Lourie, M. J. Dyer, K. Moloni, T. F. Kelly, and R. S. Ruoff, “Strength and Breaking Mechanism of Multiwalled Carbon Nanotubes Under Tensile Load.,” *Science*, vol. 287, no. 5453, p. 637, Jan. 2000.

[75] J.-P. Salvetat, A. J. Kulik, J.-M. Bonard, G. A. D. Briggs, T. Stockli, K. Metenier, S. Bonnamy, F. Beguin, N. A. Burnham, and L. Forro, “Elastic Modulus of Ordered and Disordered Multiwalled Carbon Nanotubes,” *Advanced Materials*, vol. 11, no. 2, pp. 161–165, 1999.

[76] D. A. Walters and L. M. Ericson, “Elastic strain of freely suspended single-wall carbon nanotube ropes.,” *Applied Physics Letters*, vol. 74, no. 25, p. 3803, Jun. 1999.

[77] J. P. Lu, “Elastic Properties of Carbon Nanotubes and Nanoropes,” *Phys. Rev. Lett.*, vol. 79, no. 7, p. 1297, 1997.

[78] N. Yao and V. Lordi, “Young’s modulus of single-walled carbon nanotubes.,” *Journal of Applied Physics*, vol. 84, no. 4, p. 1939, 1998.

[79] Y. Jin and F. G. Yuan, “Simulation of elastic properties of single-walled carbon nanotubes,” *Composites Science and Technology*, vol. 63, no. 11, pp. 1507–1515, Aug. 2003.

[80] H. W. Zhang, J. B. Wang, and X. Guo, “Predicting the elastic properties of single-walled carbon nanotubes,” *Journal of the Mechanics and Physics of Solids*, vol. 53, no. 9, pp. 1929–1950, Sep. 2005.

[81] B. I. Yakobson, C. J. Brabec, and J. Bernholc, “Nanomechanics of Carbon Tubes: Instabilities beyond Linear Response,” *Phys. Rev. Lett.*, vol. 76, no. 14, p. 2511, Apr. 1996.

[82] G. D. Seidel and D. C. Lagoudas, “Micromechanical analysis of the effective elastic properties of carbon nanotube reinforced composites,” *Mechanics of Materials*, vol. 38, no. 8–10, pp. 884–907, 2006.

[83] C. Li and T.-W. Chou, “A structural mechanics approach for the analysis of carbon nanotubes,” *International Journal of Solids and Structures*, vol. 40, no. 10, pp. 2487–2499, May 2003.

[84] C. W. S. To, “Bending and shear moduli of single-walled carbon nanotubes,” *Finite Elements in Analysis and Design*, vol. 42, no. 5, pp. 404–413, Feb. 2006.

[85] M. Meo and M. Rossi, “Prediction of Young’s modulus of single wall carbon nanotubes by molecular-mechanics based finite element modelling,” *Composites Science and Technology*, vol. 66, no. 11–12, pp. 1597–1605, Sep. 2006.

[86] G. I. Giannopoulos, P. A. Kakavas, and N. K. Anifantis, “Evaluation of the effective mechanical properties of single walled carbon nanotubes using a spring based finite element approach,” *Computational Materials Science*, vol. 41, no. 4, pp. 561–569, Feb. 2008.

[87] B. Yakobson and P. Avouris, “Mechanical Properties of Carbon Nanotubes,” in *Carbon Nanotubes*, 2001, pp. 287–327.

[88] D. Srivastava, M. Menon, and K. Cho, “Nanoplasticity of Single-Wall Carbon Nanotubes under Uniaxial Compression,” *Phys. Rev. Lett.*, vol. 83, no. 15, p. 2973, Oct. 1999.

[89] T. Belytschko, S. P. Xiao, G. C. Schatz, and R. S. Ruoff, “Atomistic simulations of nanotube fracture,” *Phys. Rev. B*, vol. 65, no. 23, p. 235430, Jun. 2002.

[90] T. W. Ebbesen, H. J. Lezec, H. Hiura, J. W. Bennett, H. F. Ghaemi, and T. Thio, “Electrical conductivity of individual carbon nanotubes,” , *Published online: 04 July 1996; | doi:10.1038/382054a0*, vol. 382, no. 6586, pp. 54–56, Jul. 1996.

[91] B. T. Astrom, *Manufacturing of Polymer Composites*. CRC Press, 1997.

[92] C. D. L. Deborah, *Carbon Fiber Composites*. Elsevier, 1994.

[93] R. Haggenmueller, C. Guthy, J. R. Lukes, J. E. Fischer, and K. I. Winey, “Single Wall Carbon Nanotube/Polyethylene Nanocomposites: Thermal and Electrical Conductivity,” *Macromolecules*, vol. 40, no. 7, pp. 2417–2421, Apr. 2007.

[94] P. Bonnet, D. Sireude, B. Garnier, and O. Chauvet, “Thermal properties and percolation in carbon nanotube-polymer composites,” *Appl. Phys. Lett.*, vol. 91, no. 20, pp. 201910–3, Nov. 2007.

[95] A. Yu, M. E. Itkis, E. Bekyarova, and R. C. Haddon, “Effect of single-walled carbon nanotube purity on the thermal conductivity of carbon nanotube-based composites,” *Appl. Phys. Lett.*, vol. 89, no. 13, pp. 133102–3, 2006.

[96] F. Du, C. Guthy, T. Kashiwagi, J. E. Fischer, and K. I. Winey, “An infiltration method for preparing single-wall nanotube/epoxy composites with improved thermal conductivity,” *Journal of Polymer Science Part B: Polymer Physics*, vol. 44, no. 10, pp. 1513–1519, 2006.

[97] Y. Xu, G. Ray, and B. Abdel-Magid, “Thermal behavior of single-walled carbon nanotube polymer-matrix composites,” *Composites Part A: Applied Science and Manufacturing*, vol. 37, no. 1, pp. 114–121, Jan. 2006.

[98] C. H. Liu, H. Huang, Y. Wu, and S. S. Fan, “Thermal conductivity improvement of silicone elastomer with carbon nanotube loading,” *Appl. Phys. Lett.*, vol. 84, no. 21, pp. 4248–4250, May 2004.

[99] Y. S. Song and J. R. Youn, “Influence of dispersion states of carbon nanotubes on physical properties of epoxy nanocomposites,” *Carbon*, vol. 43, no. 7, pp. 1378–1385, Jun. 2005.

[100] L. Thien-Nga, K. Hernadi, E. Ljubovic, S. Garaj, and L. Forro, “Mechanical Purification of Single-Walled Carbon Nanotube Bundles from Catalytic Particles,” vol. 2, no. 12, pp. 1349–1352, 2002.

[101] R. Andrews, D. Jacques, M. Minot, and T. Rantell, “Fabrication of Carbon Multiwall Nanotube/Polymer Composites by Shear Mixing,” *Macromolecular Materials and Engineering*, vol. 287, no. 6, pp. 395–403, 2002.

[102] O. Breuer and U. Sundararaj, “Big returns from small fibers: A review of polymer/carbon nanotube composites,” *Polymer Composites*, vol. 25, no. 6, pp. 630–645, 2004.

[103] L. Jin, C. Bower, and O. Zhou, “Alignment of carbon nanotubes in a polymer matrix by mechanical stretching,” *Appl. Phys. Lett.*, vol. 73, no. 9, pp. 1197–1199, 1998.

[104] D. Qian, W. K. Liu, and R. S. Ruoff, “Load transfer mechanism in carbon nanotube ropes,” *Composites Science and Technology*, vol. 63, no. 11, pp. 1561–1569, Aug. 2003.

[105] F. H. Gojny, M. H. G. Wichmann, B. Fiedler, and K. Schulte, “Influence of different carbon nanotubes on the mechanical properties of epoxy matrix composites - A comparative study,” *Composites Science and Technology*, vol. 65, no. 15–16, pp. 2300–2313, Dec. 2005.

[106] E. T. Thostenson and T.-W. Chou, “On the elastic properties of carbon nanotube-based composites: modelling and characterization,” *Journal of Physics D: Applied Physics*, vol. 36, no. 5, pp. 573–582, 2003.

[107] S. Wang, Z. Liang, B. Wang, and C. Zhang, “Statistical characterization of single-wall carbon nanotube length distribution,” *Nanotechnology*, vol. 17, no. 3, pp. 634–639, 2006.

[108] P. D. Spanos and M. Esteva, “Effective Elastic Properties of Nanotube Reinforced Composites with Slightly Weakened Interfaces,” *Proceedings of the PACAM X- Pan American Congress of Applied Mechanics*, Jan. 2008.

[109] M. Esteva, “Hybrid Finite Elements Nanocomposite Characterization by Stochastic Microstructuring,” Rice University, 2008.

[110] C.-W. Nan, G. Liu, Y. Lin, and M. Li, “Interface effect on thermal conductivity of carbon nanotube composites,” *Appl. Phys. Lett.*, vol. 85, no. 16, pp. 3549–3551, Oct. 2004.

[111] N. Shenogina, S. Shenogin, L. Xue, and P. Keblinski, “On the lack of thermal percolation in carbon nanotube composites,” *Appl. Phys. Lett.*, vol. 87, no. 13, pp. 133106–3, 2005.

[112] S. T. Huxtable, D. G. Cahill, S. Shenogin, L. Xue, R. Ozisik, P. Barone, M. Usrey, M. S. Strano, G. Siddons, M. Shim, and P. Keblinski, “Interfacial heat flow in carbon nanotube suspensions,” *Nat Mater*, vol. 2, no. 11, pp. 731–734, Nov. 2003.

[113] O. M. Wilson, X. Hu, D. G. Cahill, and P. V. Braun, “Colloidal metal particles as probes of nanoscale thermal transport in fluids,” *Phys. Rev. B*, vol. 66, no. 22, p. 224301, Dec. 2002.

[114] M. B. Bryning, D. E. Milkie, M. F. Islam, J. M. Kikkawa, and A. G. Yodh, “Thermal conductivity and interfacial resistance in single-wall carbon nanotube epoxy composites,” *Appl. Phys. Lett.*, vol. 87, no. 16, pp. 161909–3, Oct. 2005.

[115] C.-W. Nan, R. Birringer, D. R. Clarke, and H. Gleiter, “Effective thermal conductivity of particulate composites with interfacial thermal resistance,” *J. Appl. Phys.*, vol. 81, no. 10, pp. 6692–6699, May 1997.

[116] D. P. H. Hasselman and L. F. Johnson, “Effective Thermal Conductivity of Composites with Interfacial Thermal Barrier Resistance,” *Journal of Composite Materials*, vol. 21, no. 6, pp. 508–515, Jan. 1987.

[117] Q. Z. Xue, “Model for the effective thermal conductivity of carbon nanotube composites,” *Nanotechnology*, vol. 17, no. 6, pp. 1655–1660, 2006.

[118] T. B. Lewis and L. E. Nielsen, “Dynamic Mechanical Properties of Particulate-Filled Composites,” *Journal of Applied Polymer Science*, vol. 14, pp. 1449–1471, 1970.

[119] R. L. Hamilton and O. K. Crosser, “Thermal Conductivity of Heterogeneous Two-Component Systems,” *Industrial & Engineering Chemistry Fundamentals*, vol. 1, no. 3, pp. 187–191, 1962.

[120] H. Hatta and M. Taya, “Effective thermal conductivity of a misoriented short fiber composite,” *J. Appl. Phys.*, vol. 58, no. 7, pp. 2478–2486, Oct. 1985.

[121] J. D. Eshelby, “The Determination of the Elastic Field of an Ellipsoidal Inclusion, and Related Problems,” *Proceedings of the Royal Society of London. Series A, Mathematical and Physical Sciences*, vol. 241, no. 1226, pp. 376–396, Aug. 1957.

[122] D.-L. Shi, X.-Q. Feng, Y. Y. Huang, K.-C. Hwang, and H. Gao, “The Effect of Nanotube Waviness and Agglomeration on the Elastic Property of Carbon Nanotube-Reinforced Composites,” *J. Eng. Mater. Technol.*, vol. 126, no. 3, pp. 250–257, Jul. 2004.

[123] P. D. Spanos and A. Kontsos, “A multiscale Monte Carlo finite element method for determining mechanical properties of polymer nanocomposites,” *Probabilistic Engineering Mechanics*, vol. 23, no. 4, pp. 456–470, Oct. 2008.

[124] C.-W. Nan, Z. Shi, and Y. Lin, “A simple model for thermal conductivity of carbon nanotube-based composites,” *Chemical Physics Letters*, vol. 375, no. 5–6, pp. 666–669, Jul. 2003.

[125] D. Shi, J. Lian, P. He, L. M. Wang, F. Xiao, L. Yang, M. J. Schulz, and D. B. Mast, “Plasma coating of carbon nanofibers for enhanced dispersion and interfacial bonding in polymer composites,” *Appl. Phys. Lett.*, vol. 83, no. 25, pp. 5301–5303, Dec. 2003.

[126] Thostenson E.T., Ren Z., and Chou T.-W.[1], “Advances in the science and technology of carbon nanotubes and their composites: a review,” *Composites Science and Technology*, vol. 61, pp. 1899–1912, Oct. 2001.

[127] H. Lee, S. Mall, P. He, D. Shi, S. Narasimhadevara, Y.-H. Yun, V. Shanov, and M. J. Schulz, “Characterization of carbon nanotube/nanofiber-reinforced polymer composites using an instrumented indentation technique,” *Composites Part B: Engineering*, vol. 38, no. 1, pp. 58–65, Jan. 2007.

[128] X. Li, H. Gao, W. A. Scrivens, D. Fei, X. Xu, M. A. Sutton, A. P. Reynolds, and M. L. Myrick, “Nanomechanical characterization of single-walled carbon nanotube reinforced epoxy composites,” *Nanotechnology*, vol. 15, no. 11, pp. 1416–1423, 2004.

[129] R. Hill, “Elastic properties of reinforced solids: Some theoretical principles,” *Journal of the Mechanics and Physics of Solids*, vol. 11, no. 5, pp. 357–372, Sep. 1963.

[130] M. Ostoja-Starzewski, “Microstructural Randomness Versus Representative Volume Element in Thermomechanics,” *J. Appl. Mech.*, vol. 69, no. 1, pp. 25–35, Jan. 2002.

[131] M. Ostoja-Starzewski, “Material spatial randomness: From statistical to representative volume element,” *Probabilistic Engineering Mechanics*, vol. 21, no. 2, pp. 112–132, Apr. 2006.

[132] A. Kontsos, M. Esteva, A. Tamer, and P. D. Spanos, “Polymer nanocomposites characterization by a stochastic multiscale approach,” *Proceedings of the Fifth International Conference on Computational Stochastic Mechanics*, pp. 393–400.

[133] "Aluminum-(Silicon Carbide) Composite." [Online]. Available: http://www.alphamaterials.com/AlSiC.htm. [Accessed: 03-Jan-2009].

[134] D. Mandal, B. K. Dutta, and S. C. Panigrahi, "Effect of wt% reinforcement on microstructure and mechanical properties of Al-2Mg base short steel fiber composites," *Journal of Materials Processing Technology*, vol. 198, no. 1–3, pp. 195–201, Mar. 2008.

[135] Y. S. Song and J. R. Youn, "Evaluation of effective thermal conductivity for carbon nanotube/polymer composites using control volume finite element method," *Carbon*, vol. 44, no. 4, pp. 710–717, Apr. 2006.

[136] Y. Li and H. Shimizu, "High-shear processing induced homogenous dispersion of pristine multiwalled carbon nanotubes in a thermoplastic elastomer," *Polymer*, vol. 48, no. 8, pp. 2203–2207, Apr. 2007.

[137] O.-K. Kim, J. Je, J. W. Baldwin, S. Kooi, P. E. Pehrsson, and L. J. Buckley, "Solubilization of single-wall carbon nanotubes by supramolecular encapsulation of helical amylose," *J. Am. Chem. Soc.*, vol. 125, no. 15, pp. 4426–4427, Apr. 2003.

[138] S. S. Park, N. Bernet, S. de la Roche, and H. T. Hahn, "Processing of Iron Oxide-epoxy Vinyl Ester Nanocomposites," *Journal of Composite Materials*, vol. 37, no. 5, pp. 465–476, Mar. 2003.

[139] R. Schueler, J. Petermann, K. Schulte, and H.-P. Wentzel, "Agglomeration and electrical percolation behavior of carbon black dispersed in epoxy resin," *Journal of Applied Polymer Science*, vol. 63, no. 13, pp. 1741–1746, 1997.

[140] J. Gou, B. Minaie, B. Wang, Z. Liang, and C. Zhang, "Computational and experimental study of interfacial bonding of single-walled nanotube reinforced composites," *Computational Materials Science*, vol. 31, no. 3–4, pp. 225–236, Nov. 2004.

[141] J. Lee, K. Yamamoto, and K. Morita, "Surface tension of liquid Fe-Cr-O alloys at 1823 K," *Metallurgical and Materials Transactions B*, vol. 36, no. 2, pp. 241–246, 2005.

[142] I. Karatzas and S. E. Shreve, *Brownian Motion and Stochastic Calculus*, 2nd ed. Springer, 1998.

[143] S. Howell, D. Kuila, B. Kasibhatla, C. P. Kubiak, D. Janes, and R. Reifenberger, "Molecular Electrostatics of Conjugated Self-Assembled Monolayers on Au(111) Using Electrostatic Force Microscopy," *Langmuir*, vol. 18, no. 13, pp. 5120–5125, Jun. 2002.

[144] J. Loos, N. Grossiord, C. E. Koning, and O. Regev, "On the fate of carbon nanotubes: Morphological characterisations," *Composites Science and Technology*, vol. 67, no. 5, pp. 783–788, Apr. 2007.

[145] C. Park, J. Wilkinson, S. Banda, Z. Ounaies, K. E. Wise, G. Sauti, P. T. Lillehei, and J. S. Harrison, "Aligned single-wall carbon nanotube polymer composites using an electric field," *Journal of Polymer Science Part B: Polymer Physics*, vol. 44, no. 12, pp. 1751–1762, 2006.

[146] L. Liu, B.-M. Zhang, D.-F. Wang, and Z.-J. Wu, "Effects of cure cycles on void content and mechanical properties of composite laminates," *Composite Structures*, vol. 73, no. 3, pp. 303–309, Jun. 2006.

[147] B. J. Herzog, "Characterization Of The Void Content Of Fiber Reinforced Polymer (frp) Composite Materials Fabricated By The Composites Pressure Resin Infusion System (compris)," Dissertation, The University of Maine, 2004.

[148] H. A. Kelleher, "Air-gaps Via Thermally Decomposable Polymers And Their Application To Compliant Wafer Level Packaging (cwlp)," Dissertation, Georgia Institute of Technology, 2004.

[149] K. A. Chowdhury, R. Talreja, and A. A. Benzerga, "Effects of Manufacturing-Induced Voids on Local Failure in Polymer-Based Composites," *J. Eng. Mater. Technol.*, vol. 130, no. 2, pp. 021010–9, Apr. 2008.

[150] A. Krach and S. G. Advani, "Influence of Void Shape, Void Volume and Matrix Anisotropy on Effective Thermal Conductivity of a Three-Phase Composite," *Journal of Composite Materials*, vol. 30, no. 8, pp. 933–946, May 1996.

[151] B. S. Hayes and L. M. Gammon, *Optical Microscopy of Fiber Reinforced Composites*. ASM International, 2010.

[152] G. Polizos, E. Tuncer, I. Sauers, and K. L. More, "Physical properties of epoxy resin/titanium dioxide nanocomposites," *Polymer Engineering & Science*, vol. 51, no. 1, pp. 87–93, Jan. 2011.

[153] A. M. Díez-Pascual, J. Guan, B. Simard, and M. A. Gómez-Fatou, "Poly(phenylene sulphide) and poly(ether ether ketone) composites reinforced with single-walled carbon nanotube buckypaper: II – Mechanical properties, electrical and thermal conductivity," *Composites Part A: Applied Science and Manufacturing*, vol. 43, no. 6, pp. 1007–1015, Jun. 2012.

[154] S. Yesil and G. Bayram, "Effect of carbon nanotube purification on the electrical and mechanical properties of poly(ethylene terephthalate) composites with carbon nanotubes in low concentration," *Journal of Applied Polymer Science*, vol. 119, no. 6, pp. 3360–3371, 2011.

[155] T. W. Ebbesen, P. M. Ajayan, H. Hiura, and K. Tanigaki, "Purification of nanotubes," , *Published online: 10 February 1994; | doi:10.1038/367519a0*, vol. 367, no. 6463, pp. 519–519, Feb. 1994.

[156] I. W. Chiang, B. E. Brinson, R. E. Smalley, J. L. Margrave, and R. H. Hauge, "Purification and Characterization of Single-Wall Carbon Nanotubes," *Journal of Physical Chemistry B*, vol. 105, no. 6, pp. 1157–1161, 2001.

[157] K. B. Shelimov, R. O. Esenaliev, A. G. Rinzler, C. B. Huffman, and R. E. Smalley, "Purification of single-wall carbon nanotubes by ultrasonically assisted filtration," *Chemical Physics Letters*, vol. 282, no. 5–6, pp. 429–434, Jan. 1998.

[158] S. Bandow, A. M. Rao, K. A. Williams, A. Thess, R. E. Smalley, and P. C. Eklund, "Purification of Single-Wall Carbon Nanotubes by Microfiltration," *Journal of Physical Chemistry B*, vol. 101, no. 44, pp. 8839–8842, 1997.

[159] B. Gao, C. Bower, J. D. Lorentzen, L. Fleming, A. Kleinhammes, X. P. Tang, L. E. McNeil, Y. Wu, and O. Zhou, "Enhanced saturation lithium composition in ball-milled single-walled carbon nanotubes," *Chemical Physics Letters*, vol. 327, no. 1–2, pp. 69–75, Sep. 2000.

[160] V. Georgakilas, D. Voulgaris, E. Vázquez, M. Prato, D. M. Guldi, A. Kukovecz, and H. Kuzmany, "Purification of HiPCO Carbon Nanotubes via Organic Functionalization," *J. Am. Chem. Soc.*, vol. 124, no. 48, pp. 14318–14319, 2002.

[161] B. Zhao, H. Hu, S. Niyogi, M. E. Itkis, M. A. Hamon, P. Bhowmik, M. S. Meier, and R. C. Haddon, "Chromatographic Purification and Properties of Soluble Single-Walled Carbon Nanotubes," *J. Am. Chem. Soc.*, vol. 123, no. 47, pp. 11673–11677, 2001.

[162] J. Zhu, J. Kim, H. Peng, J. L. Margrave, V. N. Khabashesku, and E. V. Barrera, "Improving the Dispersion and Integration of Single-Walled Carbon Nanotubes in Epoxy Composites through Functionalization," *Nano Lett.*, vol. 3, no. 8, pp. 1107–1113, Aug. 2003.

[163] T. Kashiwagi, F. Du, K. I. Winey, K. M. Groth, J. R. Shields, S. P. Bellayer, H. Kim, and J. F. Douglas, "Flammability properties of polymer nanocomposites with single-walled carbon nanotubes: effects of nanotube dispersion and concentration," *Polymer*, vol. 46, no. 2, pp. 471–481, Jan. 2005.

[164] K. J. Ziegler, U. Rauwald, Z. Gu, F. Liang, W. E. Billups, R. H. Hauge, and R. E. Smalley, "Statistically Accurate Length Measurements of Single-Walled Carbon Nanotubes," *Journal of Nanoscience and Nanotechnology*, vol. 7, pp. 2917–2921, Aug. 2007.

[165] H. Fukunaga, T. W. Chow, and H. Fukuda, "Probabilistic Strength Analysis of Inter Laminated Hybrid Composites," *Composites Science and Technology*, vol. 14, pp. 331–335, 1989.

[166] S. . Engelstad and J. . Reddy, "Probabilistic methods for the analysis of metal-matrix composites," *Composites Science and Technology*, vol. 50, no. 1, pp. 91–107.

[167] R. L. Smith, “The random variation of stress concentration factors in fibrous composites,” *Journal of Materials Science Letters*, vol. 2, no. 8, pp. 385–387, 1983.

[168] A. P. Roberts and M. A. Knackstedt, “Structure-property correlations in model composite materials,” *Phys. Rev. E*, vol. 54, no. 3, p. 2313, 1996.

[169] G. L. Povirk, “Incorporation of microstructural information into models of two-phase materials,” *Acta Metallurgica et Materialia*, vol. 43, no. 8, pp. 3199–3206, Aug. 1995.

[170] S. C. Baxter and L. L. Graham, “Characterization of Random Composites Using Moving-Window Technique,” *Journal of Engineering Mechanics*, vol. 126, no. 4, pp. 389–397, Apr. 2000.

[171] S. C. Baxter, M. I. Hossain, and L. L. Graham, “Micromechanics based random material property fields for particulate reinforced composites,” *International Journal of Solids and Structures*, vol. 38, no. 50–51, pp. 9209–9220, Dec. 2001.

[172] L. L. Graham and S. C. Baxter, “Simulation of local material properties based on moving-window GMC,” *Probabilistic Engineering Mechanics*, vol. 16, no. 4, pp. 295–305, Oct. 2001.

[173] T. Kashiwagi, J. Fagan, J. F. Douglas, K. Yamamoto, A. N. Heckert, S. D. Leigh, J. Obrzut, F. Du, S. Lin-Gibson, M. Mu, K. I. Winey, and R. Haggenmueller, “Relationship between dispersion metric and properties of PMMA/SWNT nanocomposites,” *Polymer*, vol. 48, no. 16, pp. 4855–4866, Jul. 2007.

[174] J. Summerscales, *Non-Destructive Testing of Fibre-Reinforced Plastics Composites*. Springer, 1990.

[175] J. C. Joiner, “The Determination of Voids in Carbon Fibre Composites,” Jul. 1973.

[176] D. Purslow, “On the optical assessment of the void content in composite materials,” *Composites*, vol. 15, no. 3, pp. 207–210, Jul. 1984.

[177] B. Jiang, C. Liu, C. Zhang, B. Wang, and Z. Wang, “The effect of non-symmetric distribution of fiber orientation and aspect ratio on elastic properties of composites,” *Composites Part B: Engineering*, vol. 38, no. 1, pp. 24–34, Jan. 2007.

[178] R. Y. Rubinstein and D. P. Kroese, *Simulation and the Monte Carlo Method*, 2nd ed. Wiley, 2007.

[179] H. Hatta and M. Taya, “Thermal conductivity of coated filler composites,” *J. Appl. Phys.*, vol. 59, no. 6, pp. 1851–1860, Mar. 1986.

[180] H. Hatta and M. Taya, “Equivalent inclusion method for steady state heat conduction in composites,” *International Journal of Engineering Science*, vol. 24, no. 7, pp. 1159–1172, 1986.

[181] T.-K. Lai, “Thermal stress due to disturbance of uniform heat flow by an ellipsoidal inclusion,” Ph.D., Northwestern University, 1977.

[182] A. Tamer, *Monte Carlo Simulation Based Determination of Nanocomposites Thermal Conductivity*. ProQuest, 2009.

[183] J. Hone, M. Whitney, C. Piskoti, and A. Zettl, “Thermal conductivity of single-walled carbon nanotubes,” *Phys. Rev. B*, vol. 59, no. 4, p. R2514, Jan. 1999.

[184] Z. H. Karadeniz and D. Kumlutas, “A numerical study on the coefficients of thermal expansion of fiber reinforced composite materials,” *Composite Structures*, vol. 78, no. 1, pp. 1–10, Mar. 2007.

[185] L. Valentini, J. Biagiotti, J. M. Kenny, and S. Santucci, “Morphological characterization of single-walled carbon nanotubes-PP composites,” *Composites Science and Technology*, vol. 63, no. 8, pp. 1149–1153, Jun. 2003.

[186] P. Keblinski, J. A. Eastman, and D. G. Cahill, “Nanofluids for thermal transport,” *Materials Today*, vol. 8, no. 6, pp. 36–44, Jun. 2005.

[187] M. L. Dunn, M. Taya, H. Hatta, T. Takei, and Y. Nakajima, “Thermal Conductivity of Hybrid Short Fiber Composites,” *Journal of Composite Materials*, vol. 27, no. 15, pp. 1493–1519, Jan. 1993.

[188] D. S. Wilkinson, W. Pompe, and M. Oeschner, “Modeling the mechanical behaviour of heterogeneous multi-phase materials,” *Progress in Materials Science*, vol. 46, no. 3–4, pp. 379–405, 2001.

[189] S. R. Bakshi, R. G. Batista, and A. Agarwal, “Quantification of carbon nanotube distribution and property correlation in nanocomposites,” *Composites Part A: Applied Science and Manufacturing*, vol. 40, no. 8, pp. 1311–1318, Aug. 2009.

[190] R. B. Pipes, S. J. V. Frankland, P. Hubert, and E. Saether, “Self-consistent properties of carbon nanotubes and hexagonal arrays as composite reinforcements,” *Composites Science and Technology*, vol. 63, no. 10, pp. 1349–1358, Aug. 2003.

[191] G. Gao, T. Cagin, and W. A. G. III, “Energetics, structure, mechanical and vibrational properties of single-walled carbon nanotubes,” *Nanotechnology*, vol. 9, no. 3, pp. 184–191, 1998.

[192] H. Hatta, T. Takei, and M. Taya, “Effects of dispersed microvoids on thermal expansion behavior of composite materials,” *Materials Science and Engineering A*, vol. 285, no. 1–2, pp. 99–110, Jun. 2000.

[193] Y. K. Hamidi, L. Aktas, and M. C. Altan, “Effect of Nanoclay Content on Void Morphology in Resin Transfer Molded Composites,” *Journal of Thermoplastic Composite Materials*, vol. 21, no. 2, pp. 141–163, Mar. 2008.

[194] Y. K. Hamidi, S. Dharmavaram, L. Aktas, and M. C. Altan, “Effect of Fiber Content on Void Morphology in Resin Transfer Molded E-Glass/Epoxy Composites,” *Journal of Engineering Materials and Technology*, vol. 131, no. 2, p. 021014, 2009.

[195] N. Judd and W. Wright, “Voids and their effects on the mechanical properties of composites- an appraisal,” *Sampe Journal*, vol. 14, pp. 10–14, 1978.

[196] M. L. Scott, *ICCM-11 [v4]*. Woodhead Publishing, 1997.

[197] S. R. P. Silva, *Properties of Amorphous Carbon*. Institution of Engineering and Technology, 2003.

[198] W. Hurler, M. Pietralla, and A. Hammerschmidt, “Determination of thermal properties of hydrogenated amorphous carbon films via mirage effect measurements,” *Diamond and Related Materials*, vol. 4, no. 7, pp. 954–957, May 1995.

[199] Q. Bao and C. Pan, “Electric field induced growth of well aligned carbon nanotubes from ethanol flames,” *Nanotechnology*, vol. 17, no. 4, pp. 1016–1021, Feb. 2006.

[200] V. K. Rangari, M. Yousuf, S. Jeelani, M. X. Pulikkathara, and V. N. Khabashesku, “Alignment of carbon nanotubes and reinforcing effects in nylon-6 polymer composite fibers,” *Nanotechnology*, vol. 19, no. 24, p. 245703, Jun. 2008.

[201] H. G. Chae, M. L. Minus, and S. Kumar, “Oriented and exfoliated single wall carbon nanotubes in polyacrylonitrile,” *Polymer*, vol. 47, no. 10, pp. 3494–3504, May 2006.

[202] L. Ci, J. Suhr, V. Pushparaj, X. Zhang, and P. M. Ajayan, “Continuous Carbon Nanotube Reinforced Composites,” *Nano Lett.*, vol. 8, no. 9, pp. 2762–2766, Sep. 2008.

[203] R. Haggenmueller, H. H. Gommans, A. G. Rinzler, J. E. Fischer, and K. I. Winey, “Aligned single-wall carbon nanotubes in composites by melt processing methods,” *Chemical Physics Letters*, vol. 330, no. 3–4, pp. 219–225, Nov. 2000.

[204] H. Huang, C. H. Liu, Y. Wu, and S. Fan, “Aligned Carbon Nanotube Composite Films for Thermal Management,” *Advanced Materials*, vol. 17, no. 13, pp. 1652–1656, 2005.

[205] H. Peng, X. Sun, and T. Che, “Polymer Composites with Carbon Nanotubes in Alignment,” in *Carbon Nanotubes - Polymer Nanocomposites*, S. Yellampalli, Ed. InTech, 2011.

[206] B. Harris, “Fatigue behaviour of polymer-based composites and life prediction methods,” in *Durability Analysis of Structural Composite Systems (ed. A.H. Cardon)*, Taylor & Francis, 1996.

[207] J. A. Nairn and S. Hu, “Micromechanics of Damage: A Case Study of Matrix Microcracking, Chapter 6,” in *Damage Mechanics of Composite Materials (ed. R. Talreja)*, Elsevier, 1994.

[208] G. P. Sendeckyj, “Life Prediction for Resin-Matrix Composite Materials, Chapter 10,” in *Fatigue of composite materials (ed. K.L. Reifsnider)*, Elsevier, 1991.

[209] W. W. Stinchcomb and C. E. Bakis, “Fatigue Behavior of Composite Laminates, Chapter 4,” in *Fatigue of composite materials (ed. K.L. Reifsnider)*, Elsevier, 1991.

[210] J. A. Bannantine, J. J. Comer, and J. L. Handrock, *Fundamentals of metal fatigue analysis*. Prentice Hall, 1990.

[211] K. L. Reifsnider, “Damage and Damage Mechanics, Chapter 2,” in *Fatigue of composite materials (ed. K.L. Reifsnider)*, Elsevier, 1991.

[212] U. Hansen, “Damage Development in Woven Fabric Composites During Tension-Tension Fatigue,” *Journal of Composite Materials*, vol. 33, no. 7, pp. 614–639, Apr. 1999.

[213] R. A. Naik, S. R. Patel, and S. W. Case, “Fatigue Damage Mechanism Characterization and Modeling of a Woven Graphite/Epoxy Composite,” *Journal of Thermoplastic Composite Materials*, vol. 14, no. 5, pp. 404–420, Sep. 2001.

[214] “Offshore Standard DNV-OS-F101 Submarine Pipeline Systems.” Det Norske Veritas AS, 2012.

[215] T. A. Osswald and G. Menges, *Materials Science of Polymers for Engineers*. Hanser Verlag, 2003.

[216] Z. Zhang and G. Hartwig, “Relation of damping and fatigue damage of unidirectional fibre composites,” *International Journal of Fatigue*, vol. 24, no. 7, pp. 713–718, 2002.

[217] M.-H. R. Jen, Y. S. Kau, and C. L. Ong, “Effect of matrix resin on the response in a centrally notched composite laminate,” *Composite Structures*, vol. 29, no. 1, pp. 99–106, 1994.

[218] S. Nemat-Nasser and M. Hori, *Micromechanics: Overall Properties of Heterogeneous Materials*. Elsevier, 1999.

[219] Y. . Fu, Y. . Wong, C. . Tang, and C. . Poon, “Thermal induced stress and associated cracking in cement-based composite at elevated temperatures—Part II: thermal cracking around multiple inclusions,” *Cement and Concrete Composites*, vol. 26, no. 2, pp. 113–126, Feb. 2004.

[220] C. M. Manjunatha, A. C. Taylor, A. J. Kinloch, and S. Sprenger, “The tensile fatigue behaviour of a silica nanoparticle-modified glass fibre reinforced epoxy composite,” *Composites Science and Technology*, vol. 70, no. 1, pp. 193–199, Jan. 2010.

[221] S. G. Long and Y. C. Zhou, “Thermal fatigue of particle reinforced metal–matrix composite induced by laser heating and mechanical load,” *Composites Science and Technology*, vol. 65, no. 9, pp. 1391–1400, Jul. 2005.

[222] R. J. Sanford, *Principles of fracture mechanics*. Prentice Hall, 2003.

[223] K. L. Reifsnider, *Fatigue of Composite Materials*. Elsevier, 1991.

[224] R. Talreja, “Damage Characterization by Internal Variables, Chapter 2,” in *Damage Mechanics of Composite Materials (ed. R. Talreja)*, Elsevier, 1994.

[225] R. Talreja, “Damage Mechanics of Composite Materials Based on Thermodynamics with Internal Variables,” in *Durability of Polymer Based Composite Systems for Structural Applications*, 1991.

[226] X. Liang and H. William Lloyd, “Continuum damage mechanics modeling of the failure of refractory cup under thermal loading and chemical shrinkage,” *Refractories Applications from American Ceramic Society*, vol. 11, no. 3, 2006.

[227] L. Kachanov, *Introduction to Continuum Damage Mechanics*. Springer, 1986.

[228] D. Krajcinovic and G. U. Fonseka, “The Continuous Damage Theory of Brittle Materials, Part 1: General Theory,” *Journal of Applied Mechanics*, vol. 48, no. 4, p. 809, 1981.

[229] G. U. Fonseka and D. Krajcinovic, “The Continuous Damage Theory of Brittle Materials, Part 2: Uniaxial and Plane Response Modes,” *Journal of Applied Mechanics*, vol. 48, no. 4, p. 816, 1981.

[230] J. Lemaitre and J.-L. Chaboche, *Mechanics of Solid Materials*. Cambridge University Press, 1994.

[231] J. Choi and K. K. Tamma, “Woven fabric composites—part I: Predictions of homogenized elastic properties and micromechanical damage analysis,” *International Journal for Numerical Methods in Engineering*, vol. 50, no. 10, pp. 2285–2298, 2001.

[232] J. Choi and K. K. Tamma, “Woven fabric composites—part II: Characterization of macro-crack initiation loads for global damage analysis,” *International Journal for Numerical Methods in Engineering*, vol. 50, no. 10, pp. 2299–2315, 2001.

[233] S. Araki and K. Saito, “Micromechanics of Stiffness Damage in Ceramic-Based Fiber-Reinforced Composites,” *International Journal of Damage Mechanics*, vol. 11, no. 3, pp. 205–222, Jul. 2002.

[234] J. P. Fan, C. Y. Tang, and C. L. Chow, “A Multilevel Superelement Technique for Damage Analysis,” *International Journal of Damage Mechanics*, vol. 13, no. 2, pp. 187–199, Apr. 2004.

[235] Z. Sun, I. M. Daniel, and J. J. Luo, “Statistical damage analysis of transverse cracking in high temperature composite laminates,” *Materials Science and Engineering: A*, vol. 341, no. 1–2, pp. 49–56, Jan. 2003.

[236] Z. Sun, I. M. Daniel, and J. J. Luo, “Modeling of fatigue damage in a polymer matrix composite,” *Materials Science and Engineering: A*, vol. 361, no. 1–2, pp. 302–311, Nov. 2003.

[237] J.-M. Berthelot, A. E. Mahi, and J.-F. Le Corre, “Development of transverse cracking in cross-ply laminates during fatigue tests,” *Composites Science and Technology*, vol. 61, no. 12, pp. 1711–1721, Sep. 2001.

[238] H.-C. Wu and V. C. Li, “Stochastic Process of Multiple Cracking in Discontinuous Random Fiber Reinforced Brittle Matrix Composites,” *International Journal of Damage Mechanics*, vol. 4, no. 1, pp. 83 –102, Jan. 1995.

[239] T. W. Clyne and P. J. Withers, *An Introduction to Metal Matrix Composites*. Cambridge University Press, 1995.

[240] M. R. Kabir, W. Lutz, K. Zhu, and S. Schmauder, “Fatigue modeling of short fiber reinforced composites with ductile matrix under cyclic loading,” *Computational Materials Science*, vol. 36, no. 4, pp. 361–366, Jul. 2006.

[241] G. M. Odegard, T. S. Gates, K. E. Wise, C. Park, and E. J. Siochi, “Constitutive modeling of nanotube-reinforced polymer composites,” *Composites Science and Technology*, vol. 63, no. 11, pp. 1671–1687, Aug. 2003.

[242] G. M. Odegard, T. C. Clancy, and T. S. Gates, “Modeling of the mechanical properties of nanoparticle/polymer composites,” *Polymer*, vol. 46, no. 2, pp. 553–562, Jan. 2005.

[243] T. Mura, *Micromechanics of Defects in Solids*. Springer, 1987.

[244] Y. P. Qiu and G. J. Weng, “On the application of Mori-Tanaka’s theory involving transversely isotropic spheroidal inclusions,” *International Journal of Engineering Science*, vol. 28, no. 11, pp. 1121–1137, 1990.

[245] K. Takahashi, K. Harakawa, and T. Sakai, “Analysis of the Thermal Expansion Coefficients of Particle-Filled Polymers,” *Journal of Composite Materials*, vol. 14, no. 1, pp. 144 –159, Jan. 1980.

[246] UL IDES, “Prospector Plastics Database of Data Sheets & UL Yellow Cards - Generic Epoxy.”

[247] J. Zhu, H. Peng, F. Rodriguez-Macias, J. L. Margrave, V. N. Khabashesku, A. M. Imam, K. Lozano, and E. V. Barrera, “Reinforcing Epoxy Polymer Composites Through Covalent Integration of Functionalized Nanotubes,” *Advanced Functional Materials*, vol. 14, no. 7, pp. 643–648, 2004.

[248] J.-W. Jiang, J.-S. Wang, and B. Li, “Thermal expansion in carbon nanotubes and graphene: nonequilibrium Green’s function approach,” *arXiv:0909.1917*, Sep. 2009.

[249] N. Marimuthu, “Determination Of Coefficient Of Thermal Expansion Of Single Walled Carbon Nanotubes Using Molecular Dynamics Simulation,” *Electronic Theses, Treatises and Dissertations*, Aug. 2005.

Appendices

A – Degradation of Elastic Modulus

B – Degradation of Poisson's Ratio

C – Degradation of Coefficient of Thermal Expansion

D – Degradation of Thermal Conductivity

E – Hatta-Taya Method

Appendix A – Degradation of Elastic Modulus

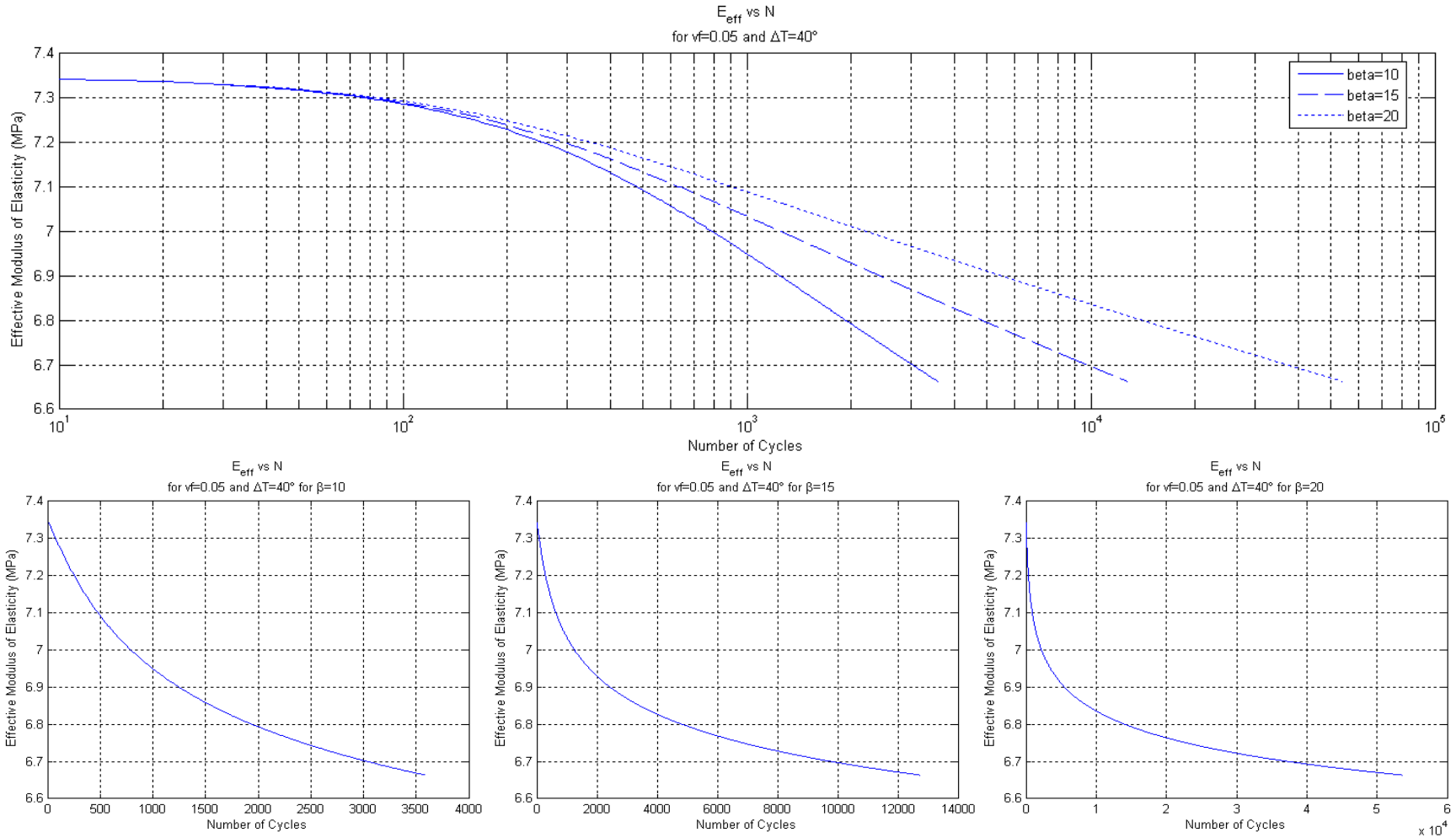

Figure A-1. Variation of elastic modulus (E) w.r.t. number of thermal cycles (N) for various Weibull shape parameter, beta values.
Top – Comparison of all beta values in semi-log scale. **Bottom –** Individual beta values.

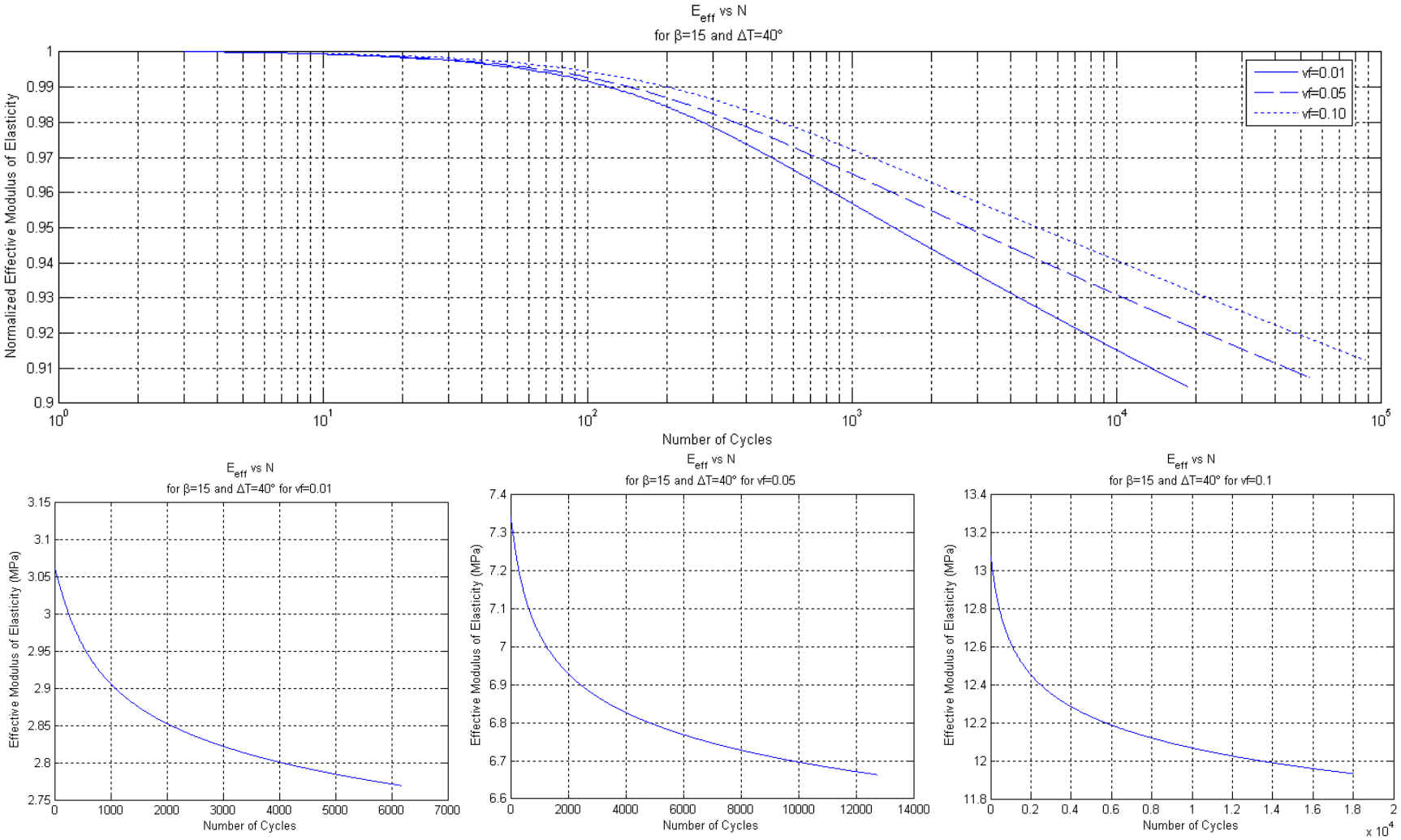

Figure A-2. Variation of elastic modulus (E) w.r.t. number of thermal cycles (N) for various SWCNT volume fraction, vf values.
Top – Comparison of all vf values in semi-log scale. **Bottom –** Individual vf values.

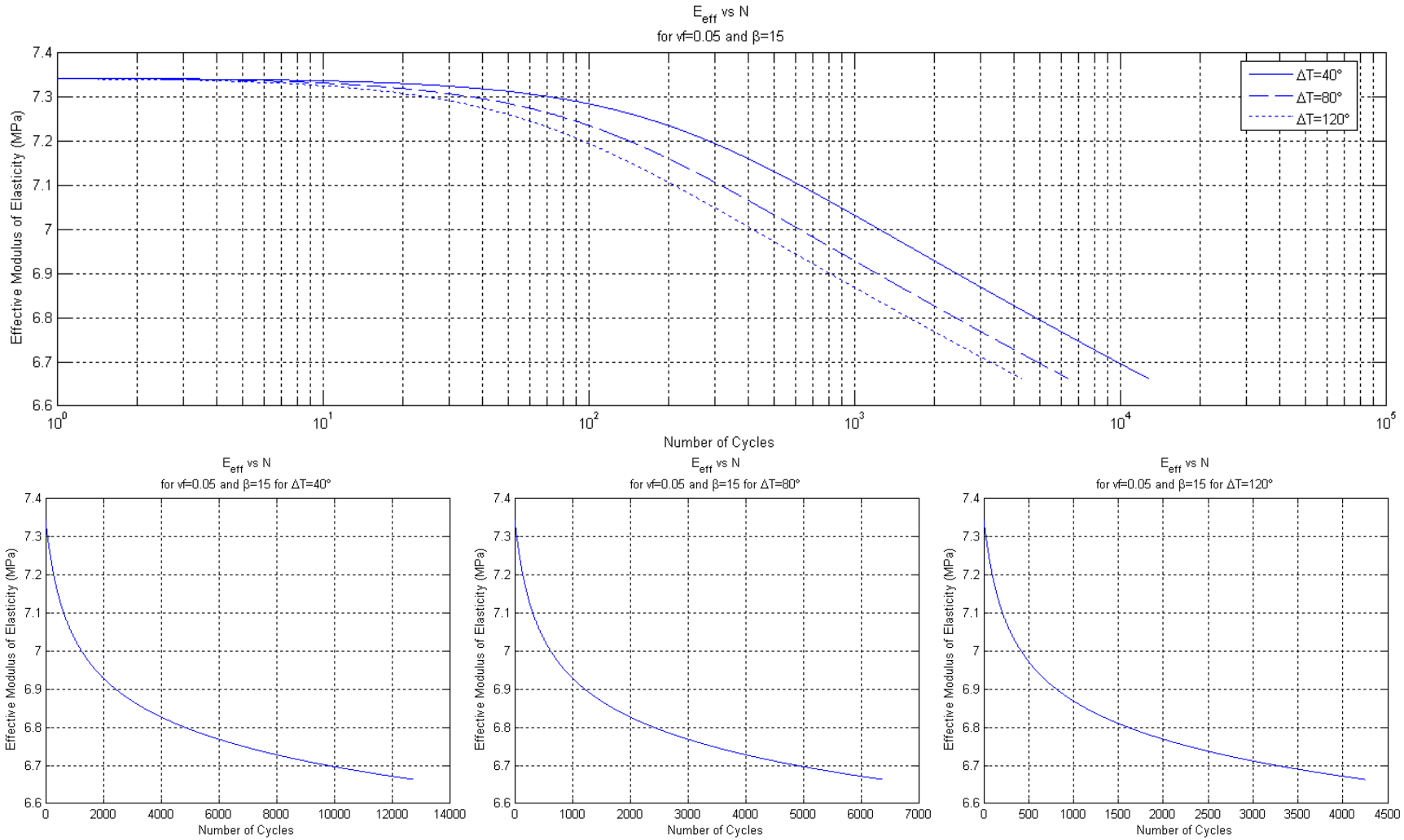

Figure A-3. Variation of elastic modulus (E) w.r.t. number of thermal cycles (N) for various temperature change, ΔT values.
Top – Comparison of all ΔT values in semi-log scale. **Bottom –** Individual ΔT values.

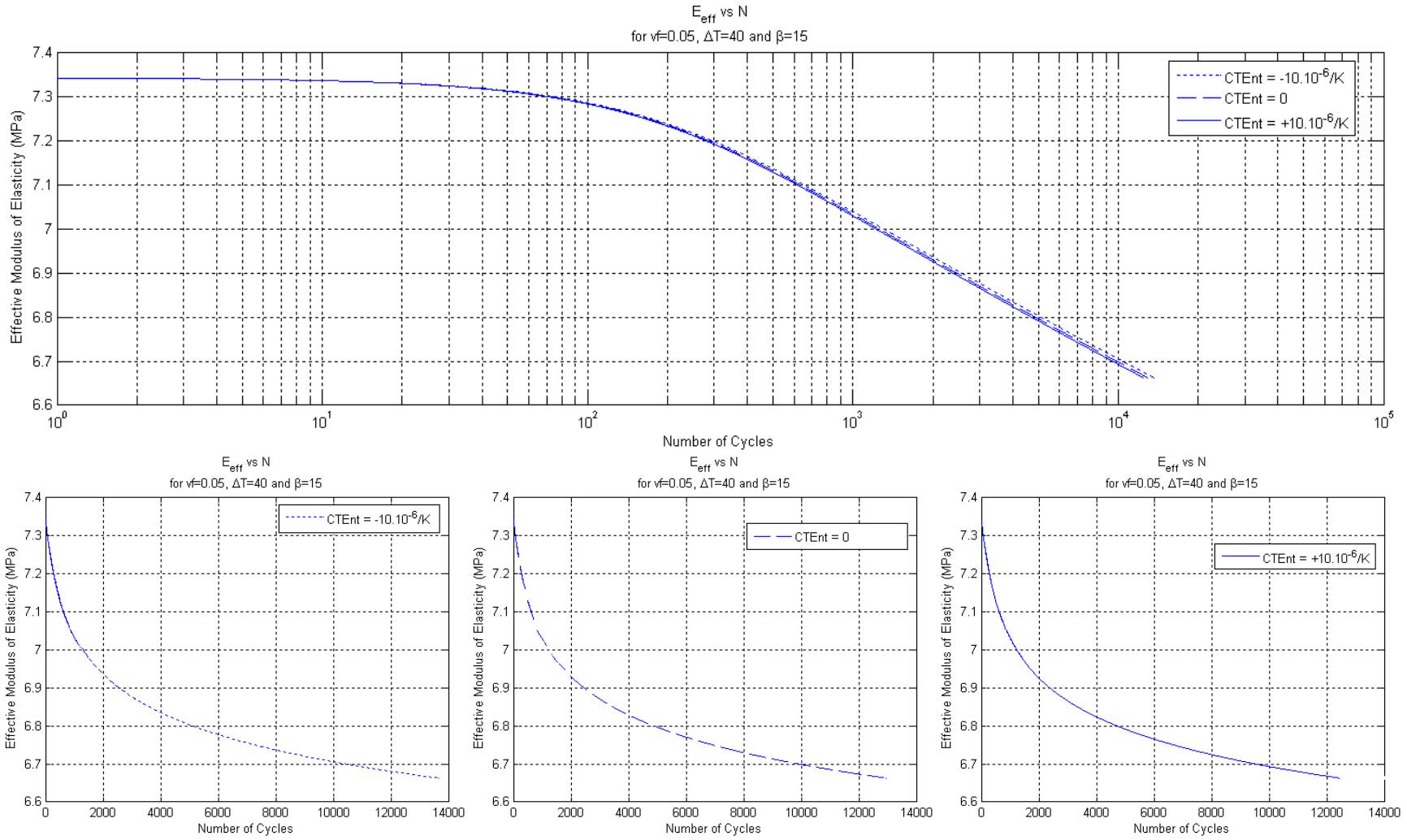

Figure A-4. Variation of elastic modulus (E) w.r.t. number of thermal cycles (N) for various SWCNT CTE values.
Top – Comparison of all SWCNT CTE values in semi-log scale. **Bottom –** Individual SWCNT CTE values.

Appendix B – Degradation of Poisson's Ratio

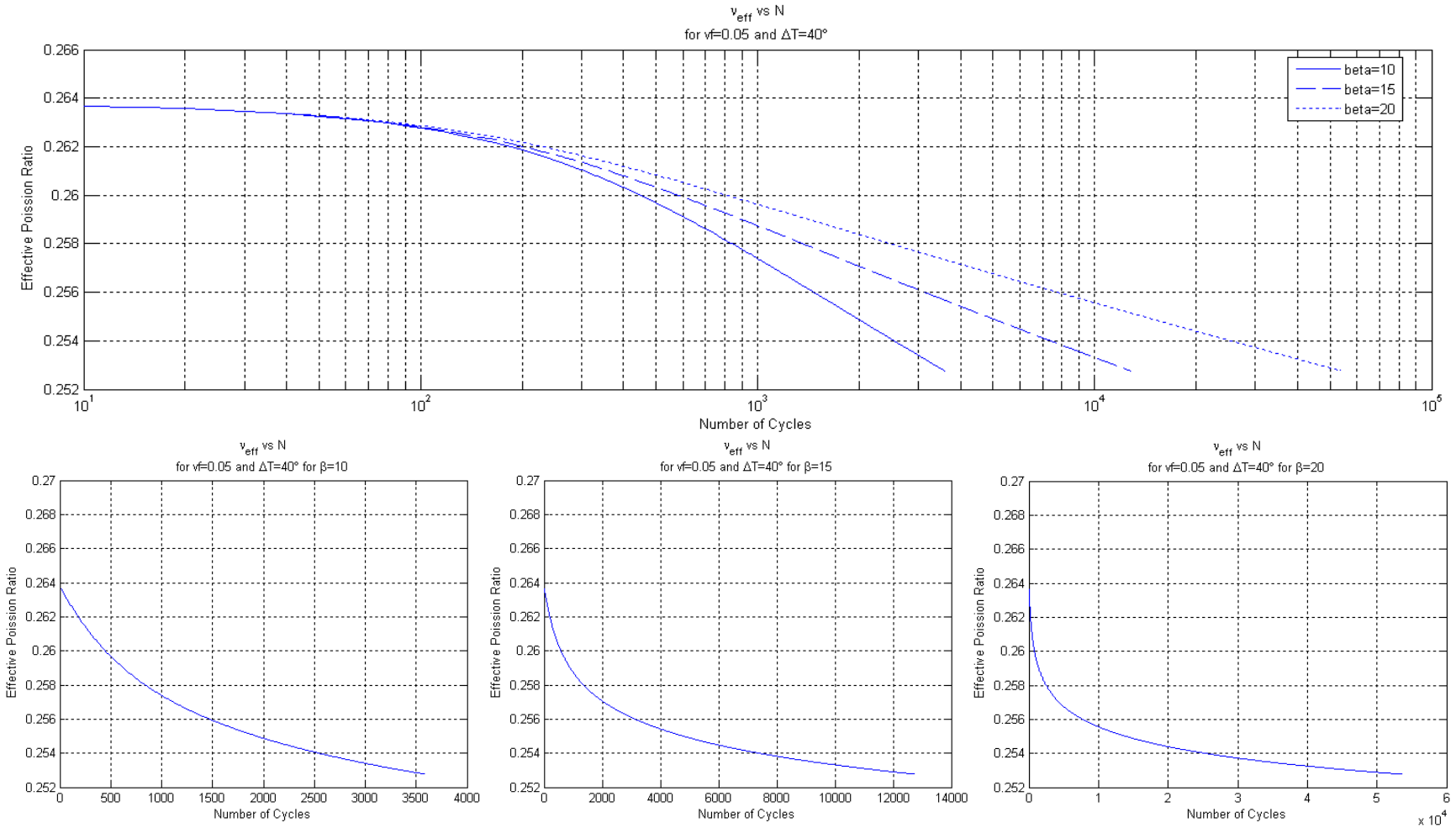

Figure B-1. Variation of Poisson's ratio (ν) w.r.t. number of thermal cycles (N) for various Weibull shape parameter, beta values.
Top – Comparison of all beta values in semi-log scale. **Bottom –** Individual beta values.

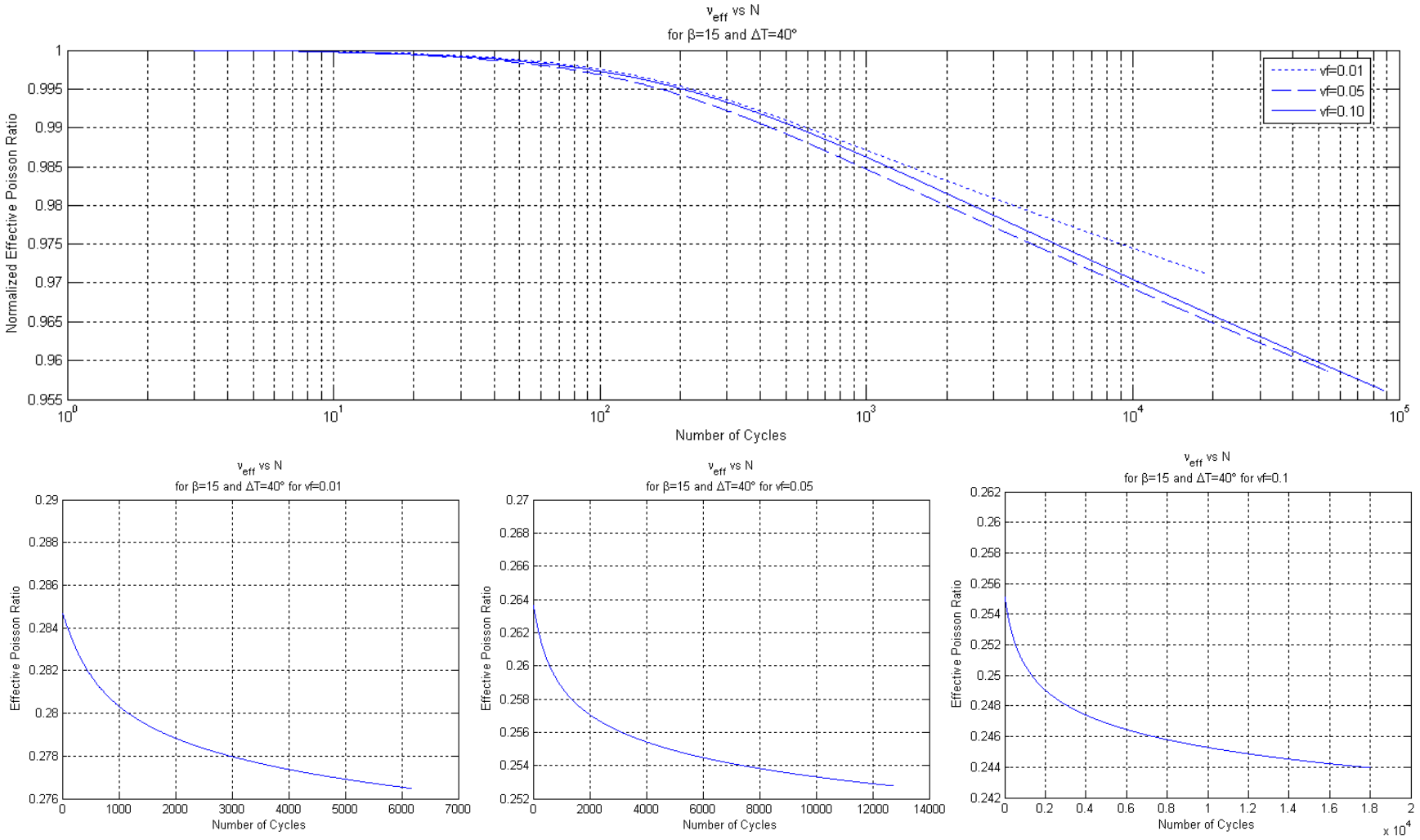

Figure B-2. Variation of Poisson's ratio (ν) w.r.t. number of thermal cycles (N) for various SWCNT volume fraction, vf values.
Top – Comparison of all vf values in semi-log scale. **Bottom –** Individual vf values.

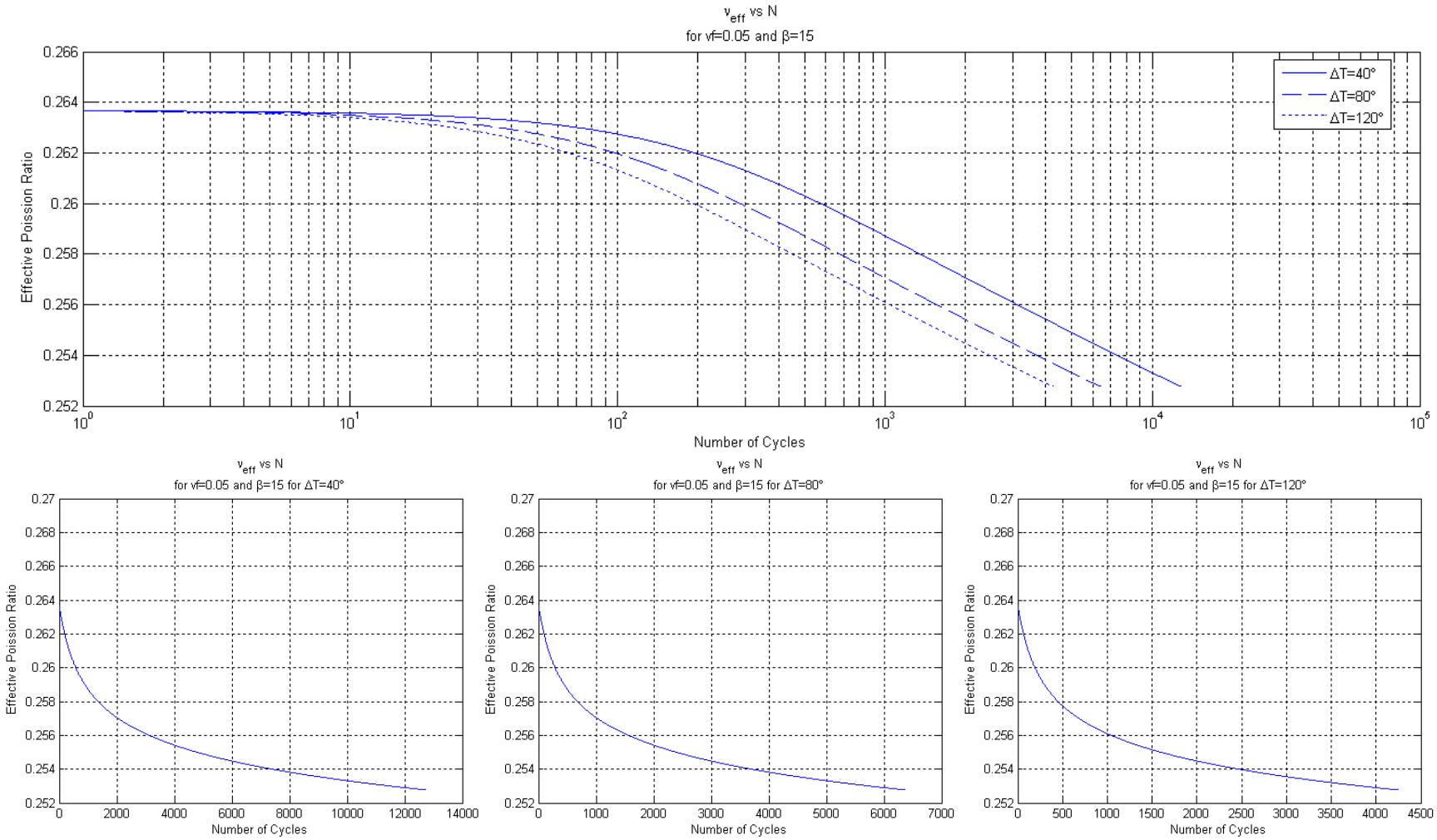

Figure B-3. Variation of Poisson's ratio (ν) w.r.t. number of thermal cycles (N) for various temperature change, ΔT values.
Top – Comparison of all ΔT values in semi-log scale. **Bottom –** Individual ΔT values.

Appendix C – Degradation of Coefficient of Thermal Expansion

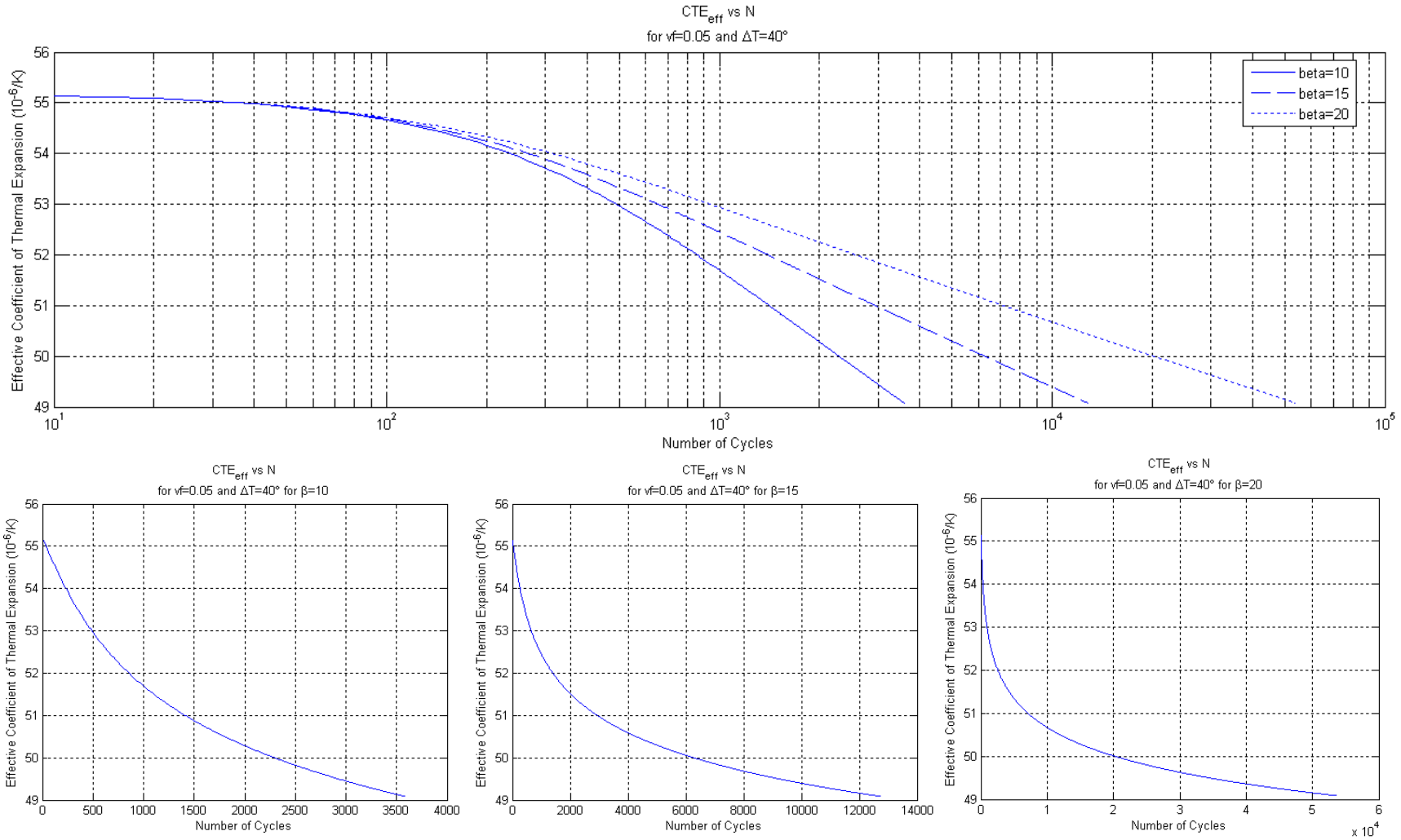

Figure C-1. Variation of coefficient of thermal expansion (CTE) w.r.t. number of thermal cycles (N) for various Weibull shape parameter, beta values. **Top –** Comparison of all beta values in semi-log scale. **Bottom –** Individual beta values.

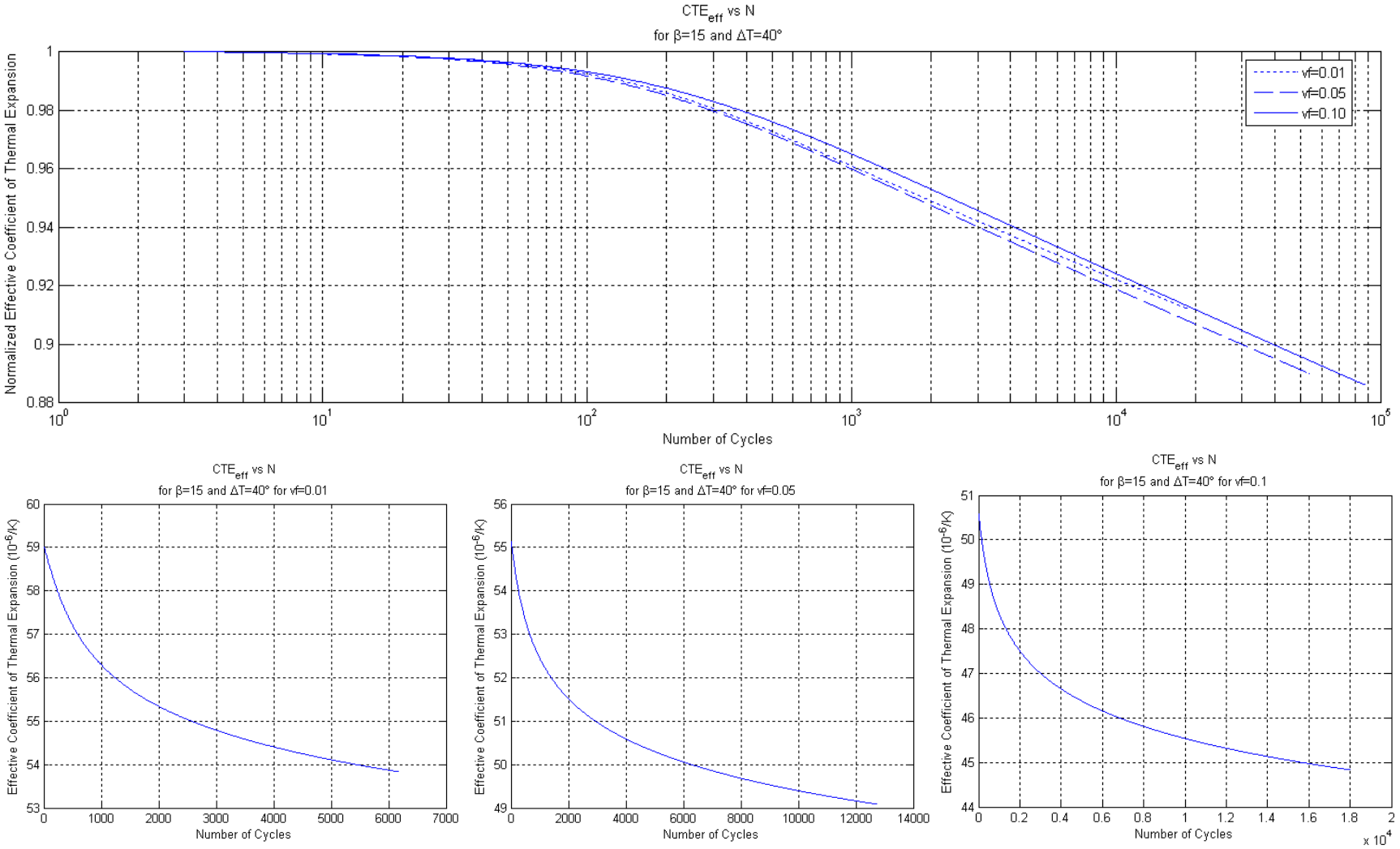

Figure C-2. Variation of coefficient of thermal expansion (CTE) w.r.t. number of thermal cycles (N) for various SWCNT volume fraction, vf values. **Top –** Comparison of all vf values in semi-log scale. **Bottom –** Individual vf values.

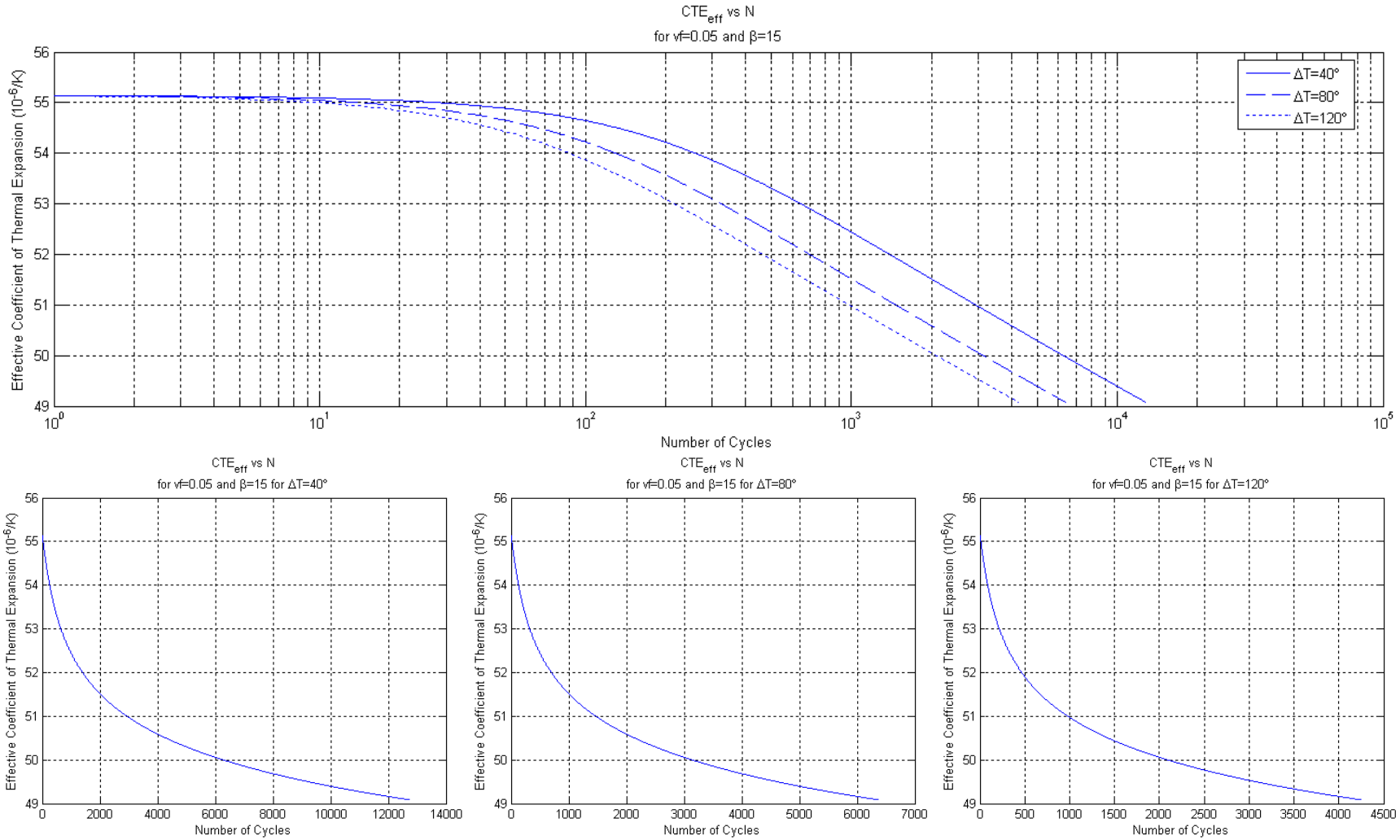

Figure C-3. Variation of coefficient of thermal expansion (CTE) w.r.t. number of thermal cycles (N) for various temperature change, ΔT values. **Top –** Comparison of all ΔT values in semi-log scale. **Bottom –** Individual ΔT values.

Appendix D – Degradation of Thermal Conductivity

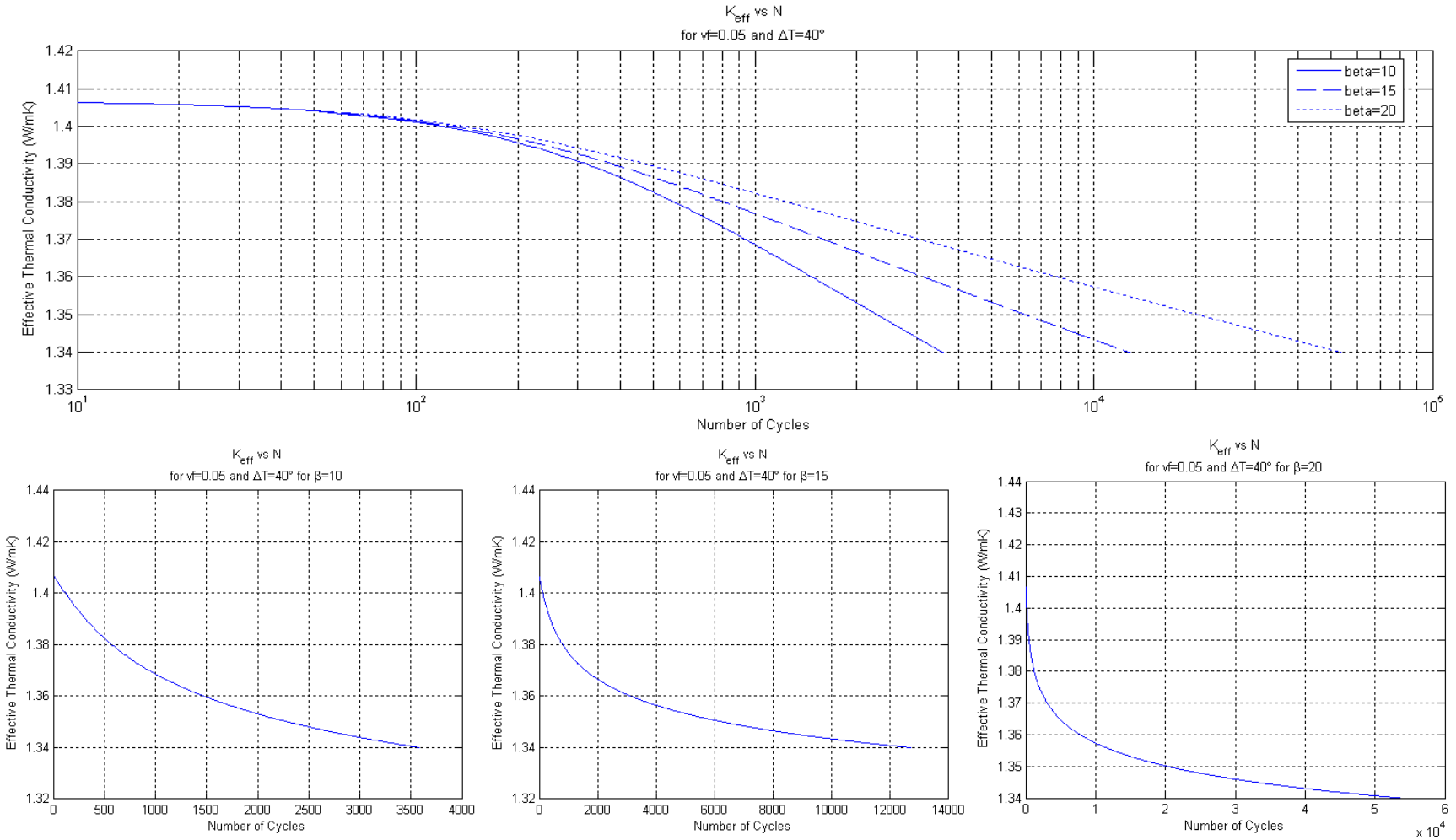

Figure D-1. Variation of thermal conductivity (K) w.r.t. number of thermal cycles (N) for various Weibull shape parameter, beta values.
Top – Comparison of all beta values in semi-log scale. **Bottom –** Individual beta values.

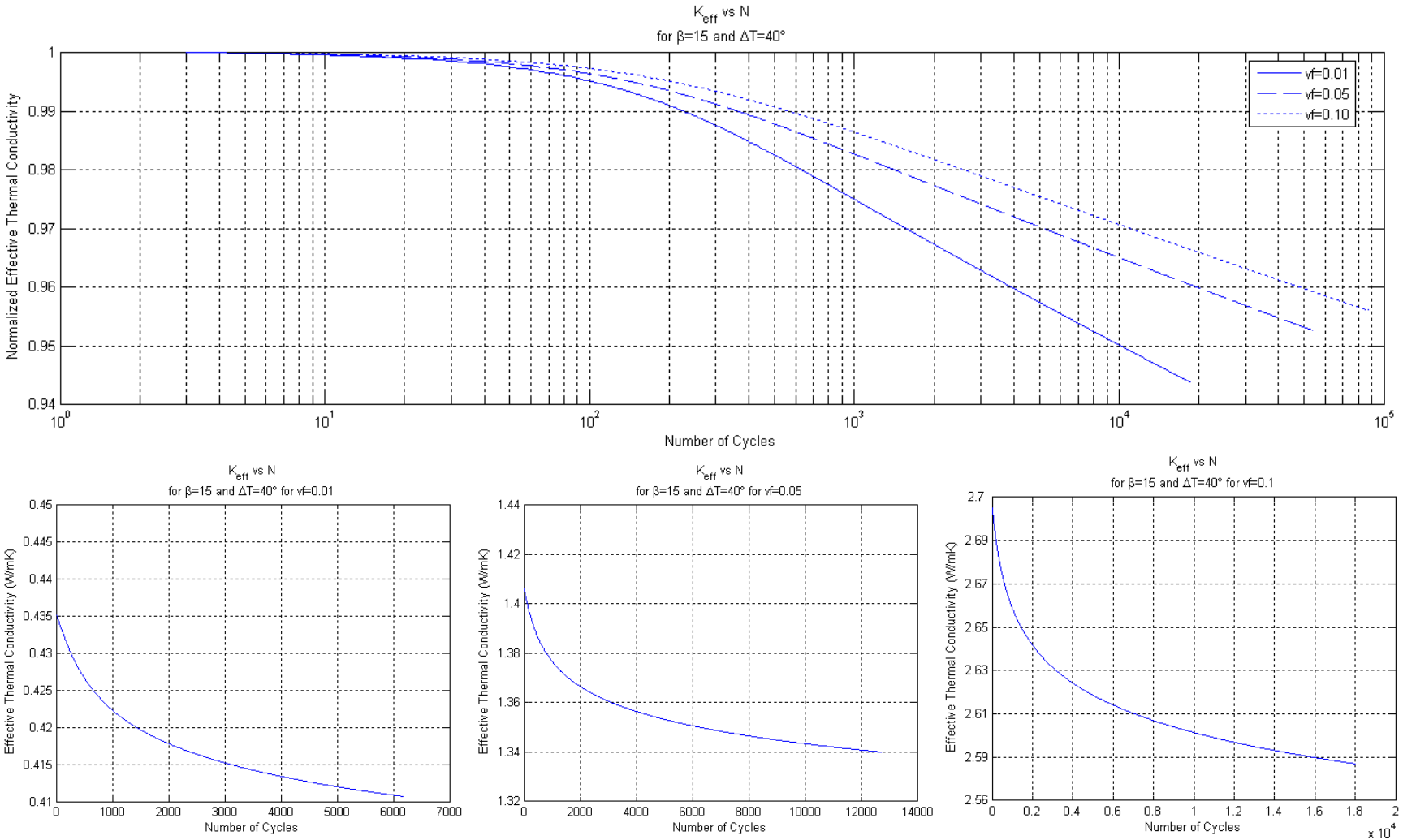

Figure D-2. Variation of thermal conductivity (K) w.r.t. number of thermal cycles (N) for various SWCNT volume fraction, vf values.
Top – Comparison of all vf values in semi-log scale. **Bottom –** Individual vf values.

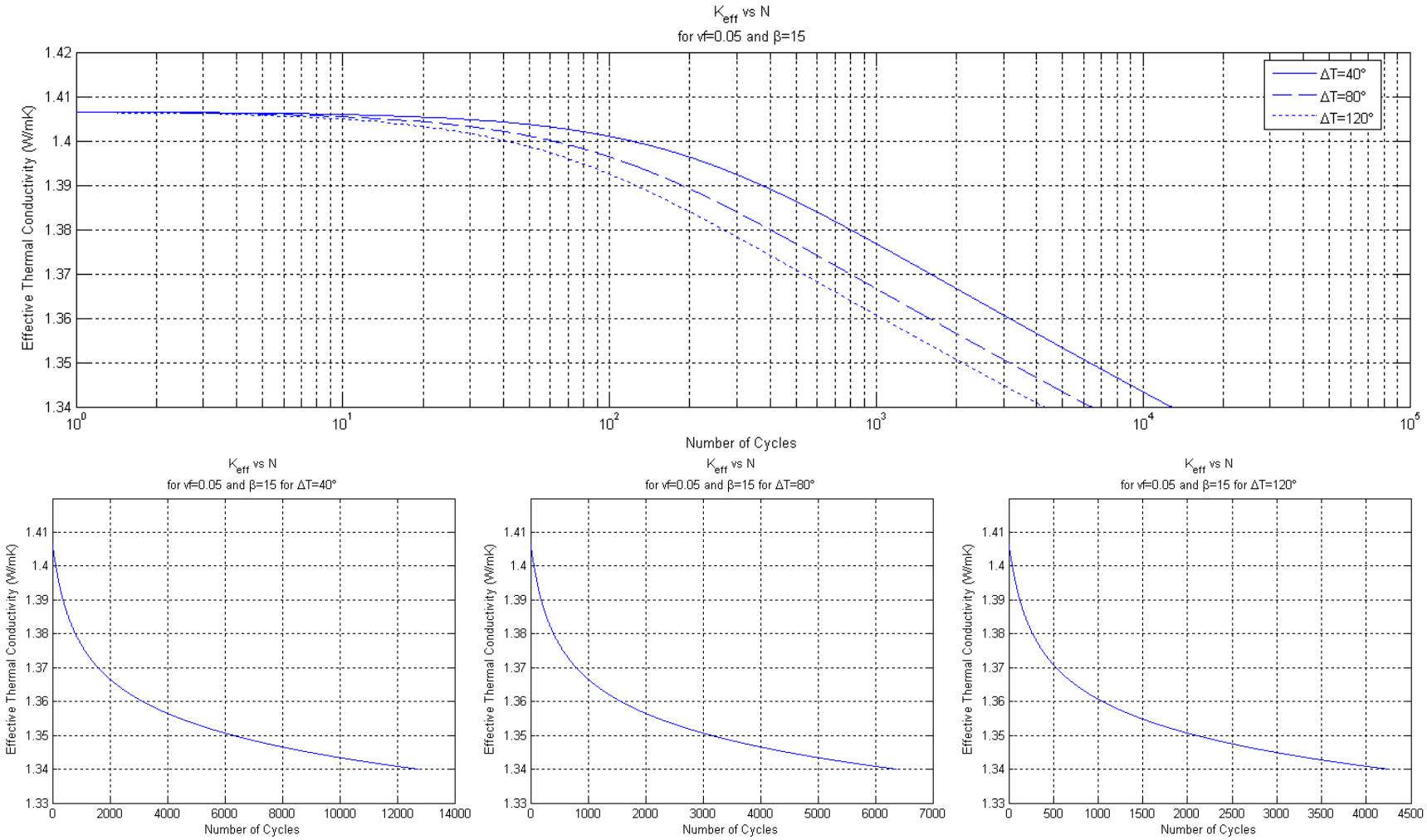

Figure D-3. Variation of thermal conductivity (K) w.r.t. number of thermal cycles (N) for various temperature change, ΔT values.
Top – Comparison of all ΔT values in semi-log scale. **Bottom –** Individual ΔT values.

Appendix E – Hatta – Taya Method

The characteristics of the Hatta-Taya method are

I. Uses Equivalent Inclusion Method for steady state heat conduction, analogous to Eshelby's, and thermal counter part of Mori-Tanaka;

II. Replaces the actual inclusion by an equivalent one made of matrix material, which has appropriate misfit temperature gradient, such that the flux is the same as for the actual inclusion;

and

III. Takes into account the interaction among multiple inclusions.

Two phase Hatta-Taya (matrix and one type of multiple inclusion) is described below.

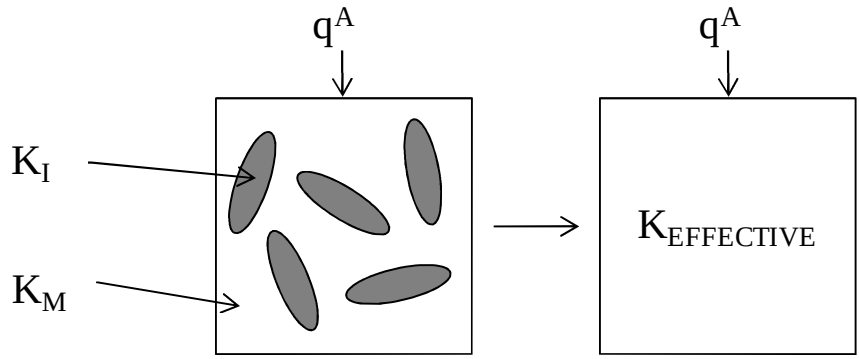

Figure E-1. Schematic of Hatta-Taya homogenization.

The overall heat balance equation of the homogeneous composite is

$$q^A = K_{Eff} < T_{,i} > , \qquad \textbf{E.1}$$

where

q^A is the applied heat flux;

K_{Eff} is the effective thermal conductivity of the homogenized composite;

and

$< T_{,i}>$ is the average composite temperature gradient.

The average composite temperature gradient is related to the applied and the disturbed temperature gradient at the rate of the volume fraction of the inclusions. Specifically,

$$q^A = K_{Eff} < T_{,i}> = K_{Eff} (T^A_{,i} + f \ T^T_{,i}) , \qquad \textbf{E.2}$$

where

f is the volume fraction of inclusions,

$T^T_{,i}$ is the disturbed temperature gradient due to mismatch.

$T^T_{,i}$ can be obtained via equivalent inclusion method.

$$K_I (T^A_{,i} + T^C_{,i} + <T_{,i}>_M) = K_M (T^A_{,i} + T^C_{,i} + <T_{,i}>_M - T^T_{,i}), \qquad \textbf{E.3}$$

where left hand side is the actual inclusion flux, and right hand side is the equivalent inclusion flux, and

$T^C_{,i}$ is the constrained temperature gradient,

$<T_{,i}>_M$ is the mean matrix temperature gradient due to inclusions (interaction term).

The relationship between $T^C_{,i}$ and $T^T_{,i}$ is given by a transformation tensor, S, similar to Eshelby's, which is a function of aspect ratio of the inclusions.

$$T^C_{,i} = S \ T^T_{,i} \qquad \textbf{E.4}$$

Term $\langle T_{,i} \rangle_M$ is obtained through internal flux balance based on the effective field theory as

$$(1-f)\langle q \rangle_M + f \langle q \rangle_I = 0 , \quad \textbf{E.5}$$

where the mean matrix flux is

$$\langle q \rangle_M = K_M \langle T_{,i} \rangle_M , \quad \textbf{E.6}$$

and

the mean inclusion flux is

$$\langle q \rangle_I = K_M (T^C_{,i} + \langle T_{,i} \rangle_M - T^T_{,i}) . \quad \textbf{E.7}$$

Therefore,

$$\langle T_{,i} \rangle_M = -f (T^C_{,i} - T^T_{,i}) . \quad \textbf{E.8}$$

Then, the disturbed temperature gradient can be obtained as functions of

$$T^T_{,i} \Rightarrow (T^A_{,i} , f , S , K_M , K_I) . \quad \textbf{E.9}$$

Finally, plugging the above terms into overall heat balance equation (E.1) gives the effective thermal conductivity of the homogenized composite.